Modeling and Simulation of a Solar Air-Based Façade-Integrated Decentralized System for Retrofits

Edvinas Bigaila

A Thesis

In the Department

of

Building, Civil and Environmental Engineering

Presented in Partial Fulfillment of the Requirements

For the Degree of

Doctor of Philosophy (Building Engineering) at

Concordia University

Montreal, Quebec, Canada

August 2018

CONCORDIA UNIVERSITY

SCHOOL OF GRADUATE STUDIES

This is to certify that the thesis prepared

By: Edvinas Bigaila

Entitled: Modeling and Simulation of a Solar Air-Based Façade-Integrated
Decentralized System for Retrofits

and submitted in partial fulfillment of the requirements for the degree of

Doctor Of Philosophy (Building Engineering)

complies with the regulations of the University and meets the accepted standards with respect to originality and quality.

Signed by the final examining committee:

_____ Chair
Dr. Ion Stiharu

_____ External Examiner
Dr. Mikhail V. Sorin

_____ External to Program
Dr. Georgios Vatistas

_____ Examiner
Dr. Radu Grigore Zmeureanu

_____ Examiner
Dr. Hua Ge

_____ Thesis Supervisor
Dr. Andreas Athienitis

Approved by_____
Dr. Fariborz Haghighat, Graduate Program Director

November 6, 2018   _____
Dr. Amir Asif, Dean
Gina Cody School of Engineering and Computer Science

Abstract

Modeling and Simulation of a Solar Air-Based Façade-Integrated Decentralized System for Retrofits

Edvinas Bigaila, Ph.D

Concordia University, 2018

There is a significant amount of research on air-based photovoltaic/thermal (PV/T) solar collectors. However, the installed area of all air-based solar thermal systems is only 1% compared to all solar thermal systems installed.

With open-loop mechanically ventilated air-based building integrated photovoltaic/thermal (BIPV/T) collectors, the silicon based photovoltaic panels can be operated at close to optimal power production levels all year long, without overheating in summer. In efficient, highly insulated and airtight buildings, requirements for fresh air are higher, thus solar air collectors integrated with high efficient envelopes and HVAC systems are an important part of a highly efficient building.

This thesis is focused on development of a BIPV design methodology for solar façade applications in building envelope retrofit projects with BIPV, BIPV/T, STPV (semitransparent photovoltaics), BIPV shading devices and double skin façades with BIPV glazing. A BIPV/T assisted heat pump system and a radiant panel with short term phase change thermal storage with PCM (RPCMP) is also studied as a potential retrofit system.

The retrofit methodology is applied to a case study office building, demonstrating that the solar façade application can contribute to energy consumption reduction in perimeter zones by up to 84%. Cases with the most promising techno-economic results demonstrate the possibility to reach energy consumption reductions by up to 56%. The most promising case selection was done using

the proposed methodology employing the Net Present Value/Investment ratio over the energy savings cost ratio. Different design options are shown to be feasible for different climatic regions of Canada.

A model with Simulink/Matlab was developed for design, optimization and operational performance studies of a novel concept for a prefabricated façade module, which consists of an air-based building integrated photovoltaic/thermal (BIPV/T) solar collector assisting a small scale decentralized exhaust heat pump integrated in or linked to façade in which heating of a perimeter zone in an office building is supplied through a radiant panel. Fresh air could be supplied by an air-based BIPV/T system in a displacement ventilation mode and extracted through central exhaust or decentralized heat recovery ventilator. With the developed model annual simulations for Prairies climate, show that there is a potential to reach net-zero energy targets for the perimeter zone with this solution. The model for the perimeter zone studies was incorporated into the existing Simulink toolbox CARNOT (2017) for future work on the system and control optimization.

Acknowledgements

Table of Contents

Abbreviations

BIPV	Building-integrated Photovoltaic panel
BIPV/T	Building-integrated Photovoltaic/Thermal collector
BOMA	Building Owners and Managers Association of Canada
COP	Coefficient of Performance
CV-RMSE	Root mean square error coefficient of variation, %
CDD	Cooling degree days
DOE	U.S. Department of Energy
EPoG	Energy producing glazing
EVA	Ethylene-vinyl acetate
EUI	Energy Use Intensity
FF	Fill factor
HDD	Heating degree days
HP	Heat Pump
HVAC	Heating, ventilation and air-conditioning
IGU	Insulated glazing unit
Mono-Si	Mono-crystalline Silicon
NMBE	Normalized mean biased error, %
NRCan	Natural Resources Canada
NPV	Net-present value
PCM	Phase Change Material
PF	Packing factor - the area of photovoltaic cells over the area of active glazing
PV	Photovoltaic
PVB	Poly-vinyl butyral
RTD	Resistance temperature detector
SHGC	Solar heat gain coefficient
STPV	Semi-transparent photovoltaic
STC	Standard testing conditions
TABS	Thermally-Activated Building System
TRNSYS	Transient System Simulation Tool
UV	Ultra-violet
WWR	Window-to-wall ratio

Nomenclature

Symbols

A	Surface area, m^2
C_i	Specific heat, J/kg K
D	Diameter, m
E	Electrical power generated by the photovoltaic panel W
F	View factor between surfaces
F'	Radiant panel efficiency or heat removal factor
I	Current, A
G	Insolation, W/m^2
L	Length, m
Nu	Nusselt number
R	Thermal resistance, m^2K/W
Re	Reynolds number
Pr	Prandtl number
Q	Energy rate, W
Slope	Slope of BIPV/T collector, degrees
Spacing	BIPV/T air gap channel thickness, m
T	Temperature, K
U	Thermal conductance, W/m^2 K
V	Voltage, V
V_{wind}	Wind speed, m/s
W	Distance between the tube and the centerlines, m
d_h	Hydraulic diameter, m
e	Electron charge, 1.6 x 10^{-19} Coulombs
f	Friction factor
g	Acceleration due to gravity, m/s^2
h	Convective film coefficient, W/ m^2-K
k_{fluif}	Thermal conductivity of air, W/m-K
$\dot{m}$	Mass flow rate of the radiant panel, kg/s
skew	Skewness factor
slope	Slope of the transition between phases

t_{insu}, t_{pcm}	Thickness of the insulation and of PCM layer, m
q_e	Photovoltaic system power production, W/m^2
w	Temperature range of PCM panel phase change, K
y, $\triangle$y	Length and element region of length of the pipe, m

Greeks Symbols

α	Absorptivity of a material
$\gamma_{mpp,ref}$	Photovoltaic module temperature efficiency modifier, 1/oC
δ	Material thickness, m
ε	Emissivity of material
η	Efficiency of photovoltaic module
λ	Conductivity of material, W/m-K
ρ	Density of air, kg/m^3
τ	Transparency of photovoltaic module glass
ϑ	Viscosity of material, kg/m-hr

1   Introduction

1.1   Background and Rationale

The commercial sector includes a large variety of different building types, operating in a wide range of climatic conditions, and as such, there is a great variation in how energy is used in commercial buildings. In Canada, the largest end use for energy is for space heating (45%), then for auxiliary equipment (19%), lighting (12%) and 5% for space cooling (NRCan-OEE, 2013a). In milder U.S or European climates the lighting and office equipment often drive "internal loads" in commercial buildings that make their total energy use less dependent on climatic conditions than residential buildings. The remainder of energy use in commercial buildings is for water heating, refrigeration, and other purposes. Commercial/institutional buildings energy use in Canada by end-use are shown in Figure 1.1 (NRCan-OEE, 2013a).
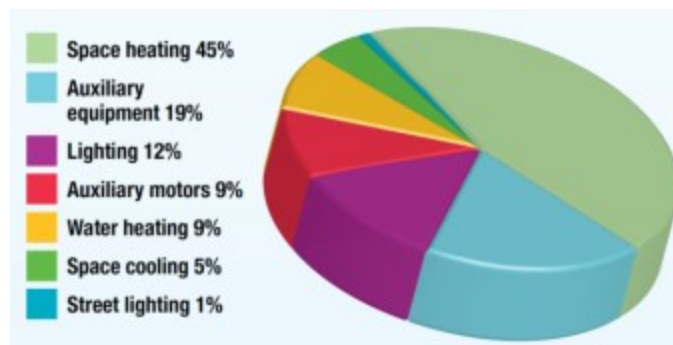
Figure 1.1: Commercial/institutional energy use by end-use in Canada (NRCan-OEE, 2013a) .

Commercial sector energy use has been growing at a rapid pace, in part due to economic trends and the shift from manufacturing to services (Waide and Amann, 2007). Often newer buildings as a whole are no more efficient than older ones. Figure 1.2 shows EUI levels for buildings by year of construction. Commercial buildings constructed from prior to 1919 through 1959 use, on average, appreciably less energy per unit of floor space than more recent construction. Differences in service levels, types of equipment in place, and building use may explain some of this phenomenon, but

overall it appears that new designs are not matching energy performance expectations, and the impact of energy codes is not necessarily showing up in the average stock of new construction (DOE, 2005; Waide and Amann, 2007).
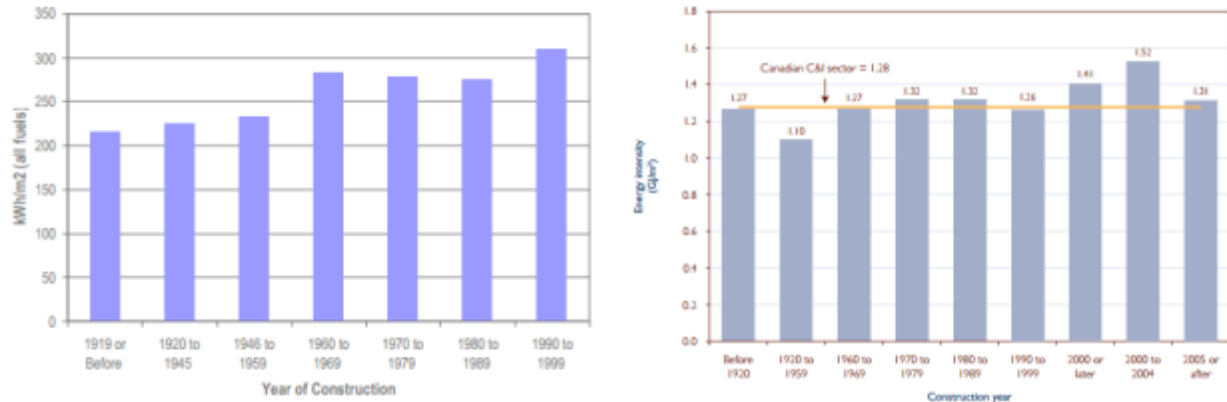
Figure 1.2: Commercial and Institutional Building Energy Intensity by Year of Construction. North America left (DOE, 2012) and Canada right (NRCan-OEE, 2013b).

For reference, commercial sector buildings categorized by floor space, number of buildings, and percentage of total sector energy consumption are shown in Table 1.1. The three principal building types of office, mercantile and education account for almost half of commercial sector energy use (Waide and Amann, 2007). As shown in Table 1.2, a substantial portion of commercial floor space was built prior to 1980 year and a large number of buildings built in the first half of the 20th century are still in operation. 18% of the commercial building estate per floor area is government owned and 57% is non-government owned and owner occupied, 23% non-owner occupied and 2% unoccupied (DOE, 2012).

Table 1.1: Share of Commercial Buildings by Type and Primary Energy Consumption (DOE, 2005).

Building type	Total Floor space	Total Buildings	Primary Energy Consumption
Office	18%	16%	22%
Warehouse/Storage	16%	13%	8%
Mercantile	15%	14%	15%

Table 1.1: Share of Commercial Buildings by Type and Primary Energy Consumption (DOE, 2005) (cont.).

Building type	Total Floor space	Total Buildings	Primary Energy Consumption
Education	13%	7%	10%
Public Assembly	7%	7%	6%
Lodging	7%	3%	7%
Service	5%	10%	6%
Health Care	4%	3%	8%
Food Service	3%	7%	7%
Public Order/Safety	2%	2%	1%
Food Sales	1%	4%	4%
Vacant	8%	12%	2%
Other	2%	2%	3%
	100%	100%	100%

Table 1.2: Commercial Building Vintage (DOE, 2005).

Year of Construction	Percent of Total floor space
Prior to 1919	6%
1920 – 1959	23%
1960 – 1979	34%
1980 – 1989	21%
1990 – 1999	16%

In addition, it is reported that in Canada there are approximately 83,500 non-medical commercial office buildings covering 147.5 million square meters of floor space and having an average energy use intensity (EUI) of 333 ekWh/m^2 (NRCan-OEE, 2013b). 80% of Canada's non-medical office buildings were constructed before the year 2000, which results in 79% of the total commercial building related energy use (NRCan-OEE, 2013b). Approximately 57% of these buildings had not undergone any type of retrofit yet by the year 2009 (NRTEE, 2009). Buildings account for approximately 31% of the energy consumed in Canada, with commercial and institutional sector contributing 12.5% of Canadian energy use and 11% of Canadian greenhouse gas emissions (NRCan-OEE, 2013a).

The building industry is conscious that many office buildings urgently require improvement. Many certification tools, such as 'Leed EB:OM', 'ENERGY STAR', 'BOMA BESt' (Canada and USA), 'Breeam' (UK), 'DGNB' (GER) have been developed, which judge a building project for its sustainability and energy performance. However, having the certification tool at hand does not help to find the most appropriate technical solution. Refurbishment in general – and façade refurbishment in particular – is a complicated planning task. Buildings always demand individual technical solutions. The refurbishment has to deal with existing structural conditions and given design. Often too little is known about the building stock and its technical parameters, which results in costly planning and rather rigorous refurbishment approaches. Usually, outdated office buildings are either demolished, or they are substantially refurbished by removing the façade, technical installations, and all finishing. Intermediate solutions are very rare and building owners worry about the impact of refurbishment and the economic consequences. Therefore, many buildings with a high refurbishment potential are kept in the poor technical state as long as possible. On the other hand, many buildings are demolished, which is a waste of capital, embodied energy and often architectural identity and much waste that often goes to landfills. Current practice is often lacking innovative and practical refurbishment concepts for office facades (Ebbert, 2010).

Energy performance in the commercial sector often focuses on improving the efficiency of the heating, cooling or lighting equipment. However, optimizing these systems depends also on the thermal properties of a building's outer shell. Improvements made to the windows, walls and roof of a commercial building reduce energy cost while also reducing mold and other moisture problems, equipment breakdown and discomfort (Waide and Amann, 2007). A wide variety of materials are used in the construction of commercial buildings, providing more variance in building shell efficiency than in the residential sector. For instance, many large commercial office buildings are constructed with steel, which can dramatically increase the thermal conductivity of a building's shell without proper insulation. On average, heat transfer and air infiltration through walls account

for 21% of total heat losses from commercial buildings during heating months (DOE, 2012). Although insulation upgrades can save considerable energy at relatively low cost in many buildings, commercial building owners tend to focus on equipment upgrades. Over the past 25 years, insulation upgrades have been installed in 5% of the existing building stock. The retrofit rates for lighting and HVAC systems are roughly three times as high (DOE, 2012).

1.2 Problem statement

Photovoltaic (PV) products exist for several decades now and the most common technology – silicon PV cells – are a mature and cost competitive technology in the energy technology sector. The rising popularity is attributed to the falling PV module prices, governmental subsidies and already achieved grid parity in some countries. Other factors are increased awareness of the environmental problems, due to climate change, pollution and waste production by humans and energy efficiency interest in built environment, as a result.

Integrating PV technologies with building materials, like laminated glazing, creates an opportunity to manufacture energy producing construction elements, called building-integrated photovoltaics (BIPV) or energy producing glazing (EPoG). The application of these active construction materials opens up the opportunities to study the potential of applying them in facade retrofit projects. BIPV can, in addition to electricity produce also useful heat when a heat recovery fluid is used to extract heat from the PV   (BIPV/T) or also transmit useful daylight in the case of semitransparent photovoltaic (STPV) windows. Thus, solutions with BIPV glazing or EPoG can be used as cladding material, to construct a spandrel-integrated BIPV or BIPV/T, STPV glazing, shading devices with BIPV and second skin façades with BIPV. A holistic design strategy in a retrofit project, where the energy reduction and on-site renewable energy application opportunities are investigated to assist the development of retrofitted net-zero buildings, or net-zero energy perimeter zones, needs to be developed.

To reach net-zero performance targets in an efficient way for retrofits, service-integrated prefabricated façade concept is getting more attention in recent years (Fraunhofer ISE, 2012; IEA, 2014; IEA ECBCS, 2011; MEEFS, 2013; Ochs, 2014). These systems are attractive in façade retrofits, where an opportunity to integrate both energy supply systems and improve energy efficiency of the perimeter spaces, by reducing the environmental impact on thermal loads, providing good quality daylight and condition the space is possible. In this case old and inefficient mechanical systems can be either reduced in size and capacity or removed. Higher comfort and energy efficiency can be achieved by decentralizing the energy supply systems, distribution losses are eliminated and occupancy based control could result in lower energy consumption.
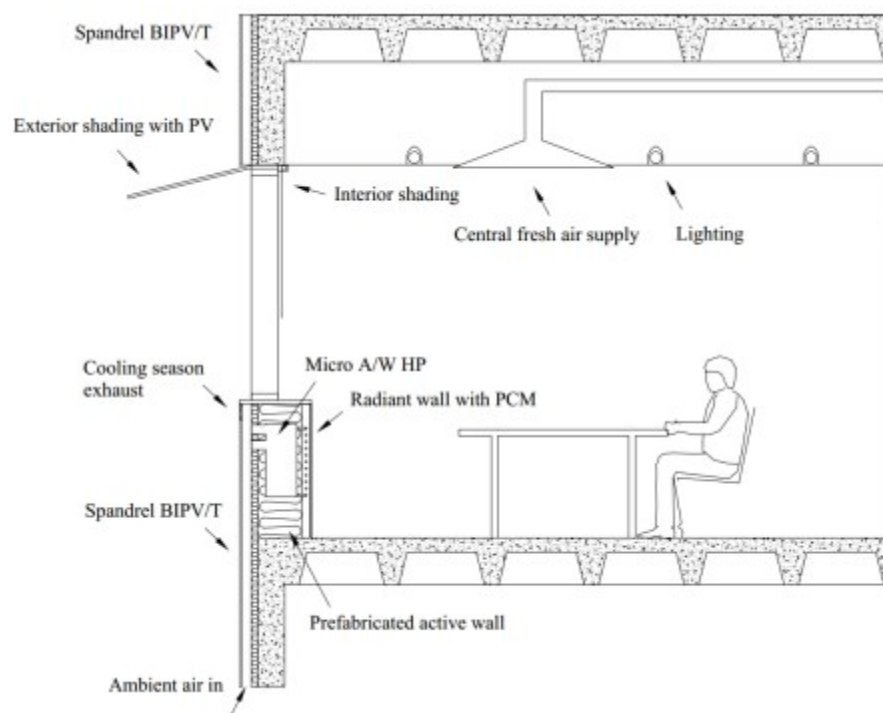
Figure 1.3: A cross section of a perimeter zone with a decentralized solar assisted system with integrated short term thermal storage for a commercial building façade retrofit (studied further in this thesis).

A concept of a solar façade with decentralized solar assisted system is presented in Figure 1.3. Currently there is a lack of design tools and insufficient research and development activities on these systems. There are only few commercial or prototype phase products. Issues are numerous, related to either architectural limitations to lack of sufficient data on their performance, economy and durability.

One of the challenges is the lack of design tools for integrated systems. The quasi-steady state models used to simulate façade integrated BIPV/T systems thermally coupled with building model in TRNSYS Type56 are not representing the true potential of these systems due to lack of mathematical models of new improved designs. One of them is the multiple inlet BIPV/T with STPV panels (Yang, 2015) studied at Concordia University. Also, transient effects of thermally massive façade systems are not included in the BIPV/T model, which eliminates the potential to study various innovative operation modes, like cycling of the PV/T and some storage systems to increase the system performance.

Concerning small scale heat pump models, the performance map based heat pump models do not take into account the cycling and defrosting losses of the heat pump. Plus, promising configurations, like exhaust air heat pump working in various configurations with up- or downstream to HRV or BIPV/T, cannot be easily simulated, if these maps are not provided by the manufacturers. Also, air enthalpy downstream from either heat pump condenser or evaporator is usually not provided. New models are needed, in order to facilitate innovative designs of heat pumps, especially for façade integrated applications.

Simulation of low temperature heating and high temperature cooling systems can be simulated with most commercial thermal building models. However, systems with innovative configurations, like capillary pipes embedded in encapsulated or panelized PCM with gypsum plaster cannot be simulated with tools like TRNSYS, due to the linear conduction transfer method used for solving the

heat transfer in the wall phenomena, which uses constant wall parameters, to estimate the transfer function coefficients. Modeling of these systems requires expert knowledge of the design parameters.

Finally, the system design configurations, sizing and performance dependence from the mentioned components physical parameters and system operation is crucial, but unfortunately no focused and extensive studies exist, yet.

Concerning BIPV applications in envelope retrofit studies, there is a lack of systematic studies that evaluate the techno-economic potential of these technologies, including the various options such as BIPV/T and STPV. A methodology to systematically evaluate these technologies in a holistic way alongside traditional envelope insulation techniques needs to be developed.

1.3   **Thesis scope**

This thesis provides a systematic study of solar façade design and a decentralized system potential in façade retrofit cases:

- Experimental work of an innovative multiple inlet BIPV/T solar-air collector prototype design, construction, testing and performance characterization;
- Numerical model development and parametric study. Optimal design analysis and potential for future development investigations;
- BIPV/EPoG design methodology development;
- A case study building model development and a complete holistic study of a retrofit for several Canadian climates and conventional and solar façade design options investigated. Retrofit methodology presented and the most promising cases identified for several Canadian climatic regions;

- A decentralized BIPV/T assisted heat pump with PCM radiant panels integrated in façade system design and numerical model development. The system numerical model integration into a Matlab/Simulink based toolbox CARNOT (2017) for solar system studies. The introduced model can be used for future design and control optimization studies.

1.4   Thesis overview

This thesis follows the manuscript-based format. Chapter 2 provides a literature and technology overview of BIPV and BIPV/T collectors and systems. Performance of different BIPV/T designs is discussed. A review on decentralized and solar-assisted façade-integrated technologies is also presented. Chapter 3 presents an experimental procedure for the characterization of an air-based multiple inlet BIPV/T collectors. A BIPV/T prototype design and experimental study is performed. Several design parameters are identified and a parametric study is performed. A design methodology for BIPV/EPoG is presented. Chapter 4 presents a solar façade retrofit study for a case study building in several Canadian climates. Numerical models for spandrel-integrated BIPV, second skin façade with BIPV, STPV glazing and solar shading with BIPV are presented and a feasibility study methodology is presented to identify the most promising solar façade designs in a retrofit project from techno-economical point of view. A shading factor for façade integrated BIPV in north latitudes is proposed. Chapter 5 is dedicated for a numerical model development of a retrofit system for a façade retrofit. The system consists of a spandrel-integrated air-based BIPV/T collector assisting a small-scale façade integrated air-to-water heat pump that delivers the heat to the office space through a radiant panel with PCM. The model is developed and introduced into a Matlab-based toolbox CARNOT (2017) for building integrated solar system studies. Finally, Chapter 6 summarizes the main contributions of this thesis and research needs.

2   Literature review

In this chapter a review on related physics, modeling techniques and system behavior in the scientific literature and design guides on the PV technologies, BIPV and BIPV/T concepts is presented. Also a review on solar façade types and their behavior is provided. Finally, a review section is dedicated on major products and research projects on solar-assisted façade-integrated decentralized HVAC systems.

2.1   **Façade state of art**

Before discussing the integrated façade concept, typologies of post-war facades are explained with a focus on office buildings.

The development of the western office building façade in the North America and Europe can be divided into 4 phases: the post-war massive facades in reinforced concrete structure (1945-1965), reinforced concrete with perforated façade (1960-1980), skeleton construction with precast concrete (1975-1990) and skeleton construction with curtain wall façade (1975-2010s) (Fraunhofer ISE, 2012).

The perception on building design has changed since the 1980's due to peoples' awareness of their natural environment, making stricter demands on thermal insulation and energy saving. Both minimal legal requirements for building energy consumption and improvements in façade technologies are constantly increasing.

2.1.1   *Glazing unit development*

Improvements in glass industry has resulted in development of glazing units with u-values as low as 0.5 W/m^2-K with vacuum glass. Figure 2.1 shows the thermal conductance for different types of glass. The widest acceptance for double pane insulated glass is with low-e coating and air or argon.

Double-glazed low-e argon windows have become the new standard in Europe and North America. Recently, similar triple glazed windows with two low-e coatings and two argon filled cavities have been introduced, increasing the thermal performance significantly.

Triple pane glasses with argon or krypton achieve high thermal performance, but issues related to bulkiness of the IGU and price reduces its wide spread use so far. The overall optimization of glazing system design must take into account also the glazing performance in visible light spectrum and shading strategies to reach the optimal performance of the façade system.
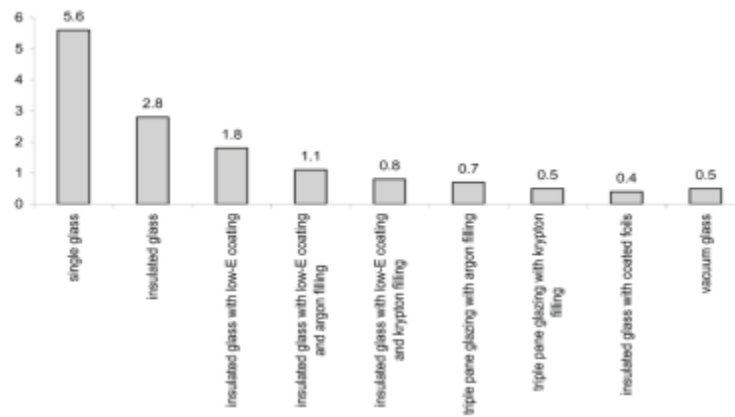
Figure 2.1: U-values (W/m²-K) of different types of glass (Ebbert, 2010).

2.1.2   Double façade

The need to reduce the heating demand in office buildings with high glazing area, for better daylight performance, led to the development of a double façade concept in the early 1903 in the Steiff factory building in Giengen/Brenz (Germany) (Ebbert, 2010). Due to the developments in glass industry, with IGU's having u-value as low as 0.5 W/m²-K, the office building did not suffer from extensive heat loss anymore, but tended to overheat from solar and internal gains all year round in milder climates. This caused severe needs for air-conditioning and fueled the call for a reduced portion of transparent building parts and use of passive cooling methods, like natural ventilation

and solar shading. But the desire to build all-glazed buildings and legal obligations to reduce the building energy demand resulted in the need to find new strategies to deal with high cooling loads.

The new double facades are equipped with a layer on the inside position and an additional exterior layer, and depending from the design either inside or outside layer can be insulated. The cavity provides a buffer zone and space for sun-protection devices. The additional glass layer gives noise protection in case the windows shall be opened by users. The classification of double facades depends on the way the cavity is formed (box window, multistory façade, corridor façade, shaft-box façade), from type of ventilation (natural, mechanical or hybrid), depending from the air flow path (exhaust air, supply air, reversible air flow, outdoor air curtain or indoor air curtain). The second layer can be installed over an opaque façade section or transparent façade section. A possibility exists to integrate the double façade with photovoltaic modules and generate electricity or act as a sort of air collector to pre-heat the ventilation air during the heating season for some double facade typologies (ECBCS, 2009; Fallahi, 2009).

The major advantages of double facades are a good protection against exterior noise source and against wind loads, which allows opening windows in high rise buildings. For the natural night cooling by opening windows and purging the building with fresh air, the additional glass provides protection against burglary. In terms of building installations, the protected cavity offers space to place standard or advanced sun protection systems. The disadvantages are potential overheating problems in summer, opening windows causing operation discontinuity for central air handling system due to mass flow rate differences, the incoming air in summer may be hotter than the outside air temperature and in winter the warm air may condensate on the outer glass pane. That is why a double façade design has to be developed in combination with the whole building concept and with respect to the surrounding climate conditions, which result in custom solutions for each building and naturally higher construction costs (up to 2.5 times). In recent projects, double facades

are not a preferred option anymore and instead the additional layer is only placed in those zones where necessary, for example to protect operable solar blinds or on the side of a building that are exposed to wind and noise (Ebbert, 2010; Knaack et al., 2007).

Double facades can be feasible option for refurbishment of office buildings. An existing façade can be improved by adding an exterior layer. Thus, the original façade may be allowed to stay in place. New building services can be installed in the façade cavity, which makes it possible to technically update the building without interfering with the interior (Ebbert, 2010).

2.1.3   Façade integrated with HVAC systems

In order to reach an optimal performance of a building, the façade has to be planned in combination with the ventilation concept and the technical building services. Since 1990s the concept of placing the most of the building services in the façade zone occurs. The major problem of such de-centralized concepts always used to be the control and maintenance of the enormous number of components. Only with progress in information technology and facility-management software these HVAC-components became practice. Several examples of existing systems include Post Tower, Bonn (Germany) (Compagno, 2002; Ebbert, 2010), TEmotion by Hydro building systems (Hovels, 2007) and the "Capricorn Façade" by Gatermann und Schossig (Ebbert, 2010) and will be discussed later.

The integration of de-centralized service/HVAC components into the façade provides many advantages in comparison to central air-conditioning systems. Energy savings can be achieved, since there is no need to distribute large quantities of air through a building. De-centralized systems condition the air directly at the palace where it is needed, hence, warm or chilled water is transported through the building instead of air, which occupies less space and needs less service energy, since the water has higher heat capacity. It is also potentially easier to provide individual comfort control for every office space and the need for air distribution ducting that takes a lot of

space is reduced or eliminated. Elimination of plenums with no suspended ceiling allows using concrete ceilings for heat storage or precooling.

Some issues are very large number of maintenance points, which needs a well administered facility management system (that can be addressed with BMS-installations and adequate software), maintenance costs for such installations are similar to that of centralized building services. Also disadvantages due to limited access for maintenance, limited mass flow rates since noise and draughts occur, space planning influences the performance of the system, air humidification and dehumidification is complex, wind effects and outdoor air temperature affects the performance of the system, air exhaust is complex and short-circuits are possible. Also a major issue is the unclear responsibility of different parties, which can be solved by co-operation of specialist companies. Another challenge is the acceptance of such facades by planners, designers and clients. Well developed products, like mentioned above have not been used often, as many stakeholders found them too restrictive, which leads to a need for a more open system and modular concept. Nevertheless, the idea to combine facades and building services is very promising for refurbishment. Placing new installations in the façade layer allows a building process almost fully independent from the interior. Also such retrofits can be done in a manner that complements the main HVAC system (i.e. does not completely replace it, emphasizing utilization of solar energy and avoid enlarging it).

2.2   Façade integrated photovoltaic/thermal solar systems

In this section a detailed literature review is carried out on façade integrated air-based photovoltaic thermal systems, related technical aspects and numerical modeling.

2.2.1 Photovoltaic cells

Photovoltaic (PV) products exist for several decades now and the most common technology – silicon PV cells – are a mature and cost competitive technology in the energy technology sector. The rising popularity is attributed to the falling PV module prices, governmental subsidies and already achieved grid parity in some countries. Other factors are increased awareness of the environmental problems, due to climate change, pollution and waste production by humans and energy efficiency interest in built environment as a result (IRENA, 2012). This led to interest in PV technology research and development, some focusing on building integrated photovoltaic technologies. Now photovoltaic technology is emerging as energy generating device and also as a building envelope component, like exterior cladding, shading devices, glazing.

There are two main ways of integrating PV modules to a building: BAPV (building-attached photovoltaics) or BIPV (building-integrated photovoltaics). BAPV are commonly used for existing buildings, since the PV modules are mounted on existing building structures on the building envelope. Visually the system can be appealing, but no savings in substituted building elements are achieved. BIPV uses the PV panel as an architectural function. The traditional envelope elements are substituted with PV materials and additional installation cost savings are possible due to reduction in used materials for the envelope construction. The most common integration techniques are:

- Over-cladding (cold roof or façade);
- Enclosure (hot roof or façade);
- Shading devices.

Silicon cells are semiconductor based devices, whose electrical conductivity decreases with increasing temperature as the band gap of the semi-conductor cell is decreasing. The decrease in the band gap of a semiconductor with increasing temperature can be viewed as an increase in

energy of the electrons in the material. Lower energy is therefore needed to break the bond. In the bond model of a semiconductor band gap, reduction in the bond energy also reduces the band gap. Therefore increasing the temperature reduces the band gap. In a solar cell, the parameter most affected by the increase in temperature is the open-circuit voltage and is seen in Figure 2.2 (The German Energy Society, 2008). Reduced open-circuit voltage means reduced power output of the PV cell as seen in the equations below. A badly ventilated PV façade can result in efficiency decrease of the PV cell, which is the power generated by the PV cell over solar energy input on cell area. Temperatures above the recommended operating limits by the module producers are to be avoided due to durability issues of the modules, since operation of the photovoltaic modules outside of the recommended cell temperature range results in accelerated degradation of the PV modules (The German Energy Society, 2008). The temperature coefficients depend on the PV cell type and module construction: about 0.45%/K for crystalline silicon, 0.35%/K for CIS, 0.25%/K for CdTe and 0.2%/K for a-Si (Zondag, 2008).
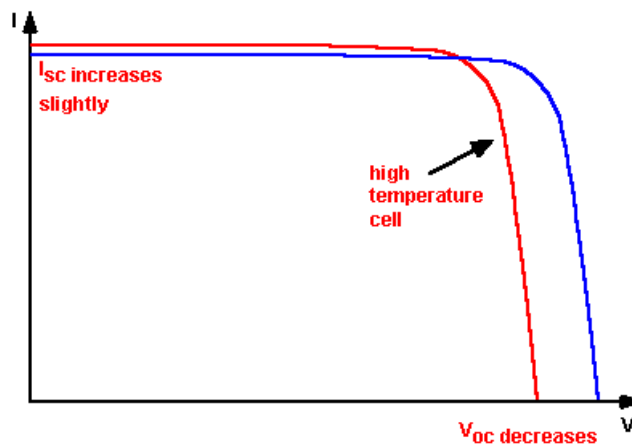
Figure 2.2: Characteristic I-V curve of a PV cell. I is the current in amperes and V is the voltage in volts (The German Energy Society, 2008).

Electric power (P_{max}) in watts (W) is calculated using equation 2.1, which shows the dependence of P_{max} from open circuit voltage (V_{oc}), short circuit current (I_{sc}) and fill factor (FF). Efficiency of solar

energy (P_{in}) conversion into electricity (η) using PV is calculated with equation 2.2 (The German Energy Society, 2008).

$$P_{max} = V_{oc}I_{sc}FF \tag{2.1}$$

$$\eta = \frac{V_{oc}I_{sc}FF}{P_{in}} \tag{2.2}$$

In order to model a PV array numerically, the following data supplied by the manufacturer are used: open circuit voltage, short circuit voltage, maximum power point voltage/current, temperature and radiation modifiers at defined standard testing conditions need to be used. Basic standard testing conditions (STC) are defined by IEC 61215 (IEC, 2006) of irradiance 1000 W/m^2, spectrum AM 1.5 and PV cell temperature of 25°C. Power output modifiers for low irradiation conditions and temperature coefficients for power, voltage and current are supplied by module manufacturers and characterization methods are described in the same standard (IEC, 2006).

Solar radiation is transmitted to the surface of the PV layer through the glass cover. A portion of this flux will be converted to electrical energy:

$$\alpha_i = \alpha_i' + q_e \tag{2.3}$$

where α_i is the irradiation input of the PV layer, α'_i is the solar radiation absorbed by the PV layer that is converted to heat and q_e is the electrical power output. Several models exist to calculate the q_e, such as one by (Buresch, 1983):

$$q_e = n.c.p[V.I_d\left(exp\left(\frac{e.V}{\sigma.d.\text{T}}\right) - 1\right) - V.I_L] \tag{2.4}$$

where T is the temperature (K) of the PV material, V the voltage at maximum power point, I_d the diode current, I_L the light generated current, d the diode factor, n the number of series connected cells, c the number of parallel connected cells, p the number of surface panels, e the electron charge (1.6 x 10^{-19} Coulombs) and σ the Stefan-Boltzman constant (1.38 x 10^{-23} W/m^{2}K^4).

The diode factor and current are given by:

$$d = \frac{e(V - V_{oc})}{n.\alpha.\text{T}_{stc}\log(\frac{I_{sc} - I_{mp}}{I_{sc}})} \qquad\qquad 2.5$$

$$I_d = \frac{I_{sc}2^{\frac{\theta - \theta_{ref}}{\lambda}}}{c.exp(\frac{e.V_{oc}}{n.k.d.T_{stc}} - 1)} \qquad\qquad 2.6$$

and the light generated current by:

$$I_L = \frac{\alpha' I_{sc}}{c.\alpha'_{stc}} \qquad\qquad 2.7$$

where λ is an empirical factor and T$_{stc,}$ V_{oc}, I_{sc}, I_{mp} and α_{stc}, are temperature, open circuit voltage, short circuit current, maximum power point current and cell insolation under STC. These are the parameters that need to be measured in a laboratory test.

2.2.2   *Air-based photovoltaic/thermal solar collectors*

A photovoltaic/thermal air-based collector is a combination of both solar air heater (SAH) and a photovoltaic cell (PV) together in one system. The PV cells usually are acting as solar radiation absorbers and the heating fluid (air) is removing the heat through forced convection phenomena. The relationships of heating and electrical power from mass flow rate at standard testing conditions are shown in Figure 2.3.
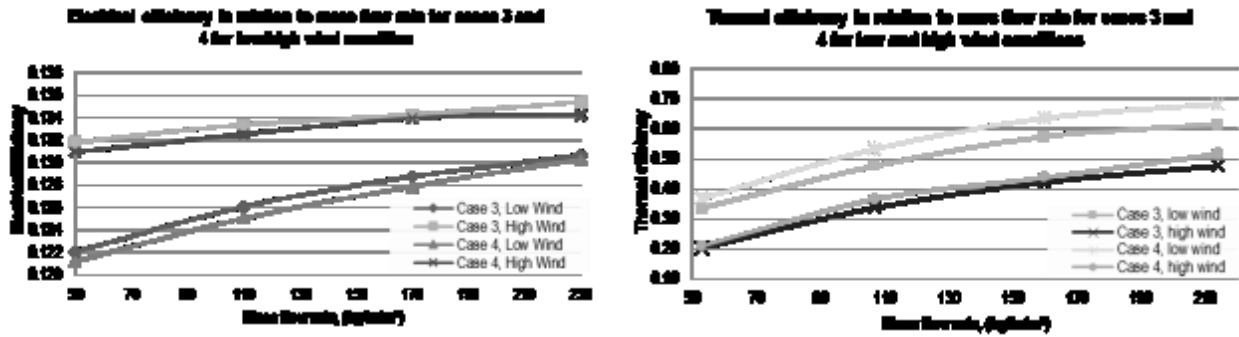
Figure 2.3: Thermal and electrical efficiency (in percentage) dependence form mass flow rate and exterior wind conditions at standard air based PV/T collector test bed (Bigaila et al., 2015).

Different air based collector design options are shown in Figure 2.4. A1 to A3 and B1 to B3 are glazed collectors. The light blue plane represents the transparent cover, the dark blue plane the absorber and the beige block represents insulation. Variants A4 and B4 are described as un-glazed. Variants B1 to B4 are part of a closed loop air heating system, thereby potentially reaching higher outlet temperatures. The variants A1 and A4 are heating ambient air in a single path through. Variant A2 and A3 could be used in both flow patterns. The blue arrow symbolizes the cold inlet air flux and the red is representing the hot air flux. From this arrows one can see, that some variants are from the point of view of the absorber, under flown (B2, B4), over flown (B1) or passed through (A1 to A4) (Kramer, 2011).
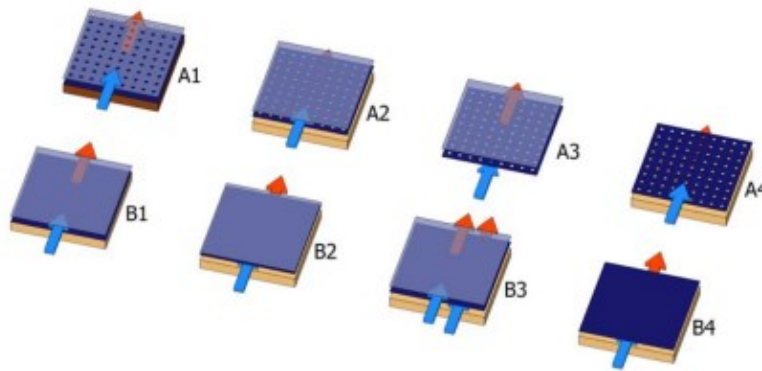
Figure 2.4: SAHC variants (Kramer, 2011).

In PV/T air collector case, the PV cells are acting as the solar absorber mainly. The other case is when the PV cells are laminated on a transparent sheet, forming an STPV, which allows a certain amount of solar radiation to be transmitted through the PV module and have been shown to be at least 5% more efficient if compared to opaque PV module systems (Yang, 2015). Comparison of different PV/T air based collector types was done by Hegazy (2000), who compared the performances of four most common PV/T concepts, shown in Figure 2.5. In the four designs, the air flow passage is located above the absorber (model 1), below the absorber (model 2), on both sides of the absorber (model 3) and a double pass mode for both sides (mode 4). The study was carried out numerically and solutions indicate that the electrical and thermal outputs for models 2 to 4 are similar and superior to that of model 1. The pumping power needed is lower for model 3 and second lowest for model 4.
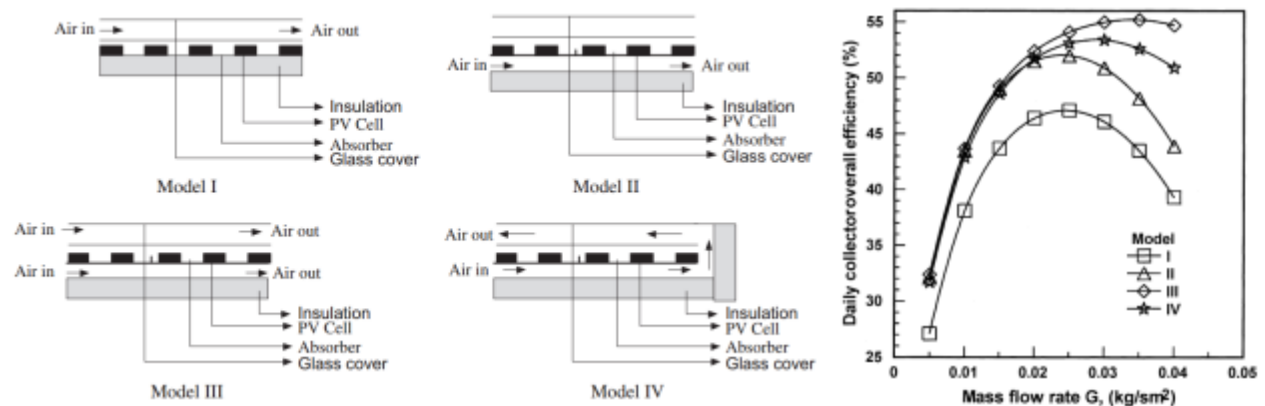
Figure 2.5: PV/T designs studied by Hegazy (2000).

A comparative experimental and numerical study was carried out by Tonui and Tripangnostopoulos (2007) on low cost improvements of PV/T performance using configurations including fins, glazing cover and with PV module as the first layer, acting as the absorber. Design schemes are shown in Figure 2.6. It was concluded that the finned PV/T has the highest thermal efficiency. The configuration with suspended metallic plate was second best and the case where PV is the exterior solar absorber was the third. The glass cover increased the thermal efficiency

significantly and all the thermal results can be seen in the Figure 2.6. The decrease of electrical efficiency due to the glazing is from 0.127 to 0.117 with reference cell temperature 25°C, while the efficiency modifier is 0.006°C^{-1}. The authors of this study also correlated the channel depth to T_{PV} and T_w for all the cases, which showed nearly 10°C increase from 0.1 to 0.5 m channel depth, but a 5°C decrease in T_{out}. The pumping power was practically the same between collector configurations, but dropped from 0.1 to 0.01 W with the channel depth from 0.05 to 0.2 m.

PV/T type	Experimental
PVT/AIR–REF	$\eta_{th} = 0.247 - 7.31\Delta T/G$
PVT/AIR–TMS	$\eta_{th} = 0.280 - 7.14\Delta T/G$
PVT/AIR–FIN	$\eta_{th} = 0.297 - 6.14\Delta T/G$
PVT/AIR–REF + GL	$\eta_{th} = 0.364 - 4.79\Delta T/G$
PVT/AIR–TMS + GL	$\eta_{th} = 0.399 - 4.93\Delta T/G$
PVT/AIR–FIN + GL	$\eta_{th} = 0.504 - 6.44\Delta T/G$
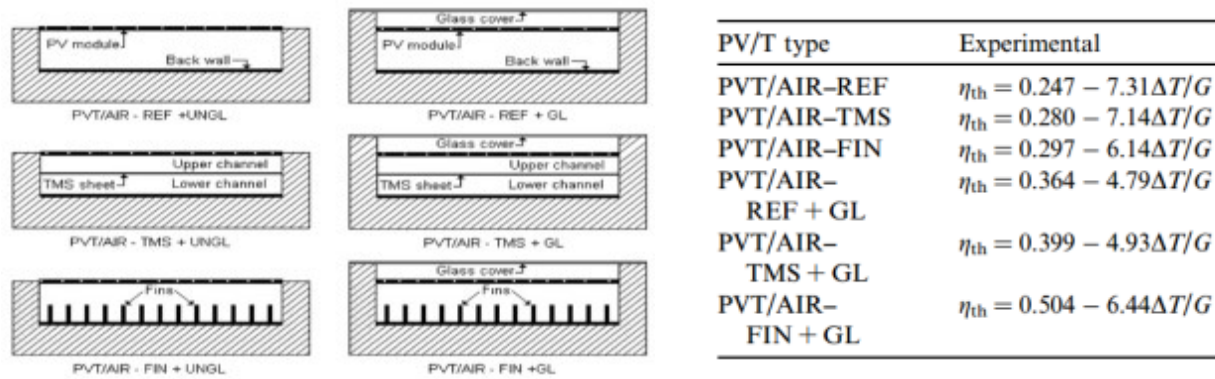
Figure 2.6: Tonui and Tripangnostopoulos cases and thermal efficiencies (2007).

Yang (2015), Bigaila et al. (2015) and Rounis et al. (2015) carried out numerical and experimental work on a multiple inlet air based PV/T collector concept. The concept utilizes several air entrance slots along the air channel, which provide higher convective heat transfer coefficients due to entrance effects. This results in more heat removed from the PV panels and higher PV and solar thermal air collector energy outputs. Experimentally Yang showed that by using the 2-inlet BIPV/T system, the thermal efficiency is increased by 5%. Although the electrical efficiency increase is marginal, it can be seen that the peak PV temperature in the 2-inlet system is lower than that in the 1-inlet system, which means that PV degradation with high temperature is reduced in the 2-inlet system and by extension in a multi inlet system. She also compared systems with 1 vs. 2 inlets and opaque and semitransparent PV module configurations. The conclusion was that the thermal performance of a BIPV/T system can be significantly improved by using semi-transparent

crystalline silicon PV modules to replace opaque ones due to the absorption of some solar radiation at the bottom surface in the BIPV/T system cavity.

2.2.2.1 *BIPV collector energy balance*

In a BIPV/T system the photovoltaic modules absorb the fraction of incident radiation that falls in the spectrum region for which the photovoltaic effect occurs and electricity is generated. The fraction that is converted into electricity is in the range of 8-19% for commercially available modules. The fraction of solar radiation that is absorbed by the photovoltaic cell depends from photovoltaic module optical properties and incidence angle of the sun. The rest of the solar irradiation is either reflected which is in the order of 5-8% or converted into heat to the exterior of the building and to the back of the PV panel through convective and longwave radiation heat transfer. Radiation heat transfer between the PV cell and the sky and between the PV cell and the back surface can be modeled using Stefan-Boltzman equation. The exterior convective heat transfer depends from wind effects on the PV panel and the interior heat transfer depends from circulating air in the channel. The radiative heat transfer portion is the remaining amount of energy transferred to the sky or surfaces in the PV/T channel. The energy balance and existing heat exchanges are shown in the Figure 2.7.
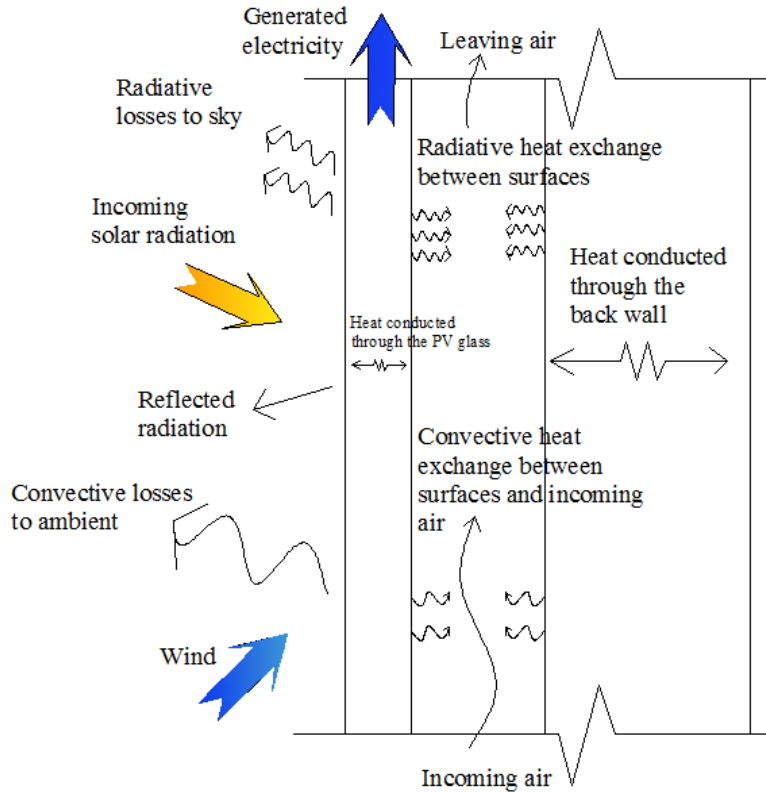
Figure 2.7: Energy transfer modes in a PV/T air collector system.

The heat balance equations can be solved for all BIPV/T area with simple lumped parameter models or discretized into smaller control volumes for more accurate results with higher resolution. The energy balance in the PV module is expressed by equation 2.8.

$$\alpha.\,G.\,A_{pv} = E_{pv} + Q_1 + Q_{ra} + Q_c + Q_r \qquad\qquad 2.8$$

where αGA_{pv} is the solar radiation absorbed by the PV module, E_{pv} is the electricity generated by PV modules, Q_l is the exterior convective loss, Q_{rs} is the exterior radiative thermal loss to the sky, Q_c is the heat removed by heat transfer fluid in the channel, in this case air, and Q_r is the radiative heat exchange between PV and the back plate surface.

The air temperature in the control volume is estimated by an exponential air temperature variation, which is the exact solution if the temperatures of the surrounding surfaces are assumed to be uniform and the average air temperature for energy balances is estimated by equation 2.9.

$$T_{av} = \int T dx / \Delta x \qquad\qquad 2.9$$

where T_{av} is the average control volume bulk air temperature.

The radiative heat transfer coefficient is estimated by equation 2.10. View factors are taken into account in the cases when the geometry of the air gap is more complex, but majority of the models initial assumption for the view factor is 1 (Yang, 2015; Candanedo, 2010).

$$h_r = \frac{\sigma F_{bpv,insu}(T_{insu}^4 - T_{bpv}^4)}{\frac{1}{\varepsilon_2} + \frac{1}{\varepsilon_3} - 1} \qquad\qquad 2.10$$

where σ is the Stephan-Boltzman constant 5.670×10^{-8} Wm^{-2}K^{-4}, F_{bpv} the view factor between plates, T_{insu} and T_{bpv} the surface temperatures, ε are emissivities of the surfaces facing each other.

The interior convective heat transfer correlations are specific for each air collector type and geometry due to heating asymmetry, non-developed flow conditions and framing effects on flow type. The Nusselt number correlations developed for pipes and ducts with uniform boundary conditions are applied by some researchers and in some modeling tools, but in most of the cases this results in not correct PV/T output simulations, since these tend to underestimate the convective heat transfer, due to framing and structure imperfections acting as turbulence promoters and inlet effects due to developing flow conditions, where turbulence is more intensive (Candanedo, 2010). That is why new air collector designs require case specific expression for Nusselt number estimation. This can be done with laboratory measurements.

Electrical efficiency model can be either based on the electrical model described by equation 3 or a simple linear model taking into account PV module efficiency variations due to temperature effect adopted from (Duffie and Beckman, 2006), shown in equation 2.11.

$$\eta_{PV} = \eta_{mpp}T_{PV,ref} - \gamma_{mpp,ref}(T_{PV} - T_{PV,ref}) \qquad\qquad 2.11$$

where η_{PV} is the efficiency of PV module, η_{PV} the efficiency at reference temperature, $T_{PV,ref}$ is PV module reference temperature, $\gamma_{mpp,ref}$ is efficiency modifier from temperature, T_{PV} is the PV module temperature.

Changing transmittance, reflectance and absorptance in PV system modeling as a function of solar incidence angle is considered by some researchers (Candanedo et al., 2010; Duffie and Beckman, 2006):

$$G = \tau\alpha_b(\theta)(\tau\alpha)_n I_T \qquad\qquad 2.12$$

where $\tau\alpha_b(\theta)$ is the incidence angle modifier for transmitted and absorbed solar radiation by PV module glass, $(\tau\alpha)_n$ the transmittance and absorptance of PV module glass and I_T is the solar radiation incident.

Pressure drop in the BIPV/T system is a function of the geometric configuration of the channel, like framing system, wall roughness, etc. The pressure drop is usually much smaller than the one in the ducts, but on the other hand in depends from the cavity design. The air pressure drop is a function of friction factors and mass flow rates in the BIPV/T system.

The thermal efficiency is determined by the ratio of available power per square meter of collector surface and irradiance:

$$\eta = \frac{Q_c}{I_t A} \qquad\qquad 2.13$$

Most common modeling approach is a steady state approach not taking into account thermal capacitance of materials in the BIPV/T system. Transient models, using fully-explicit finite difference methods (Ito et al., 1999; Candanedo, 2010) are useful if STPV modules are used and back wall is absorbing majority of the solar radiation or a double pass configuration is used, creating a thermal lag in the system. In that case the transient models would be more suitable for system behavior studies, development of control algorithms for air flow rate.

The performance characterization of air-based photovoltaic/thermal solar collectors is not standardized yet. Guidelines for liquid non-concentrating PV/T solar collectors and solar air collectors are found in EN 12975-2 (2011) and EN ISO 9806:2014 (2014). Basic energy efficiency curves are determined by manufacturers for standard testing conditions, but for physical model development and usage in energy simulation tools, physical convective heat transfer correlations and efficiency modifiers must be determined separately (Bigaila et al., 2015; Delisle and Kummert, 2012).

2.2.3 Technical aspects of air-based façade-integrated BIPV/T solar collectors

2.2.3.1 Mixed forced and natural convection

In air collectors, the air is always transported through a channel. However, the thermal performance of air collectors is not as high as the performance of liquid collectors. This is due to two effects:

- Air has a thermal conductivity that is 24 times lower than for water. Since h = Nu x k/D this reduces the heat transfer. This leads to the fact that for air collectors, the channel height has a large influence on the thermal efficiency. (Note that the channel height has no effect on the Reynolds number, since the decrease in flow velocity is compensated by the increase in channel width as can be seen from Re = UD/n = ΦL/n, in which Φ is the specific flow rate and L the collector length).

- Air has a much lower heat capacity. Therefore, the flow rate in an air collector is necessarily much larger than in a liquid collector. Due to the fact that C_{pwater}/C_{pair} = 4.2 x 10^6/1.2 x 10^3 = 3.5 x 10^3, a conventional fluid flow rate of 50 l/m^2 /h for a liquid collector corresponds to an airflow of 175 m^3/m^2/h, which is too high to be feasible in practice. Therefore, in practice a flow rate is used that is typically in the order of 40 m^3/m^2/h.

These effects dictate obvious research focus for most research activities on air based solar collectors and PV/T collectors with focus on improving the heat transfer to the air by means of a range of techniques using fins, roughening techniques. The following table will have a condensed review on some research efforts in increasing the heat removal from absorber to air in air collector systems.

Forced convection of façade integrated systems in majority of installations is not very common. But the newer studies on BIPV/T, especially in Canada, study mainly forced BIPV/T systems, since the thermal output of BIPV/T system is integrated with HVAC of the building (Bambara et al., 2011; Bigaila et al., 2015; Candanedo, 2010; Chen, 2009; Yang, 2015).

Because of the critical heat transfer to the air, it is very important to model the heat transfer properly. First of all, one should be aware that for a sufficiently wide channel, the hydraulic diameter is twice the channel height. Next, for laminar flow, the entrance length is often substantial. Eicker (2003) presents an overview of entrance-effect heat transfer relations for air collectors, showing a variation of about 10% in average Nusselt number when integrated over the entrance length. For fully developed laminar flow she recommends to use the fixed Nusselt value of 5,4. For turbulent flow, she compares the Petukhov equation and the popular and simpler relation of Tan and Charters which she indicates to be both sufficiently accurate.

$$Nu = 0.0158Re^{0.8} + (0.00181Re + 2.92)exp(-0.03795L_c/d_h) \qquad \text{2-14}$$

where *Re* is the Reynolds number, L_c is the flow channel length and d_h is the hydraulic diameter of the channel.

Both correlation produce sufficiently exact values for the convective heat transfer coefficients.
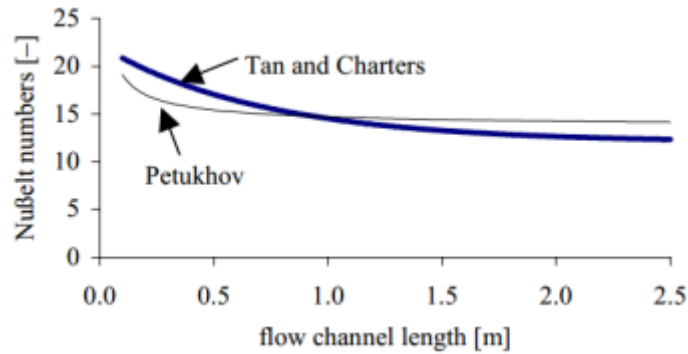
Figure 2.8: Nusselt correlations for forced convection (Eicker, 2003).

The Tan and Charters relation is also used by Hegazy (2000), Sopian and Othman (Zondag, 2008). Bazilian and Prasad (2002) makes a comparison of different heat transfer relations for turbulent flow (comparing equations by Cengel, Petukhov, Brinkworth and the Dittus-Boelter equation) and finds for his configuration a variation of about 25% in the resulting Nusselt number. He concludes that the difference significantly affects the results and that the Petukhov equation is in closest correlation with his experimental findings.

Infield performed a study on the Mataro library PV/T façade system. The existing system has 7900 m^3/h of ventilation air drawn mechanically, with the dimensions of the façade 6.5 x 36 x 0.14 m (H x W x D) resulting in flow velocities in the order of 0.5 m/s and thermal efficiencies of 30%. The low velocity results in high importance of natural convection and the mixed convection is calculated with the equations 2.15-2.17. As reported, the original air filters were the reason for large flow resistance and were replaced and also it was found that the effect of the wind has a substantial importance and for easterly wind the cavity air was even forced in the downward direction (Zondag, 2008).

$$Re_{free} = \sqrt{Gr/2.5} \quad Nu_{lam} = 0.664 Re^{0.5} Pr^{0.33} \hspace{4cm} 2.15$$

$\text{Re}_{\text{forced}} = \text{UL}/\text{v} \quad \text{Nu}_{\text{turb}} = 0.037\text{Re}^{0.8}\text{Pr}/(1 + 2.443\text{Re}^{-0.1}(\text{Pr}^{0.67} - 1))$
<div align="right">2.16</div>

$\text{Re} = \sqrt{\text{Re}_{\text{free}}^2 + \text{Re}_{\text{forced}}^2} \quad \text{Nu}_{\text{turb}} = 0.037\text{Re}^{0.8}\text{Pr}/(1 + 2.443\text{Re}^{-0.1}(\text{Pr}^{0.67} - 1))$
<div align="right">2.17</div>

Candanedo (2010) did a study on convective heat transfer coefficient determination for a ventilated roof with integrated PV cells. He developed Nusselt number correlations for smooth and ribbed BIPV/T framing configurations for laminar and turbulent flow regimes, determined the thermal development lengths for laminar and turbulent flow in smooth and ribbed BIPV/T systems. Natural convection effects on Nusselt number have been studied as well, in terms of Grashof and Rayleigh numbers for the smooth BIPV/T system. He found that most of the data falls in the mixed convection region established by the Metais and Eckert map (Metais and Eckert, 1964). All the experimental data is above the limits of Grashof numbers established by the Petukhov correlations for vertical and horizontal pipes that established the limit where the deviation from Nusselt number from the forced convection value would be higher than 1%. It was found that in the laminar region (for the smooth case) the effective Nusselt number can be approximated by the addition of the forced and natural convection components. For the turbulent region, the best approximation can be taken by assigning the power n to 0.638. The Nusselt number distributions for the development length, x, has been calculated for the top surface for the whole length of the BIPV/T system (39Dh). They are expressed with the equations 2.18-2.19.

For laminar region, $250 \leq \text{Re} \leq 2400$

$$Nu_{top}(x) = 0.039Re^{0.78}Pr^{0.4}e^{-\frac{x}{20Dh}} + 0.034Re^{0.78}Pr^{0.4}$$
<div align="right">2.18</div>

For turbulent region, $2400 < \text{Re} \leq 7100$

$$Nu_{top}(x) = 0.012Re^{0.78}Pr^{0.4}e^{-\frac{x}{9.09Dh}} + 0.049Re^{0.78}Pr^{0.4}$$
<div align="right">2.19</div>

The equation 2.18 gives on average Nusselt 2.6 times higher than the equation given by Dittus-Boelter, which is developed for smooth pipes. The fully developed solution for the laminar flow (Re<2300) by Hallman as recommended by Candanedo:

$$\frac{x}{D_h} > 0.0425 RePr \qquad \text{2.20}$$

For the turbulent region, the development length is shorter and it can be estimated, as recommended by Candanedo, by:

$$\frac{x}{D_h} \approx 4.4 Re^{1/6} \qquad \text{2.21}$$

Yang (2015) developed Nusselt number correlations for frameless multiple inlet BIPV/T air collector, created a lumped parameter mathematical model a validated it experimentally. Her setup consisted of two 0.5 m² each PV panels assembled in a way so the air could be collected from both bottom PV panel and the air gap between the PV panels. This method proved to increase the thermal efficiency by 5% if compared to one inlet, since the developing boundary layer is broken and new air stream introduced in the channel removes more heat from PV cells due to larger temperature difference. She developed Nusselt number correlations in the case of one inlet system for bottom and top plates for turbulent region:

$$Nu_{top}(x) = 8.188 Re^{0.77} Pr^{3.85} e^{-\frac{x^{0.2}}{2.8 D_h}} + 0.061 Re^{0.77} Pr^{3.85} \; 2300 < Re < 9500 \qquad \text{2.22}$$

$$Nu_{bot}(x) = 4.02 Re^{1.09} Pr^{19.3} e^{-\frac{x^{0.2}}{14 D_h}} + 0.005 Re^{1.09} Pr^{19.3} \; 2300 < Re < 9500 \qquad \text{2.23}$$

And for the laminar region:

$$Nu_{top}(x) = 0.6883 Re^{0.7} Pr^{0.8} e^{-\frac{x^{0.2}}{6.45 D_h}} + 0.0124 Re^{0.7} Pr^{0.8} \; 1190 < Re < 2300 \qquad \text{2.24}$$

$$Nu_{bot}(x) = 50 Re^{0.5} Pr^{0.2} e^{-\frac{x^{0.2}}{1.37 D_h}} + 0.428 Re^{0.5} Pr^{0.2} \; 1190 < Re < 2300 \qquad \text{2.25}$$

2.2.3.2   Inlet effects

Inlet effects can significantly affect the performance of an air-based solar system. Direct numerical simulations on the detailed fluid flow have been carried out by Bazilian and Prasad (2002), investigating the effect of the PV frame edges on the airflow, which he found to cause recirculation areas. He found that the size of these recirculation zones could be reduced by means of airfoils attached to the frame. Gandini (Zondag, 2008) carried out a direct numerical study on the airflow distribution within a facade, where he found strong localized turbulence due to the inlet and an inhomogeneous heat transfer.

As reported by Charron (2004) and Brinkorth (2000) the inlet and outlet regions are factors that can affect the overall efficiency of the ventilated façade due to flow disturbances in the localized zones. The shape, roughness and design of the inlet/outlet (height of the inlet/outlet relative to the gap width, aspect ratio, size, distribution, etc.) are very important and the overall effect of this parameter was negligible for small gaps widths, but could have a significant impact when cavity was wider than 0.6 m.

2.2.3.3   Air leakage

Air leakage is often ignored in the ventilated façade modeling. Saelens (2002) did an extensive review of experimental and theoretical work, mentions of the importance of considering air leakage in a model. Leakage can alter the flow velocity and the total energy balance.

Welz et al. (2014) developed a model taking into account pressure drop, leakage and inlet mass flow to find the optimal mass flow rate for air collector system optimizing for fan consumption taking into account the mentioned physical phenomena. Mass flow rates and pressure drop models have been developed and if combined with appropriate thermal inlet models, the inlet and outlet effects could be modeled.

2.2.3.4 Exterior convection and wind effects on mass flow

Wind has the largest effect on the exterior convective film coefficient. Several correlations exist in the literature for calculating the convective part of it. These include the correlations by Test (1981) (equation 2.26), Sharples and Charlesworth (1998) (equation 2.27) and McAdams (1954) (equation 2.28) (Duffie and Beckman, 2006) as a function of the wind speed in m/s. Candanedo (2010) evaluated all correlations for the BIPV/T roof of the EcoTerra Solar house. The results are shown in Figure 2.9 and as can be seen the Sharples and Charlesworth correlation gives the closest results to measured top of the BIPV/T channel temperature.

$$h_o = 8.55 + 2.56 V_{wind} \qquad\qquad 2.26$$

$$h_o = 11.9 + 2.2 V_{wind} \qquad\qquad 2.27$$

$$h_o = 5.7 + 3.8 V_{wind} \qquad\qquad 2.28$$
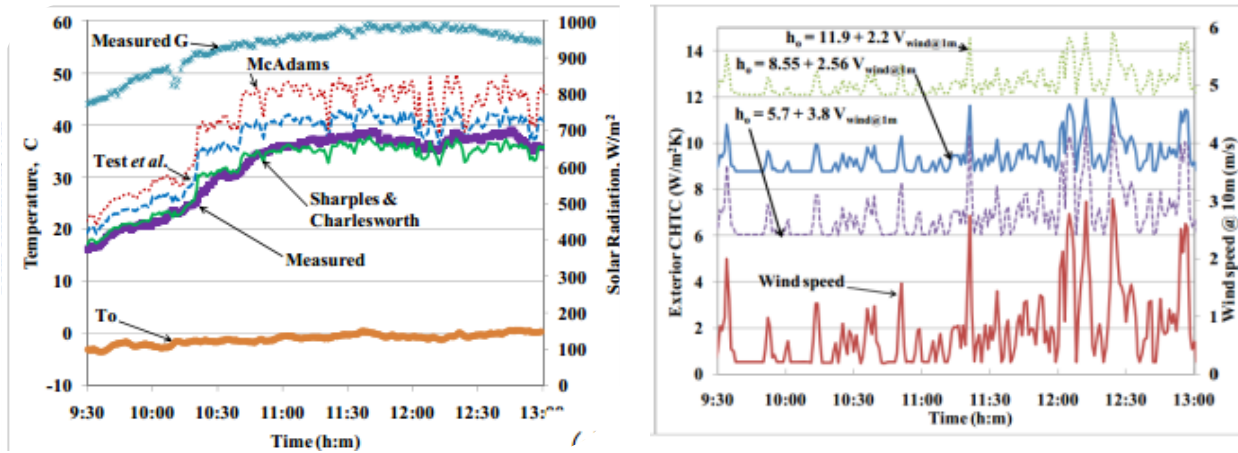
Figure 2.9: Exterior convective heat transfer coefficient dependence from wind (Candanedo, 2010).

Wind effect on performance of different solar collector types is shown in the Figure 2.10. For an evacuated tube collector (ETC) the external convective losses are significantly reduced by the vacuum. For a standard flat plate collector (FPC) with a transparent cover and some gap between the absorber and the cover optimized to have no internal convection transporting significant heat from the absorber to the front cover, the wind dependency can be measured, but has often proven

to be in a low range. Wind effects may be more pronounced on collectors, where the front cover is either in direct contact with the heat transfer medium, or collector designs without any protection against convection losses (such as unglazed), and these effects must be quantified. The values from the measurements can then be used for calculations and simulations.
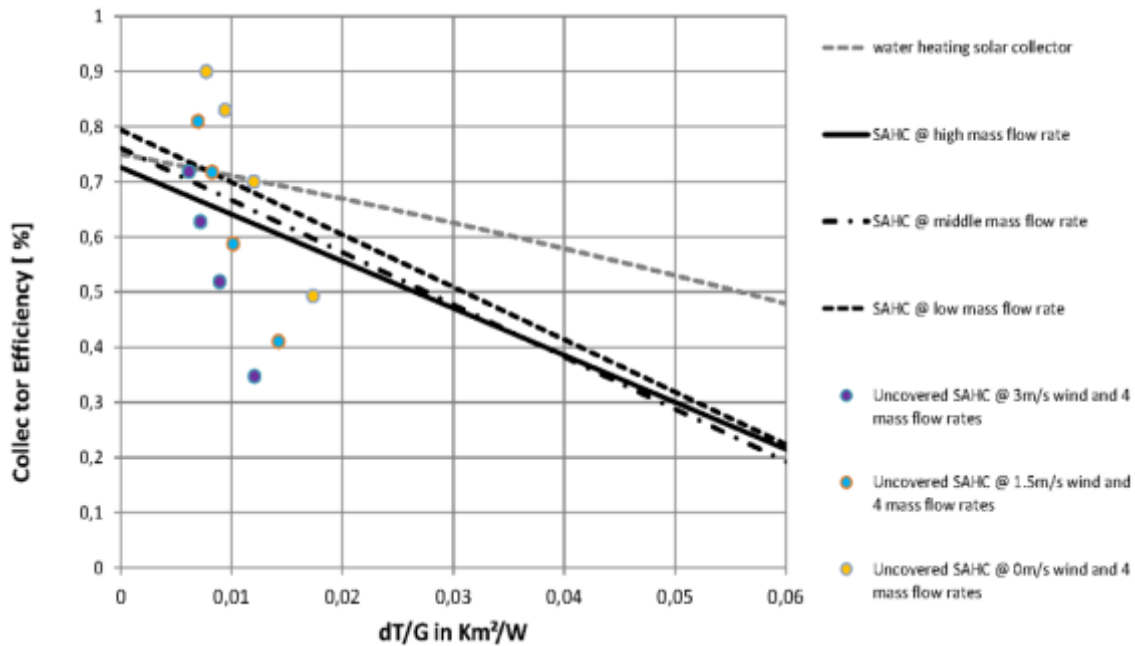
Figure 2.10: Collector performance dependencies on dt/Gm mass flow rates and wind speed by Kramer (2013).

In the case of flat plate glazed solar air collectors the wind is affecting the exterior convective heat transfer coefficient. But in the case of transpired air collectors, PV/T facades and multiple inlet collectors the wind is also affecting the mass flow rates. The following table will describe the findings by researchers addressing wind effects on façade air collectors.

Infield (2004) performed a study on Mataro library PV/T façade system mentioned above. It was found that the effect of the wind has a substantial importance and for easterly wind the cavity air was even forced in the downward direction. Dymond and Kutscher (1996) did a study on UTC air collector modeling and laboratory experiments. He showed that the efficiency, defined as the

amount of energy recovered by the air divided by the total irradiation received by the collector, was little affected by wind when using large suction velocities (about 0.05 m/s). If suction decreases, efficiency decreases accordingly, since the collector temperature increases and it becomes more sensitive to wind. Theoretical studies showed that UTC could reach 80% efficiency, when the air suction is about 0.05 m/s. At this speed, the collector is not wind sensitive. Radiation is the main mechanism of heat loss. Correspondingly, when reducing suction, the UTC becomes wind sensitive, the plate temperature rises, efficiency drops, radiation losses raise. Gunnewiek et al. (2002) did a study on UTC modeling with introduced wind effects on the flow and found out, that to avoid the reverse flow effect, the minimum suction speed during 5 m/s wind increased from 0.0125 m/s to 0.026 m/s for a wind towards the building, and 0.039 m/s for a wind at 45 degrees . The pressure distribution field analysis induced by the wind showed that to prevent reverse flow under wind conditions, it was better not to build the UTC all the way to the top of the building. Fleck and Meier (2002) studied an experimental setup of UTC performance at different wind conditions showed, that performance tended to increase when the wind coming from above by the building created a recirculation/stagnation zone, wind coming to the collector face increased effectiveness while a side wind reduced it. In addition, the effectiveness decreased with increasing turbulence around the collector. Cordeau and Barrington (2011) studied UTC installations on two barns equipped with 1% perforated collector facades. Measurements with 7% uncertainty show, that wind factor has the greatest influence on the efficiency (after irradiation) of 63% at 2 m/s to 25% at 7 m/s. Rounis (2015) did an experimental and numerical study of wind effects on flow distribution in a multiple inlet BIPV/T façade system and found that highest negative pressure occurs, if wind direction towards BIPV/T façade surface is from 90 to 180 degrees, but the thermal losses are related generally to higher exterior convective heat transfer coefficient and not reversed mass flow. No pressure drop correlation between exterior wind speed and direction were done however.

2.2.3.5   Glazing and absorber properties, loss mechanisms and management

In the case of ventilated PV facades, PV modules are acting as rain screen cladding and solar absorbers or the cell laminates are glues on structural materials. Gluing commercial PV laminates over structural surfaces reduces the thermal performance of the PV/T system, due to increased thermal resistance between PV and absorber and also additional gluing step is not optimal for commercial manufacturing, furthermore backsheet rear is generally introducing large reflection losses. Lamination of whole package of top cover, PV cells and electrical insulation and absorber together in one step would be a more advanced solution. Electrical insulation between cell and absorber must be provided, which could be insulating foil between the cells and the absorber or electrically insulating coating. While laminating, a slight bend will occur due to thermal expansion differences between metal and glass, so a possibility to use top foil, like clear backsheet, is possible, but then the rigidity issues must be addressed.

Also moisture issues must be addressed with respect to durability issues in PV/T modules used for façade installations, since bad encapsulating quality can lead in color change in PV modules during the life time of PV/T façade. This can be assured using durability testing methods of encapsulating techniques used: silicon sealing from sides, framing strips or high quality laminating techniques. For example Komp (1982) for the electrical insulation first applies a layer of silicone over the absorber onto which he presses a layer of cloth, followed by a second layer of silicone for the fastening of the cells. However, for commercial production silicones have some drawbacks as they are difficult in terms of handling and have the risk of air entrapment.

As mentioned by Zondag (2008), whichever technique is chosen, one should take care that the encapsulants (and any foils that may be used) are able to withstand the high temperatures that occur in stagnating glazed PV/T modules, which can be as high as 130°C (note the difference between the glazed PVT modules and BIPV/T air collectors, where the maximum temperature can reach 85 °C). In addition, the optical properties of the PV cells should be sufficiently good - not all

commercially available PV cells are equally suitable for PV/T application due to differences in reflection losses in the infrared light spectrum.

Concerning the PV module optical characteristics, 4 effects affect the thermal efficiency of a PV/T collector:

1. the absorption factor of the PV-surface is lower than the absorption factor of a conventional collector surface due to reflections at the various layers in the PV laminate;
2. the PV-surface is not spectrally selective, resulting in large thermal radiation losses;
3. the heat resistance between the absorbing surface and the heat transfer medium is increased due to additional layers of material. This implies a relatively hot surface of the PVT-panel, leading to additional heat losses and a small decrease in electrical performance;
4. the energy that is converted to electrical output is lost for the thermal output. However, as this effect is intended, it will not be discussed further.
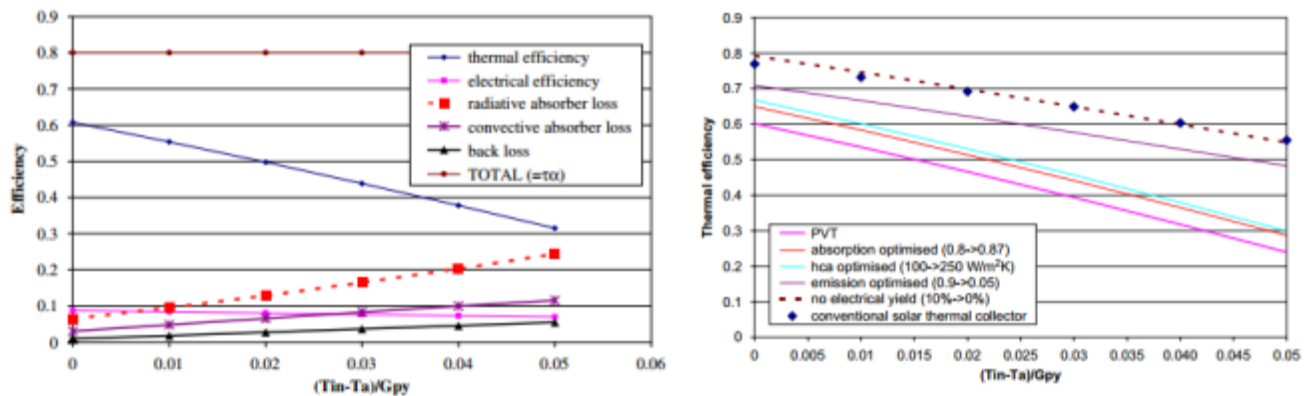
Figure 2.11: PV absorber losses influence from optical PV glazing properties (Zondag, 2008).

Reduction of reflective losses depends from materials used in the PV module in the ventilated façade case or PV/T collector. This is usually addressed by PV module glass manufacturers. Anti-reflective coatings are applied as a cost effective solution, also patterned glass can be used, which reduces the reflective component due to reflections redirected to the glass again from micro structured components in the glass, but this could reduce the transmission.

Thermal losses in PV/T collectors are not only from the top loss, which is the most important, but also back insulation, thermal bridges between the absorber and the collector casing. The top loss mechanisms are convection and radiation to the ambient from the absorber, which is the PV module. In the case of glazed PV/T collector, the loss mechanism is through convection or radiation from the PV/T absorber through the spacing and the PVT top cover to the ambient. Concerning reduction of the convective heat transfer with the ambient, solutions that do not significantly reduce the PV cell output due to shading and are feasible to manufacture have not been proposed yet.

What concerns reduction of the convective component to the ambient, not that many practically applicable solutions have been proposed, which would not compromise the solar gain to the PV cells and manufacturing ease.

The reduction of radiative component from exterior surface of PV or glazing can be controlled by employing plastic covers that reduce the long wave infrared radiative loss or applying spectrally selective coatings for the top glass that would reflect the infrared back to the absorber in the glazed collector case or would reduce the infrared loss to the sky from the top cover. As suggested by Zondag (2008), the problem of such coatings at present is the reduced transmission in the solar part of the spectrum. The glass database in the LBNL program WINDOW gives 76% solar transmission at best for a glazing of 30% emissivity, while a glazing of 5% emissivity would have a transmission of at best 60%. In theory spectrally selective glazing has a substantial potential for increasing the thermal efficiency of a PVT collector, for commercially available spectrally selective glazing the transmission is too low to increase the PVT performance. Although transmission values are presently too low for PVT applications and it will be difficult to increase the transmission substantially, this may be promising for the future.

Two standard techniques exist for the creation of a spectrally selective coating:

1. A coating that is transparent for long-wave radiation and has a high absorption in short-wave radiation (e.g. a semiconductor) on top of a reflective surface.
2. A coating that is highly reflective for long-wavelength radiation and highly transparent for short-wavelength radiation on top of an absorbing surface.

Of course, whereas the first technique is more standard in solar thermal collectors, for PVT only the second technique is suitable. Such coatings are applied in highly efficient glazing. A problem is the limited transmission of such coatings for the solar spectrum, as indicated above for the top cover.

2.2.3.6 Packing factor

Packing factor is the ratio between the PV cell area over PV module area in the case, when a transparent backing sheet is used. In this case the PV module becomes a semi-transparent photovoltaic module (STPV) and a portion of solar radiation is transmitted through it. For a solar air collector this means, that the collector becomes glazed, if the back surface has optical properties that of a solar absorber, which can result in higher thermal efficiency, since exterior convective losses are reduced. On the other hand a smaller amount of PV per area would be installed, some shading from frames will occur and depending on the channel design, interior convective heat transfer might be lower.

It was demonstrated, that the thermal efficiency of a BIPV/T collector would increase, if STPV modules would be used instead of opaque, by 5% if the packing factor would be 80% (Yang, 2015). Several studies demonstrated contradictory results, if total energy production is considered (Ooshaksaraei et al., 2013; Vats et al., 2012), which points out to a need for more research on this topic to determine overall optimal designs.

2.2.3.7 Channel dimensions and pressure drop

Air gap spacing has an effect on the thermal performance of the collector, since it affects the velocity of the air in the channel, which results in different air flow characteristics, heat removal

and as a result it affects the thermal loads of the building, PV electricity generation and fan power consumption.

Tonui and Tripangnostopoulos (2007) performed a study on the performance of the air PV/T collector varying the channel depth. It was shown that the thermal efficiency drops by almost 80% with increasing channel depth from 0.05 m to 0.5 m for airflow rates between 30 and 100 m³/h. The electrical efficiency drops as well, since the increased channel results in smaller velocities and higher temperatures of the collector surfaces. Although, the T_{out} is not affected that much, the power consumption of the fan is reduced significantly. The main graphs showing these relationships are given in the Figure 2.12.
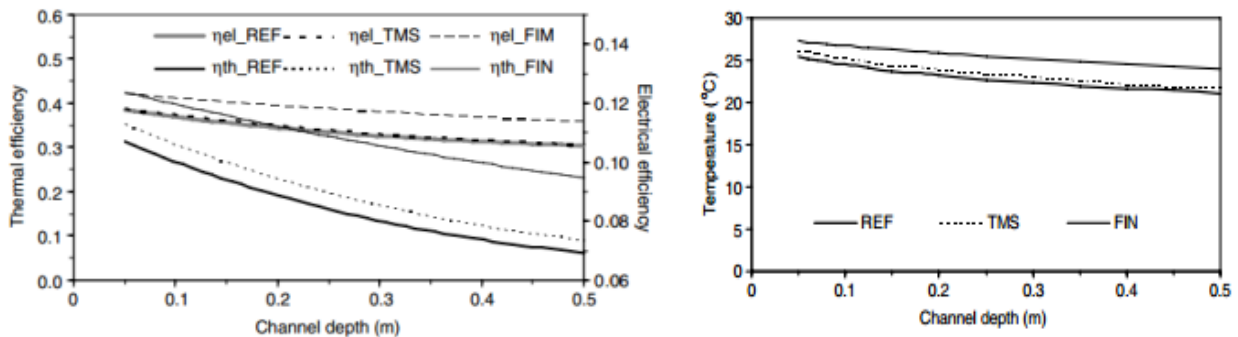
Figure 2.12: Graph showing the channel depth effect on air PVT performance.

Candanedo (2010) in his thesis discussed the pressure drops in the BIPV/T collector system, that was installed in EcoTerra building. The measured pressure drops for the smooth channel are relatively small - for a flow rate of 19 L/s (40 CFM), the pressure drop is around 7 Pa. Assuming that the combined efficiency of the electric motor and the fan is only 20%, the resulting electric power consumption would be: (0.019 m3/s)(7 Pa)/0.20 = 0.66 W. For the framing case, the pressure drop at 19 L/s (40 CFM) is around 62 Pa. These result illustrate the usefulness of air-based BIPV/T systems, as the required power consumption for driving the flow in the channel is small in comparison with the recovered energy (in this case, 68 W of electric power, and hundreds of watts

of thermal energy). This information is very useful for design purposes: it suggests that it is advisable to optimize the ducting system and connecting manifold, since the most significant pressure drops will be much larger there than in the BIPV/T channel. He also did the measurement of friction coefficients and comparison with Blasius friction factor correlation. For the smooth case, the ratio of the measured friction factor to the Blasius friction factor is in the range of 5 to 6. For the framing case, this ratio is in the range of 44 to 52. As a comparison, the ratio of the measured friction factors to the friction factor predicted for turbulent flow in a circular smooth pipe using the Blasius relationship is calculated for the turbulent region. The Blasius relationship is given by equation 2.29:

$$f_b = \frac{0.3164}{Re^{0.25}}$$ 2.29

The friction factor for the laminar region, Re<2300 (ASHRAE, 2009), is calculated using the equation 2.30:

$$f_{lam} = \frac{64}{Re}$$ 2.30

2.2.3.8 Active and passive air mass flow control strategies

Air velocity can be controlled through having an adequate cross-sectional area. The suction air velocity must be at optimal level, which is a compromise between fan electricity consumption, preheated air temperature needed, cooling or heating of the ventilated façade seasonal operation requirements, optimal PV cell operation and the used HVAC system optimal operation.

One option to control the mass flow rate is based on the required temperature differential between ambient and needed outlet temperature, although this could be limited to a set of assumptions for what is the best operation of a ventilated façade (Charron, 2004). Some work still is needed to establish a good operating point taking into account both thermal behavior of the ventilated façade, zone and HVAC system optimal performance requirements.

One option of optimal flow rate is the building requirement for fresh air. This is applicable for heating season and air could be drawn from the ventilated façade all the time except in the case of noise issue. In the summer season the operation should still continue, but the air should be rejected, to not increase and possibly decrease the cooling loads of the building.

2.2.3.9 BIPV/T effects on building thermal loads

BIPV/T affects positively the thermal zone during heating season in cold sunny locations, since the ventilated PV rain screen cladding results in higher cavity temperatures during sunny winter, shoulder season days and reduces the conductive loss through opaque walls. If the fully glazed façades are used, the performance depends from the operation and design of the facade system, location and building type (ECBCS, 2009). During the cooling season, solar facades usually tend to increase the cooling load in all locations, due to higher temperature in the cavity, which results in energy gain to the zone. On the other hand, some investigations demonstrate, that reduction in cooling load is possible, if massive wall is used and heat discharge is performed during night from the wall.

Hauser and Heibel (1998) analyzed a solar thermal system integrated in a curtain wall for preheating ventilation air. He considered a retrofit option. The heat gain in their study was the reduction of transmission heat loss in comparison with a reference wall. They came up with a recommendation for optimal air gap for curtain walls of 0.02-0.04 m, optimized for heat gain and fan energy consumption. They stated that the thermal efficiencies of such systems make sense for all orientations, since they are recovering the heat loss from façade and reusing it in the ventilation system of the building.
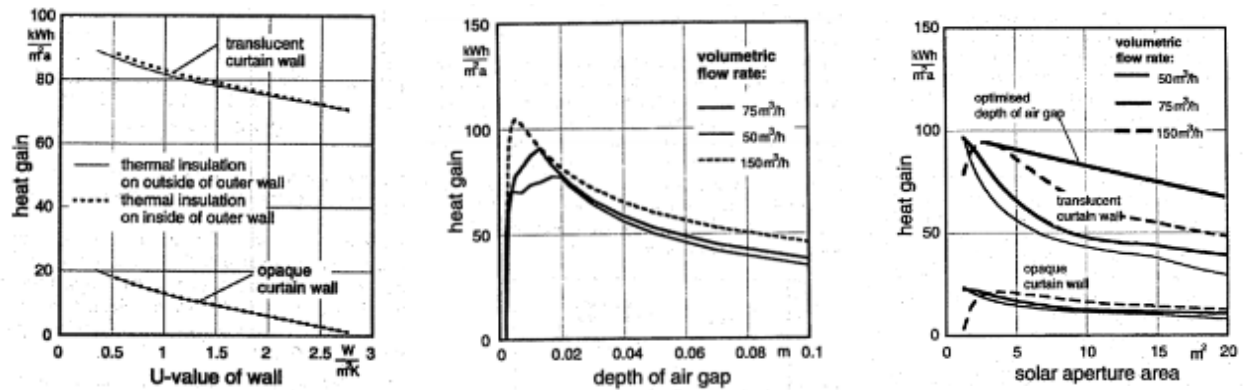
Figure 2.13: Ventilated curtain wall performance (Hauser and Heibel, 1998).

Peng et al. (2013) placed a PV panel on the outside of a south facing outer wall (5-25 cm air gap between the PV panel and outer wall) and they found that this BIPV structure could reduce 51% of the heat gain during summertime in Hong Kong compared with regular south-facing outer walls. The reduction of heat gain per unit outer wall area each year was 52.1 kWh/m^2, thus reducing the air conditioning load by 18.6 kWh/m^2.

Kim et al. (2012) did a study on three types of BIPV facades: BIPV, vented BIPV with outdoor air and vented BIPV with room air. For the case of the building with BIPV/T that circulates the outdoor air, the heating load was slightly increased because of the cooling of the external wall by forced inflow of cold outdoor air.

Mei et al. (Infield et al., 2004; Mei et al., 2006) studied Mataro library and transparent BIPV façade system. The results showed that the cooling loads were marginally higher for the building with PV façade for all the locations, while the impact of the façade on the heating load depended on the location.
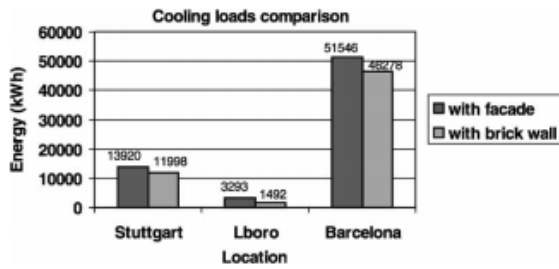
Fig. 16. Cooling loads comparison.
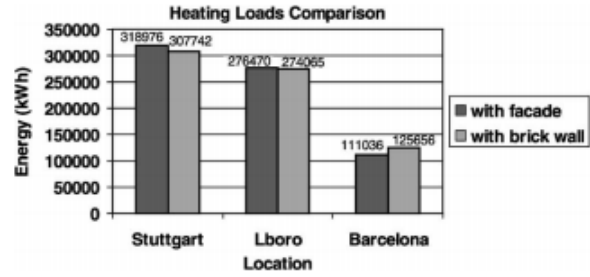
Fig. 17. Heating loads comparison.

Figure 2.14: Eicker and Mei studies on STPV ventilated facades.

Moaveni et al. (2011) studied the energy stored into the wall, when a UTC is in place as well as its effect onto the wall temperature. For the building they monitored in Minneapolis, they found out that the wall outside temperature at night, when having an UTC was about 8°C higher than without. Additional energy stored into the wall varies during the monitored time from 2.6 GJ/m³ to 18.1 GJ/m³. The authors conclude that the amount of energy stored into the wall is significant and should be accounted in the collector efficiency calculation.

Vats and Tiwari (2012) did a performance evaluation of a STPV-BIPV system on roof and façade and effect on building thermal loads for cold Indian climate. It is observed that there are maximum (18.0°C) and minimum (2.3°C) rise in room air temperature for semitransparent photovoltaic thermal (SPVT) roof without air duct and opaque photovoltaic thermal (OPVT) facade with air duct respectively.

2.3   **The holistic design case**

Building façade design has a major effect on the total building consumption, where improved thermal insulation and passive design means can result in building total energy consumption from 100 kWh/m²-a down to few kWh per square meter per year for heating needs. The total electricity consumption for a building with an energy-optimized building shell can be reduced by 50% at most. The cooling of current best practices is recorded for UK climate of as low as 36 kWh/m²a for a

cellular office type building with natural ventilation, 61 kWh/m²a for an open plan office with natural ventilation and 132 kWh/m²a for an air-conditioned office building. The prerequisite for low energy cooling design is appropriate sun-protection strategy to reduce the external loads transmission via windows, night cooling, the mentioned natural ventilation and thermal mass distribution (Eicker, 2003).

About 50% of internal loads are caused by office equipment such as PC's (typically 150 W including the monitor), printers (190 W for laser printers, 20 W for inkjets), photocopiers (1100 W) etc., which leads to an area-related load of about 10–15 W/m². Modern office lighting has a typical connected load of 10–20 W/m² at an illuminance of 300–500 lx. The heat given off by people, around 5 W/m² in an enclosed office or 7 W/m² in an open-plan one, is also not negligible. Typical mid-range internal loads are around 30 W/m² or a daily cooling energy of 200 Wh/m²d, in the high range between 40–50 W/m² and 300 Wh/m²d.

External loads depend greatly on the surface proportion of the glazing as well as the sun-protection concept. On a south-facing facade, a maximum irradiation of 600 W/m² occurs on a sunny summer day. The best external sun-protection reduces this irradiation by 80%. Together with the total energy transmission factor (SHGC) of sun-protection glazing of typically 0.65, the transmitted external loads are about 78 W per square meter of glazing surface. In the case of a 3 m² glazing surface of an enclosed office, the result is a load of 234 W, which creates an external load of just about 20 W/m² based on an average surface of 12 m². The reducing coefficients of sun-protection devices depend particularly on the arrangement of the sun protection: external sun protection can reduce the energy transmission of solar radiation by 80%, whereas with sun protection on the inside a reduction of at most 60% is possible.

With this in mind, there is an obvious optimization task in order to both reject as much as possible heat during cooling season, transmit the necessary amount of solar heat during heating season,

collect and when necessary store as much as possible available solar energy for space heating, DHV or use it in solar conditioning systems. The amount of light on the work plane in administrative buildings has to be at minimum 500 lx during operating hours, which can lead to a need for compromise between temperature and visual comfort and energy consumption. External shading devices and façade integrated solar systems can result in self-shading issues and rise tasks for optimizing both for energy generation, passive gains and occupant comfort. There has been no research done on correlating these interconnected relationships and developing advanced energy generating façade design guidelines.

A holistic design, especially if solar façade is concerned, is a multidisciplinary task and requires advanced methodologies and design tools that are able to address multi-physical phenomena and complex interrelations between domains, which basically include the whole building design spectrum: solar energy retention and rejection, daylighting and lighting design, thermal and moisture balance through the envelope, ventilation design, power system integration and design, aesthetics, costs and other standard design questions related to safety and comfort.

2.4   Façade integration aspects

Vapor transfer is a physical parameter and an important one for BIPV/T systems. One must consider the absorber or the glazing as an external vapor barrier. Usually the vapor moves within the wall from the warmer interior to the cooler exterior of the building, which is basis for a rule, that a more open to diffusion layer is installed on the outer layer to avoid destructive condensation within the wall construction. This relation can be reversed by a hot integrated absorber as the outer layer of the wall (Maurer et al., 2015), which implies, that in this case the vapor should be allowed to exit the wall to the interior of the building, by installing more open to diffusion inner layers (Bergmann & Weiss, 2002). This especially true for water based collectors without back ventilation, closed loop air-based collectors and potentially PV/T collectors with STPV as front sheet and wall

integrated absorber. It is necessary to carry out WUFI+ simulations for entirely new façade systems (Cappel et al., 2014).

Hydraulic components integrated in façade generally follow the same rules as roof installations. Both high and low flow systems are possible. The challenge can be to achieve pressure equalization for custom collectors of different shapes and arrays of different size. For air-based systems, pressure drop equalization can be achieved by installing either appropriate dimension pipes or dampers to regulate the pressure drop in these sections. In the case of façade integrated air-based systems vibration and noise issues are also a concern. Depending from design of the hydraulic system, thermal bridges in the façade, due to piping or ducting embedded in the envelope must be addressed. Due to a small amount installed, the information about practical issues and methods are hard to find.

Photovoltaic array design has some basic design considerations: The array designer must take into account the temperature gradient over the PV modules in a BIPV/T system and solar radiation shading from exterior objects. PV-cells that are connected in series have to operate at the same current, while PV-cells that are connected in parallel have to operate at the same voltage. The IV-characteristics depend on the temperature. If a temperature gradient exists over the BIPV/T, not all cells may be able to operate at their maximum power point at the same time. Only a very small effect of the temperature in the case of series connection (1%) can be observed, but a large effect in the case of parallel connection of about 17% loss (Zondag, 2008). This means, that series strings may be represented by their average temperature and that cells at different temperatures should be connected in series and not parallel. Shading on the other hand, for a series connection, will result in reduction of total current produced by the whole string, based on the current produced by the shaded PV module. For parallel connection the power output would be reduced only by subtracting the current drop from the shaded module, which results in a higher total power output

if compared to series system with the same amount of modules (The German Energy Society, 2008). This has to be managed accordingly by a PV array or a BIPV/T designer, when a façade or roof integrated system is designed in an area with shading effects and large temperature gradients for optimal power production.

Structural design depends from the kind of solar and façade system is chosen to be used in the building. Façade technologies and architectural aspects for facades were already discussed. The degree of building shell substitution needed defines what kind of solar system is most appropriate for façade integration. Some examples, like *Grammer system,* replace only a part of the building shell and the air collectors are placed on an opaque structural façade, like concrete or bricks. Other option is to use a ventilated rain screen cladding as an air collection system. The structural system would be similar to that of a stick or unitized mullions curtain wall with introduced air inlets in the cladding as shown in Figure 2.15. Another example is to integrate the air collectors into post-beam or steel frame construction of the façade and the whole surface is covered by glass. The collectors used here would be not standard collectors, but made according to building requirements and could be called as second skin facades, mentioned before.
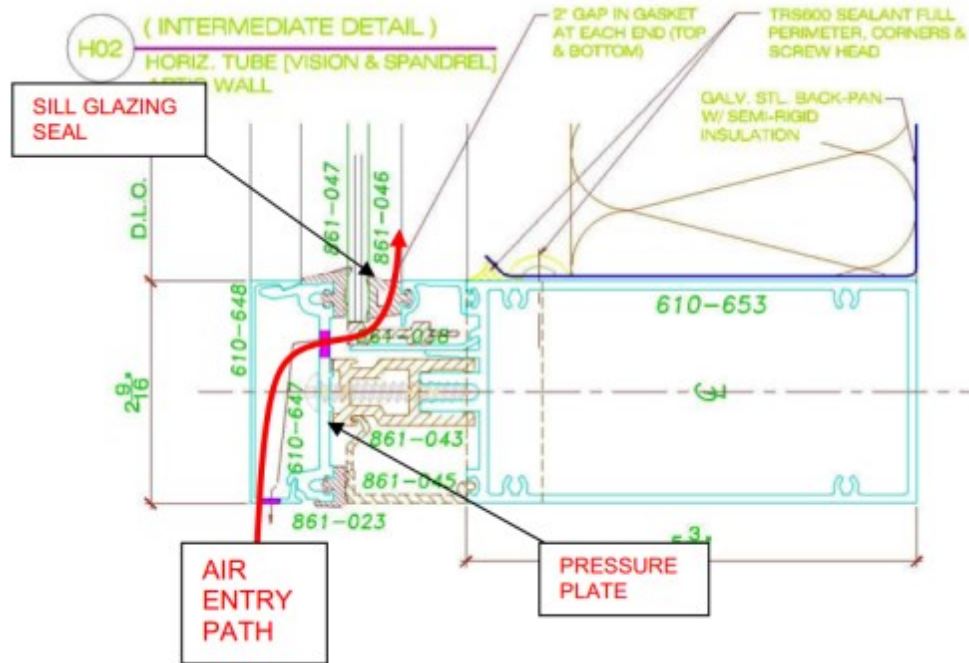
Figure 2.15: An example of an air inlet system in a curtain wall (Richman and Pressnail, 2010).

2.5   Solar-assisted façade integrated decentralized HVAC systems

The following literature review is focused on advanced façade design topics, which includes façade integrated solar energy system energy output aspects, façade design influence on energy performance of the building and solar air collector passive and active coupling with building.

2.5.1   Yields of a façade integrated air-based solar collector

One of the biggest obstacles for market penetration and promotion of façade integrated solar systems is the performance of real façade integrated system data (Cappel et al., 2014). The performance indices include energy output of solar collector, envelope performance, durability aspects and also the effect on building thermal loads, to mention a few. Scarce literature is available, but a complete database with necessary details is a major gap in this field. The following literature will be focused on air-based spandrel integrated collectors and their energy output.

Richman and Pressnail (2010) developed an analytical model and tested the performance of a solar dynamic buffer zone (SDBZ) within a curtain wall system. Solar dynamic buffer zone is a low cost method for gathering solar energy efficiently by using the movement of air. Given the example design conditions, the analysis showed that the SDBZ can act to replace up to 90% of required fresh air for a typical mid-rise commercial building while significantly reducing the cost by preheating during daytime hours. The spandrel integrated SDBZ performance was investigated for Toronto climate during heating season and demonstrated approximately 40% thermal efficiencies, 150-210 kWh/m² heating power production, temperature lifts of up to15°C in January for design conditions with mass flow rates of 15 – 290 m³/m²-h.
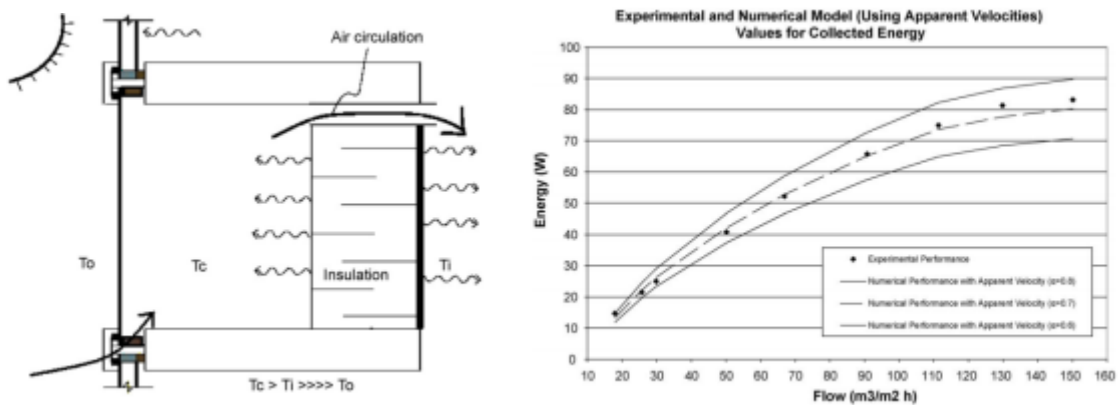
Figure 2.16: Spandrel design with forced air circulation and experimental results of heating power output of a 0.551m² prototype.

Ubertini and Desideri (2003) developed a spandrel integrated solar air collector system for winter heating and summer ventilation for Italian climate. The collector had a double pass channel with finned absorber inside and exhaust air channel next to it, increasing the potential of heat recovery from exhaust air. Air supply grill was in the sill under the window. This system in winter mode is shown in the Figure 2.17. Ubertini and Desideri developed a numerical model and performed parametric analysis and laboratory experiment. The air flow rate varied between 270 – 280 m³/h,

for a collector with dimensions 1.1 x 1.36 (width x length, m), channel depth 31 and 46 mm, the temperature lifts are from 13 – 24°C at different irradiation levels (wind speed is not indicated).
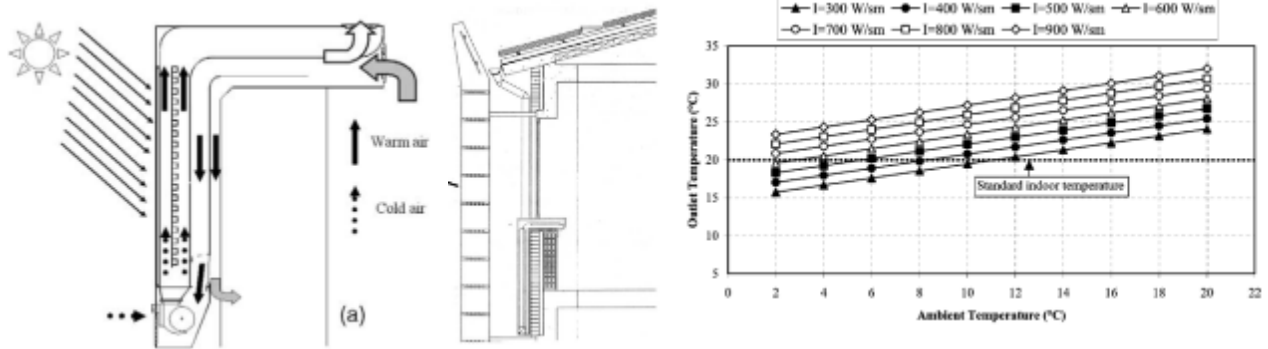
Figure 2.17: Spandrel air collector for fresh air supply in winter designs and temperature lift for given conditions.

One can conclude that there is a large amount of research on solar air collection systems, but the research methods used to quantify the performance of various designs are lacking standardized protocols to produce a representable database of performance of various collector designs under standard and non-standard conditions. In particular ambient temperature effect, wind speed effect, mass flow rate effect and irradiation effect on the total energy and outlet temperature output. Standardized characterization methods would provide crucial information and help the designers to include these devices into their designs easier. A lack of studies on air-based systems for non-residential buildings in cold climate is also observed.

2.5.2   Façade integrated solar air collector active and passive coupling with building aspects

Air-based collectors integrated into façade have an advantage of simple and risk free installation. Large ventilation needs in office buildings increase the potential for façade air collectors installed in front of conditioned zone, where fresh air is needed. Generally the same HVAC designs are applicable as for residential buildings, however large commercial buildings have higher internal gains, thus resulting in higher cooling energy need even in winter, which depends from

volume/surface area ratio, climate, occupancy patterns, building type, envelope design and condition.

Solar air-based façade systems heat utilization means are few: 1) heating of incoming ventilation air; 2) circulating the room air through a solar collector; 3) circulating heated air through a cavity in the building envelope or the floor, where the heat can be brought to the room by passive or active means; 4) heating water through air-to-liquid exchanger, after which the heated water can be used for DHW, space heating or upgraded with a heat pump; 5) assisting the building ventilation by means of natural convection, through use of PV façade as a natural chimney or hybrid ventilation.

2.5.2.1 *Heating of incoming ventilation air*

This is the simplest sort of solar air system. The collectors have fresh air flowing through them, which is then blown into the building in heated form. There is no exhaust air system; the exhaust air leaves the building by leakage or through exhaust air flaps. The installation required for blowing solar-heated feed air into the building is minimal. All that is necessary is to conduct the air into the required rooms. This system is used mostly for retrofitting into existing buildings. If the required hygienic air change is brought into the building via the solar air collector system, every degree of temperature increase brings with it an energy saving. Thus, for example, with an outside temperature of –10°C (14°F) and a desired room temperature of +20°C (68°F), a temperature increase in the solar air collector of only 15 K reduces the ventilation-heat requirement by 50% (German Solar Energy Society, 2010).
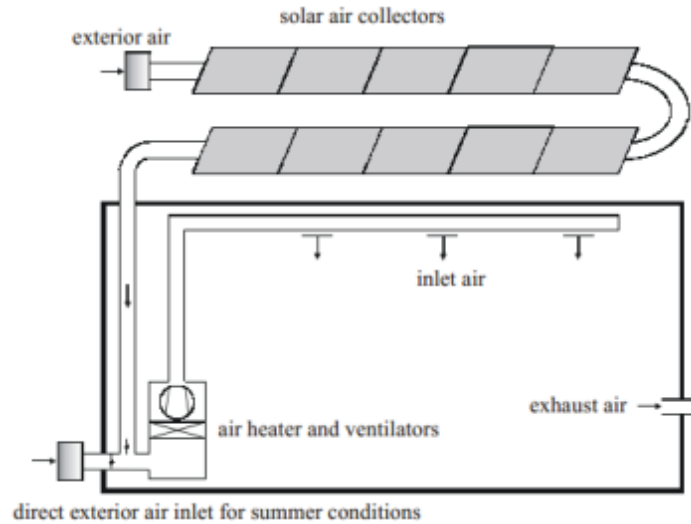
Figure 2.18: Solar fresh air system (Eicker, 2003).

Office buildings are a potential application for solar air-collectors, since the fresh air heat requirements are highest during the day, when both the solar radiation and occupant densities are highest. As a result the solar system can be easily installed, replacing exterior cladding materials with solar collectors. The possibility to integrate the preheated air to central feed and return lines sometimes is easily possible, particularly for new buildings, such as the Concordia JMSB building (Bambara et al., 2011).

Preheating fresh air systems are used in buildings without heat recovery systems. With decentralized air collector fields within the parapet area of a facade with an air intake into the space behind, the entry and exit air distribution system always necessary for heat recovery can be omitted. Even in an energy-optimized low-energy building, a commercial air collector can produce heating energy savings of between 150 kWh/m^2 in a lightweight construction and 210 kWh/m^2 in a massive construction for northern European climatic conditions. Flow rates recommended by the manufacturers are typically 60 m^3/m^{2}h (Eicker, 2003).

The combination of an air collector system with heat recovery from the space exhaust air reduces the effectively possible heating energy savings by the air collector. During fresh air pre-heating the air collector and heat recovery system compete, with the potential saving being limited in total. With an air collector between the outside air inlet and the heat recovery unit, savings of 25–60 kWh/m² of collector are possible. If the collector is placed behind the heat recovery unit to provide additional temperature rises of the room inlet air, the air collector system is energetically more favorable. In a low-energy building, between 60 and 110 kWh/m² of air collector surface of heating energy can be saved in this way.

2.5.2.2 Circulating the room air through a collector

Apart from purely fresh air pre-heating, the warm air produced in air collectors can also be used for direct heating, if the outlet temperatures are at least 5 K above the room temperature. Systems for direct heating are usually operated with lower specific flow rates, to guarantee high rises in temperature even with low irradiances in winter (20–40 m³/m²h).
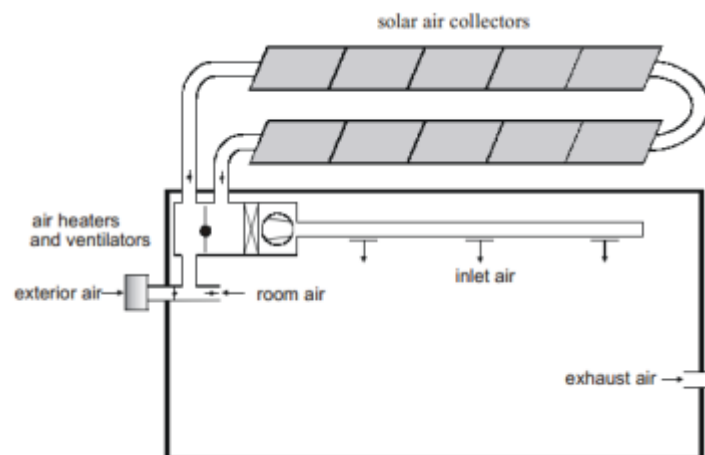
Figure 2.19: System of air heating with air collectors and mixed-air operation (Eicker, 2003).

2.5.2.3 Direct storage systems

When there is a high heating requirement in rooms, the amounts of air necessary to provide the heating can lead to uncomfortably high injection rates. To improve thermal comfort, the solar-heated warm air can be led into ceiling or wall cavities in a closed cycle (so-called hypocausts) or heat storage in conventional hot water tanks by means of an air–water heat exchanger and the room can be warmed by radiant heat. For reasons of cost and efficiency, special stone stores have not gained acceptance in buildings.

In buildings equipped with such systems, it is recommended to subdivide the collector output into part feeding the storage system and part for direct room heating or assisting a ventilation system, since in the corresponding storage component can only absorb a limited amount of heat.

2.5.2.4 Heating water through air-to-liquid exchanger

When space heating is not a priority, the solar air collectors can be used to heat domestic hot water, through air-to-water heat exchanger. Generally, it is considered not effective, since the temperature lifts are not high enough, and solar water collectors are preferred for this application, since the annual yields are higher.

Integrated designs show higher potential for air based systems. In a Net Zero residential house in Canada, air collector was linked to a hypocaust system with a by-pass to DHW preheat tank (Chen, 2009). In a passive apartment house in Switzerland a façade air collector was used with a Solar Box to assist in charging a hot water tank for space and DHW heating. The Solar box was either supplying fresh air or branched with outdoor air supply for an HRV unit (Gutermann, 2002), see Figure 2.20. This is the most common integration scheme of air collectors with a residential combi-system.
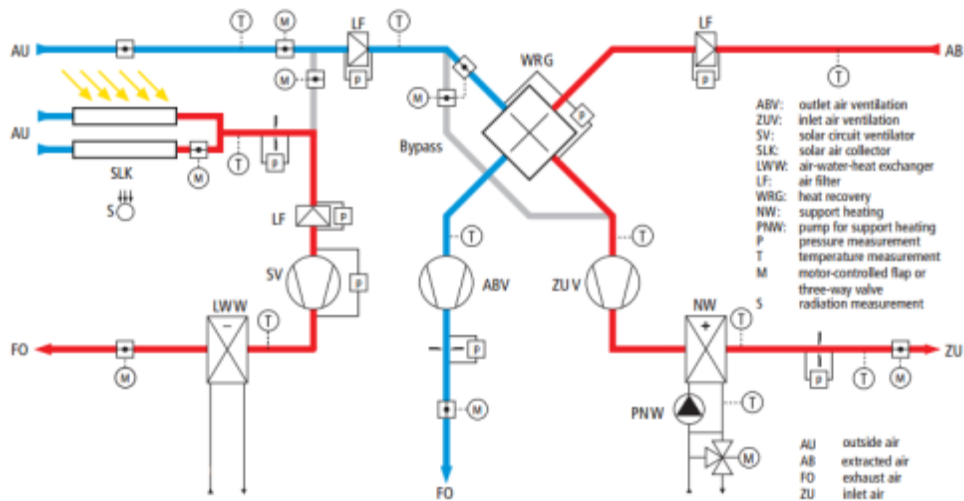
Figure 2.20: Air collector integration with heat recovery and air-to-water HX (German Solar Energy Society, 2010).

The solar system can often supply the necessary heating energy in combination with a heat pump as a heat recovery system. However, it is necessary to consider here the primary energy balance in connection with the number of hours of operation of the heat pump over the year. For safety, low-temperature electrical convectors can be installed to cover the residual heat requirement on very cold days.

In low heat demanding buildings, like highly insulated modern 'passive' houses, the need for either fresh air or space heating can be small. Since the DHW heating application becomes the major heating load in a house, it might be worthwhile to consider water based system due to higher annual yield, since air based system can be highly effective only few months in a year.

It is known thought, that a PV/T collector has a higher exergy than a side-by-side solar thermal modules and PV panels (Torío, Angelotti, & Schmidt, 2009). It is much easier to keep the PV efficiencies high with open to ambient air-based PV/T systems, than with water-based PV/T systems all year round, but this depends from the inlet temperature in water-based PV/T system.

This rises system design and operation related research questions, which needs more investigation and hasn't been covered widely yet.

2.5.2.5 Thermally driven cooling

Solar assisted thermally driven cooling systems are also a promising application in commercial buildings, due to coincidence between building cooling load and solar air collector output during the cooling season. This has already been applied both using solar air-based systems and solar water-based systems (Henning, 2007) with success.

Air-based systems are used with desiccant systems. A desiccant cooling unit driven by heat from a solar air collector (solar-thermally autonomous system) has four modes based on increasing cooling load and moisture content in fresh air: free ventilation, indirect evaporative cooling, combined evaporative cooling and desiccant cooling.

During desiccant cooling mode, regeneration heat must be supplied in order to remove the adsorbed water from the desiccant material. The required heat is at relatively low temperature, in the range of 50 to 100°C, depending on the desiccant material and the degree of dehumidification.

Due to the needed regenerative heat, only façade solar system might not be enough for high cooling and dehumidification loads. For example in Mataro library, the solar air based façade PV/T system (225 m^2, 20% required heat supply) with roof PV/T sheds (300 m^2, 37% required heat supply) supplying 6000-12000 m^3/h heat (average 65°C) to a 81 kW solid desiccant chiller with a vapor compression backup (see Figure 2.21). It was estimated, that a roof solar air collector potentially could be installed (105 m^2, to supply additional 43% of required heat). The overall system shows average COP of 0.52 and average solar fraction of 0.93 over the summer season. During winter the system supplies one third of the heating demand.
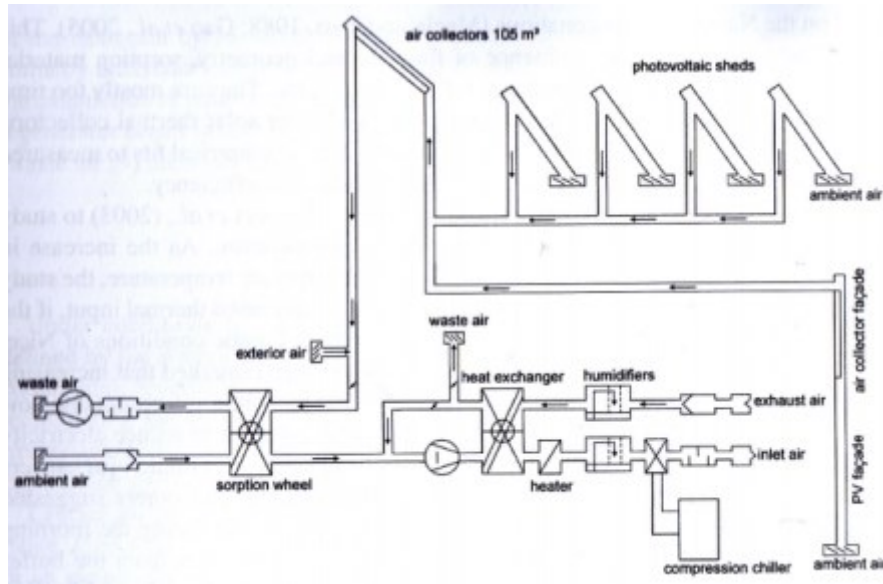
Figure 2.21: Mataro library solar-thermally autonomous desiccant cooling system with a ambient air solar air collector with a backup vapor compression chiller (Eicker, 2003).

2.5.3   Solar-assisted service integrated facades

A solar assisted service integrated façade is a type of decentralized wall integrated HVAC unit. The functionality of the systems varies depending on the design considerations.

2.5.3.1   Decentralized solar-assisted ventilation systems

As mentioned before, assisting fresh air supply is one of the most effective ways of using a solar air collector. A façade integrated air-base solar collector linking to centralized system technically is complicated and depends from the type of building is under consideration. If the air collector is near fresh air intake points, preheated fresh air could be used. However, for facade integrated air-collectors this is rarely the case and decentralized systems could be applied.

In general, ventilation strategies are categorized into three types: natural ventilation, mechanical ventilation, and hybrid ventilation. Hybrid ventilation (HV) combines natural ventilation and typical mechanical ventilation to reduce HVAC energy demand based on outdoor thermal conditions.

Natural ventilation (NV) is an effective passive cooling strategy to save energy and to provide good indoor air quality (Kim & Baldini, 2016). Typical decentralized ventilation (DV) is a type of traditional mechanical ventilation that implements in similar method to fan-assisted natural ventilation. However, fresh outdoor air is supplied and distributed into the room by passing through a compact decentralized air-handling unit rather than being utilized directly. All systems are shown in Figure 2.22.
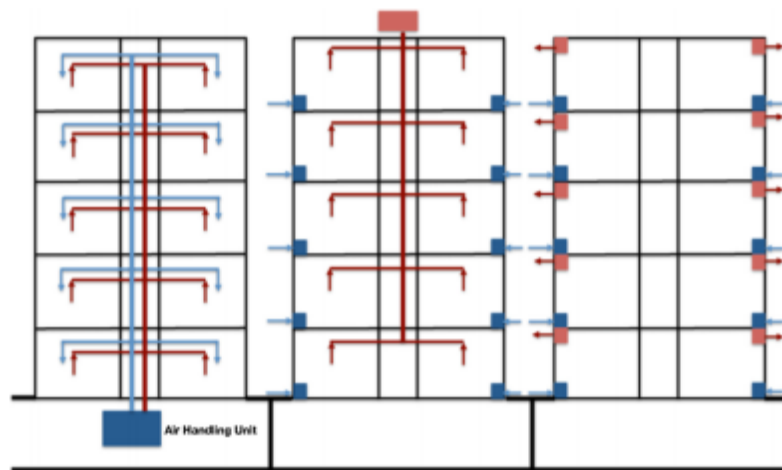
Figure 2.22: Comparison between centralized, hybrid and decentralized ventilation (Kim & Baldini, 2016).

DV of façade integrated ventilation units (FIV) can be sill-mounted, where only the air intake and the air exhaust protrude the façade and units where the entire functional unit for ventilation is to a great extend situated horizontally in the ´jamb´ of the window. They are approximately 0.90 to 1.10 m wide and project approximately 0.20 to 0.30 m into the room. FIV units integrated in the raised floor are up to 1.25 m wide and 0.60 to 0.65 m deep whereof less than 0.30 to 0.35 m from the grille for air supply and extract. The remaining 0.30 cm are walkable and covered by the raised floor construction. The height of the FIV units is between 18 and 25 cm which in return also defines the height of the necessary raised floor construction. Wall-integrated (vertical) FIV units are usually project-specific custom-made units. They are characterized by little depth to be integrated in the

structural glazing system. One commercially available unit is approximately 16 cm thick and intended for use together with a vacuum insulation panel on the outer side (Gruner, 2012). Figure 2.23 demonstrates all the concepts.
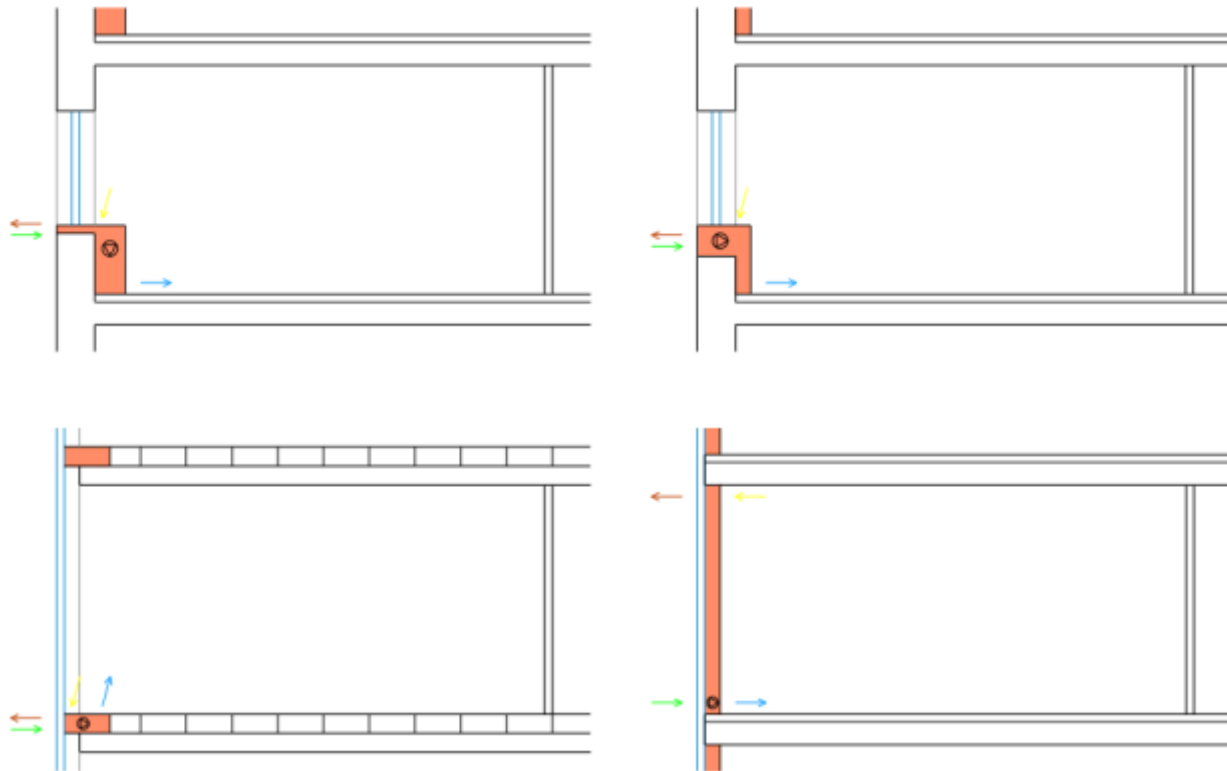
Figure 2.23: Location of FIV units: sill-mounted, jamb-mounted, raised floor, wall-integrated (Gruner, 2012).

The basic components of FIV units are air supply unit, heat exchanger unit (2 or 4 pipe systems), extract air unit, heat recovery unit, secondary air unit, PCM unit. The FIV units provide all the functions of air supply system: air supply/exhaust, secondary air, heat recovery, heating/cooling, de-/humidification.

A monitoring, survey and simulation study of 20 buildings with similar decentralized ventilation concept systems with various heating and heat recovery concepts exists (Bine.info, 2009). The conclusion on these systems was that it can result in 18% annual savings in heating and 76% in

electricity if compared to central systems, less space and floor area required for new buildings (elimination of suspended ceiling saves 0.6 m per floor), no need for supply shafts or fire dampers for ventilation ducts, exact consumption-based cost accounting possible for each room or zone, individual ventilation and temperature control of rooms and increased occupant satisfaction.

The disadvantages were that with excessive air flow problems due noise and draughts occur, air humidification and dehumidification is complex, maintenance and filter replacement require more time and effort, individual devices, heat recovery is relatively complex (alternative is a centralized exhaust), higher consumption with open plan offices or central controllers, wind pressure and outdoor temperatures at the building envelope influence the functioning of the devices. From cost effectiveness point of view, the systems in year 2006 were on the level of medium to high standard office buildings.

There is not much research on decentralized ventilation systems for buildings in cold climate, like Canada. Gruner (2012) did a research on potential of FIV units for Nordic climate (Oslo) based on published technical literature, case studies and personal communications. It was concluded, that for cold climate, FIV systems working in displacement ventilation mode are not recommended for heating, since the ventilation effectiveness falls below mixed ventilation effectiveness when temperature difference between supply and room air becomes <+1K. The cooling and dehumidification function can be effective and research and development on façade integrated systems is progressing (Kim & Baldini, 2016), discomfort issues can be avoided if the supply air is 0.5 – 2 K below room air temperature. In intermediate season 4 pipe systems must be used, since heating and cooling must be carried out within the same day. For this TABS or radiant panels are used, which demonstrate very good results with regard to comfort and required capacities (Gruner, 2012; Kim & Kim, 2012; Kim & Baldini, 2016). The energy delivered by the FIV is comparable to centralized systems if energy supply strategy is chosen which focuses on renewable sources.

A solar assisted FIV concept was proposed by Egolf et al. (2014) consisting of a transparent insulation with PCM storage and heat recovery unit. The system is supposed to be able to condition the ambient air while passing through a heat recovery unit and later through a transparent insulation with PCM before entering the room. Another design included evaporative cooling unit integrated in façade. No data on performance of this system is published, however the transparent insulation with PCM unit was studied separately for Swiss climate and showed a mean energy flux of 13 W/m^2 during highest temperature difference possible for this climate and only 1% of the time energy loss to outside through this facade (Manz et al., 1997).
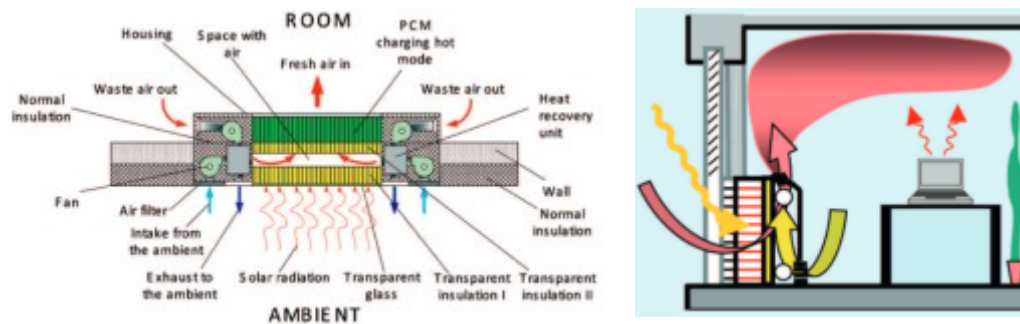
Figure 2.24: Decentralized solar assisted fresh air supply system by Egolf et al. (2014).

A solar air collector with a heat recovery unit for residential façade retrofit is applied by an Austrian company GAP Solutions (Gap Solutions GmbH, 2014). The façade applied solar air collector is a prefabricated façade retrofit system with includes transparent insulation with glazing. One air collector covers approximately 2 m^2 of exterior façade, transparent insulation can be applied with conventional thermal insulation from residential building exterior. A small plate HRV unit (15-90 m^3/h) with 76% efficiency (dimensions 40.9x38.8x19.6 cm) is installed in every room of the building to provide fresh air to retrofitted apartments. This concept was applied in Austria in several apartments and non-residential buildings with different mechanical systems, however, no publications on performance of these systems and retrofitted buildings performance are available.
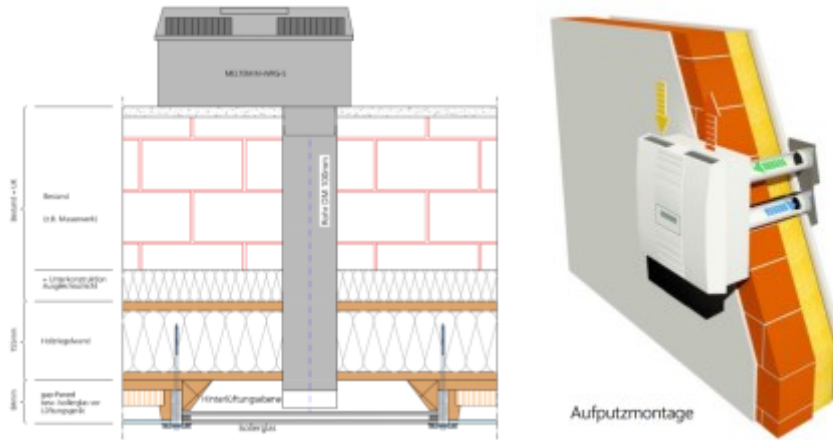
Figure 2.25: Gap Solutions residential building retrofit scheme using solar air collectors and HRV (Gap Solutions GmbH, 2014).

An early example of positioning building service components into the zone of the façade is the 'Post-Tower' in Bonn, Germany. The 162.5m high office tower was built from 1998 -2002. The double façade is divided into 1 storey high zones. The climate installation concept is based on de-centralized induction units, placed in the top-floor zones along the façade. Fresh air is taken into the façade cavity. There it is pre-conditioned by solar irradiation. The induction units take this air and heat it to the desired temperature. Depending on the outside weather conditions the ventilation rate of the cavity is adjusted. Used air is extracted through big winter gardens in the central zone of the building (Compagno, 2002). The major development task in this building was the control and maintenance of the HVAC components. All openings in the façade, as well as the ventilation units are controlled by a facility-management-software. As the amount of components exceeded any previous project every floor is treated by the software as one building itself. Nevertheless, the complex control allows a feasible performance and individual maintenance intervals for all components (Ebbert, 2010)
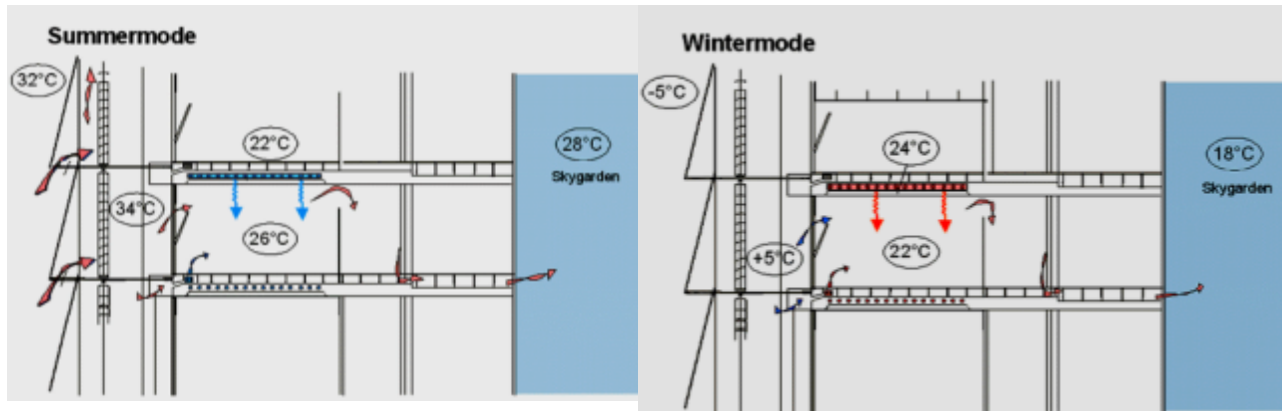
Figure 2.26: Post – Tower HVAC system and operation modes.

A concept 'TEmotion' developed by Wicona (Hydro Building Systems) and University of Dortmund is a combination of a box window and an installation element within one unitized element. The box window is permanently closed. The exterior pane protects the solar blind. All functions of ventilation and air conditioning are placed in an opaque vertical element. It is possible to open parts of this element for natural ventilation. Additionally, there is a mechanical de-centralized HVAC unit that allows ventilation with heat-recovery and air conditioning.

The combination and dimension of the transparent and the functional elements can be chosen freely, which can give the designer of the building a certain design freedom. The entire control system is integrated in the façade-unit. All functions can be monitored by a BUS-installation. Thus, it is possible to mount different components in the service unit without major changes in the building's installation system. The product never left the prototype status as it held two disadvantages that made marketing difficult: the façade was composed of existing products, which caused rather big dimensions and design possibilities with this unitized façade were limited, which led to a lack of acceptance among architects (Ebbert, 2010; Hovels, 2007).
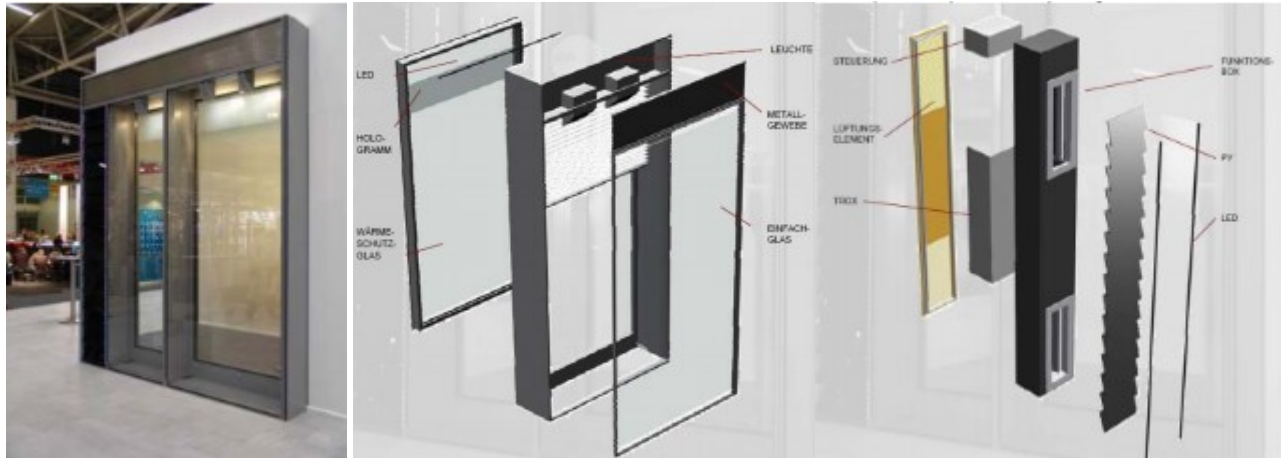
Figure 2.27: TEmotion façade with functional module components break-up.

Another example is the Capricorn institution façade. The architects and engineering team together developed a solution, in which all building services should be provided from the façade. In this case the unitized aluminum façade is equipped with specially designed de-centralized building service units. These units are minimized in size. With approximate dimensions of 1.20/1.00/0.20 m the climate units can be placed in the parapet level of the façade. The installation provides ventilation with heat recovery, heating and cooling. Furthermore, the façade elements are equipped with operable box-windows, venetian blinds in the cavity and artificial lighting.

The module was based on the idea of the architects to produce a façade that helps to be free in the interior building planning by placing all kinds of building services inside the façade. The functions that have been placed inside this module are individually controllable ventilation combined with heating, cooling and air circulation and possibly night cooling.

In short, the outside air enters the module by a closable gap on the outside of the façade and goes through a fine dust filter, a volume flow limiter, a heat recovery unit (air-air heat exchange with the exhaust air), a ventilator and a heat exchanger to the room. The air enters the room trough a kind of grate in the parapet. The exhaust air leaves the room through an exhaust valve in the parapet and

goes through a rough dust filter, a heat exchanger and a ventilator to the outside. The users of the façade can individually control the system. Figure 2.28 gives a complete picture of the functioning of the module.
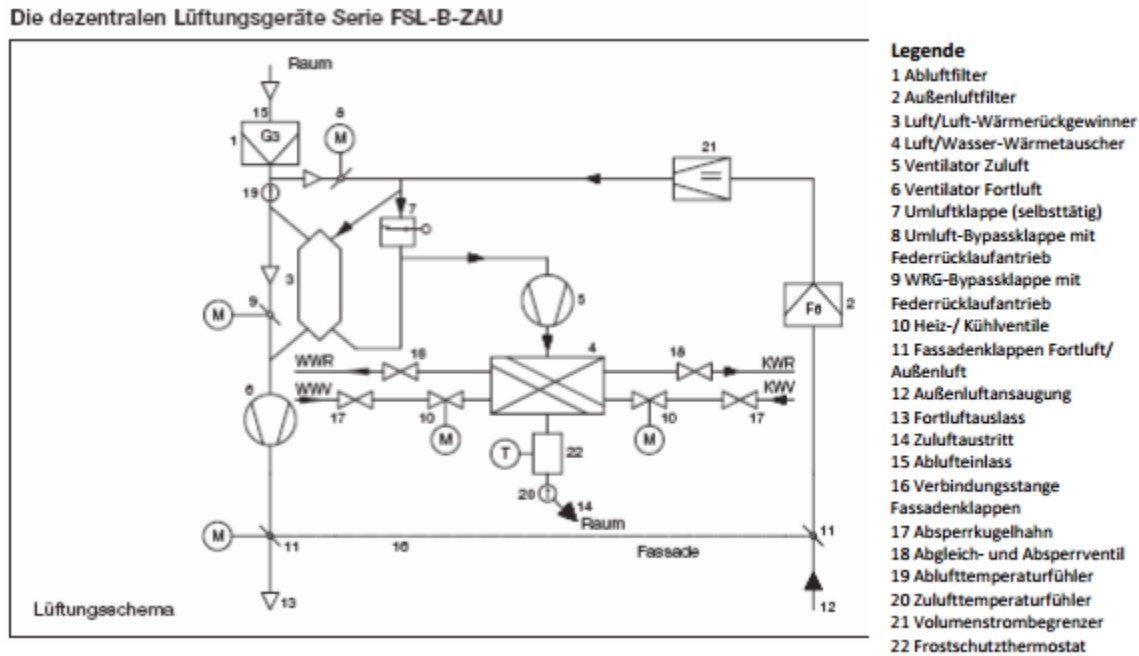
Figure 2.28: Scheme of the air stream of the Trox climate unit in the Capricorn House (Ebbert, 2010).

A concept of using a downscaled heat pump for façade integrated system for retrofits is developed by Feist et al. (2014), Gustafsson et al. (2015), Ochs, (2014). The micro heat pump (μHP) works on the same principles as any air source heat pump, using a compressor cycle that exploits the physical heat–pressure relationship to upgrade heat from the cold ambient air source to an indoor space. The concept works either with water-based systems using radiators or underfloor heating, or air based systems that directly pump hot air into the building. The prototype is an extract air-to-air model in combination with a mechanical ventilation with heat recovery (MVHR). The innovative element is the integration factor - because the heat pump must form part of a nonintrusive façade, it is significantly smaller than a typical heat pump, both physically and in heating capacity terms. The

basic concept of compact units – extract air heat pumps, with storage for hot water – has been used in the Passivhaus field for some fifteen years already. The innovative importance of the work lies in separating space heating from water heating, down scaling the heat pump and integrating it into the façade. The heat pumps range from 1 to 1.5 kWp heating capacity – relatively miniature. They are designed for buildings with high-energy efficiency ratings or Passivhaus or EnerPhit specification, which have extremely low heating demand – in the region of 15-25 kWha/m². Technical efficiency is not so important because of the low demand. Another novelty of the micro heat pump is that it works in conjunction with the mechanical ventilation system and a larger heat recovery unit (MVHR), and can use both ambient air and extract air from the ventilation system as the heat source. One of the great advantages of integration into the external façade, is that almost everything can be prefabricated, so installation causes minimal disturbance. As the micro heat pump shares the system used for ventilation, only one air distribution system is required within the building. Experimental and simulation based studies demonstrated that decreasing the compressor frequency COP tend to be higher, but optimization for highest system SPF is needed, since the performance of the whole system depends from climate and indoor conditions. A comparison for different climates using on/off and PI control was performed as well and it was observed, that PI control is usually performing 15% better that on/off with constant compressor frequency, which is a result of the inability to supply energy at peak load using on/off control at constant speed, which is a result of sizing requirements for constant speed heat pumps.
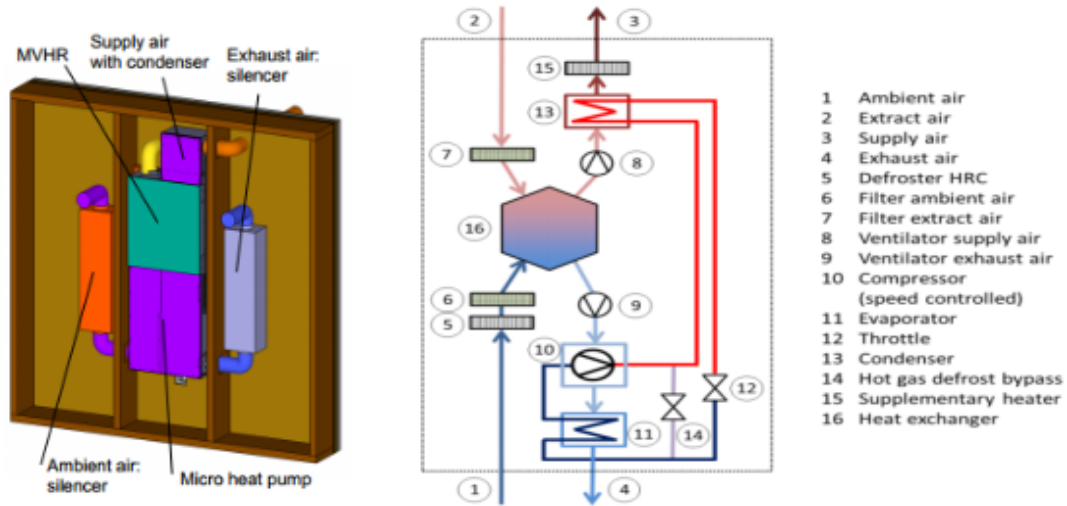
Figure 2.29: Micro Heat pump developed in iNSPIRE project.

2.5.3.2   Air collector with heat pump façade systems

The principles of heat pump operation is described in an basic thermodynamic text book (S. Klein & Nellis, 2012) or technology overview publications (NRCan, 2004). Integration of heat pumps with solar collectors was studied under IEA SHC task 44/HPP Annex 38 „Solar and Heat pump systems", where several concepts were described (Haller et al., 2014). One of the conclusions was that the seasonal performance factor (SPF, the ratio of useful heat delivered for space heating and DHW to the total electricity consumption of all components) largely depends from the system concept, climate and the heat load. Seasonal performance factor (SPF) (the ratio of useful heat delivered for space heating and DHW to the total electricity consumption of all components in the system) was estimated for air source heat pumps with unglazed solar water based collectors in Central Europe climate. The results are shown in the Figure 2.30. It is visible, that the addition of solar collector, improves the SPF of the heat pump system. Also, it is visible, that a series/parallel system doesn't outperform significantly a series air source heat pump and solar system.
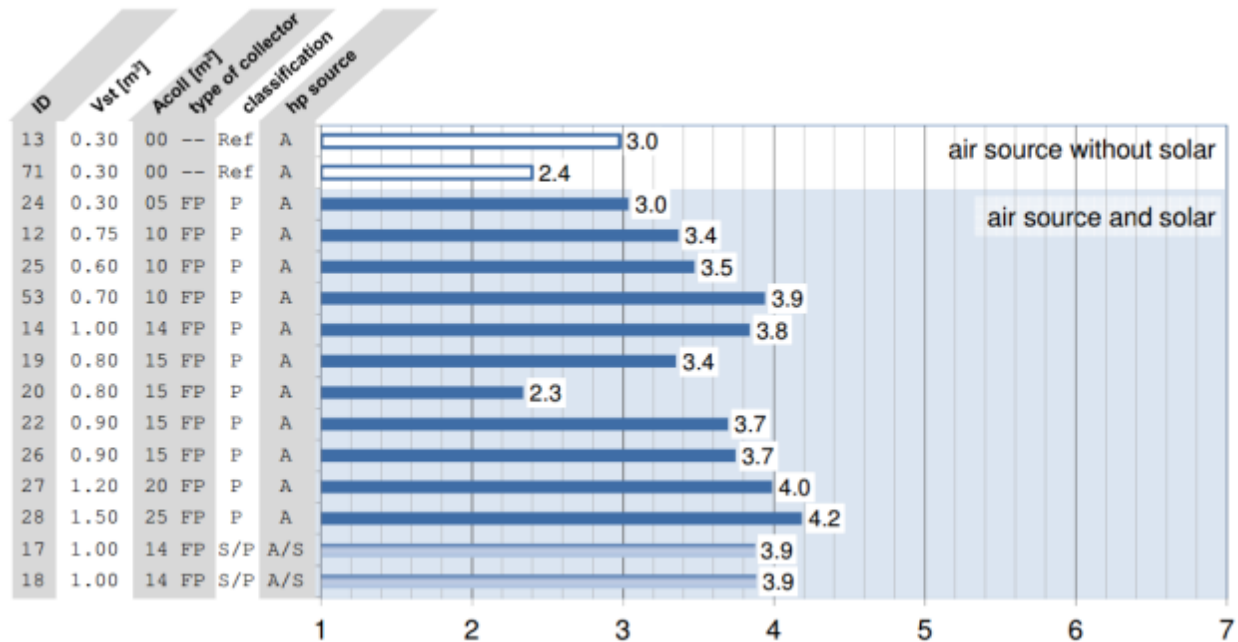
Figure 2.30: SPF of systems with air as the main heat source for the heat pump (Haller et al., 2014).

Research of PV/T assisted heat pumps dates back to 1970's, with the focus on PV/T collectors, with the main aim of increasing the energy efficiency. In 1979 a system was suggested by Tysenhaus (Zeimes, 1979). The idea was to use the solar preheated air on the evaporator side and use the condenser side as a heat source for water tank or direct room heating. The evaporator can be excluded from the circuit by valve directing the heated air along bypass duct. Heat storage devices can thus be charged by being fed the heated air either along bypass duct or through the solar collector. Fresh air can be fed to the duct to prevent the evaporator reaching too high a temperature by opening throttle valve. The heat delivered from the air circuit by the heat pump can either be fed directly to a heat delivery system for space or water heating or it can be stored, until wanted, in a heat storage device. This concept was used later by many system designers and researchers as an option for introducing solar collector heat to heat pump.
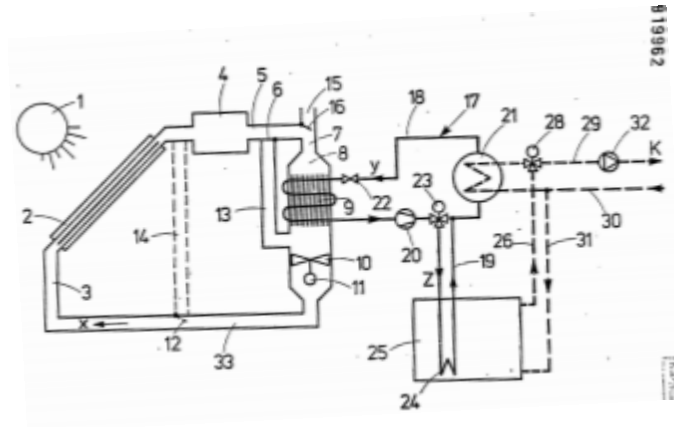
Figure 2.31: A patent by Tyssen Industrie of solar air collection system with air/water heat pump (Zeimes, 1979).

In 1984 Pfeifer (Pfeifer, 1984) filed a patent for a built in heat pump component for building openings like windows or doors. The component had an air channel formed between two panes that led to the evaporator. The feed air flows from below via an air inlet opening into the air channel and thus reaches the evaporator. The evaporator is followed by centrifugal fan, which forwards the feed air over a condenser heated by the compressor into the interior space. Similar concept was applied to a building in Solar Center in Frankfurt/Oder, Germany. The building has a modular façade, which supplies fresh air and daylight through windows equipped with outside blinds over which a rigid daylight control system is installed – artificial light is only activated by light detector when needed. Integrated in the spandrel area of the façade are the thermal air collectors and a photovoltaic system. Behind is a heating, air-conditioning and ventilating machine with heat exchanger. Active air flow is supplied through two window panes (an air gap between conventional pane and insulating pane). In winter the incoming air is heated over the air collector and then led to the heat exchanger. There, another rise in temperature follows due to the heat energy absorbed from the used air. Afterwards the pre-heated outside air comes to a conventional heater in the room. In this way, fresh air and heat is supplied to the office. On sunny days the output from collectors and the heat gain for the room's heating system are both adequate, and the used air

is then led outside through the space between the windowpanes. Over the course of a year the photovoltaic system delivers the needed energy for the operation of the ventilation system. The collectors are turned off in the summer via a summer-winter circuit because the warm outside air comes in direct contact with the heat exchanger and there the cooler inside air can cool it. On very hot days cold water from an underground reservoir flows through the heaters, turning the heating system into a cooling system. Soil serves as the cold source. The heating and ventilation production is 58 kWh/m²/a and the lighting demands were halved compared to a conventional building in addition, the workspace conditions were pleasant and adequate, during summer, the rooms didn't overheat (Hug, 2010).
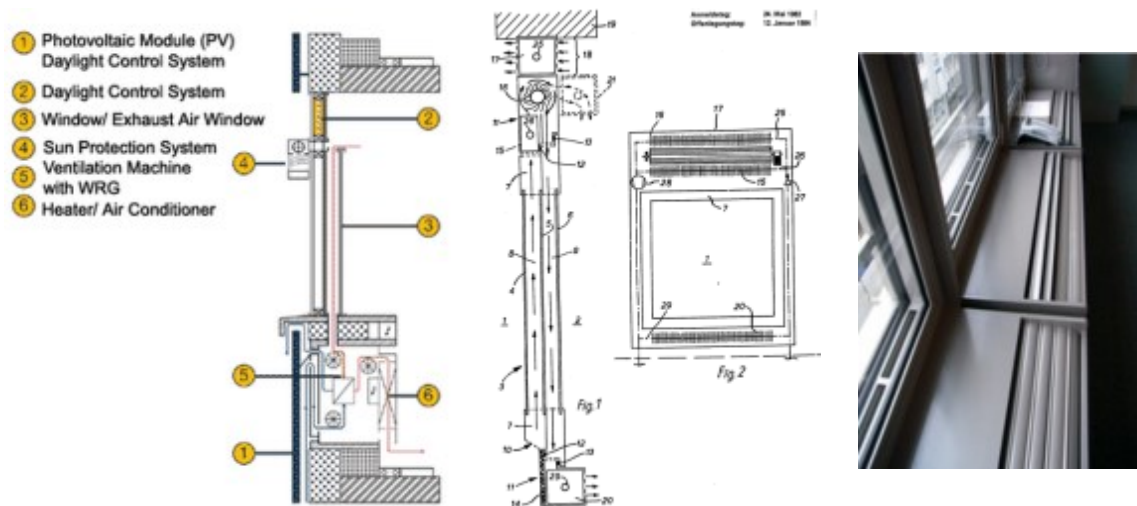
Figure 2.32: BINE project modular façade and patent scheme and a built in device (Hug, 2010).

Candanedo and Athienitis (2008) did a performance evaluation of different combinations of air based PV/T collector assisting a heat pump through air to water heat exchanger and charging a water tank, a PV/T direct charge of water tank, a PV/T with two parallel heat pumps/water tank and a ground source heat pump/water tank. If one heat pump would be assisted by air based PV/T, in near-optimal conditions (high flow rates and high BIPV/T temperatures), over 20 kW could be delivered to the tank with a COP higher than 5. The heat delivery could range from 7 kW – 23 kW if

BIPV/T temperatures would be from -2 to 40°C. For an average heat delivery output rate of about 14-15 kW, eight hours of operation (typically, between 8:00 and 16:00) could deliver about 112-120 kWh of thermal energy to the TES tank, which represents about one day of heating autonomy. Two parallel heat pumps would result in better part load performance (Candanedo, 2011).

In the EU funded 7th Framework Programme project Cost-Effective-Renewables an unglazed solar collector integrated in façade was developed Ruschenburg et al. (2011). They developed a heating/cooling system for high-rise buildings using active solar façade elements to take advantage of the available unglazed vertical surface. The system is composed of a cost effective active solar façade coupled to a reversible heat pump. The active façade works as a low temperature solar collector as well as an atmospheric heat exchanger and a nighttime heat-dissipater in order to boost the heating/cooling efficiency of the system. The collector was connected to the storage tank and an air source heat pump working at the cooling mode was connected and supplying additional heat to the tank. During the heating season the heat pump was supplying 25% of the heating load to the tank, while 75% was supplied by façade collector. This was 70% of the total heating load of the house for DHW. Dynamic models were developed and simulations carried out. The assembled heat pump on the test rig has proven its functionality regarding heating and chilling. However, its performance regarding heating capability and efficiency is too low to fulfill its role in the system. This is explained by the prototype character of the heat pump. It can be anticipated that a redesign based on the same requirements would achieve the intended characteristics. The performance of the whole system depends strongly on the interaction between solar source and heat pump. In the original case, the solar source contributed just 28% of the required source energy. The low performance was explained by a). Solar source is adding a lot of value to the heat pump performance and a larger solar collector would help to boost the performance more, but it is hard to do it for façade integrated systems, due to aesthetic reasons and mandatory window sizes for non-residential buildings; b). Experimentally it was seen, that heat pump is insensitive to source

71

temperatures above 10°C and is explained by the use of thermostatic expansion valves (TEV) in the prototype, which have a non-linear relation between source temperature and superheating for TECs is undesired. For solar assisted heat pumps, relatively high source temperatures (up to 25°C would result in higher efficiencies if electronic expansion valves would be used; c). moderate scaling up for whole floor heating would result in higher auxiliary losses due to the heat distribution, but the solar source would be higher and a potential of outperforming the central system is still high. Prefabrication would be an issue.

the WP3.5 concept (simplified scheme)
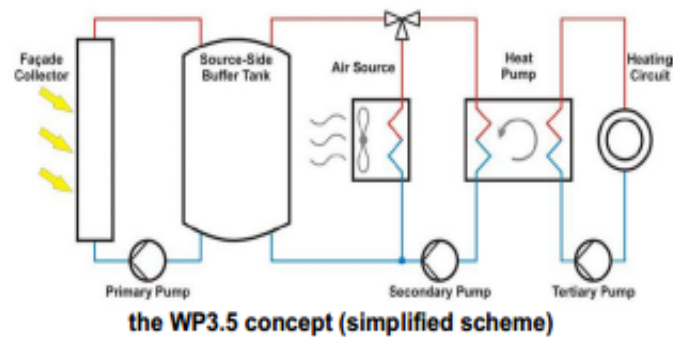
Figure 2.34: A developed prototype of façade integrated heat pump assisted by unglazed water collector and air source (Ruschenburg et al. (2011)).

Decentralized ventilation systems as described above perform well in moderate Central Europe climate covering heating and cooling demands in office buildings with concrete core tempering. Moderate climate results in good U-values of the facades and reduced losses through thermal bridges due to openings in façade, which results in low-area related heating and cooling capacity. The concrete core is operated at close to room temperatures which allows to use passive energy, like energy pile installations, geothermal probes, well water or free cooling at night (Mahler & Himmler, 2008).

Recent innovations have also demonstrated that these systems demonstrated higher exergy and energy efficiencies in hot and humid climates, where dehumidification of fresh air is needed

compared to all air systems (Kim et al., 2014). A chilled ceiling panel for sensible cooling and an decentralized ventilation system with free reheat was designed by Baldini et al. (2014) (Guo et al., 2017).

Regarding high heating loads, it was reported, that the façade integrated decentralized displacement ventilation concept is not advisable due to lower ventilation effectiveness (Gruner, 2012). Also if exhaust is integrated in façade, room depth is advised to be maximum 6 m to facilitate a return of the impurer air to the façade units.

2.6 **Research opportunities**

According to the extensive literature review that covered aspects of the BIPV and BIPV/T collectors, façade integration aspects, solar assisted and façade integrated HVAC systems, the selected research opportunities are as follows:

- The design and modeling of a prefabricated BIPV and BIPV/T façade needs to be covered to present different design and integration possibilities and identify the main design parameters for standardized products suitable for retrofits. Also a standard performance characterization method needs to be identified for BIPV/T collectors for performance comparison of different designs of standard certified products;

- A BIPV design methodology needs to be developed. This is a new approach to design the PV products that are tailored for building retrofit applications – an energy producing glazing that is based on structural glazing technology;

- A solar façade in a retrofit project design methodology needs to be developed. A holistic comparison method, that would allow the designer to systematically identify optimal choices and configurations is required;

- There is a need/opportunity for modeling and numerical analysis of a façade integrated air-collector assisting a façade integrated decentralized micro-heat pump with low temperature heating system (modular radiant panel) and short term thermal storage (PCM). This innovative concept will be modeled to evaluate the performance numerically and identify design and development opportunities.

- There is a need for integration of semitransparent photovoltaics into retrofit methodologies.

All of the above needs will be addressed in this thesis.

3 EPoG and BIPV/T design methodology and experimental prototype development

In this chapter a discussion about the architecturally integrated BIPV cladding design methodology will be carried out, an energy model for a BIPV panel will be presented, an experimental prototype of a prefabricated BIPV/T panel unit will be described, experimental results presented, performance analysis and parameter discussion carried out. A decentralized façade system for retrofits will be introduced.

3.1 BIPV (EPoG) design methodology

A simplified BIPV glazing or an EPoG (Energy producing glazing) design methodology consists of the steps shown in the flowchart in Figure 3.1. Each step will be described in the following sections for EPoG's based on multi- and mono-crystalline silicon cell PV technology.
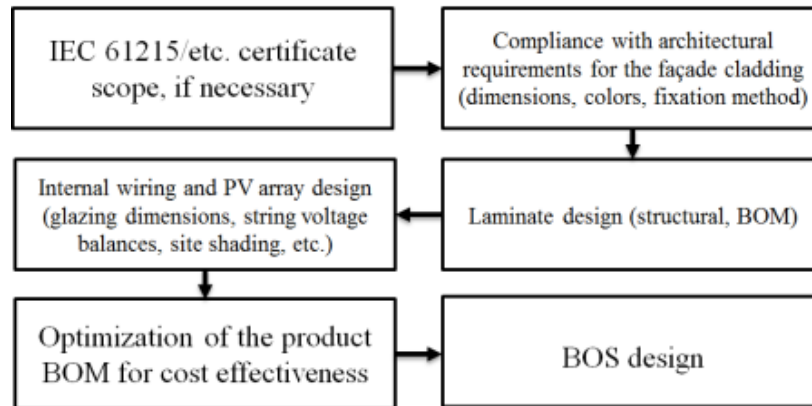
Figure 3.1: Simplified EPoG design methodology.

3.1.1 PV standards and EPoG glazing technologies

The façade or roof integrated BIPV panels or EPoG's are a subject to standards applicable to standard photovoltaic panels: *Design qualification and type approval testing for PV modules according to IEC 61215-1 (2016) / IEC 61215-1-1 (2016) / IEC 61215-2 (2016)* and *Safety*

qualification testing for PV modules according to IEC 61730-1 (2007), IEC 61730-2 (2007) and UL1703 for the North American markets and other derivative regional standards. This is generally not an issue to the BIPV producers, if their standard certified panel type covers the power output, bill of material and dimensions of the glazing for a given project. Since the standard allows 20% variation in power and 10% variation of the dimensions (for the same glass thickness), there is a certain range that the producer can cover with his products, however, the majority of BIPV projects are exceptional designs with variation in sizes, shapes, colors, power and fixation systems, which are outside of the producers certification range. This poses a problem for the competitiveness to the majority of the current producers in the BIPV market.

Since the BIPV is a glazing with PV cells used as a construction material, the panel is also a subject to the regional structural building safety regulations, which normally impose a certain glass deflection limit for a Serviceability Limit State. If the client or a control office are strict, the standard PV panel glass thickness is not going to be compliant with the maximum deflection requirements by the building structural codes and this will lead to an increase in a number of types that need to be certified by the producer, to be able to cover the range of products needed to satisfy the demands of clients and architects.

There is an obvious need for a special certification for a BIPV or EPoG products, since the current PV module certification framework does not address the fact, that a BIPV or EPoG panel is more a structural glazing product than a PV module with completely different applications and design goals.

3.1.2   Architectural integration aspects

The BIPV panels are essentially a laminated safety glazing with PV cells laminated between the glass panes. For building applications, panels with backsheet can be accepted, if the local control office accepts the different mechanical and fire safety characteristics, but normally this is outside

the structural safety regulations as mentioned in Section 3.1.1. The Figure 3.2 describes briefly the main types of BIPV with their BOM and effect on performance and potential applications.

To be able to integrate the glass into the architectural design of the building, the BIPV must be able to come in different shapes and colors. Since the BIPV is also producing solar electricity and potentially preheating air, the overall design task is to optimize between the power output and esthetics. Various techniques and products exist which are normally an industry know-how. Some basic examples are shown in the Figure 3.2.

- Opaque white;
- High reflectivity 2nd interlayer;
- Solar grade glass with anti-reflective coating;
- Highest possible electrical output;
- Limited-to-none façade integration opportunities.

- Opaque with black ribbons and black high reflectivity 2nd interlayer;
- Solar grade front glass;
- Reduced power output due to higher cell temperature, but higher heat recovery potential.

- Transparent laminate;
- Limited architectural integration, due to cavity visibility;
- Increased thermal performance, since air collector becomes glazed.

Figure 3.2: Examples of BIPV/EPoG glazing.

- Opaque, semi-transparent;
- 1st or 2nd interlayer is colored;
- Solar grade front glass;
- Limited number of available colored films and compromised electrical properties of the PV laminate;
- Power output is defined based on the film chosen.

- Patterned front glass;
- Surface #2 can be screen printed;
- Similar performance to glass with anti-reflective coatings;
- Limited products in market.

- Surface #1 or #2 digitally screen printed;
- Surface #1 can be etched, with anti-reflective coating, patterned;
- Patterns are limitless;
- Paint intensity and pattern defines the power output of the panel.

- Surface #1 or #2 digitally screen printed with single color;
- Surface #1 can be etched, with anti-reflective coating, patterned;
- Paint intensity can be varied.

- Special glass with anti-reflective surface #1;
- Spectrally selective high transmission coating on surface #2;
- Only several colors available;
- Data on durability not yet available.

- Colored patterns printed on surface #2 with lithography;
- Power output/visual performance is optimized varying the dot size, pattern, color and distance between the dots.

Figure 3.2: Examples of BIPV/EPoG glazing (cont.).

3.1.3 Façade integration aspects

Façade integration is a structural design task, common in glazing industry, covered by ISO 1288 "Glass in buildings" and other standards. There are four major types of glass fixation: clamping, adhesion, punctual fixation and linear fixation. Each type can be advantageous depending from the building structural and architectural requirements. For glazing industry this is a common practice, however for BIPV suppliers, this is an optimization and iteration process to find a compromise between the project architectural and technical requirements, like cell layout, glass thickness, color and power output, potential subsidies and necessity to comply with IEC and other PV and building integration standards.

Special particularities for the BIPV's are that the cabling paths. Several points that require attention are: 1. Building envelope water-tightness; 2. Installation, maintenance and replacement accessibility; 3. Cable lengths, sizes and voltage drops; 4. Junction-box types that exist in the market and are compatible with the glass fixation system; 5. Constructability; 6. PV array testing and commissioning.

Compliance with fire safety is an important detail. Generally each PV producer can perform a fire class testing for their products and mandatory in some cases (for example, to obtain a UL1703 certificate, fire class testing is mandatory). The fire class testing of a standard PV panel consists of *Spread of Flame* and *Burning Brand* tests, according to the results of which, the product receives a Fire Classification A, B and C according to UL1703 and IEC 61730-2 standards. For building added or integrated PV panel the minimum class is B.

However, glazing integrated in buildings is a subject to fire resistance classification for each country or state. Generally the requirements take into account separately the glass and laminate fire resistance classes, however as a building material, the BIPV is a subject to EN 13501 and DIN 4102

classification tests, which poses the same problem as the issues discussed in Section 3.1.1 – the additional testing of the same product for PV and building standards.

3.1.4 Life cycle analysis – cradle to crave energy, cost and ecology

The BIPV is an energy generating construction product. The standard methodology to evaluate the environmental impact of the EPoG is described in ISO 14064, ISO 1404/44 and PAS 2050 (ISO, 2006 a; ISO, 2006 b; PAS, 2011).

The CO_2 emissions during the production of the PV panel depend from the BOM used by the producer and also the producers utility energy mix. The carbon emissions per production stage and per component are shown in the Figures 3.3 for a product produced in Belgium (Issol, 2018). As can be seen, the largest amount of carbon share per production stage is from raw materials, accounting to 97%. This depends from the location the factory is in, for example, if a factory is in China, the manufacturing share would be significantly larger. This is reflected in the carbon emissions per component pie chart, where the cells are normally from Chinese or Taiwanese suppliers, whilst the rest of the materials are available in the EU region.

The production of green electricity contributes to reduction of the greenhouse emissions through its lifecycle approximately 0.6 tonnes/kWp installed depending from the location/local energy mix. The energy payback of the panels are within 1-4 years, depending on the installation (ISSOL, 2018).

By the end of the lifecycle of the product, the reduction of the CO_2 emissions can reach 17.6 tonnes/kWp, if installed in Norway, with a low carbon energy mix. In this case, the CO_2 payback is within 4 years. The energy produced is 30 – 150 times higher than needed for the BIPV production. After the end of the lifecycle, the product can be reused in the construction industry as a construction material as described in Section 3.1.5.

The BIPVs or EPoGs are, from cradle to crave, environmentally friendly, clean and safe materials, contributing to greenhouse gas emission reduction and clean energy production.
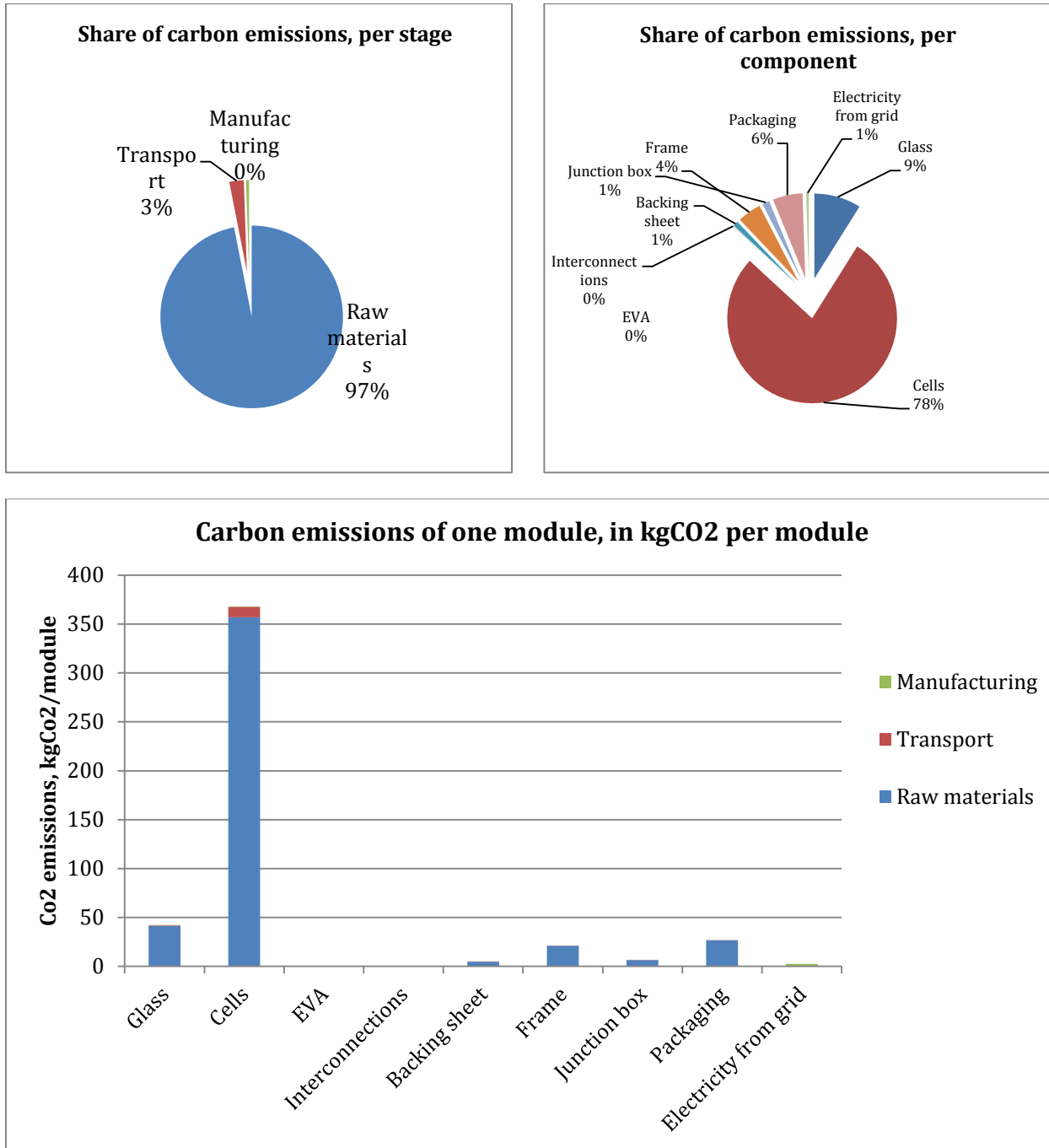
Figure 3.3: The CO2 emission calculations for a EPoG produced in Belgium following the ISO 14064, ISO 1404/44 standards.

3.1.5   PV and BIPV recycling

The BIPV panels have a lifetime of more than 25 years. In the initial stages of the life cycle of the product, the BIPV panels are producing green electricity, thus reducing the need for the owner to use electricity from the grid, reducing the CO_2 emissions for energy consumption. The product also acts as a construction material – a laminated safety glazing. At the end of the life cycle, the BIPV panels can be reused as laminated safety glazing for other structures or building materials (greenhouses or cold frames), the electronic parts (cables, diodes and junction boxes) can be reused or recycled as well. There is a possibility to recycle the laminated glass, by separating the interlayer from the glass, broken glass can be mixed with concrete to create terrazzo flooring, the melted glass can be melted and remanufactured into fiberglass or glass can be incorporated into glassphalt. More technical and economic solutions are possible and is a subject to active R&D as part of an circular economy cycle.

3.2   **BIPV/T prototype for prefabricated retrofit experimental and numerical study**

A multiple inlet open-loop building-integrated photovoltaic/thermal air collector was developed, assembled and tested in Concordia university Solar Simulator laboratory. This study main objective was to categorize an air based BIPV/T prototype using experimental data gathered in Concordia University Solar Simulator Laboratory. The BIPV/T prototype is made to be a modular plug and play solution for building façade applications. It is built as a prefabricated wall element using curtain wall extrusions to attach PV modules on the wall as exterior rain screen cladding. This concept enables air collection behind the PV panels. The air is preheated by cooling the PV panels, which increases the PV electrical efficiency and the warm air can be used in building HVAC system. This type of design simplifies the installation of BIPV systems over opaque areas of buildings and the prefabricated wall element can be used as a new building wall, roof or for as a retrofit solution if designed accordingly.

3.2.1 Experimental BIPV/T prototype

The experiments were carried out in an indoor solar simulator test facility to fully characterize the collector thermal and electrical performance. The BIPV/T wall prototype consists of 3x60 W 1030x548 mm monocrystalline silicon (c-Si) cell PV panels mounted on a standard insulated 5cm x 10cm stick wall with aluminum extrusions used in curtain wall industry to create a 7 cm gap for air circulation beneath the PV panels. Total area of the BIPV/T air collector test specimen was 1.73 m². PV array was connected in series. Multiple inlets are created for higher thermal and electrical efficiency. The thermal resistance of the insulated BIPV/T collector back wall corresponds to 2.13 m² . K/W. On the BIPV/T collector side's buffer panels were created, to replicate a continuous wall mounted on a building façade with same thermal conditions in the air channel, to eliminate heat transfer to the sides of the collector. Two PV panels were opaque with black polyvinyl fluoride (PVF) back cover and one was with semitransparent PVF back layer for better thermal efficiency. The PV panels were custom made in PV module manufacturer factory. The assembled prototype under test conditions is visible in Figure 3.4. This BIPV/T air collector prototype is open to ambient, meaning it is taking outdoor air in and preheating it for further use in the building.

3.2.2 Experimental setup

The experiments were carried out in Concordia University, Montreal, Canada, Solar Simulator and Environmental Chamber Laboratory. The experimental setup is shown in Figure 3.4. The test area is illuminated by a lamp field, which consists of 8 Metal Halide Lamps (MHG) with 4.6 kW maximum power each. These lamps provide a spectral distribution, which fulfills the specifications of standards EN 12975:2006 and ISO 9806-1:1664. The lamp field can be inclined from 0° to 90° and each lamp row can be moved electrically. Each lamp can be dimmed separately from 100% to 75% of maximum power output to achieve required irradiation levels and homogeneity over the test specimen area. The Concordia University Solar Simulator is able to achieve 1000 W/m² irradiance

with a homogeneity of +/- 5% for a 1.0x2.0 m specimen. Artificial sky, which is mounted on the lamp field, removes the longwave infrared radiation emitted by the high temperature MHG lamps, by circulating cooled air between 4 low-iron with anti-reflective coating glass modules. An X-Y scanner with pyranometer, solar cell and anemometer is used to measure the wind speed and irradiation levels over the test area. External wind is created by a ventilation unit with two cross-flow fans.

Air collection is performed with solar air collector test stand with volume flow range from 30-530 m^3/h. The system is open loop, seen in Figure 3.4, meaning it is taking room air as collector input for performance tests. This is a huge limitation, since not all necessary points for performance evaluation could be obtained, due to small temperature ranges inside the air channel, that are required by IEC 60904-5 or other relative standards. Improvement could be doing tests in environmental chamber with solar simulator or outdoors, but this increases the experiment time, due to weather and repeatability related issues. The setup includes orifice plate for pressure drop and mass flow measurements, pressure drop over collector measuring device, a temperature sensor to measure air mass temperature at the outlet of the solar air collector and measuring devices for absolute room pressure, humidity and temperature measuring. All of these values were measured every 15 seconds.

26 T-type thermocouples were used to measure temperature distribution on the back surface of PV panels, 47 thermocouples for back wall temperature distribution measurements, 22 thermocouples for air temperature measurements along and across the channel for air flow. These measurements were carried out every 5 second with +/-0.5 K accuracy. Additional thermocouples and RTD's were added to measure ambient temperature, inlet air temperature, air temperature above the PV panels along the collector. A total of 102 T-type thermocouples and 9 RTD's were used to measure the temperature distribution in the BIPV/T collector system. Also infrared pictures were taken at

steady state conditions to identify the thermal performance of the PV/T collector through infrared imaging studies.

The PV cells were connected to an electronic load that allowed to keep the PV operating at optimal power point. The load resistance had to be inputted manually through some iterations, thought. At steady state conditions quick switch to I-V curve tracer allowed to take the electrical output information of the PV string and plug PV panels to the electric load afterwards. For modeling purposes emissometer was used to measure the emissivity values of PV and channel back surfaces.

For mass flow model, air velocity inside the channel was measured at different mass flow rates and irradiation levels at different points in the channel, to identify the mass flow distribution in different BPV/T collector sections. The measurements were carried out with an anemometer with air velocity range from 0.1m/s up to 30m/s with accuracy of +/-2.0% of reading at every steady state. Some drawbacks of this measuring method were observed and more discussion about mass flow and wind effect for this BIPV/T air collector is done by Rounis et al. (2015).

To gather sufficient data for characterization of the thermal and electrical PV/T collector performance in an open-loop configuration indoors the prototype was tested in 25 groups under 134 different conditions, varying irradiation levels, mass flow rates, exterior wind speeds and dimensions of the inlets and air channel. All measurements were done at steady state condition. The time constant was 30 min +/-10min.

3.2.3   *Procedures to experimentally characterize the performance of the collector*

Measurements were obtained varying mass flow rate between 50-400 kg/hr, at three different exterior wind conditions (0, 0.6 and 2.5 m/s) and varying irradiation levels between 1010 and 535 W/m^2. The collector was at 90° tilt, simulating vertical façade application.
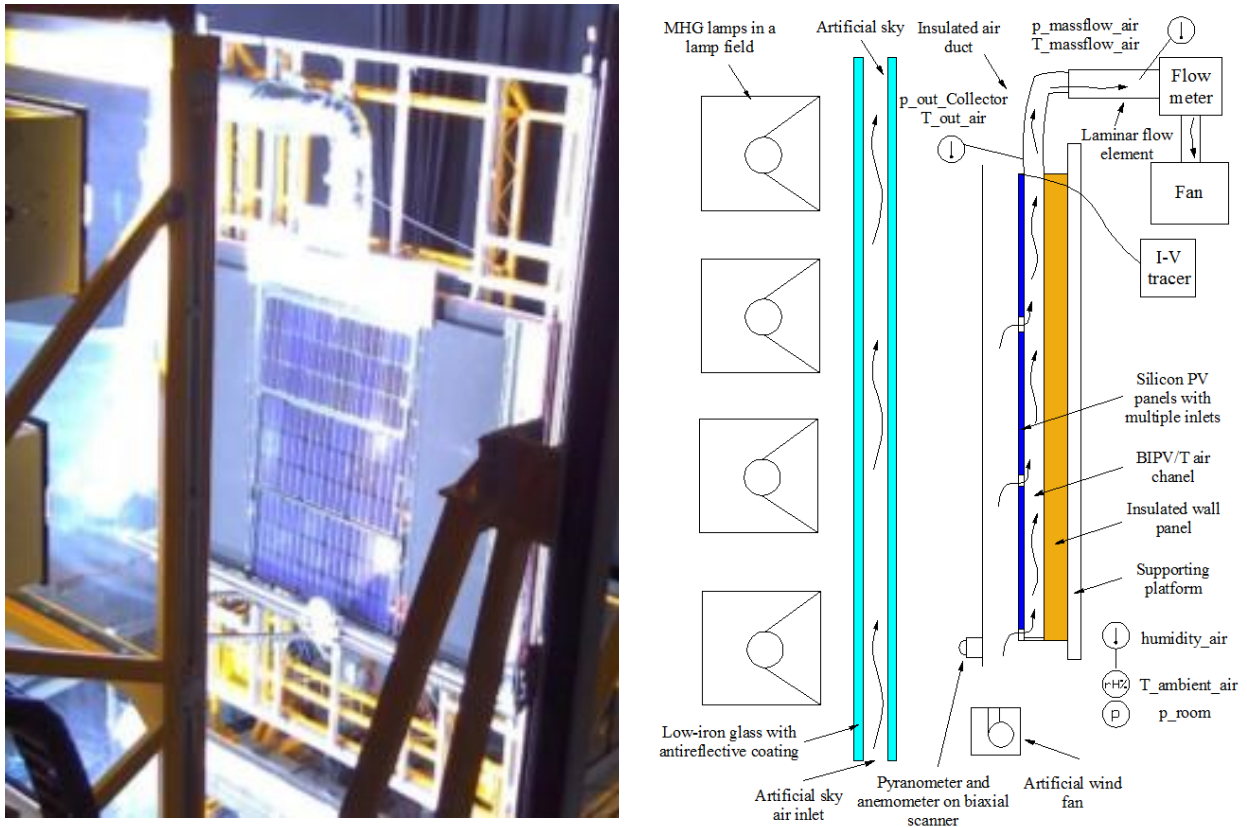
Figure 3.4: BIPV/T prototype experimental setup in Concordia Solar Simulator (left) and open loop setup schematics (right).

To characterize experimentally an open-loop multiple inlet building integrated photovoltaic thermal unglazed air collector in an indoor solar simulator 5-plot system was used (Delisle and Kummert, 2012). The results for measured cases are presented in the Figure 3.9 along the validated energy model simulation results.

The first plot is describing the thermal efficiency as a function of mass flow rate. One plot can be obtained only for one wind speed only. Thermal efficiency is calculated as show in equation 3.1. The second graph shows the temperature rise in the collector dependence from mass flow rate and irradiation levels. Temperature rise is the temperature difference between ambient room air temperature and temperature measured at the outlet of the collector. The second plot is obtained by varying mass flow rate levels at the same irradiation level. Plot three shows the temperature rise

and ambient temperature influence on outlet temperature. The outlet temperature and irradiation level influence to temperature of photovoltaic cells is shown in plot 4. And from photovoltaic cell temperature obtained in plot 4 and irradiation levels, maximum power point of the PV modules can be estimated.

$$\eta_{th} = \frac{m_o \cdot c_p \cdot (T_o - T_{in})}{G \cdot A}$$
\hfill 3.1

To characterize Photovoltaic cell electrical performance dependence from temperature, temperature coefficient was obtained measuring photovoltaic module average back temperature distribution and maximum power point production with I-V curve tracer at steady state conditions at the same irradiation levels and varying cell temperature by changing mass flow rates. This was done only for one irradiation level, but in future prototype testing, more irradiation levels will be used, for performance curves at different irradiation levels. This also applies for 5-plot system measurements.

The photovoltaic string efficiency dependence from temperature is presented in Figure 3.5. The average and highest back surface of PV temperature was used to compare the effect on the temperature coefficient correlation for the electrical output of the PV cell. According by IEC 60904-5, equivalent cell temperature must be used to obtain the temperature coefficients for PV cells. The procedure requires, that the PV cell temperature would be kept uniform and varied within 30°C while measuring the cell electrical output. In practice, with in multiple inlet PV/T collector this is impossible to achieve, since the variations of PV back surface are sometimes more than 30°C and since the tests are done indoors, the room temperature doesn't allow to vary the ambient temperature at the necessary ranges. That is why the average PV back temperature was used to obtain temperature coefficient value, later used in PV/T collector mathematical model. The temperature distribution in the range of 45 and 75°C was obtained by varying the wind speed and

mass flow rates. Based on manufacturer data, the PV cell efficiency is 18.30%, the PV module consists of 18 cells connected in series.
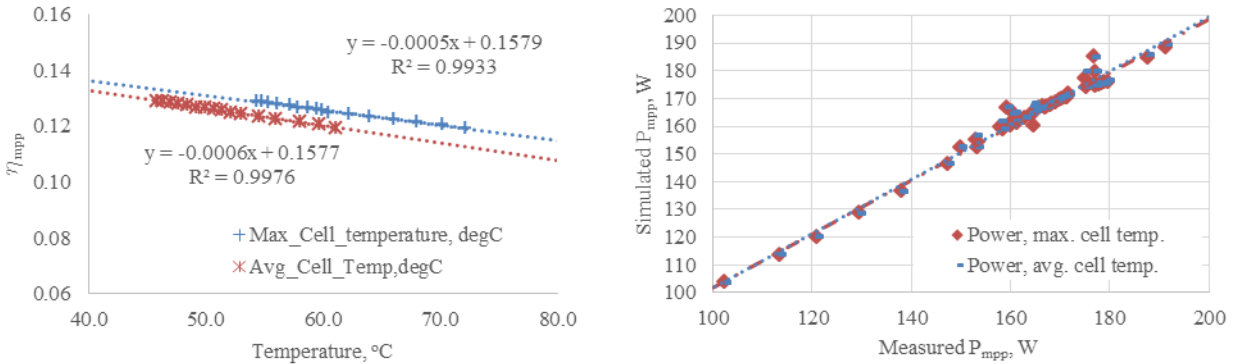
Figure 3.5: Estimated PV efficiency temperature modifier (left) and measured and simulated power of the PV string (right).

3.2.4 BIPV/T numerical modeling

A mathematical model based on experimental data was developed. BIPV/T system testing and modeling activities have been done based on previous experiences and findings of similar systems in Concordia University (Candanedo, 2010; Yang and Athienitis, 2014; Charron, 2006, Chen et al., 2007; Candanedo et al., 2007). This air collector design involves numerical models as follows:

- Optical absorption model
- Flow distribution model
- Thermal model
- Electrical model
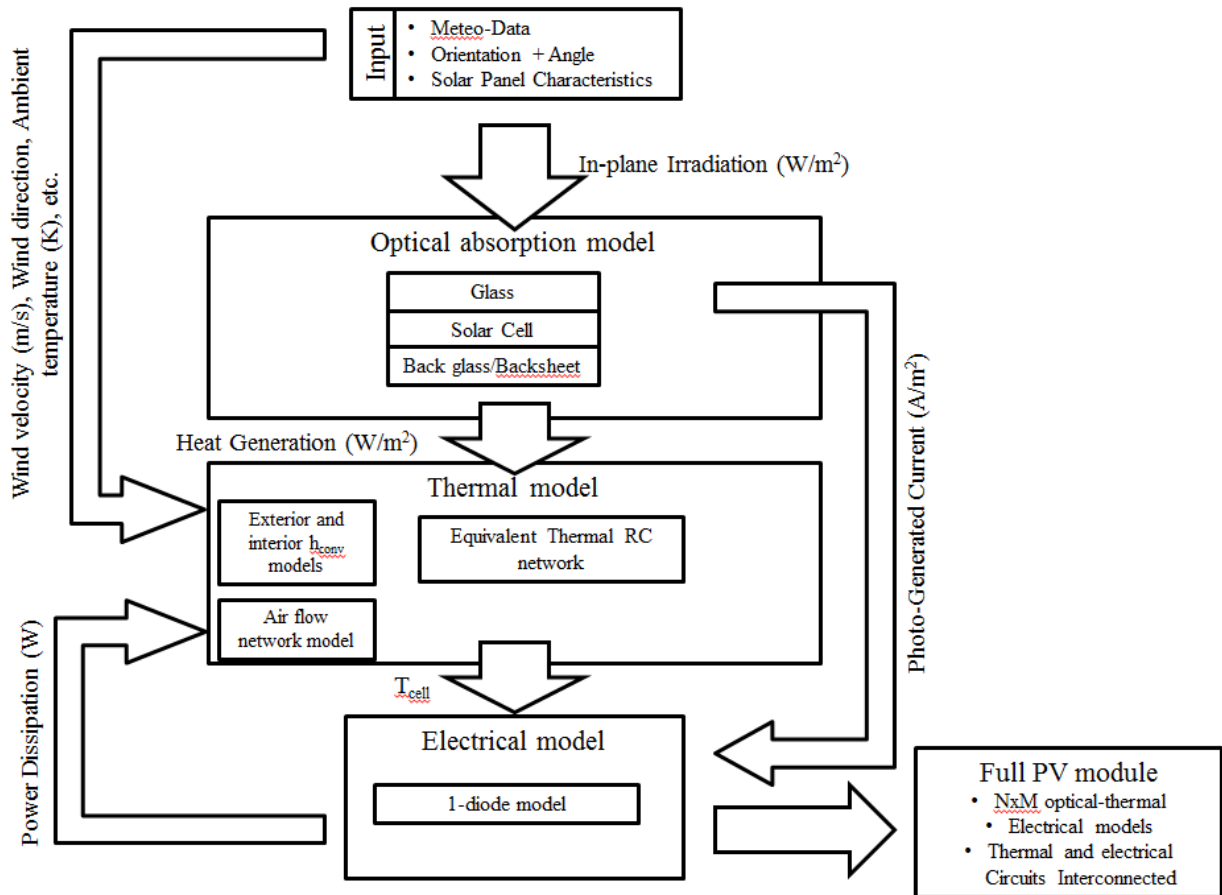
Figure 3.6: Schematic representation of the BIPV/T (EPoG) energy model.

Due to framed PV panels used in the BIPV/T prototype design a significant temperature rise of up to 20°C was observed at the first control volumes of the channel, where the outdoor temperature enters the solar air collector channel. To model this inlet heat exchange model was applied. The current model uses a correlation developed by Kutscher (1994), which gives a satisfactory result.

Flow distribution analysis in a multiple inlet solar air collector is one of the most important factors in this kind of collector modeling, since the thermal efficiency depends strongly from the mass flow rates in the air channel. Air collectors tend to be leaky and experimentally it was observed, that infiltration was a significant factor affecting the mass flow distribution ratios, which lead to different heat removal at different sections of the collector depending from air collection rates. This

shows that more research needs to be done on mass flow, pressure drop (including pressure drop due to framing systems) and leakage related modeling for multiple inlet air collector (Welz et al., 2013). These problems were addressed using flow network modeling by Rounis et al. (2015)

The applied model is a steady state one dimensional fully-explicit finite difference scheme. The details are described by Candanedo (2010). The exterior convective heat transfer coefficient is estimated using the Sharples and Chralesworth correlation for the experimental setup (Sharples and Charlesworth, 1998). Several correlations existing in the literature was applied to calculate a satisfactory interior convective heat transfer coefficient for the top and bottom of the collector channel (Candanedo, (2010); Yang and Athienitis, (2014); Dittus and Boelter, (1930); Bazilian et al., (2001)). The average Nusselt number coefficient correlations shown in equations 3.2 and 3.3 gives a satisfactory result for developed model comparing to experimental results (Candanedo, 2010) for Reynolds numbers between 250 and 7500.

$$Nu_{top} = 0.052 \cdot \mathrm{Re}^{0.78} \cdot \mathrm{Pr}^{0.4} \qquad\qquad 3.2$$

$$Nu_{bot} = 1.017 \cdot \mathrm{Re}^{0.471} \cdot \mathrm{Pr}^{0.4} \qquad\qquad 3.3$$

Interior and exterior radiative heat transfer was calculated using the exact value of the radiative heat exchange between two plates and is well described by Candanedo (2010) and Yand and Athienitis (2014). The view factor value is 1, since the plates are parallel to each other. For future model view factor calculations will be taken into account for radiative heat transfer modeling.

Electrical efficiency model is a simple linear model taking into account PV module efficiency variations due to temperature effect (Delisle and Kummert, 2012). In this model the PV string efficiency temperature modifier was estimated experimentally, applied and shown in equation 3.4.

$$\eta_{PV} = \eta_{mpp}(T_{PV,ref}) - \gamma_{mpp,ref} \cdot (T_{PV} - T_{PV,\mathrm{Re}f}) \qquad\qquad 3.4$$

To model this kind of collector, in addition to thermal energy, mass flow distribution through each inlet must be determined. For this a flow network model is created. The algorithm solves the flow and thermal network models iteratively until a global convergence is achieved.

The flow is modeled using pipe network analogy (Dymond & Kutscher, 1996). The pressure drops in channels from entrance losses, friction losses, wind created pressure drop, buoyancy, mixing and channel sudden contraction and expansion. The flow network problem is shown in Figure 3.7.
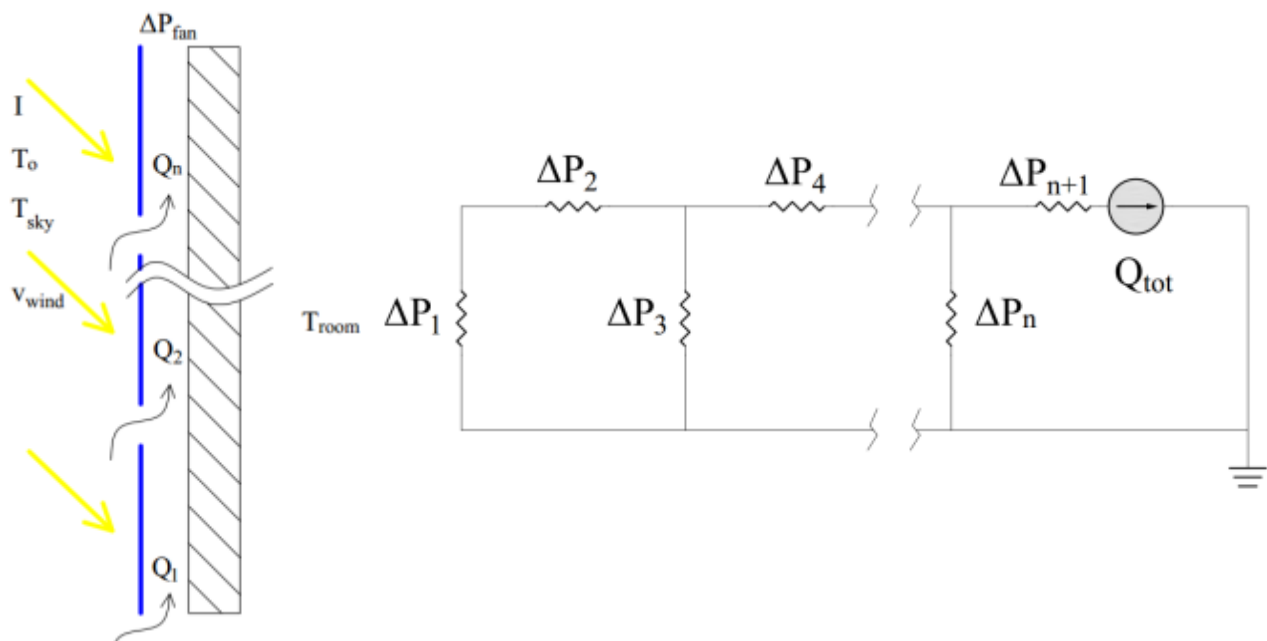
Figure 3.7: A multiple inlet BIPV/T air flow distribution representation using a pipe network analogy.

The main inputs for the BIPV/T air collector are obviously solar irradiation I, ambient temperature T_o, sky temperature T_{sky} and wind speed v_{wind}. The air collector is operated by fan created negative pressure in the channel ΔP_{fan}, which results in a certain distribution of mass flow rates in each channel Q_1, Q_2, ..., Q_n, which affects to total heat removal from PV panels and as a result thermal and electrical energy output. The goal in this case is to optimize the overall energy output by maximizing the heat removal from PV panels furthest from the fan, which have the highest total

pressure drop ΔP_1, ΔP_2, ΔP_3, ΔP_4, ..., ΔP_n. As reported by Rounis (2015) the highest energy losses are at the entrances through the inlets and framing in the air channel at each section end. The optimization is performed by reducing the pressure drop for the furthest inlets by increasing the inlet dimensions, thus allowing higher mass flow rates and as a result, higher heat removal from PV panels.

The model consists of conservation of mass equations and conservation of energy equations. Conservation of mass is expressed with equation 3.5 and conservation of energy is expressed with equation 3.6.

$$\sum_{i=1}^{No\ of\ flows} \rho_i Q_i = 0 \qquad\qquad 3.5$$

$$\sum_{i=1}^{No\ of\ p} \Delta P_i = 0 \qquad\qquad 3.6$$

The conservation of mass is expressed as volumetric air flows into and out of junctions of the pipes. The conservation of energy is derived from Bernoulli's equation and applied for steady-state incompressible flow by setting the sum of all pressure drops (change in fluid energy) around any closed loop equal to zero. For example for the first loop in the Figure 3.6, the energy conservation is described in equation 3.7.

$$\Delta P_1 + \Delta P_2 - \Delta P_3 + P_{wind1} - P_{wind3} = 0 \qquad\qquad 3.7$$

where ΔP_1 and ΔP_3 are pressure drops due to sharp edge entrances;

ΔP_2 is channel friction and framing pressure drops in the channel;

P_{wind1} and P_{wind3} are pressure created by wind at the inlet;

The entrance pressure drop is expressed by equation 3.8

$$\Delta P_i = \frac{C_D \rho_i v_i^2}{2} \qquad\qquad 3.8$$

where: C_D is the local loss coefficient, which needs to be experimentally obtained for each inlet design. Initially 0.6 is used.

ρ_i, v_i are the density and velocity of air bulk entering the channel.

The channel friction loss and the pressure drop due to framing is expressed with equation 3.9

$$\Delta P_i = \frac{f_i L_i \rho_i v_i^2}{D_{h,i} 2} + \frac{C_D \rho_i v_i^2}{2} \qquad\qquad 3.9$$

where: f_i is the friction factor;

L_i and $D_{h,i}$ are the length and hydraulic diameter of the channel;

C_D is the loss coefficient due to framing in the channel, which can be expressed as sharp edge entrance loss as well.

The wind pressure estimation methodology using flow modeling and wind tunnel tests is described by Rounis (2015) in his master thesis.

After the flow distribution is calculated, the obtained mass flow rates are used in the air collector model to estimate the temperatures of the PV surfaces and air bulk. The thermal network of the BIPV/T façade system is shown in Figure 3.8. Each PV section is solved as one control volume. The energy balance and relevant heat transfer correlations used are described in chapter 2.2.2.1, as mentioned. The model is transient and a fully explicit finite difference scheme is employed.
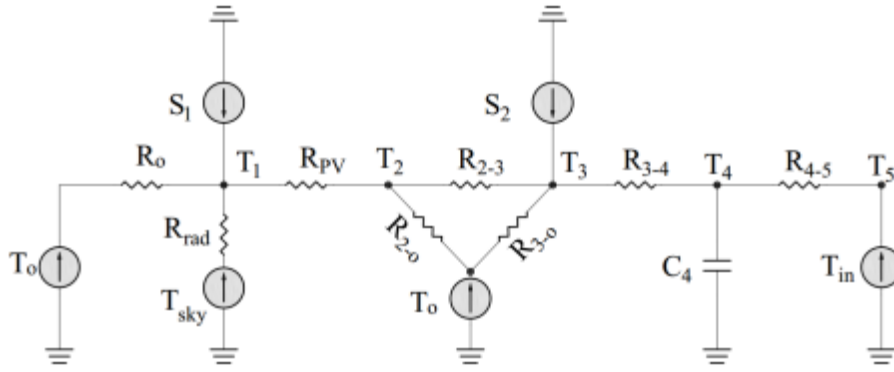
Figure 3.8: BIPV/T air collector thermal network.

Iterative process is used to reach convergence both separately for flow and thermal model and global convergence between both models, due to variation in air density from temperature. The system of equations is solved using non-linear equation solver in Matlab.

The thermal and electrical performance of the prototype is demonstrated in Figure 3.9 as a 5-plot adopted from Delisle and Kummer (2012). Since in a standard indoor solar simulator with an open loop system it is not possible to vary the external temperature, which is also the inlet temperature in an open loop air solar thermal collector, the possible performance points were collected and compared against the developed numerical thermal model of the collector. The limitations are that these plots apply only to the tested and simulated cases (one exterior wind speed value, ambient pressure and humidity values, PV cell mounting approach, etc.).
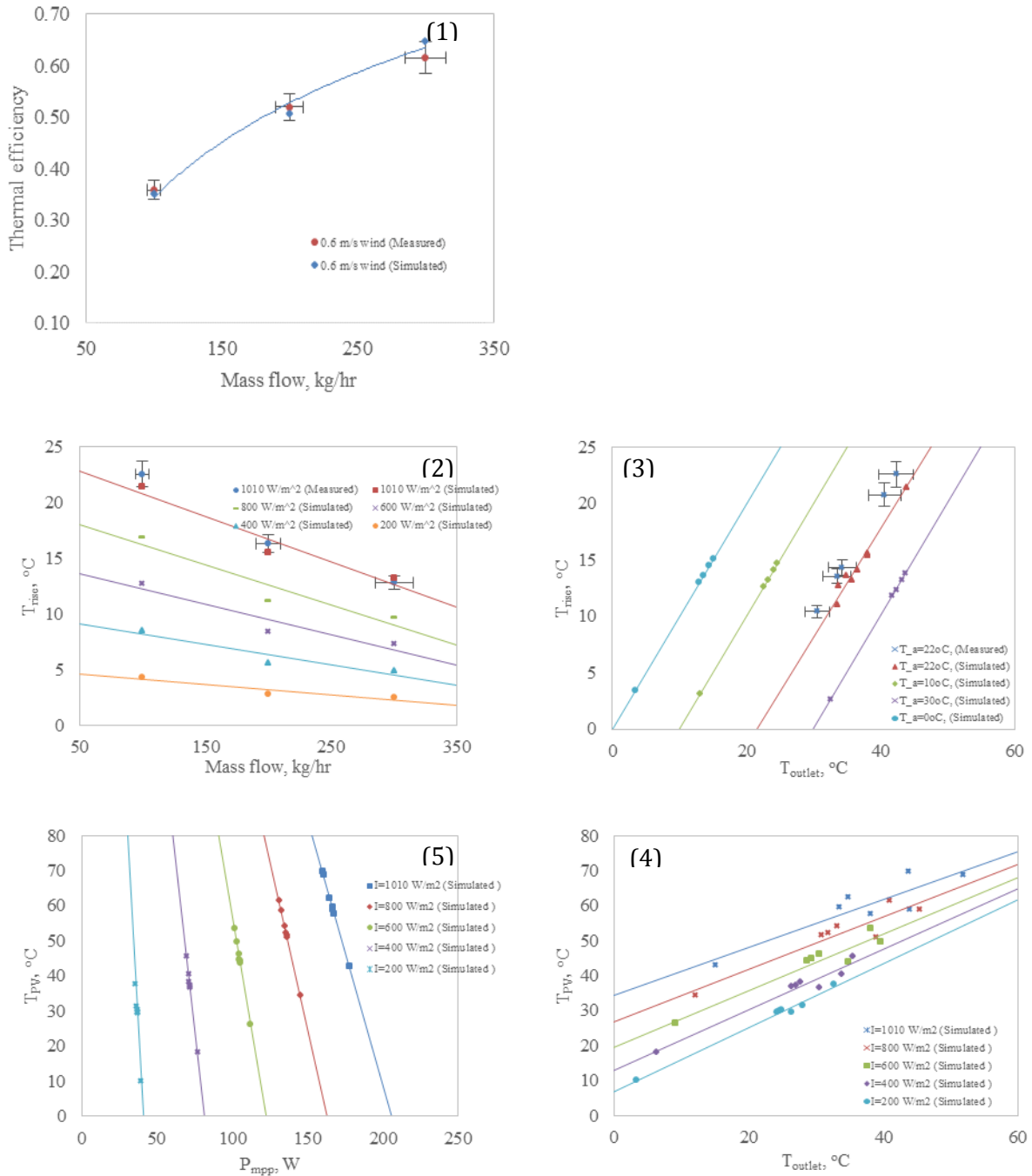
Figure 3.9: 5-plot system representing open loop air based BIPV/T collector.

3.2.5   Steady state parametric analysis of a BIPV/T output

The developed model was used to study several design parameters, to identify the sensitivity of several important design parameters for an air based BIPV/T solar collector for future prototype

improvements. The most important loss mechanisms in the air collectors are radiative loss to the sky, convective exterior loss due to exterior wind and the main useful heat removal mechanism is instigated by interior connective heat transfer, which is a function of mass flow rate and geometrical parameters of the channel that create various levels of turbulence and friction in the air channel at various air velocities. As a result, several parameters were identified that could help to further improve the performance of the prototype:

- Packing factor;

- Low-e coating;

- Gap thickness.

The developed air collector model was used for studies of these parameters. The inputs for the model are solar radiation, ambient temperature, sky temperature, wind speed, air collection mass flow rate, ambient pressure, relative humidity. Collector geometry (PV panel dimensions) and framing (PV frame and inlet dimensions) are constant, since in the "as-built" framed PV/T air collector model the convective heat transfer correlations used are not validated for different geometries of PV panels and frame shapes and inlet dimensions. This is an opportunity for further BIPV/T model improvement. The variables for this study are cavity depth, packing factor, optical properties of PV surfaces. The model calculates electrical and thermal output as mentioned before, using energy balance method. The results are given in the further sections.

3.2.5.1 Packing factor effect

The packing factor is the amount of PV cells mounted on the semi-transparent PV sheet and is expressed as a percentage of PV cell area over all PV module area. The tested PV modules had 18 PV cells wired in series with total of 78.7W nominal power at 21°C and 1000W/m^2 as measured with flash test by the manufacturer.

The full scale BIPV/T setup showed that the STPV modules had always a lower average PV panel temperature and higher thermal and electrical output. The proof of concept experiments, didn't allow to evaluate the packing factor effect on the BIPV/T performance, so the developed model was used to study this effect.

Simulations were done for a case with no wind, emissivity of the first BIPV/T surface of 0.89 as measured and 1000 W/m² irradiation on the surface with 0° angle of incidence. Mass flow collection rate is 200 kg/hr, which results in a 0.62 m/s average air speed in the cavity. The first case is the opaque PV panel with 18 cells wired in series and the second case is the STPV panel with 18 cells, which results in a 0.88 % packing factor. The simulation results output electrical and thermal power and efficiencies, PV module back (T_{bpv}), insulation surface (T_{insu}), output temperature (T_{outlet}) temperatures. The results are shown in Table 3.1. As visible, the STPV module with the same amount of cells outperforms the opaque one by 5 % from thermal performance point of view and a marginal electrical performance increase. This is due to the fact, that the transferred solar energy is absorbed in the back surface, which then reduces the convective losses to the ambient, since the PV panel acts as a glazing for the thermal air collector. Also the PV cells perform better, since the PV temperature is smaller, due to the transmitted portion of solar irradiation to the back wall, acting as an absorber. The simulation results are as measured by Yang (2015).

Table 3.1: Comparison of opaque and semi-transparent PV/T air collector performance.

Number of cells	Packing factor	T_{insu}	T_{bpv}	T_b	T_{outlet}	dT_{rise}	t_{eff}	Q_{Heat}	P_{elect}	el_{eff}
18	Opaque	10.0	30.4	1.8	3.1	3.1	34.8%	173.9	57.9	13.2%
18	0.88	17.9	28.1	2.1	3.6	3.6	40.5%	202.2	58.5	13.4%

The variation of packing factor results in change of the solar radiation transmitted through the PV glass and absorbed by the back insulation. The smaller the packing factor, the larger amount is transmitted and absorbed in the back surface, the larger the thermal output of the PV/T collector is.

This is achieved by having a highly absorptive back surface paint, a high transmittance PV glass layer and a high heat removal from the back surface using air. The smaller the packing factor, the smaller amount of PV cells is installed in the PV panels. This results in smaller photovoltaic electricity generation. A method to compare the PV/T configurations and find the optimal configurations is done analyzing the Instantaneous Solar Savings (ISS) for the specific locations with local fuel prices to study the potential benefits of BIPV/T design options. ISS is calculated as solar savings ($/m^2) = Heating fuel savings ($/m^2) + Electricity fuel savings ($/m^2).

Heating and electricity fuel savings are solar savings of heating and electricity fuel per Wh, not taking into account the BOS costs, property taxes, insurance and maintenance and other costs associated with the BIPV/T system price, operation and maintenance. For this example, the energy prices and values used for energy conversion are given in Table 3.2, representing the Montreal area fuel prices for 2014 year (Hydro Quebec, 2018; Energir; 2018).

Table 3.2: Energy prices for Montreal for 2014 year and hypothetical costs for comparison.

Electricity price, $/kWh	Natural gas price, $/kWh	Oil price, $/kWh
0.0722	0.05	0.09
	Natural gas price, $/m3	Oil price, $/l
	0.47	1.03

From energy point of view, the packing factor decrease can result in an almost 50% increase in thermal efficiency and around 1% increase in electrical efficiency, as well as reduced total electrical power, due to lower number of cells installed. The trends are shown in the Figure 3.10.
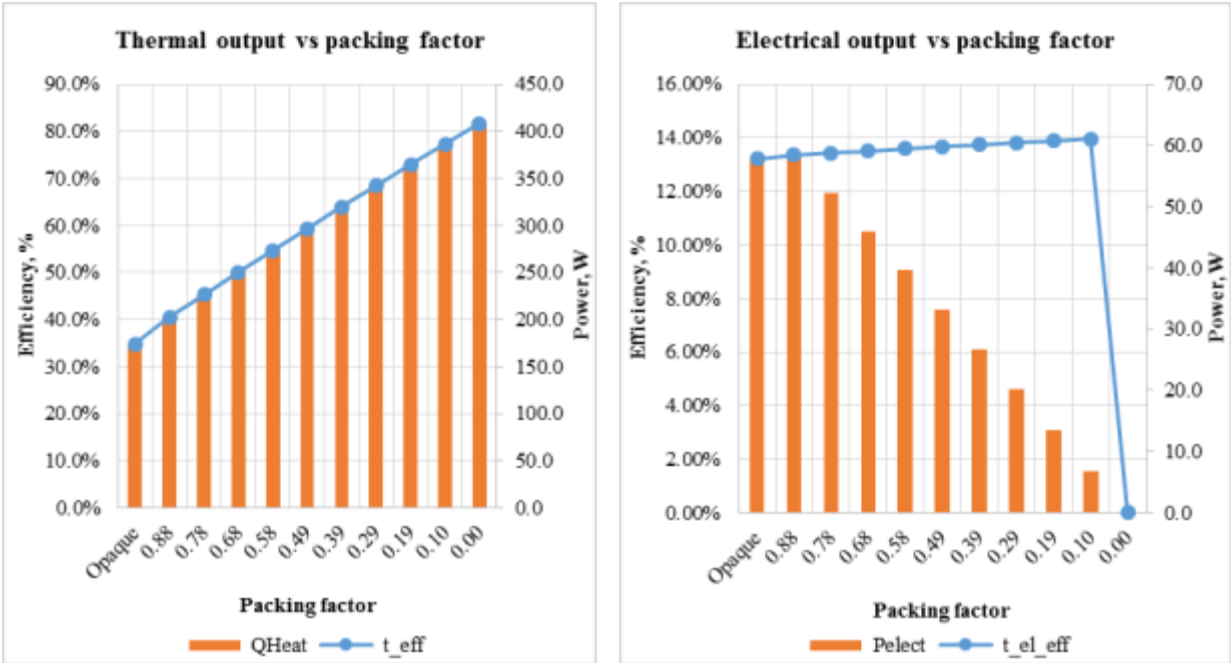
Figure 3.101: Packing factor effect on thermal (left) and electrical (right) outputs.

The reduction of PV cells mounted on BIPV/T façade gives a large amount of flexibility in finding the most feasible solutions for solar facades, since the photovoltaic system can lead to larger investment rates. The economy of the BIPV facades is a case specific design problem, depending from the local energy prices, governmental incentives for PV and solar systems, existing rebates, etc. For the design purpose of BIPV/T the proposed solar saving is used, which is calculated as mentioned above. For the case of Montreal, with electricity price being 0.07 $/kWh and electricity used for heating and power, the lowest packing factor makes most sense, since the produced electricity doesn't result in large savings. For the case, where electricity prices are high, higher packing factors start to be more feasible, since the solar savings become higher, due to higher electric and thermal fuel savings. The results are shown in Figures 3.11 and 3.12.
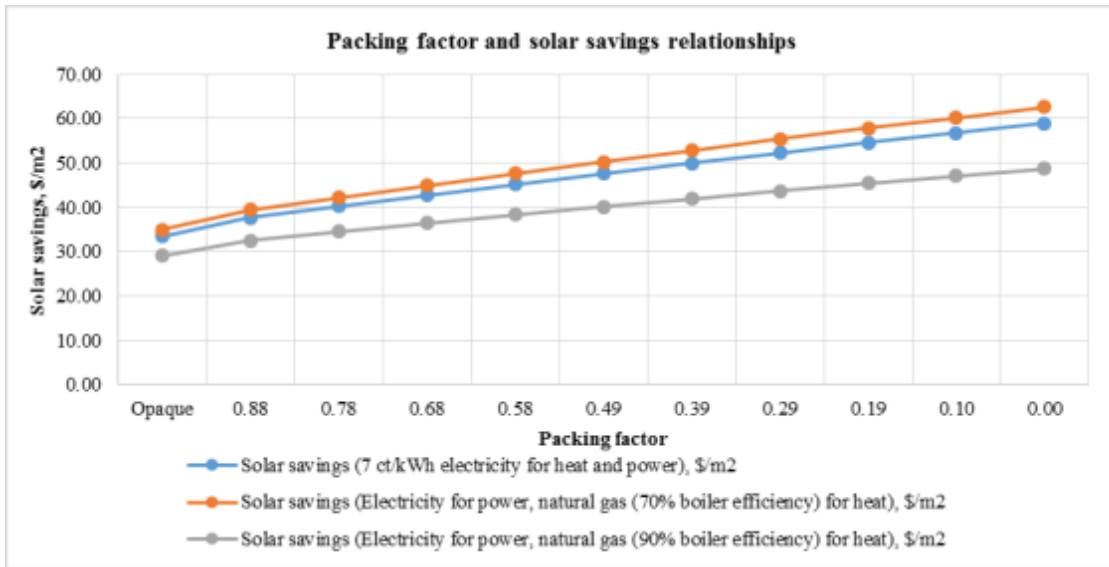
Figure 3.11: Packing factor and solar savings relationship for all electric and electric and natural gas systems.
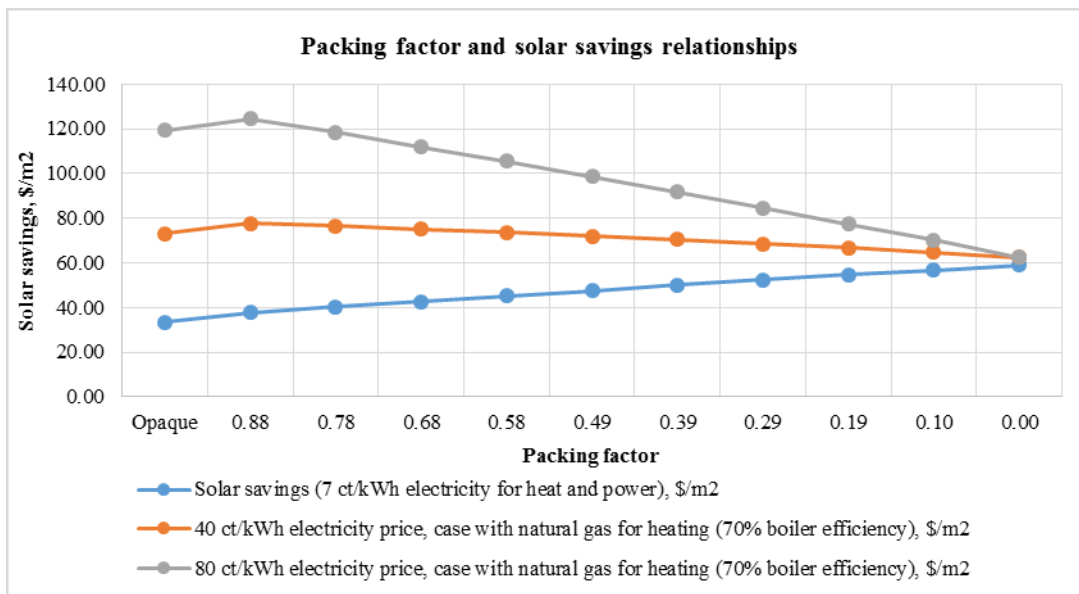
Figure 3.12: Packing factor and solar savings relationships for different electricity price cases.

Exterior convective losses due to wind are significant in the case of BIPV/T systems, since the PV panels act as an absorber. For façade integrated systems, the exterior wind speeds are high, resulting in large convective heat transfer coefficients. If STPV panels are used, then the back

100

surface acts as absorber, thus resulting in lower convective losses to the ambient. Figure 3.13 shows the packing factor and wind speed effect on the thermal BIPV/T air collector efficiencies. As can be seen, the lowest thermal efficiency is for the opaque panel and the increase of exterior wind speed results in nearly 20% drop in thermal efficiency. For the cases with lower packing factors, the thermal efficiencies are higher and also the loss due to wind speed is reduced from nearly 20% to less than 5%.
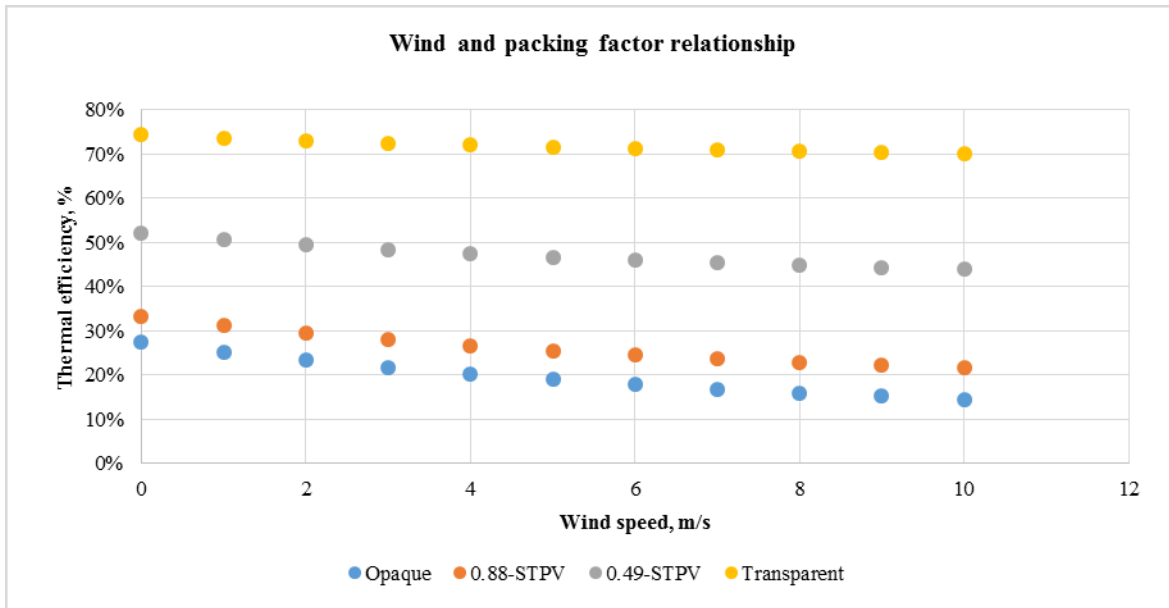
Figure 3.13: Wind speed effect on BIPV/T with different packing factors.

3.2.5.2   Air channel height effect

The reduced air channel height results in larger air velocities in the air cavity, which results in larger thermal efficiencies for the same mass flow rates, since higher convective heat transfer coefficients are achieved. On the other hand smaller gap thickness results in larger pressure drop in the channel. The gap thickness must be optimized for the thermal efficiency and pressure drop. In the case of STPV panel, the mullion height also results in shading losses at higher incidence angles as seen in Figure 3.14. Also, the mullion height is a variable that needs to be optimized for lowest shading loss, which is a tangential relationship with height of the mullion.
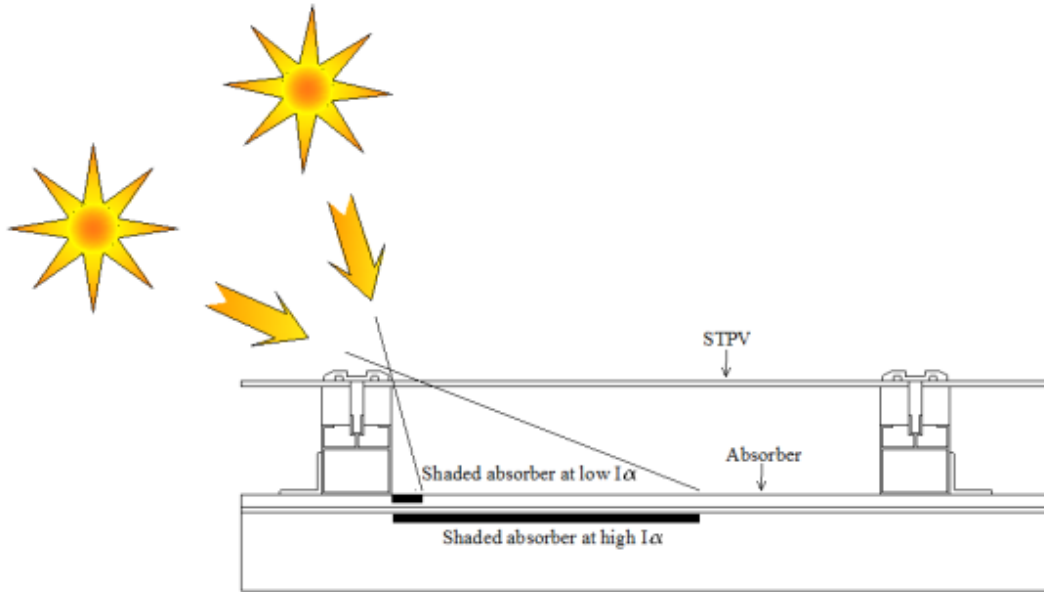
Figure 3.14: Shading loss due to mullion at different solar incidence angles.

Thermal efficiency dependence from air channel thickness is shown in Figure 3.15, where the fan consumption is plotted on the secondary axis. It is visible that channel thickness below 0.05 m gives a rapid thermal efficiency rise, but also the fan power consumption increase is exponential and goes from nearly negligible 0.09W to 12W for 200kg/h mass flow rate. The following graph shows the relationship of thermal efficiency to channel gap and also the effect of angle of incidence.
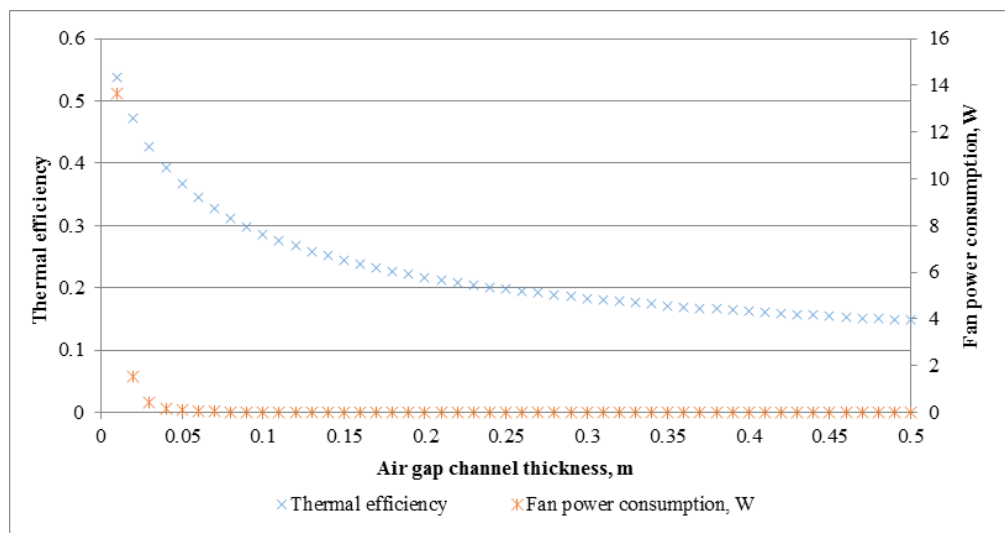
Figure 3.15: Thermal efficiency and fan power consumption relationship to air channel thickness.

Figure 3.16 is created for a BIPV/T with 0.88 packing factor and 200 kg/hr mass flow rate at 1000W/m² irradiation. For smaller packing factor values, smaller amount of solar radiation is absorbed by the PV cells and the shading effect as a function from mullion height is increased, since larger amount of irradiation is transmitted through the PV glass and absorbed by the back of the wall or shaded due to mullions at high incidence angles. For this specific case the engineer can optimize the channel gap looking into the fan consumption effect and shading effect to have the best combination of both factors. In practice, the BIPV/T mounting is not only optimized for the fan consumption, but also for structural properties. Also, for framed systems, the friction losses are higher with higher mass flow rates due to increased dynamic pressure drop at the inlet. For the simulated case the optimal range is 0.05-0.16 m, since with smaller gaps, the fan consumption is too high and for larger mullions the shading losses become significant at angle of incidence of 70 degrees.
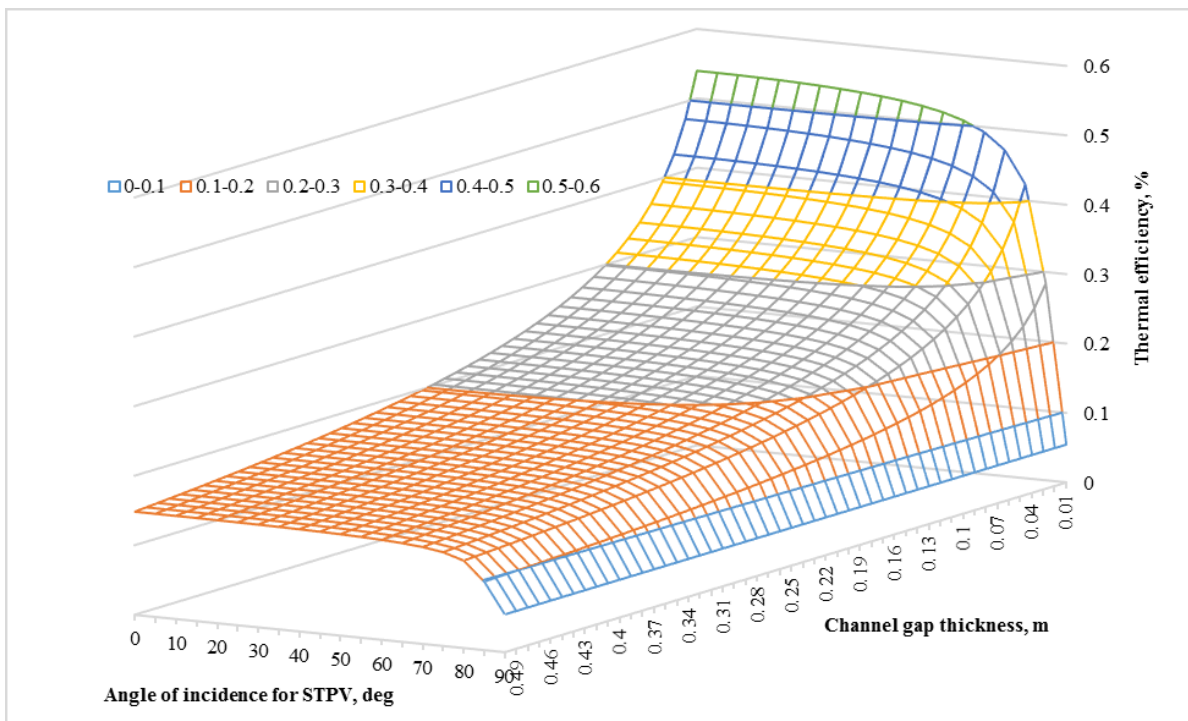
Figure 3.16: Thermal efficiency dependence from channel gap thickness and angle of incidence for BIPV/T with 0.88 packing factor.

3.2.5.3 *Low emissivity coatings on exterior surface of air collectors*

Radiative losses from the PV surface to the sky results in nearly 20% of the thermal efficiency loss. This can be controlled using low emissivity for long wave thermal radiation and high transmissivity for short wave radiation coatings, called selective low-e coatings. Innovations in selective coating technologies can help to improve the air collector performance by applying low-e coatings on exterior surface of BIPV/T air collectors. Selective coatings are used for solar thermal collector absorbers already, but the difference is, that they are used on the inner surfaces of the collector and not exposed to ambient conditions, which soft low-e coatings are sensitive to. A diamond like carbon selective low-e coating was developed by Mahtani et al. (2011), who demonstrated physical capabilities of being used on exterior surfaces of windows or solar collectors. A simulation was carried out using a constant transmissivity value and variable emissivity from PV to the sky value to determine the potential of using these coatings with respect to thermal and electrical efficiency. The simulation was carried out varying the emissivity value from 0-90% and observing the effect on performance of the collector for different sky temperatures.

As seen from Figure 3.17, the increase in thermal efficiency from 5-10% is possible with additional selective low-e coating strategies, with increased transmission values and reduced emissivity values. On the other hand the electrical efficiency drops with added coating, since the PV temperature increases. The efficiency drop is from 0.3-0.7%.
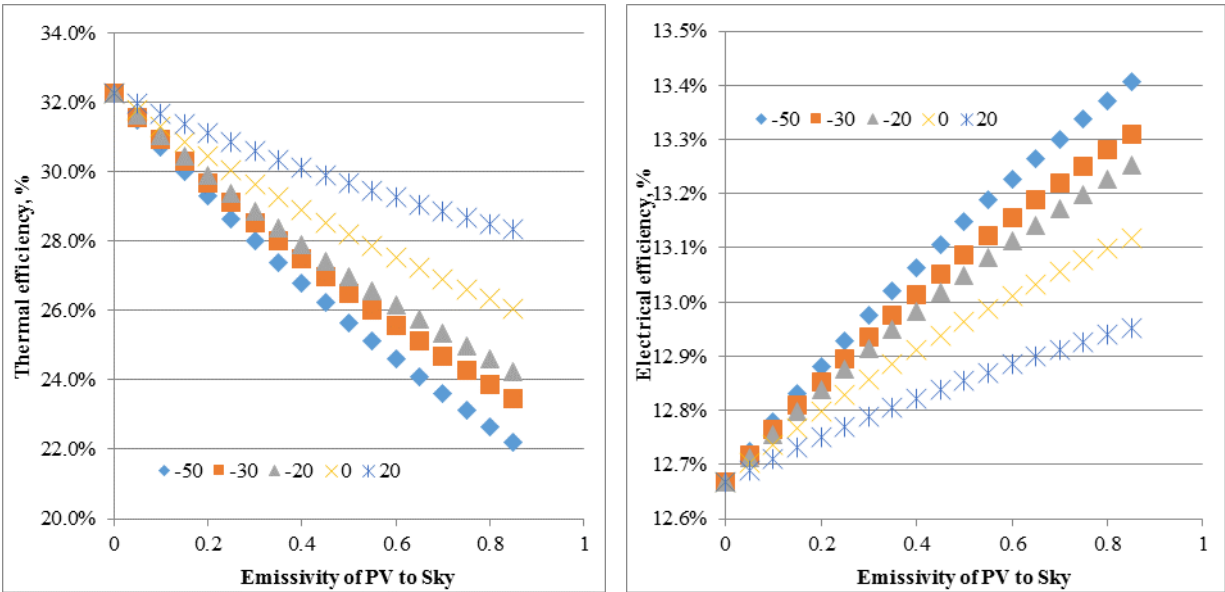
Figure 3.17: Thermal and electrical efficiency variation from different emissivity and sky temperatures.

3.2.6 Optical performance of EPoG glass

The optical absorption model is essentially a transmission coefficient of the front glass. This coefficient variation is significant in the case of BIPV (EPoG), which depends from the type of the front glass that is used. As mentioned in Section 3.1.2, some of the main architectural integration criteria are shape and color. Several parameters were studied within the Horizon 2020 project Smart-Flex (2017) for dotted patterns described in Section 3.2.6.1 and a spectral measurement study of several glasses suitable for BIPV (EPoG) carried out in the Applied Research Institute for Prospective Technologies (Protech) in Vilnius, Lithuania as part of this thesis.

3.2.6.1 Paint intensity effect

The paint color and intensity has an influence of the glazing optical performance and as a result output of the PV cells. Measurements of glazing electrical performance was done within a project Smart-Flex (2017) with glazing with dots painted in custom patterns with different levels of opacity and intensity on the glass. Several sample glasses are shown in Figure 3.18 and the output summary

is shown in Figure 3.19. As can be seen, certain levels of opacity, can result in electricity production losses only within 80%, while visually appearing as an opaque colored glazing.
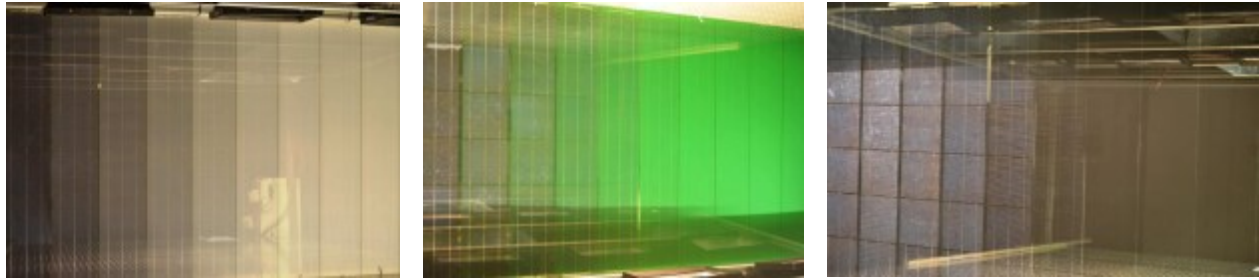
Figure 3.18: EPoGs with dotted patters measurement samples within the Smart-Flex (2017).
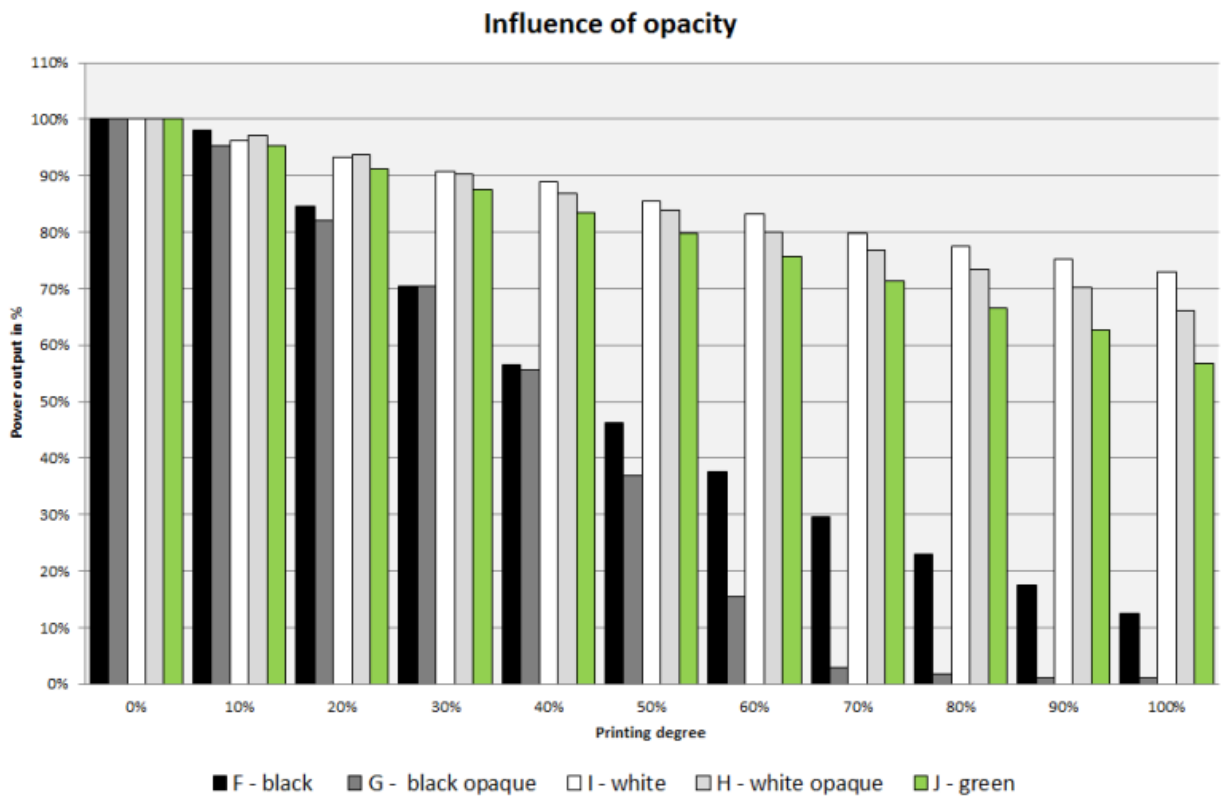
Figure 3.19: Paint intensity and color effect on the output of the EPoG power output compared to reference case with extra-clair glass.

3.2.6.2 Spectral transmisivity of painted glass

The tests to identify the spectral transmisivity of several types of glass used for EPoG were carried out for the glass samples shown in Table 3.3. As identified in Section 3.2.6.1, the effect of the color and opacity of the paint, has a significant influence on the overall output of the PV cells behind this glass. The cell spectral response is not the same for all producers, since the newer cells tend to have a higher spectral response in the low UV region. Generally a good BOM selection practice involves a good material compatibility and spectral matching of the front glass, encapsulant and cell is one of the main steps to reach for higher peak output of the PV modules at STC conditions. The measurement data here should serve as a reference for engineers wiling to optimize the power and esthetical outputs of the BIPV's (EPoG's). Results of the spectral transmisivity are shown in Figure 3.20.

Table 3.33: EPoG front glass samples selected for spectral transmisivity measurements with the RAL and pain intensity level.

| RAL9010 60% | RAL5026 60% |
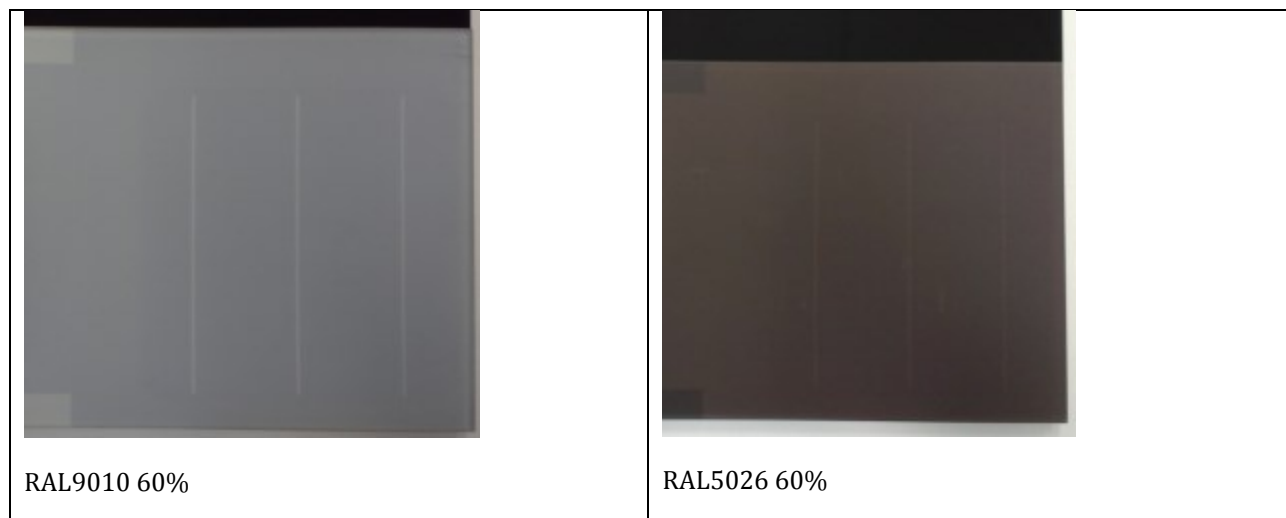
Table 3.33: EPoG front glass samples selected for spectral transmisivity measurements with the RAL and pain intensity level (cont.).
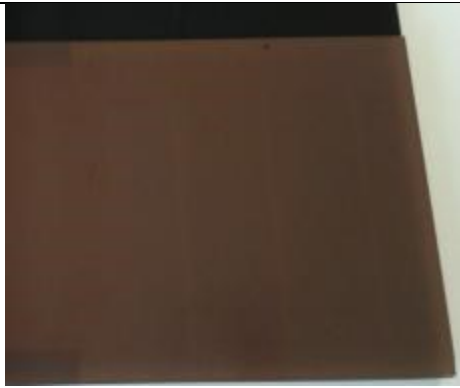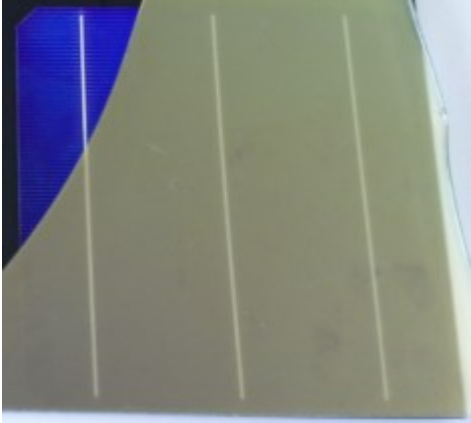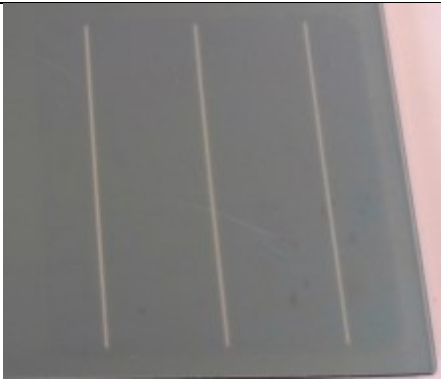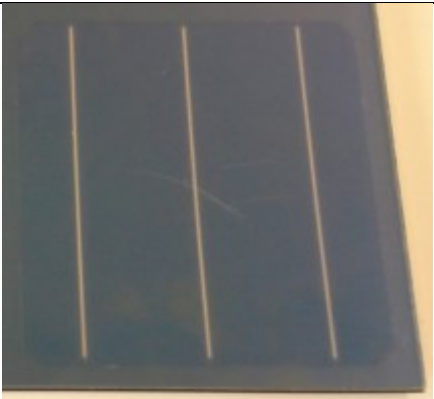
RAL3007 60%	RAL7033 60%
RAL5025 60	RAL1001 60
Kromatix GREY	Kromatix Terra Cota

Table 3.33: EPoG front glass samples selected for spectral transmisivity measurements with the RAL and pain intensity level (cont.).

Kromatix GREEN	Kromatix BLUE
Maristika Matt L	Maristika Matt Sm
FLOAT GLASS	
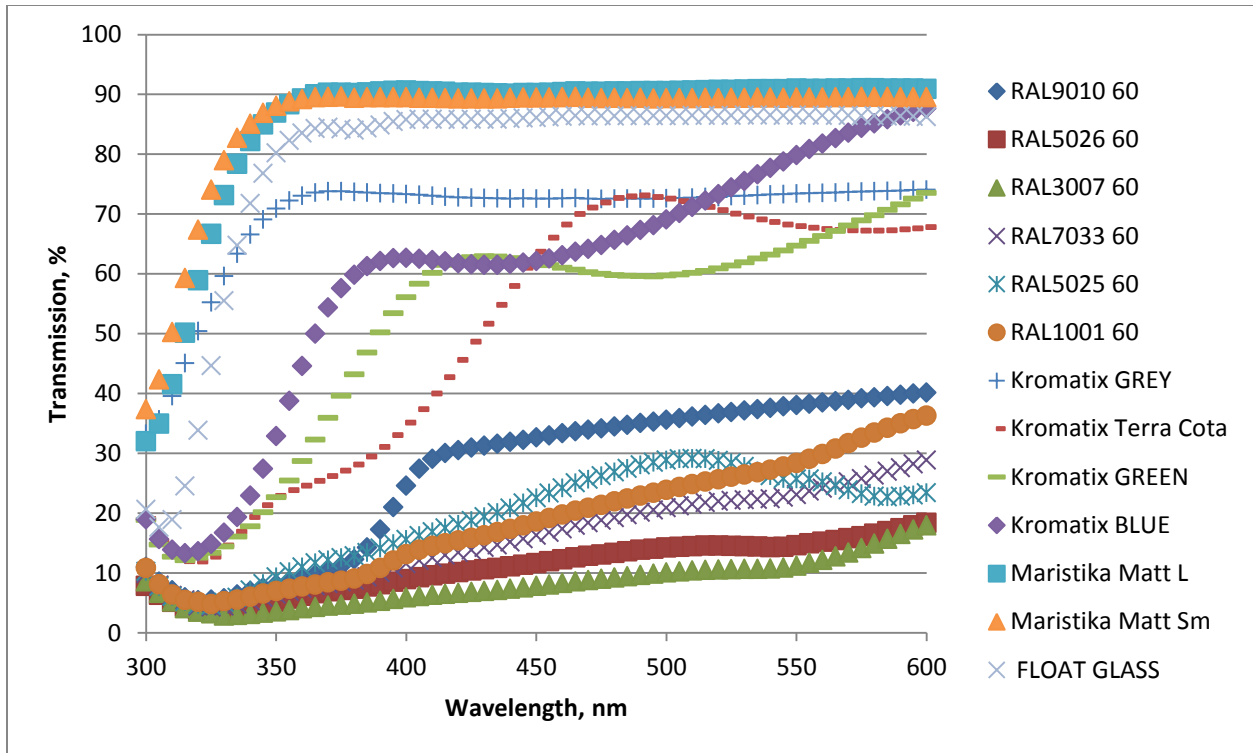
Figure 3.20: Spectral transmission of different glass types used for EPoG design.

3.2.6.3   Transmission of the front glass expression in the model

The spectral measurement data can be used as an input in the equation 3.10. Since the spectral measurement is not always available, the theoretical methodology suggested by Frontini et al. (2016) can by applied:

$$\tau = \tau_{tr} * \tau_{co} * \tau_{pat} \qquad\qquad 3.10$$

where:

τ_{tr} - is the transparency of layers in front of the cells (0 – 0.95);

τ_{pat} - is the transparency of glass surface pattern (0 – 1);

τ_{co} - is the transparency of layer's color (0 – 1);

$$\tau_{co} = 1 - (0.40 * LRV) \qquad\qquad 3.11$$

where:

LRV - is the light reflectance value and can be found in paint datasheets.

3.3 Conclusions

A BIPV module design methodology was presented in this chapter. Several design challenges/limitations were mentioned, like the IEC certification for PV modules, which results in limitation of the design possibilities for the BIPV or EPoG producers. This can be viewed as design flexibility limitations. Some EPoG designs were developed and applications presented in Section 3.1.3. Life cycle analysis for the modules was carried out to demonstrate the energy and CO2 paybacks, which are within 4 years for a plant in a country with low carbon emission utilities.

An open-loop air-based BIPV/T solar collector prototype study was carried out. One of the limitations of the air-based PV/T collectors is the lack of standard product performance characterization methods. One of the methods suggested is the 5-plot system, where the main electrical and thermal performance parameters can be mapped.

An experimental prototype of a multiple inlet BIPV/T solar air collector was designed, constructed and the performance characterized using the 5-plot system in the Concordia Solar Simulator laboratory. A numerical model was developed, validated and the model was utilized to perform a parametric study on the design parameters of the BIPV/T air collector. It was observed, that the BIPV/T collectors with STPV module outperforms BIPV/T with opaque module and the same amount of cells by 5 % in thermal efficiency and 0,2% in electrical efficiency. The cell number per module (packing factor) demonstrated a significant effect on the thermal efficiency and a reduced loss from wind with smaller packing factors. A method to optimize the BIPV/T thermal and electrical outputs was suggested using the Solar Savings factor.

The existing BIPV/T model was improved with the optical model to take into account one of the main architectural requirements – colored glazing. A study on the optical performance of the front glazing produced for BIPV applications was carried out. Spectral transmission was measured and the colored BIPV glazing was characterized. Parametric study was carried out for glass with different painting intensity and color. A method to calculate the transmission for other types of glazing is proposed in Section 3.2.6.3.

4   Solar façade potential in a cold climate office building retrofit case

Chapter abstract

Retrofit of existing buildings, as an evolving field of research, represents vast possibilities for increasing the energy efficiency of buildings. Façade design plays a crucial role in the retrofit of a building, and can offer additional benefits by incorporating possibilities of energy production. A façade retrofit study was carried out alongside a thorough analysis of a solar façade application for several different climatic conditions in Canada applying a developed methodology.

A multi-zone energy model of a commercial building was created to simulate the energy consumption after façade retrofit. Energy models of solar façade and building-integrated photovoltaics (BIPV) were created to investigate the energy and cost efficiency potential of solar electricity and heat generation.

It was observed, that in the sunny and cold Prairies climate with 5831 heating degree days (HDD), addition of a façade-integrated spandrel and shading BIPV elements on south, west and east facades can be a cost and energy efficient retrofit strategy alongside conventional façade insulation measures. For the less sunny and warmer Pacific Coast climate with 2501 HDD, the façade insulation measures are less cost and energy efficient, than an addition of a spandrel-integrated BIPV. And for sunny and cold Great Lakes/St. Lawrence climate with 4457 HDD the façade insulation measures are more effective than for the other two climates.

4.1   Introduction

Future buildings must consume less energy, provide comfortable environment for their occupants and be resilient. A design goal of being net-zero or grid independent is an important future research

and engineering challenge due to predicted supply shortages of traditional energy sources and the need to reduce GHG emissions (EUROSTAT, 2012).

To achieve this, the deployment of urban-scale new and renewable energy systems integrated in energy efficient high-quality buildings is necessary. These building envelope integrated systems can contribute to demand reduction and create flexible demand profiles, which can facilitate the integration of energy supply technologies using intermittent variable renewable energy sources (Bigaila and Athienitis, 2017).

The integrated design can be performed using appropriate detailed dynamic models to be able to benchmark various innovative advanced façade design concepts.

This paper describes a simulation based solar façade design methodology applied in a façade retrofit projects. It consists of three main parts: demand reduction strategies, application of solar technologies integrated in a façade and a techno-economical analysis taking into account different urban density levels.

4.1.1   Envelope requirements for cold climate buildings

The need to retrofit old buildings lies in the fact, that energy use and energy related emissions from existing building stock is dominant compared to new – energy efficient buildings (Voss, 2000). Investing in conservation and efficiency measures in old existing (and new) office buildings reduces greenhouse gas (GHG) emissions, energy consumption costs, improves tenant health and productivity and increase the value of the building, which in turn create higher revenue for the building owner and/or renter (Martinez, 2014).

A significant percentage of existing building stock in both North America and Europe was constructed post-World War II era, which is characterized by strong structural systems, but inefficient envelopes, which as a result of abundant and cheap energy led to strong reliance on new

mechanical air conditioning systems of that time, displacing the use of passive design features, like natural ventilation, daylight harvesting and solar heat retention or rejection (Lechner, 2014; Martinez et al., 2000). In Canada there are approximately 83,500 non-medical commercial office buildings covering 147.5 million square meters of floor space and having an average energy use intensity (EUI) of 333 ekWh/m^2 (NRCan-OEE, 2013). 80% of Canada's non-medical office buildings were constructed before the year 2000, which results in 79% of the total commercial building related energy use (NRCan-OEE, 2013). Approximately 57% of these buildings had not undergone any type of retrofit by the year 2009 (NRTEE, 2009).

Reasons for a building retrofit can range from failure of building envelope, structure or mechanical components, need for increased comfort inside the building or energy performance requirements (Voss, 2000). It is recommended by Buildings Owners and Managers Association (BOMA) to consider the low cost solutions for retrofit first, like internal equipment replacement, controls, lighting retrofits, mechanical systems. (Gnanam, 2013). This approach is preferred, since estimated simple payback years are between 2 to 12 years (Gnanam, 2013). The issue with this approach is that if the envelope is not complying with existing requirements for U-values, air tightness, glazing type, appropriate solar control, window to wall ratios, etc. defined by provincial and local requirements, the total potential energy efficiency targets for the building may be not achieved. Both commercial and residential building's energy use for heating, cooling, ventilation and lighting accounts to more than 50% of the total energy consumption in the building, which is directly linked to façade design and performance (Bigaila et al., 2016).

A high performance façade is capable of not only separating the indoor environment from outdoor, transmitting daylight and solar heat, but also assisting or replacing oversized ventilation, heating and cooling systems, adapting to changing climate conditions and generating and storing energy (Quesada et al., 2012).

4.1.2   Solar façade design in a retrofit project

For this study a commercial building façade retrofit project in several Canadian climates is considered. An integrated energy model was developed to search for a techno-economic optimum between the energy saving methods of envelope retrofit and energy generation with envelope-integrated systems, such as building-integrated photovoltaics (BIPV) also referred as energy producing glazing (EPoG), second skin facade, solar shading and semi-transparent photovoltaic windows (STPV).

Design guidelines are scarce for such projects and this research study in part addresses this need. The majority of existing buildings lack proper documentation and necessary performance data. Consequently developed building models are with high uncertainty (Heo et al., 2012). Usually, a perceived optimal retrofit case is chosen based on a compromise between cost and estimated performance, which is usually done based on the expertise of the designers (Rysanek et al., 2013). Estimations are done using building energy models and in order to choose optimal retrofit approach several methodologies exist: physical modeling and optimization techniques using third-party automated programs (Christensen et al., 2006), quasi-steady-state building energy models for (usually) single zone energy balance to quickly estimate the energy performance of a larger set of retrofit options (van Dijk et al., 2005) and high-fidelity surrogate models based on regression techniques (Rysanek et al., 2013; Eisenhower et al., 2012). Existing retrofit toolkits can be empirical data driven, normative or using advanced energy tools with pre-simulated building model databases. These toolkits are usually limited to existing conventional retrofit approaches and emerging technologies are hard to evaluate, if multiple retrofit measures are considered and challenges with model calibration exist (Lee et al., 2015).

The use of solar systems for building retrofit application is still at an early research stage. Already, the solar systems for building heating and cooling are competitive from energy and life cycle cost

point of view (Henning et al., 2012). The mature solar thermal and photovoltaic systems are available for building integration and were applied in number of residential, commercial and industrial projects (Athienitis et al., 2011; Hastings, 1999; Zondag, 2008). However, they have not yet become a common part of most retrofit projects. The main reasons for low adoption of solar systems for retrofit projects are higher initial costs, lack of support from local policies, low local fossil fuel prices, lack of experience from designers, installers, suppliers, lack of installed capacity to observe long term performance and determine the durability and dynamic performance of building-integrated solar systems (Zhang et al., 2015).

In European context, an integrated study was performed for residential building refurbishment in three climates within the European HERB project (Eicker et al., 2015). It was observed, that for the Southern dry climate the envelope refurbishment investment benefit is moderate, while renewable energy integration has higher benefits. However, for the more northern regions of European continent, the envelope refurbishment specific costs were increasing in potential benefits and the opposite was the case for renewable energy sources. Another study for European temperate climate suggested that a refurbishment of a residential building façade retrofit with a second skin with PV has an investment payback time of nine years, but stated that fiscal incentives and high self-consumption are necessary (Evola and Margani, 2016). In the study it was mentioned as well, that better efficiencies, lower prices and higher self-consumption rates of solar electricity can enhance the economic profitability of such retrofits.

For successful deployment of photovoltaic systems in urban areas, assessment of local solar potential and estimation of partial shading can be performed using ray-tracing algorithms to predict the performance of various energy generating technologies, including solar, in the city boundaries (Bobinson et al., 2009; Bobinson et al., 2007; Sarralde et al., 2007), digital surface modeling of the urban region built with Light Detection and RANGING (LiDAR) surveys data linked

to Geographical Information Systems (GIS) (Esclapes et al., 2014; Redweik et al., 2013) or less complex engineering methods (Marquez-Garcia et al., 2013; Duffie and Beckman, 2006). A Tregenza sky model existing in TRNYS/SketchUp is used in this study to study the shading effect on façade solar system energy generation potential, due to reported high accuracy (Tregenza, 1987).

Photovoltaic panel on façade can be superimposed or integrated. Superimposed panels are installed over existing exterior cladding or other finishing and do not act as envelope component. Integrated panels act as envelope elements and can be a cold façade, hot façade or shadow device (Fuentes, 2007; Lai and Hokoi, 2015). Hot façade systems demonstrate lower electrical efficiency, since the PV modules tend to have higher temperatures at the same environmental conditions. The annual production difference depends on the type of PV cell used. For mono-crystalline cells the difference in annual electricity output of non-ventilated hot facade is lower by 7-13% as compared to optimally ventilated PV cladding or free standing PV rack respectively (Guiavarch and Peuportier, 2006). The heat from the PV modules can be recovered and used in non-residential buildings for fresh air preheating purposes (Bambara et al., 2011), thermally driven cooling applications (Mei et al., 2006) or stored (Chen, 2013). A prefabricated panel was developed for Portuguese residential housing façade retrofit applications with possible integration of PV modules on the exterior face and demonstrated low payback times (between 4.6-6.9 years) due to integrated design approach and combined savings of both retrofit and power production (Silva et al., 2013).

Exterior shading devices are an effective way of controlling solar gains. Depending on the type of building, climate, lighting demands, façade type and architectural requirements a number of technologies are available (Kirimtat et al., 2016). Appropriate design involves optimizing for cooling, heating and lighting energy consumption, thermal comfort in the space and glare management (Gugliermetti and Bisegna, 2006; Moeseke et al., 2007). Applying appropriate integrated design decisions and control strategies up to 45% combined annual energy demand

savings were demonstrated for Canadian climate compared to no shading and passive lighting control case (Tzempelikos and Athienitis, 2007). Integration of solar energy generation technologies such as PV panels or transpired solar thermal collectors on exterior shading devices can lead to additional energy generation (Maurer and Kuhn, 2012; Saranti et al., 2015).

PV products for non-residential retrofits were described in several studies, analyzing the integration approach, the energy balance of the solar system and the building, performance of the PV system and economic and/or environmental analysis (Voss, 2000; IEA, 2014). This work builds on the previous experiences and knowledge on solar façade design and modeling, focusing on applying an integrated design approach to evaluate the solar system potential for office building façade retrofit project in three Canadian climates: The Prairies (Saskatoon), The Great Lakes/St. Lawrence (Montreal) and The Pacific Coast (Vancouver).

4.2 Methodology

Recommended basic steps for any retrofit project are (i) ensuring the commitment from the property owner, (ii) benchmarking the performance of the existing building, (iii) energy auditing and assessment of the retrofit opportunities, (iv) identifying the retrofit measures to go from existing case to required performance level, (v) the implementation phase and (vi) continuous monitoring to ensure the system is working as planned (Gnanam, 2013). For the steps iii-iv, the following methodology is applied in this study:

1. Development of a validated building model to benchmark the existing building performance and analysis of conventional façade retrofit measures on the whole building scale. The selected building in this study is an archetypical Canadian office building, constructed in the 1970s' with an inefficient envelope and an oversized mechanical system. The building is described in Section 4.2.1;

2. Development of an integrated one floor 5-zone model with validated building parameters to study the passive façade retrofit measures and façade integrated solar system energy

generation potential. The solar façade measures studied are naturally ventilated spandrel-integrated BIPV, solar shading with BIPV, corridor type second skin with BIPV and STPV windows. Detailed designs and numerical models are described in Sections 4.2.2-4.2.6;

3. Energy and life cycle analysis of perimeter zones' façade retrofit measures;
4. Risk analysis (shading by future buildings) taking into account existing and future site solar potential estimation. For this study, shading factors for 45°-55° north latitudes developed.

4.2.1 Building model

The building considered is situated in Saskatoon, Saskatchewan State, Canada. The geographic location is 52.13° North and 106.68° West. On the near-south side of the lot there is a parking space with a possible construction site in near future. The average annual daily horizontal solar radiation is 3.89 kWh/m²/d with 5813°C-d heating degree-days (HDD) and 765°C-d cooling degree-days (CDD).

The other locations, where the same building construction is considered, are Montreal and Vancouver. Montreal is in the Canadian climate region of Great Lakes/St. Lawrence, with the average annual daily horizontal solar radiation of 3.52 kWh/m²/d with 4457°C-d HDD and 1091°C-d CDD. Vancouver is in the Pacific coast climate region, with 3.46 kWh/m²/d average annual daily horizontal solar radiation, 2501°C-d HDD and 1002°C-d CDD.

The building has four stories, in addition to a basement space and shown in Figure 4.1. The gross floor area is 6528 m². Total façade area is 2459 m², total glazing area is 857.3 m². The building slab is medium weight concrete construction. Exterior wall consists of porcelain enamel on steel spandrel panels and limestone facing, air gap, 20.32 cm clay "Terra Cotta" bricks, 5.1 cm mineral wool insulation and interior plaster with aluminum frame double pane glazing with air gap. Window-to-wall ratio (WWR) for south, east and west façades are 80%.

Figure 4.1: Case study building south and west facades (Bigaila et al., 2016).

Heating is with a natural gas-fired boiler located in the basement. The air-handling unit is roof mounted with air distribution capacity of 8495 m^3/hr. The heating coil is 166 kW at 8495 m^3/hr. The capacity of direct expansion cooling coil is 28 kW.

The building was modeled with the EnergyPlus software (U.S. DOE, 2017) and calibrated against monthly annual electricity consumption bill with CV-RMSE-12.63% and NMBE 4.01%, electricity consumption profile calibrated with CV-RMSE 5.13% (Figure 4.2) and NMBE 1.8%, monthly natural gas consumption bill with CV-RMSE 14.72% and -1.11%. The validated model facade RSI was 0.88, glazing U-value was 3.52 W/m^2-°C with solar heat gain coefficient (SHGC) 0.62, infiltration value for the perimeter zones was identified to be 1.67 ACH, plug loads - 7 W/m^2 and lighting density - 11.95 W/m^2. The EnergyPlus building model is with an 85% efficiency gas-fired boiler and a chiller with COP of 2.77. The all-air system operation set points were as follows:

- The mechanical ventilation supplies fresh air at a 20°C temperature and mass flow rate of 0.9 ACH rate between 8:00 and 18:00 during the workdays and is OFF between 18:00-8:00 on workdays and weekends;
- The heating set point is 22°C from 6:00 to 18:00 during workdays and 15°C from 18:00-6:00 during workdays and weekends;

- The cooling set point is constant at 27°C during the cooling season and 25°C during the heating season;
- The occupancy and appliances schedules are between 8:00 and 18:00 during the workdays and no occupants between 18:00-8:00 on workdays and weekends.
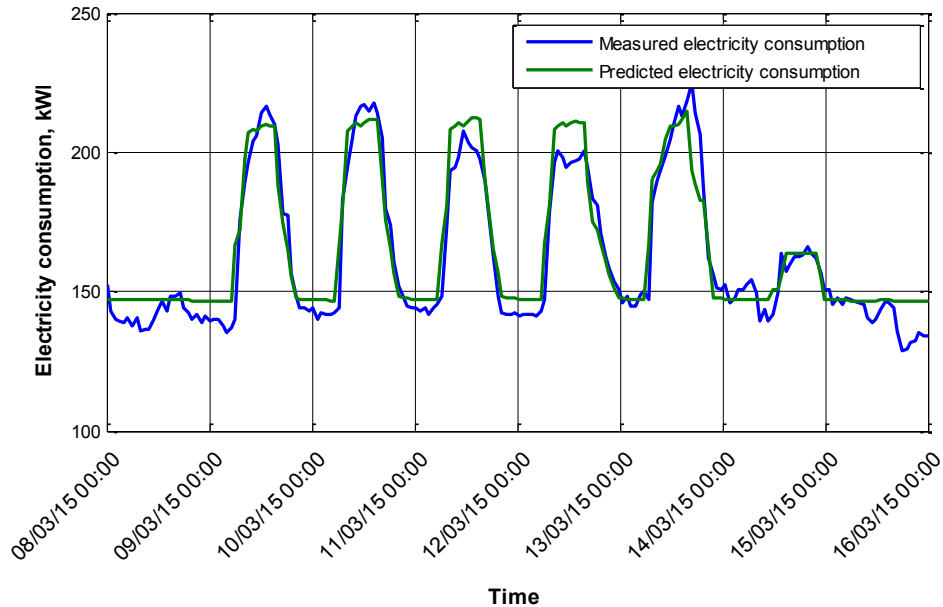
Figure 4.2: Measured and predicted electricity demand profiles.

Natural gas consumption for the considered period (2014-06 to 2015-05) is 86,384 m³ which resulted in a cost of 0.95$/m² for heating needs. Electricity consumption was 1,493,640 kWh or 228.79 kWh/m², which resulted in a cost of 18.13 $/m². Total equivalent energy consumption of the building is 365 ekWh/m²-yr. The equivalent energy is the sum of final fuel consumption in kWh.

The building energy use intensity was compared to Canadas' average commercial and institutional energy use determined by Natural Resources Canada (NRCan-OEE, 2013) from approximately 83,500 non-medical commercial office buildings in Canada covering 147.5 million m² of floor space having and average energy use intensity of 333 ekWh/m². Building Owners and Managers Association Building Environmental Standards (BOMA Best) is an organization which represents and supports the Canadian commercial building sector activity while promoting environmental stewardship (Halverson et al., 2014). Based on their established office benchmarking matrix

maximum (BOMA BESt low) and minimum (BOMA BESt high) points can be achieved for energy use intensity of 108 ekWh/m^2-yr and 388 ekWh/m^2-yr respectively (Halverson et al., 2014). The last benchmark number is obtained from a simulation study of buildings modeled according to ASHRAE 90.1-2013 requirements, which resulted in an energy use intensity of 387 ekWh/m^2-yr for a medium size office (Halverson et al., 2014). The benchmark results show, that the building overall EUI is above Canadian average and BOMA BESt low EUI case.
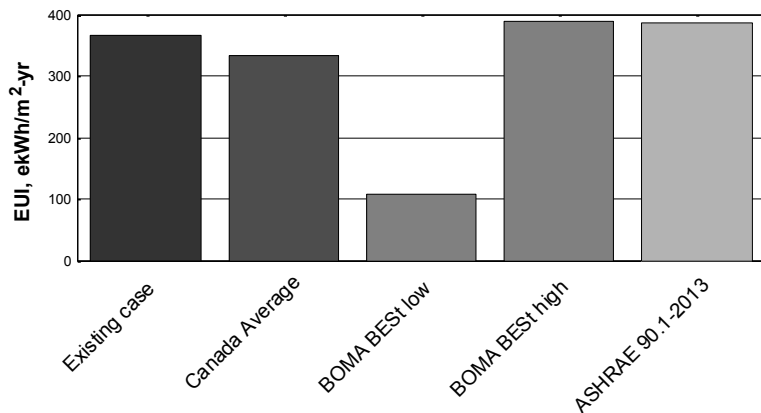
Figure 4.3: Building performance comparison against available benchmark levels.

4.2.2   Passive and active BIPV spandrel model

A photovoltaic panel installed over the structural and insulating layer of wall or roof, thus creating a cavity, transforms a standard element into a BIPV façade or roof. The cavity must be either naturally or mechanically ventilated since temperature of silicon and thin-film PV cells affects the efficiency of the sunlight conversion into electricity negatively with increasing temperatures in the range of -0.035 to -0.496 %°C^{-1} depending on the cell and PV modules type (Mattei et al., 2006).

A BIPV prototype for commercial building wall applications was tested in Concordia University (Bigaila et al., 2015). The PV modules generate electricity, while performing as a rain screen cladding with high architectural integration flexibility. Conventional silicon technology PV panels have a lifetime of at least 30 years, which offers durability of a conventional cladding material.

The model is a quasi-steady state based on energy balance of a solar air-based flat plate collector. The solar absorber is the exterior opaque plate, which is the PV panel in this case. The energy balance is solved with a lumped parameter model. The energy balance in the PV module is expressed by equation 4.1.

$$\alpha GA_{pv} = E_{pv} + Q_1 + Q_{ra} + Q_c + Q_r \qquad\qquad 4.1$$

where αGA_{pv} is the solar radiation absorbed by the PV module, E_{pv} is the electricity generated by PV modules, Q_l is the exterior convective loss, Q_{rs} is the exterior radiative thermal loss to the sky, Q_c is the heat removed by heat transfer fluid in passive mode, and Q_r is the radiative heat exchange between PV and the back plate surface.

The air temperature in the control volume is estimated by an exponential air temperature variation, which is the exact solution, if the temperatures of the surrounding surfaces are assumed to be uniform and the average air temperature for energy balances is estimated by equation 4.2.

$$T_{av} = \int T dx / \Delta x \qquad\qquad 4.2$$

where T_{av} is the average control volume bulk air temperature.

The interior convective heat transfer correlations for naturally ventilated BIPV panel were developed in Concordia University (Bigaila et al., 2015). Electrical output from the PV module is calculated using a one-diode equivalent circuit model of a modern BIPV panel (ISSOL sa/nv, 2018; Duffie and Beckman, 2006; Eckstein, 1990). The mode scheme in Trnsys (Klein et al., 2012) environment is shown in Figure 4.4.
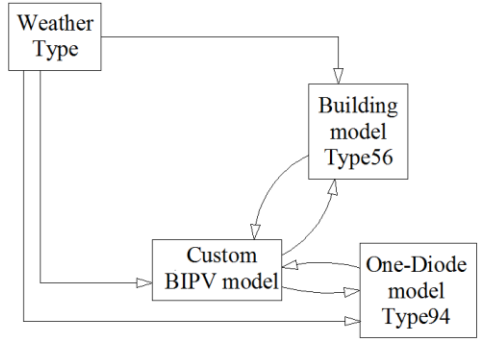
Figure 4.3: BIPV model workflow chart in Trnsys simulation software.

4.2.3 BIPV shading models

The overhang model is described by (Klein et al., 2012). The effect of façade with PV overhangs self-shading is taken into account as well. Shaded PV cells result in reduced power output of the PV string, since the string current drops to the shaded cell current levels. Shading of PV cells also results in hot spots on the PV cells, which can result in damage of the modules in the long term due to thermal stress. The algorithm how to estimate the string shading is described by Duffie and Beckman (Duffie and Beckman, 2006; Thornton et al., 2012). The model in the Trnsys environment is shown in Figure 4.5.
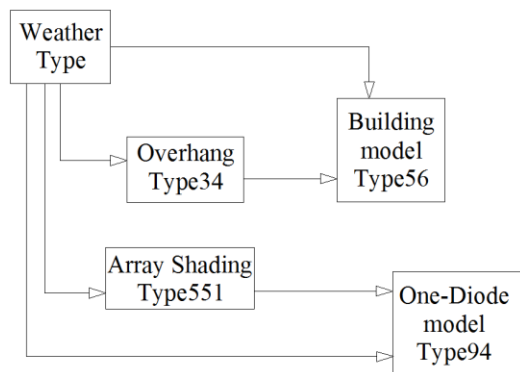
Figure 4.4: PV shading model workflow chart in Trnsys.

PV shutter is an opaque PV panel installed vertically in front of building glazing and acting as a shading device. The PV shutter has a packing factor of 50%, which means, that 50% of the window

area is shaded by an external shading device while producing electricity. It is implemented in the building model as an exterior shading device blocking 100% of direct incoming solar radiation to the building through the window and adding additional thermal resistance of 0.0714 h-m^2-K/kJ to this glazing section. A one-diode equivalent circuit model of a BIPV module was used to calculate the performance of the PV overhangs and PV solar shutters (ISSOL sa/nv, 2018).

4.2.4   Second skin model

There are several possible double skin façade designs, which depends on the way the cavity is formed (box window, multistory façade, corridor façade, shaft-box façade), from type of ventilation (natural, mechanical or hybrid), depending from the air flow path (exhaust air, supply air, reversible air flow, outdoor air curtain or indoor air curtain) (Ebbert, 2010). Generally the cavity between the second skin and the building exterior wall creates a thermal and noise buffer zone and space for sun-protection devices. The first skin can be equipped with PV laminates for double function – shading and electricity production. Other functions of second skin are noise protection to allow windows opening by users. This facilitates natural ventilation, protection from high wind loads in high rise buildings, natural cooling and purging the building with fresh air, additional glass provides protection against burglary, the preheated air can be used to assist building mechanical ventilation.

Depending on the façade design, there might be some disadvantages: overheating problems in summer, opening windows cause operation discontinuity for central air handling system due to mass flow rate differences, the incoming air in summer may be hotter than the outside air temperature, in winter the warm air may condensate on the outer glass pane. That is why a double façade design has to be developed in combination with the whole building concept and with respect to the surrounding climate conditions, which could result in custom solutions for each building.

Double facades can be feasible option for refurbishment of office buildings. An existing façade can be improved by adding an exterior layer. Thus, the original façade may be allowed to stay in place. New building services can be installed in the façade cavity, which makes it possible to technically upgrade the building without interfering with the interior (Ebbert, 2010).

The second skin façade was modeled in Trnsys using the types that are shown in the Figure 4.6. The cavity is modeled as naturally ventilated wall. Single floor corridor façade is analyzed. The cavity air and surface temperatures are iterated with the building model surface temperature. The cavity air is extracted to the exterior at the top of the façade section. The BIPV model is a one-diode equivalent circuit model and the window parameters are used to input the solar transmission data into the building model. The second skin effect on the lighting loads was not taken into account for this study. The potential to use the preheated air in the cavity for natural ventilation is a potential opportunity for a future study, since it would require a detailed analysis of the HVAC system operation adjustments for optimal performance.
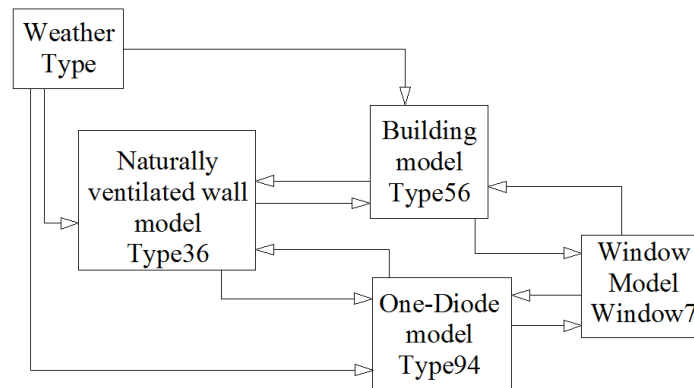
Figure 4.5: The second skin model in Trnsys of a corridor façade type with BIPV glass as exterior skin.

4.2.5   STPV model

A transparent photovoltaic laminate can be used to construct an insulated glazing unit (IGU) and used as part of building glazing design. This concept is called a semi-transparent photovoltaic glazing (STPV). The advantage of the STPV is that the glazing in this case instead of the usual climate and visual control acts as a shading device, since part of the direct solar radiation is blocked by the photovoltaic cells, while producing electricity at the same time.

In a retrofit project, if the glazing is to be replaced, replacement with STPV can create the additional advantage of saving on internal or external shading devices and also maximizing the BIPV façade covered with PV area.

The Trnsys model is presented in Figure 4.7. The IGU thermal properties described in Table 3 with integrated cells were modeled with a Window 7 tool (LBNL, 2018) and passed to the building zone model. The STPV effect on the thermal zone solar gains was modeled as a transmitted solar radiation shading factor. The photovoltaic cell temperature was obtained iterating the one-diode equivalent circuit model temperature input and the IGU shade laminated between the glazing. The STPV effect on the lighting loads was not taken into account.
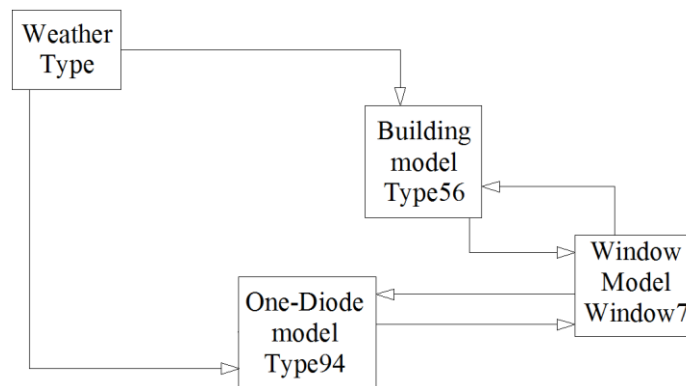
Figure 4.6: The STPV glazing model in Trnsys environment.

4.2.6   Retrofit measures considered

Façade retrofit measures and the main parameters used in the techno-economic analysis are given in Tables 4.1-4.7. Additional insulation levels include replacement of existing steel enamel panels with new metal cladding, various EPS insulation levels, labor cost. Glazing replacement takes into account IGU price plus installation costs, interior finishing costs, sealing costs. The window to wall ratio modification is considered as a complete façade reconstruction with various insulation and glazing type costs. The air-tightness improvement takes into account the cost of sealant, weather film and labor costs and is used as additional costs for the insulation and glazing upgrade. The schematic of different façade retrofit options and marking explained in Section 4.3 is shown in Figure 4.8. Costs shown in Tables 4.2-4.7 are obtained from construction material supplier catalogs, authors' personal communications and quotes supplied by vendors and contractors.
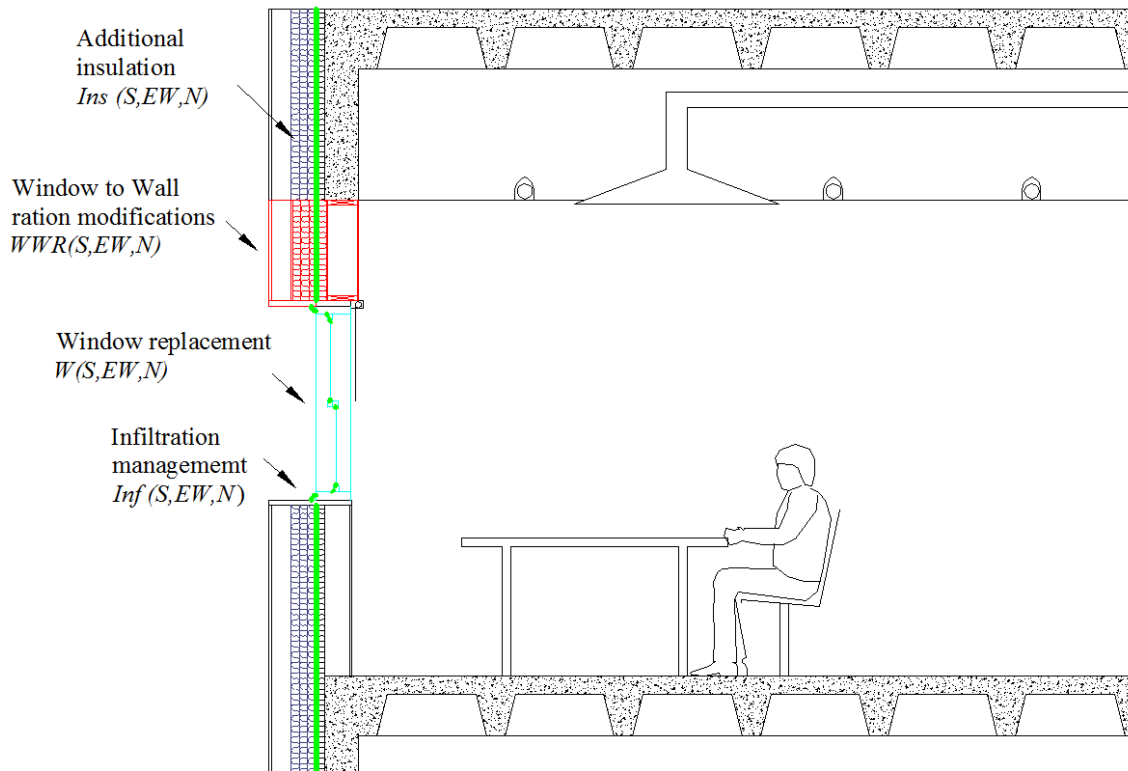
Figure 4.8: Façade retrofit measures with the case names used in Section 4.3.

Table 4.1: Solar façade cases.
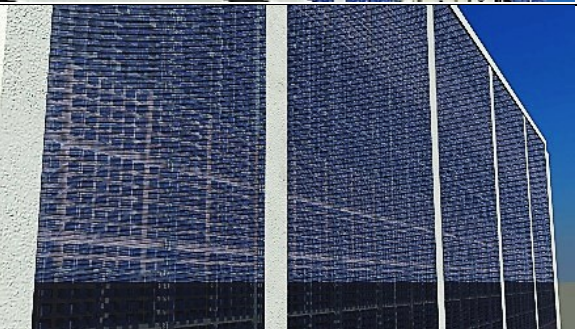
In this study a 4° sloped overhang on south, east and west facades is named O(S,EW) and if active glass is used – EPoG-O(S,EW). The installed capacity is 4.47 kWp on south façade and 4.95 kWp on East and West facades per floor.	
A horizontal shutter on south, east and west facades is named Sh(S,EW) and if active glass is used – EPoG-Sh(S,EW). The installed capacity on the south façade is 10.32 kWp and 8.50 kWp for both east and west facades per floor.	
The spandrel-integrated EPoG for south, east and west facades is named EPoG(S,E,W). The system details are shown in Table A.2. The installed PV capacity on south façade with WWR of 0.8 and 0.4 is 4.49 and 13.46 kWp respectively and for East and West - 3.49 and 11.09 kWp.	
The addition of second skin façade over the existing façade is analyzed for south and east, west façades separately. Addition of EPoG is analyzed with different packing factors (PF). The installed capacity is shown in Table A.3 for packing factors of 0.1, 0.2, 0.4, 0.6, 0.8.	
The replacement of windows with STPV glazing is considered for south, east and west facades with different packing factors (0.17, 0.39 and 0.52). Different installed capacities depend from the WWR. The installed capacities are shown in Table A.4.	

Table 4.2: Insulation upgrade costs.

Case	Insulation level, RSI	Costs, $/m²
I0 (Base case)	0.88	
I1	1.7	54.1
I2	5.5	84.7
I3	9.2	115.3
I4	13.0	145.9

Table 4.3: Glazing replacement costs.

Case	U, W/m²ºC	SHGC	Other	Costs, $/m²
W0			Base case	
W1	1.43	0.61	Argon low-e	318
W2	0.98	0.53	Argon low-e	425

Table 4.4: WWR modification costs.

Case	Costs, $/m²
I1W0	373
I2W0	403
I3W0	434
I4W0	464
I1W1	373
I2W1	403
I3W1	434
I4W1	464
I1W2	479
I2W2	510
I3W2	540
I4W2	571

Table 4.5: Airtightness improvement costs.

Case	Costs, $/m²
1.2ACH	60
0.6ACH	152

Table 4.6: Solar façade element costs.

Case	Costs, $/m²
0.5 m overhang	288
Horizontally sliding shutter	262
Second skin	870

Table 4.7: BIPV/EPoG system costs.

	Other	Costs, $/m²
0.5 m EPoG overhang		411
Horizontal BIPV shutter		459
Second skin 1	PF 10	950
Second skin 2	PF 20	964
Second skin 3	PF 40	992
STPV 1	PF 17	597
STPV 2	PF 39	630
STPV 3	PF 52	649
BIPV spandrel	Passive ventilation	382

4.3 **Results**

4.3.1 *Envelope retrofit simulations*

A total of 463 façade insulation retrofit cases were simulated. The best cases are shown in Figure 4.9 and Table 4.13. The name indicates the façade retrofit measure, for example *Ins(S,EW,N),Inf(1.2),W(S,EW,N),WWR(S,EW,N)* means that the insulation thickness has values described in Tables 4.1-4.2, an infiltration value of 1.2 air changes per hour, the window type for all facades described in Table 4.3 and with a window-to-wall ratios varying between the base case, 0.48 and 0.84. If the parameter is not shown in the name, it means a fixed base case value described in Sections 4.2.1 and 4.2.6 is kept.

The selected most promising cases for façade insulation measures are shown in Table 4.8. In general, the simulation study shows, that a façade renovation with just an effort to increase the insulation levels on the opaque part of the facade results in energy savings up to only 2%. The benefit is insignificant, because of large window to wall ratios and high infiltration levels, which were indicated during the model validation study (Bigaila et al., 2016). The façade insulation increase shows a contribution to energy savings between 21-31%, if techniques used to reduce the infiltration levels are used to reach 1.2 ACH. A replacement of windows can result in energy savings between 26-40%. A variation of WWR and a window type can result in energy savings between 31-43%.

The reduction of all perimeter zones energy consumption up to 72% can be achieved with a complete façade reconstruction and reducing the infiltration to 0.6 ACH. This parameter results in an increase in energy savings by up to 29% compared to a case with 1.2 ACH infiltration and the same insulation, WWR and glazing thermal values.

4.3.2   BIPV addition results

4.3.2.1   Overhang and shutter

The results are shown using the same method of case naming. Additional symbol O(S), means that an overhang on the south façade is applied. A symbol EPoG-O(S) means that an energy producing glazing is used as an overhang. The shutter on a south facade is described as Sh(S).

The main BIPV overhang technical specifications are shown in Appendix A Table A.1. The results for selected most promising cases for a façade retrofit with solar shading are shown in Table 4.10.

The general simulation results demonstrated that a non-active solar shading element on a façade does not result in an overall energy savings, due to the fact, that the heating load increases. This results in a total energy balance being negative even with the energy savings for cooling demand reduction. For example, the addition of the overhang, on the south façade results in an increase in equivalent energy consumption by 1.48% and 3.09% if a shutter is applied. Utilization of BIPV glazing as an overhang material results in overall 0.51% energy savings, with the electricity production from PV included in the energy balance. This expression of the final energy balance is applied for all BIPV cases in Sections 4.3.2-4.3.4. As observed from Table 4.10, one of the most promising cases with active BIPV shading demonstrated in total energy reduction of 11% and the case with the highest energy savings, whose demand profile is shown in Section 4.3.5, showed a potential of reducing the energy consumption by 19%.

4.3.2.2 Spandrel-integrated BIPV

Main simulation parameters for spandrel-integrated BIPV are shown in Table A.2 and the selected most promising case results are shown in Table 4.9. The simulations were performed for cases with BIPV glazing integrated on south, east and west facades and cases with only south façade-integrated BIPV.

In general, replacement of the spandrel cladding material with BIPV results in equivalent energy reduction by 2-6% with the south façade integrated BIPV or 4-8% with the south, east and west façade integrated BIPVs. Like mentioned in Section 4.3.2.1, the equivalent energy reduction includes the produced electricity. This contribution depends from the window-to-wall ratio. The modification of WWR can result in the PV contribution to the energy savings to 14%. However, to achieve the highest energy production from the spandrel-integrated BIPV, a façade reconstruction for higher initial investment is required.

4.3.2.3 Second Skin Facade

The parameters for the cases, where the exterior glass of the second skin was BIPV, are shown in Table A.3. The selected cases are shown in Table 4.11.

In the case of standard second skin façade without integrated PV cells, the cooling load increase cancels out the benefit of heating load decrease for south, east and west facades. A special case of using a second skin façade for the north was investigated, but the benefit was also insignificant, with equivalent energy savings for the second skin façade addition of up to 4%.

The addition of glazing with PV cells results in reduced cooling load and additional produced electricity. This design leads to combined final energy savings of up to 11%.

4.3.2.4   STPV

The STPV window electrical parameters are shown in Table A.4 and the selected cases are shown in Table 4.12. For this group, the insulation and infiltration values were kept as base case values and the window type and WWR were variables. The optimal case is with the WWR of 0.8, windows replaced to W3 and with the packing factor of 0.52 of the STPV, which results in 12.7% equivalent energy consumption reduction. With packing factors of 0.17 and 0.39, the energy savings of 11.3% and 11.9% can be achieved, which is a result of electricity production and better thermal properties of the new glazing.

4.3.3   Cost analysis

The cost effectiveness of the investment is demonstrated using Net Present Value (NPV) after 25 years of the building and façade integrated solar system operation (excluding the investment part) ratio to the investment for the retrofit case. The NPV takes into account the prices of natural gas, electricity and produced electricity feed-in-tariff, which is effective in Saskatoon (City of Saskatoon, 2018). The NPV/Investment ratio higher than 1 means, that a retrofit case has a payback within 25 years of system operation. The higher the ratio, the faster payback and higher profit for the building owner is expected. The NPV/Investment ratio is plotted against the specific cost of the energy savings - a ratio of investment per kWh saved with the façade insulation retrofit and electricity produced by the BIPV system over 25 years (Eicker et al., 2015).

In Tables 4.8 and 4.9 façade retrofit cases with spandrel-integrated BIPV on south and both south, east and west facades are shown. For the case study building the identified air leakage was high and using the economic inputs shown in Tables 4.2-4.5, it was identified, that façade sealing techniques have the highest potential from a techno-economical point of view. In Table 4.9 the same cases were evaluated, considering that the spandrel material is active glass instead of composite metal/wood panels. In this case, the extra investment is done for the fixation system designed to

support the active glass and the balance of system costs associated with the PV installation, which are included in the costs shown in Table 4.7. The benefit is the produced electricity, which can be fed into the grid, generating revenue from the feed-in-tariffs that are effective in Saskatoon (City of Saskatoon, 2018). The results show that the replacement of the spandrel material into the BIPV has a NPV/Investment ratio of 1.79 for the south, east and west facades and 1.97 for just the south façade installation. For this case the specific cost is 9.02 ct/kWh for both south, east and west and 8.02 ct/kWh for south façade, which shows the BIPV produced electricity price, which is cheaper than the utility price for electricity in Saskatoon (City of Saskatoon, 2018).

Table 4.1: Facade retrofit cases.

Name	Final energy savings, %	NPV(25 yrs) /Investment	ct/per kWh saved (25 yrs)
Ins(0.588,1.142,1.142),Inf(1.2)	23.9	1.79	1.19
Ins(0.183,1.142,1.142),Inf(1.2)	25.1	1.81	1.21
Ins(1.142,0.588,1.142),Inf(1.2)	25.0	1.80	1.24
Ins(1.142,1.142,1.142),Inf(1.2),W(N(W1))	25.2	1.41	1.51
Ins(0.588,1.142,1.142),Inf(0.6)	53.1	1.62	1.41
Ins(0.183,1.142,1.142),Inf(0.6)	53.0	1.61	1.39
Ins(1.142,0.588,1.142),Inf(0.6)	54.0	1.63	1.40

Table 4.2: Facade retrofit with BIPV cases.

Name	Final energy savings, %	NPV(25 yrs) /Investment	ct/per kWh saved (25 yrs)
EPoG(S,E,W)	4.0	1.79	9.02
Ins(1.142,1.142,0.183)+EPoG(S,E,W)	7.8	1.55	5.61
Ins(0.588,1.142,1.142),Inf(1.2)+EPoG(S,E,W)	26.7	1.82	2.19
Ins(1.142,0.588,1.142),Inf(1.2)+EPoG(S,E,W)	27.0	1.81	2.20
Ins(1.142,0.183,1.142),Inf(1.2)+EPoG(S,E,W)	27.5	1.79	2.14
Ins(1.142,1.142,1.142),Inf(1.2),W(N(W1))+EPoG(S,E,W)	27.1	1.60	2.48
Ins(0.588,1.142,1.142),Inf(1.2),W(N(W1))+EPoG(S,E,W)	27.5	1.63	2.43
Ins(0.588,1.142,1.142),Inf(0.6)+EPoG(S,E,W)	54.8	1.66	1.86
Ins(1.142,0.588,1.142),Inf(0.6)+EPoG(S,E,W)	57.5	1.65	1.86
Ins(1.142,1.142,1.142)+EPoG(S)	1.7	1.97	8.02
Ins(0.588,1.142,1.142),Inf(1.2)+EPoG(S)	24.4	1.89	1.61
Ins(1.142,0.588,1.142),Inf(1.2)+EPoG(S)	26.0	1.88	1.62
Ins(0.588,1.142,1.142),Inf(1.2),W(N(W1))+EPoG(S)	26.1	1.61	1.88
Ins(0.588,1.142,1.142),Inf(0.6)+EPoG(S)	56.1	1.65	1.57
Ins(1.142,0.588,1.142),Inf(0.6)+EPoG(S)	56.2	1.65	1.57

The selected solar shading cases are shown in Table 4.10. The benefit of adding an overhang or horizontal shading is small, since the electricity saving due to reduced cooling demand is smaller compared to the increased heating demand. On the other hand, the addition of an overhang with

BIPV is a feasible retrofit measure. As can be seen in Table 4.10, the case with addition of the BIPV on the west façade has a NPV/Investment ratio of 3.2 and the specific savings cost of 1.5 ct/kWh. The addition of an active overhang on south façade, as well as the active shutter has lower specific costs, since the high electricity production and cooling demand reduction did not cover for the increased energy demand for heating, due to the reduced solar gains on the south perimeter zone.

Table 4.3: Selected facade retrofit cases with BIPV solar shading.

Name	Final energy savings, %	NPV(25 yrs) /Investment	ct/per kWh saved (25 yrs)
Ins(1.142,0.588,1.142),W(EW(W1)),WWR(EW(0.4))+EPoG-O(East)	9.1	1.4	3.6
Ins(1.142,0.183,1.142),W(EW(W1)),WWR(EW(0.4))+EPoG-O(East)	11.0	1.4	3.2
Ins(1.142,0.588,1.142)+EPoG-O(W)	8.7	3.2	1.5
Ins(1.142,0.183,1.142)+EPoG-O(W)	2.5	1.9	6.1
Ins(1.142,0.588,1.142)+W(EW(W1)+WWR(EW(0.4)+EPoG-O(W)	9.4	1.4	3.5
Ins(0.588,1.142,1.142)+EPoG-O(S,E,W)	6.9	2.3	5.9

The addition of a corridor type second skin facade in a retrofit case results are shown in Table 4.11. The addition of just the second skin façade, just like in the case of passive shading technology, does not demonstrate a high potential from techno-economic point of view. According to the simulation results, the heating demand decrease is too small to overcome the increase in cooling demand. However, the addition of the BIPV instead of the regular glazing on the exterior skin, contributes to the solar shading and electricity production, but on the other hand increases the heating demand. The optimal designs are shown in Table 4.11. As can be seen, the PF of 4 and 5 on the south façade are the most feasible designs due to the high solar electricity production. These cases are plotted alongside other most promising cases in Figure 4.9. Since the second skin façade offers the opportunity to install the highest possible photovoltaic cell quantity on the façade, the incentive is to reduce the structure cost of the glazing support. To reach a comparable feasibility of a second skin façade with BIPV of PF 5 on south façade to a spandrel-integrated BIPV, the structure costs should be below 200 EU/m², which would allow reaching the NPV/Investment of 1.26 and specific

costs of energy efficiency of 10 ct/kWh. The discussion of the technical feasibility of a second skin glass fixation system structural optimization is not within the scope of this paper.

Table 4.4: Facade retrofit by adding a second skin with BIPV.

Name	Final energy savings, %	NPV(25 yrs) /Investment	ct/per kWh saved (25 yrs)
2nd Skin South with EPoG (PF4)	8.0	0.51	21
2nd Skin South with EPoG (PF5)	10.0	0.67	18
2nd Skin East, West with EPoG (PF5)	11.0	0.54	29

Window replacement with STPV glazing results are shown in Table 4.12. A separate case without a STPV glazing is demonstrated. The NPV/Investment ratio shows, that the STPV glazing addition for the case *W(S(W2),EW(W2)),WWR(S(0.3),EW(0.3))+STPV_PF3(S,EW)* is 0.64, as opposed to 0.37 for the case *W(S(W2),EW(W2)),WWR(S(0.3),EW(0.3)).* According to the simulation results, the addition of the STPV glazing into the window replacement efforts in a retrofit project can lead to a higher financial benefit to the building owner, than a replacement of windows with a standard glazing. The STPV IGU has higher specific energy efficiency costs, however.

Table 4.5: Façade retrofit by replacing windows with STPV.

Name	Final energy savings, %	NPV(25 yrs) /Investment	ct/per kWh saved (25 yrs)
W(S(W2),EW(W2)),WWR(S(0.3),EW(0.3))	6.1	0.37	10
W(S(W2),EW(W2)),WWR(S(0.3),EW(0.3))+STPV_PF1(S,EW)	6.9	0.45	13
W(S(W2),EW(W2)),WWR(S(0.3),EW(0.3))+STPV_PF2(S,EW)	6.7	0.59	15
W(S(W1),EW(W1)),WWR(S(0.3),EW(0.3))+STPV_PF3(S,EW)	5.8	0.63	18
W(S(W2),EW(W2)),WWR(S(0.3),EW(0.3))+STPV_PF3(S,EW)	6.4	0.64	16

4.3.4   Canadian climate effect on the results

The most promising cases described in Sections 4.3.2 and 4.3.3 were simulated for the climates of Montreal and Vancouver, in addition to Saskatoon. The results are shown in Table 4.13. The natural gas and electricity rates for small business consumers are taken for the locations under considerations (Energir, 2018; Hydro Quebec, 2018; Fortis BC, 2018a; BC Hydro, 2018b). The existing electricity consumption credits for small power producers are applied for the PV electricity

production, which is injected into the local grids (Hydro Quebec, 2018; BC Hydro, 2018 b). In Saskatoon there is a dedicated feed-in-tariff for PV power producers in Saskatchewan province (City of Saskatoon, 2018).

It may be shown, that the retrofit of a commercial building façade in the Prairies climate has a NPV/Investment ratio between 1.4-1.8 and the specific energy saving cost of 1.2-1.5 ct/kWh for the selected most promising cases. The addition of spandrel-integrated BIPV results in an increase of the NPV/Investment ratio to 1.6-2.0 and the specific energy savings cost increase to 1.6-2.2 ct/kWh. The spandrel-integrated BIPV produced electricity price is 8.0 ct/kWh for the south façade and 9.0 ct/kWh for the south, east and west façade systems combined. The BIPV overhang for this climate resulted in NPV/Investment ratio of 1.4-3.2 and 1.5-6.1 ct/kWh cost for energy savings. The second skin NPV/Investment ratio was between 0.5-0.7 and specific costs of 18.1-29.3 ct/kWh and for STPV the NPV/Investment was 0.4-06 and specific costs of 14.5-17.9 ct/kWh.

For the Great Lakes/St. Lawrence climate the façade insulation results in NPV/Investment ratio between 3.5 – 4.4 and the specific energy saving cost of 0.9-1.1 ct/kWh. The addition of spandrel-integrated BIPV results in generally a decrease of the NPV/Investment ratio to 1.0-3.5 and increase of the specific energy savings cost to 1.1-1.9 ct/ kWh. The price of electricity produced form spandrel-integrated BIPV is between 8.0-9.5 ct/kWh for the south and both south, east and west facades respectively. The BIPV overhang case Ins(1.142,0.183,1.142),W(EW(W1)),WWR(EW(0.4))+EPoG-O(East) showed the NPV/Investment ratio of 0.9 and the energy saving cost of 6.4 ct/kWh. The second skin with BIPV with PF 5 on south, east and west facades demonstrated a NPV/Investment ratio of 0.4 with a cost of 42.5 ct/kWh.

For the Pacific Coast climate it was observed, that the façade insulation NPV/Investment ratio was between 1.2-1.5 and specific energy saving costs of 1.4-1.8 ct/kWh. The spandrel-integrated BIPV addition on south façade for this climate results in NPV/Investment ratio of 2.2 at the specific

energy savings cost of 4.1 ct/kWh. The addition of BIPV overhang can result in the NPV/Investment ratios up to 0.8 with specific energy savings cost of 11.4 ct/kWh. The second skin with BIPV of PF5 addition on south, east and west facades show a NPV/Investment ratio of 0.3 with specific energy saving cost of 49.4 ct/kWh.
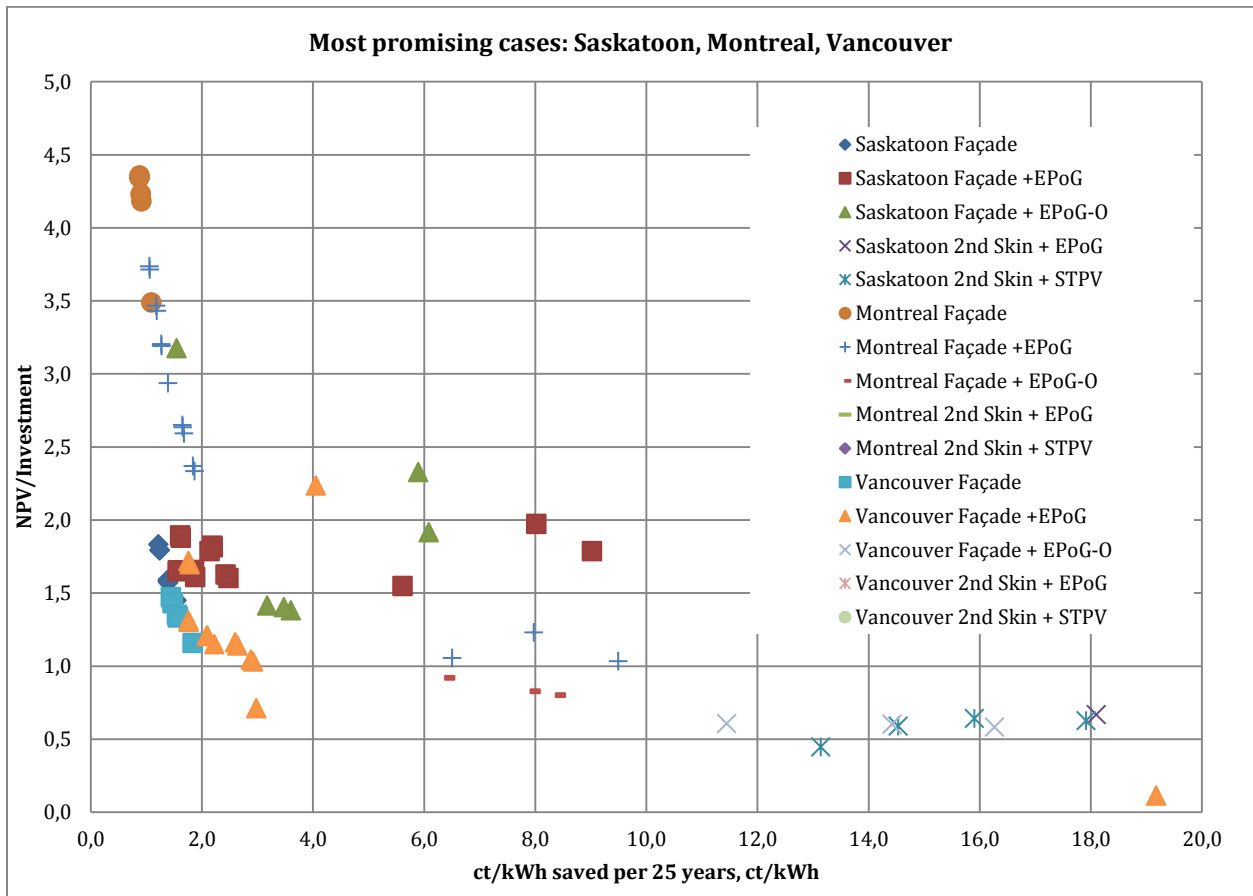
Figure 4.9: Most promising case groups for Saskatoon, Montreal and Vancouver. For detailed description see Table 4.13.

Table 4.6: The most promising cases for Saskatoon, Montreal and Vancouver climates.

Description	Name	Saskatoon		Montreal		Vancouver	
		NPV/Investment	ct/per kWh saved (over 25 years)	NPV/Investment	ct/per kWh saved (over 25 years)	NPV/Investment	ct/per kWh saved (over 25 years)
Façade retrofit	Ins(0.588,1.142,1.142),Inf(1.2)	1.8	1.2	4.4	0.9	1.5	1.4
	Ins(0.183,1.142,1.142),Inf(1.2)	1.8	1.2	4.3	0.9	1.4	1.5
	Ins(1.142,0.588,1.142),Inf(1.2)	1.8	1.2	4.3	0.9	1.4	1.5
	Ins(1.142,1.142,1.142),Inf(1.2),W(W1)	1.4	1.5	3.5	1.1	1.2	1.8
	Ins(0.588,1.142,1.142),Inf(0.6)	1.6	1.4	4.2	0.9	1.4	1.6
	Ins(0.183,1.142,1.142),Inf(0.6)	1.6	1.4	4.2	0.9	1.3	1.6
	Ins(1.142,0.588,1.142),Inf(0.6)	1.6	1.4	4.2	0.9	1.3	1.6
Spandrel-integrated EPoG addition with façade retrofit combinations	EPoG(S,E,W)	1.8	9.0	1.0	9.5	0,87	10,36
	Ins(1.142,1.142,0.183)+EPoG(S,E,W)	1.5	5.6	1.1	6.5	0,76	8,08
	Ins(0.588,1.142,1.142),Inf(1.2)+EPoG(S,E,W)	1.8	2.2	2.6	1.6	1,17	2,59
	Ins(1.142,0.588,1.142),Inf(1.2)+EPoG(S,E,W)	1.8	2.2	2.6	1.7	1,16	2,60
	Ins(1.142,0.183,1.142),Inf(1.2)+EPoG(S,E,W)	1.8	2.1	2.6	1.7	1,14	2,64
	Ins(1.142,1.142,1.142),Inf(1.2),W(N(W1))+EPoG(S,E,W)	1.6	2.5	2.3	1.9	1,03	2,92
	Ins(0.588,1.142,1.142),Inf(1.2),W(N(W1))+EPoG(S,E,W)	1.6	2.4	2.4	1.8	1,04	2,88
	Ins(0.588,1.142,1.142),Inf(0.6)+EPoG(S,E,W)	1.7	1.9	3.2	1.3	1,21	2,09
	Ins(1.142,0.588,1.142),Inf(0.6)+EPoG(S,E,W)	1.7	1.9	3.2	1.3	1,20	2,10
	EPoG(S)	2.0	8.0	1.2	8.0	1,03	8,78
	Ins(0.588,1.142,1.142),Inf(1.2)+EPoG(S)	1.9	1.6	3.5	1.2	1,36	1,90
	Ins(1.142,0.588,1.142),Inf(1.2)+EPoG(S)	1.9	1.6	3.4	1.2	1,34	1,91
	Ins(0.588,1.142,1.142),Inf(1.2),W(N(W1))+EPoG(S)	1.6	1.9	2.9	1.4	1,15	2,23
	Ins(0.588,1.142,1.142),Inf(0.6)+EPoG(S)	1.7	1.6	3.7	1.1	1,31	1,76
	Ins(1.142,0.588,1.142),Inf(0.6)+EPoG(S)	1.6	1.6	3.7	1.1	1,30	1,77
Overhang with EPoG addition with façade retrofit combinations	Ins(1.142,0.588,1.142),W(EW(W1)),WWR(EW(0.4))+EPoG-O(East)	1.4	3.6	0.8	8.4	0.6	16.3
	Ins(1.142,0.183,1.142),W(EW(W1)),WWR(EW(0.4))+EPoG-O(East)	1.4	3.2	0.9	6.4	0.6	11.4
	Ins(1.142,0.588,1.142)+EPoG-O(W)	3.2	1.5	0.3	-6.1	0.8	-10.7
	Ins(1.142,0.183,1.142)+EPoG-O(W)	1.9	6.1	0.4	-8.0	0.8	-14.9
	Ins(1.142,0.588,1.142)+W(EW(W1)+WWR(EW(0.4))+EPoG-O(W)	1.4	3.5	0.8	7.9	0.6	14.4
	Ins(0.588,1.142,1.142)+EPoG-O(S,E,W)	2.3	5.9	0.7	-15.7	1.0	-31.5
2nd Skin with EPoG	2nd Skin South with EPoG (PF4)	0.5	21.5	0.2	-87.0	0.3	-970.1
	2nd Skin South with EPoG (PF5)	0.7	18.1	0.3	-207.0	0.4	208.8
	2nd Skin East, West with EPoG (PF5)	0.5	29.3	0.4	42.5	0.3	49.4
STPV addition with façade retrofit combinations	W(S(W2),EW(W2)),WWR(S(0.3),EW(0.3))+STPV_PF1(S,EW)	0.4	13.1	0.1	153.5	0.1	-153.0
	W(S(W2),EW(W2)),WWR(S(0.3),EW(0.3))+STPV_PF2(S,EW)	0.6	14.5	0.1	276.6	0.2	-94.3
	W(S(W1),EW(W1)),WWR(S(0.3),EW(0.3))+STPV_PF3(S,EW)	0.6	17.9	0.2	-303.9	0.2	-62.6
	W(S(W2),EW(W2)),WWR(S(0.3),EW(0.3))+STPV_PF3(S,EW)	0.6	15.9	0.2	456.3	0.2	-79.7

4.3.5 Peak demand reduction and shift

Peak demand and PV production hourly graphs for a winter and summer design days are shown in Figure 4.10. Base case is shown for reference with two columns below: the most promising cases from a techno-economical point of view according to the methodology presented in Section 4.3.3 on the left column and selected cases with the highest energy reduction and BIPV electricity production presented in Sections 4.3.1 and 4.3.2 are shown on the right column.

The base case peak heating demand is 153 kW occurring at roughly 8AM during the heating season and the cooling demand peak is 11.62 kW occurring during the cooling season at roughly 17PM. According to the simulations, the heating demand peak does not significantly shift as a consequence of façade retrofit measures, but a reduction up to 56% is possible. Reduction values for the left column are 18%, 0%, 0%, 2%, 9%, for the right column 56%, 56%, 8%, 2%, 7% for the cases b, c, d, e and f respectively. The cases are shown in Figure 4.10.

The cooling load reduction for the left column is as follows: 0%, 0%, 51% (peak shit by -2h), -6%, 96%, for the right column: 58%, 58%, 96%, 59% (peak shit by -2h), 64% for the cases b, c, d, e and f respectively shown in Figure 4.10. The PV electricity production is shown as well.
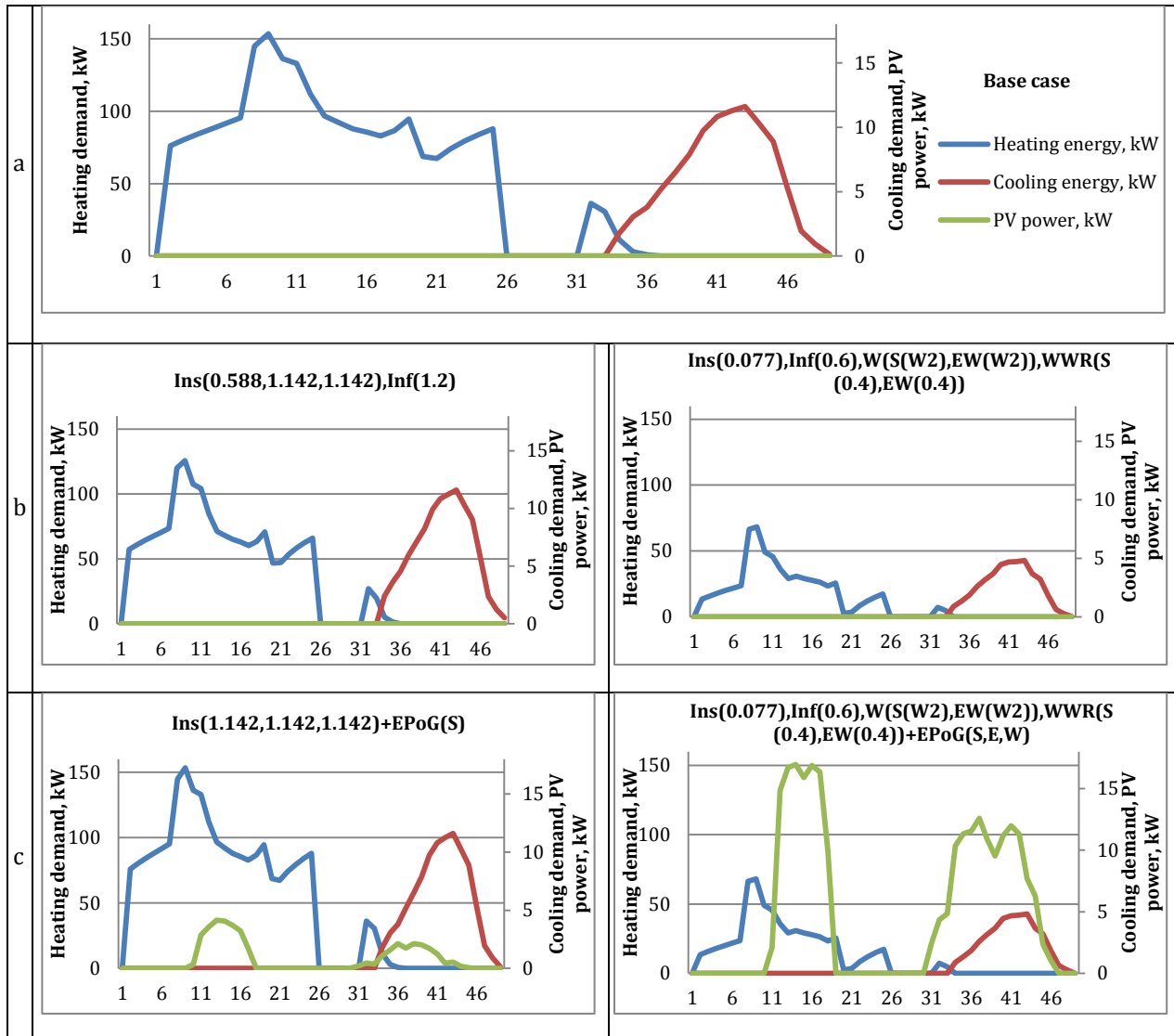
Figure 4.10: Demand curves for base case (a.) and the most promising retrofit cases according to the methodology proposed in Section 4.3 on the left column and the cases with highest energy savings and PV electricity production on the right column for each retrofit case group: façade retrofit (b), façade retrofit cases with spandrel integrated BIPV's (c), solar shading cases (d), second skin cases (e) and STPV cases (f).

Figure 4.10: Demand curves for base case (a.) and the most promising retrofit cases according to the methodology proposed in Section 4.3 on the left column and the cases with highest energy savings and PV electricity production on the right column for each retrofit case group: façade retrofit (b), façade retrofit cases with spandrel integrated BIPV's (c), solar shading cases (d), second skin cases (e) and STPV cases (f) (cont.).

4.3.6   Site shading influence on the output of BIPV systems

Site shading conditions are an obstacle for the applicability of the façade-integrated BIPV technologies in an urban environment. A model described in Section 4.2 was applied to investigate

the possible solar system yield loss for the given geographical locations from possible obstructions in an urban setting. The results are shown in Figure 4.11 for the latitude range of 45° – 55° north.

The façade urban shading factor is the reduction of total possible solar energy yield on a façade, if compared to an unshaded case. The map is showing the relationship between the height of the obstacle in front of the analyzed façade and the distance of this object to the façade. It can be seen, that for the given latitudes, the electricity production loss of up to 20% starts occurring, when the height of the obstacle is above 15 m and 10 m away from the façade or 25 m high and 40 m away from the façade. The site shading factor has a significant influence on the final results of the solar façade feasibility and has to be considered.
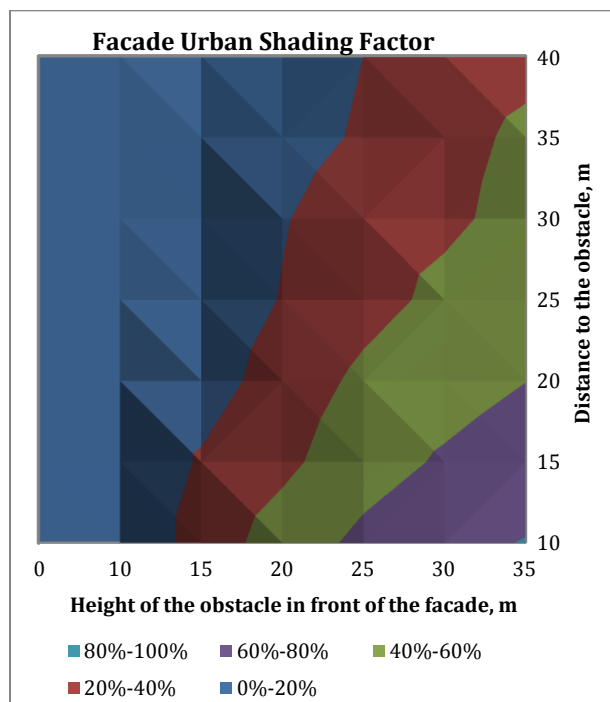
Figure 4.11: Site shading factors for a façade integrated BIPV's in an urban environment for the latitude range of 45° - 55° north.

4.4 Conclusion

This study addresses the need to consider solar technologies in a façade retrofit project in a systematic way. Façade or envelope retrofit in general is considered a risky investment to the building owner and a façade retrofit with envelope integrated PV technologies is even more so. However, the authors of this paper argue, that the addition of the BIPV/EPoG, a new generation of energy producing glazing (ISSOL sa/nv, 2018), is in fact bringing an additional benefit to the building owner, when applied in a systematic façade retrofit project of commercial buildings, as demonstrated in this study.

For the façade retrofit group (additional insulation, window upgrade, infiltration management) the highest NPV/Investment ratio, which ranges from 3.5 to 4.4, and also the lowest specific energy savings cost (ct/kWh) are for Montreal climate. Façade insulation upgrade and addition of a spandrel-integrated BIPV in Montreal climate, is a highly feasible investment. For certain cases the NPV/Investment ratio ranges from 2.6 – 3.7.

It was observed, that cladding replacement with BIPV on façade as a retrofit measure on south, east and west façade is increasing the return of investment for the façade insulation retrofit in the Prairies climate with marginal increase in specific energy efficiency costs, due to higher annual solar irradiation levels and also the existing feed-in-tariffs in Saskatoon. For the Pacific Coast climate the spandrel-integrated BIPV addition just on the south facing façade, is more feasible than façade insulation measures, with the highest NPV/Investment ratio of 2.2. Several cases for Vancouver climate have lower specific energy saving costs, but generally the inclusion of BIPV as spandrel cladding material increases the feasibility of a façade retrofit project for Vancouver and Saskatoon climates.

It was observed, that the shading techniques with BIPV glazing, have a higher potential in Saskatoon climate. For Montreal and Vancouver climates the lower NPV/Investment ratio and not feasible specific costs are observed.

The heating demand peak for Prairies climate can be reduced to 56% with façade insulation and cooling peak demand reduction of 96% is possible with an overhang, 59% with STPV and 64% with second skin additions for the Prairies climate.

Urban shading factors for latitudes between 45°-55° north have been created to estimate the façade-integrated BIPV yield loss from shading in urban environment. The obstacles' height and distance from the façade with BIPV are the inputs and it is a tool to rapidly estimate the potential yield loss in a BIPV feasibility study.

5 Modeling and simulation of a photovoltaic/thermal air collector assisting a façade integrated small scale heat pump with radiant PCM panel

Chapter abstract

Integration of photovoltaic/thermal air-based systems into office façade retrofit projects using small scale decentralized heat pumps with low temperature short term storage using a radiant phase change material panel (RPCMP) is presented for a south facing office building perimeter zone. The concept can be applied in building façade retrofits, where both façade and mechanical systems are to be replaced. A numerical study is carried out for a case study building in Saskatoon, Canada. A numerical model is developed and the concept is theoretically compared to an all-air system for several consecutive design days. Electric power demand reduction of 14,5% for these design days can be achieved, if the façade integrated photovoltaic system would be supplying energy to the perimeter zone for heating and plug load applications. A reduction in heating coil heating power demand of 11.3% is achieved for the mentioned design days when compared to an all-air system.

5.1 Introduction

A façade integrated air-based photovoltaic/thermal (BIPV/T) solar-assisted heat pump with short term PCM heat storage is analyzed. Solar-assisted façade integrated decentralized systems with integrated storage are an attractive option for building retrofits, since both envelope and mechanical systems can be retrofitted at the same time. As a result, the overall construction time and higher quality of the retrofit project can be achieved. This is beneficial to office building owners, since business operation interruptions due to construction activities are reduced. The current rigorous office building façade retrofit practices are not able to address this issue and as a result, many facades are kept in sub-standard conditions (King, 2016).

Façade-integrated solar assisted mechanical systems can supply energy in a decentralized manner and potential benefits of comfort and energy savings due to reduced distribution losses and local demand based control can be achieved (Mahler and Himmler, 2008). Another advantage of having decentralized energy supply is the opportunity to shift the financial responsibility for the energy-use from the building owner to the tenant, increased fire safety and reduced effects of stack pressure difference associated air leakage (Touchie and Pressnail, 2014).

In this paper a solar assisted façade structure integrated system concept is under investigation, to evaluate the potential in a retrofit project of a conventional office building with an all-air system. In this paper the developed energy model is described, numerical simulation is performed and compared to an all air system from energy performance point of view for several design days.

5.2   Façade integrated solar-assisted heat pump system

5.2.1   Technology review

Façade-integrated photovoltaic systems have been applied for the last two decades, when BIPV applications became more attractive to building designers due to the reduced photovoltaic panel prices and increased incentives for renewable energy sources (Zondag, 2008). Since energy production from crystalline PV panels depends on PV module temperature, the heat removal from BIPV modules provides the benefit of increased electricity production due to reduced PV temperature and preheated fresh air production Athienitis et al. (2011). In the case of crystalline photovoltaic (PV) modules, if the building integrated system is used for air preheating using forced air ventilation, the annual PV electricity generation per unit area is from 6% to 10% higher if compared to unventilated and naturally ventilated air gaps respectively for central European climate (Guiavarch and Peuportier, 2006).

Integration of BIPV cladding on prefabricated systems for façade retrofit has also been considered. A prefabricated module for residential façade retrofit was developed by Silva et al. (2013), who reported that the integrated façade retrofit payback would be 6.0 and 6.9 years if the retrofit modules would be without and with integrated BIPV system respectively.

A methodology for façade renovation using prefabricated modules was demonstrated with *TES Energy Facade* system (Heikkinen et al., 2016), where the use of 3D measurements and off site production was suggested with the benefits of precision, quality, reduction of work on-site, noise and disruption of the building inhabitants. In addition, the integration of HVAC and solar components into the retrofit modules was demonstrated. A multifunctional energy efficient façade system for building retrofitting (MEEFS) is a similar standardized façade retrofit concept integrating basic thermal insulation upgrades with technical modules, which can include decentralized ventilation units or photovoltaic and solar thermal systems (Paiho et al., 2015).

Spandrel-integrated solar air collector potential for non-residential buildings in Canada was demonstrated by Richman and Pressnail (2010). The solar dynamic buffer zone (SDBZ) within curtain wall system was studied analytically and experimentally and it was demonstrated, that this system is a low cost method, for gathering solar energy efficiently pressurizing the air gap accordingly to the solar heat availability. The spandrel integrated SDBZ performance was investigated for Toronto climate during heating season and demonstrated approximately 40% thermal efficiencies, 150-210 kWh/m^2 heating power production, temperature lifts of up to 15°C in January for design conditions with mass flow rates of 15 – 290 m^3/m^2 h (Richman and Pressnail, 2010).

The supplied air from a façade-integrated air-based solar system can be used either for fresh air preheating or the heat can be upgraded with a heat pump and used for building space heating. A major incentive to use air-based solar collectors with air source heat pumps is the improvement of

the heat pump coefficient of performance (COP) during the sunshine hours, since the COP of air source heat pumps falls with decreasing ambient temperatures (Touchie and Pressnail, 2014; Roth et al., 2009; Candanedo and Athienitis, 2008). Some design improvements for heat pumps have been used by manufacturers: sizing them for heating, instead for cooling, multiple operation compressors, increased outdoor air coil capacity, using carbon dioxide (CO_2) refrigerant cycles, mechanical liquid sub-cooling and optimization of the indoor and outdoor coil circuiting (Roth et al., 2009). The utilization of solar heat for raising the heat pump COP has been explored by a number of researchers and various system concepts have been studied Haller et al. (2014). Air-based solar collectors are considered here for façade applications, since air-based PV/T need much less maintenance and are easier to install. A type of solar buffer was demonstrated by using a glazed balcony as a source for a heat pump for residential building retrofits in Toronto, Canada (Touchie and Pressnail, 2014). A hybrid source heat pump supplying heat to both south and north zones of a residential suite demonstrated potential from energy efficiency and ecological point of view. Air-based BIPV/T solar collectors directly assisting heat pump were investigated for a net zero house in Canada (Candanedo and Athienitis, 2008). Through simulations it was shown that two parallel connected heat pumps would result in higher COP values and could work efficiently at lower mass flow rates, than one series connected heat pump. Another façade integrated heat pump concept using exhaust air as source for a micro heat pump integrated in envelope structure for façade retrofits (Gustafsson et al., 2014). Through simulations it was demonstrated, that an exhaust heat pump would demonstrate better performance than air source heat pump with a radiant system for a Nordic Stockholm climate. However, a combined system with exhaust air as source for micro heat pump and a radiator was not simulated.

Use of low temperature heating systems is another way to improve the heat pump COP, reduce the compressor cycling and improve distribution efficiency. An air to water heat pump with radiant delivery to homes was simulated in cold Denver climate low load homes and compared to an all air

system and showed a significant 31% energy savings for HVAC operation with cost effectiveness for cold climate (Backman et al., 2016). A similar system with a small scale heat pump and photovoltaic array with electrical storage as energy supply was studied for heating application in Spanish heating season for a building with 6 KW peak heat demand (Izquierdo and Augustin, 2015). The PV array was undersized and the solar fraction was 65.3%. The heat pump performance was not investigated, focusing on the experimental performance of PV-heat pump operation mainly.

In this study a radiant panel with a PCM layer is considered (named RPCMP). The RPCMP is directly connected to the heat pump and acts as a short term thermal storage (approx. 4-6 hours, to utilize the collected heat with the solar collector shifted to a period with heating load in cold climate office buildings). It has been demonstrated, that 54-67% of heat produced by an air-based solar collector during daytime can be delivered during nighttime for building heating directly charging the latent heat storage (Arkar and Medved, 2015).

To the authors best knowledge, no studies have been carried out with a complete system consisting of a façade integrated BIPV/T with a small scale heat pump with radiant heat delivery with short term storage with PCM to the office building zones. This paper is aimed at demonstrating the developed model of such a system and studying its performance.

5.2.2 *Principles of use*

The basic configuration of the decentralized solar assisted system is shown in the Figure 5.1. The BIPV/T air collector is supplying preheated air over the evaporator of the heat pump, which in turn is moving the heat to radiant panel. The RPCMP acts as a short term (a few hours) thermal storage device sized to store heat delivered by the heat pump and release it to the zone passively, when the space heating demand increases, in this case in evenings. In Figure 5.2 the perimeter zone cross section is shown with a decentralized system integrated in the façade.
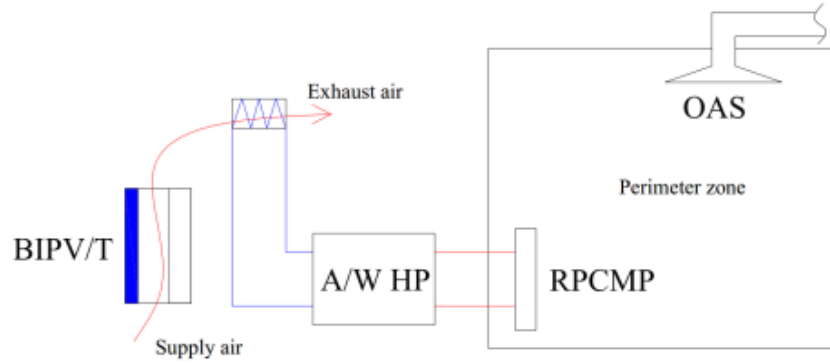
Figure 5.1: The decentralized façade integrated solar assisted heat pump system scheme.

The outdoor air supply (OAS) system is providing fresh air, cooling and acting as an auxiliary heat supply to the perimeter zone and the RPCMP is providing heat to the space from solar (BIPV/T) assisted air-to-water heat pump (A/W HP) system. RPCMP is also acting as short term heat storage.
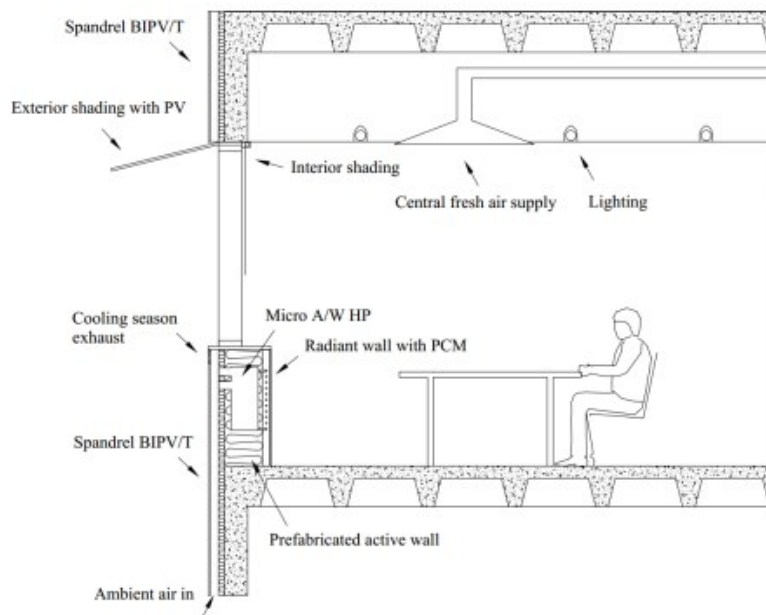
Figure 5.2: A cross section of a perimeter zone with a decentralized solar assisted system with integrated short term thermal storage for a commercial building.

The radiant panels in a retrofit project can be installed either on the wall or on the ceiling. The existing air handling system will be supplying 100% of fresh air. Ideally the heat pump system

should cover all of the space heating demand and outdoor air supply system can act as auxiliary heat supply as well. Alternative option is to use the façade integrated air collector to supply fresh air, which can be preheated with solar collector or with a façade integrated heat recovery system and the exhaust heat could be recovered by a façade integrated exhaust air source heat pump. The concept could also be applied to a balcony closed with semitransparent PV.

5.2.3 Design of the system

Base case façade design is based for a case study building in Saskatoon, Canada. The whole building model was developed and main parameters identified in a previous study (Bigaila et al., 2016). The validated model facade RSI was 0.88, glazing U value was 3.52 W/m^2 °C with solar heat gain coefficient (SHGC) 0.62, plug loads - 7 W/m^2 and lighting density - 11.95 W/m^2. The model created with Matlab/Simulink is modeled with a single zone packaged VAV unit based on ASHRAE 90.1 guidelines. Fresh air supply rate chosen based on ASHRAE 62.1, which suggests floor area rated outdoor air rate of 0.3 L/s-m^2 and occupancy based outdoor air rate of 2.5 L/s-person. This results in total outdoor air rate of 8.5 L/s-person. Heating and occupancy schedule is from 7:00 – 20:00 daily. The performance for heating period was evaluated for 4 consecutive design days: two cold days with mean ambient temperature of -10°C and two consecutive days with mean ambient temperature of -6°C. The total solar irradiation peaks on south facing façade for design days is 700/200/700/200 W/m^2.

A 3 kW air-to-water heat pump model was selected, with COP of 3.27 at 2°C source air temperature and 35°C load water temperature as a base case. The performance data is shown in the Table 5.1 and is taken from M. Gustafson study (Gustafsson et al., 2014).

Table 5.1: Heat pump performance data used in this study (Gustafsson et al., 2014).

	Water temperature [°C]	Air temperature [°C]			
		-15	2	10	30
Heating output [kW]	35	1.70	3	4.60	5.50
	55	1.30	2.70	3.80	4.70
COP	35	1.90	3.27	4.83	5.70
	55	1.16	2.12	2.87	3.45

The radiant panel design is shown in Figure 5.3. The piping and metal contact is a radiant heating panel with back-side insulation and adhered PCM layer on the front-side of the panel. The PCM layer consists of DuPont Energain panels, which are shape-stabilized panels of paraffin wax suspended in an ethylene-based polymer. These panels were characterized and modeled by V. Dermardiros, (2015). PU rigid insulation with 0.025 W/m K conductivity is considered for the back-side insulation. A 0.005 m thickness 0.51 W/m K conductivity adhesive layer between radiant panel metal sheet and Energain PCM panels (DuPont Energain, 2016).
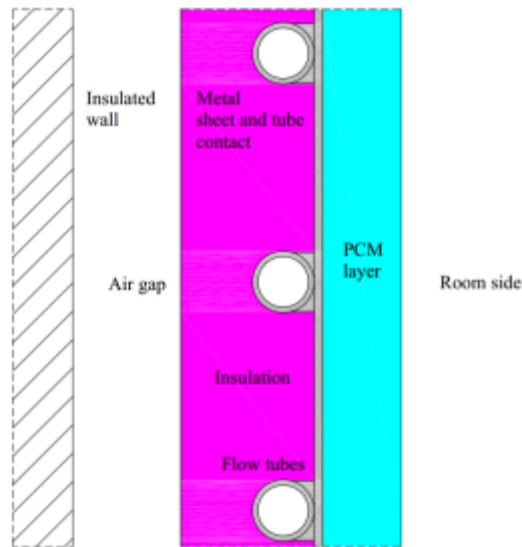
Figure 5.3: The wall RPCMP conceptual scheme.

The PV/T-air collector integrated in façade is a framed PV air-based solar thermal collector. The framing system allows the air collectors to be installed using conventional curtain wall construction elements and PV modules act as a spandrel section cladding elements. The PV modules generate

electricity and warm air, while performing as a rain screen cladding with high architectural integration flexibility. Current conventional silicon technology PV panels produce electricity up to nearly 40 years and can last longer if well designed and cooled, which offers durability similar to that of a conventional cladding materials.

The case study building façade integrated BIPV/T system was described in previous studies by Bigaila et al. (2015). Exterior wall consists of porcelain enamel on steel spandrel panels and limestone facing, air gap, 20.32 cm clay "Terra Cotta" bricks, 5.1 cm mineral wool insulation and interior plaster with aluminum frame double pane glazing with air gap. Window-to-wall ratio (WWR) for south and west façade is 48%. The office area considered for analysis width is 5 meters with a 2.2 meter high BIPV/T section. The BIPV/T system consists of 18 PV panels and results in total of 4.42 kW_p array peak power at STC. The thermal model details for the PV array are shown in Table 5.2.

Table 5.2: BIPV/T spandrel parameters.

Parameter	Unit	Value
BIPV/T geometry		
BIPV/T section width	M	4.8
BIPV/T height	M	1.4
Duct height	M	0.07
PV parameters		
STC efficiency	%	15
Temperature modifier	%/ °C	-0.04
Absorption of PV surface		0.95
Façade parameters		
Thermal resistance	m²K/W	4.5

5.3   **Numerical study**

5.3.1 Modeling

5.3.1.1 Building model

The external walls of the perimeter zone are modeled assuming one-dimensional heat flow, with each wall-layer separated into two equal partial capacities, both on surfaces of the wall layer, and partial capacities combined in a single one, in the case of joined layers (Feist, 1993). All the incoming solar radiation is assumed to be incident on the floor, which is reasonable for a large open office space. The room model performance verified with commercial building model TRNSYS was demonstrated by E. Bigaila (2016).

5.3.1.2 BIPV/T model

The model is a quasi-steady state based on energy balance of a solar air-based flat plate collector. The solar absorber is the exterior opaque plate, which is the PV panel in this case. The energy balance is be solved for all BIPV/T area with simple lumped parameter models or discretized into smaller control volumes for more accurate results with higher resolution. The energy balance in the PV module is expressed by equation 5.1.

$$\alpha GA_{pv} = E_{pv} + Q_1 + Q_{ra} + Q_c + Q_r \qquad\qquad 5.1$$

where αGA_{pv} is the solar radiation absorbed by the PV module, E_{pv} is the electricity generated by PV modules, Q_l is the exterior convective loss, Q_{rs} is the exterior radiative thermal loss to the sky, Q_c is the heat removed by heat transfer fluid in the channel, in this case air, and Q_r is the radiative heat exchange between PV and the back plate surface.

The air temperature in the control volume is estimated by an exponential air temperature variation, which is the exact solution if the temperatures of the surrounding surfaces are assumed to be uniform and the average air temperature for energy balances is estimated by equation 5.2.

$$T_{av} = \int T dx / \Delta x \qquad\qquad 5.2$$

where T_{av} is the average control volume bulk air temperature.

The interior convective heat transfer correlations are specific for each air collector type and geometry due to non-developed flow conditions and framing effects on flow type. The façade BIPV/T is a flat plate air collector characterized as a rectangle duct with asymmetric heating. A prototype BIPV/T façade system was developed by E. Bigaila and the model was experimentally validated (Bigaila et al., 2015). The Nusselt number correlations developed by L. Candanedo (2010) were used (equations 5.3 and 5.4).

For laminar region, 250 ≤Re≤2400

$$Nu_{top}(x) = 0.039 Re^{0.78} Pr^{0.4} e^{-\frac{x}{20 D_h}} + 0.034 Re^{0.78} Pr^{0.4} \qquad\qquad 5.3$$

For turbulent region, 2400 <Re≤7100

$$Nu_{top}(x) = 0.012 Re^{0.78} Pr^{0.4} e^{-\frac{x}{9.09 D_h}} + 0.049 Re^{0.78} Pr^{0.4} \qquad\qquad 5.4$$

Electrical efficiency model is a linear relationship between PV module efficiency change due to temperature effect adopted from (Duffie & Beckman, 2006) (equation 5.5).

$$\eta_{PV} = \eta_{mpp} T_{PV,ref} - \gamma_{mpp,ref}(T_{PV} - T_{PV,ref}) \qquad\qquad 5.5$$

where η_{PV} is the efficiency of PV module, η_{PV} the efficiency at reference temperature, $T_{PV,ref}$ is PV module reference temperature, $\gamma_{mpp,ref}$ is efficiency modifier from temperature, T_{PV} is the PV module temperature.

5.3.1.3 Heat pump model

The heat pump is modeled as a black-box (CARNOT, 2017). The model is a steady state empirical model with boundary conditions of the evaporator and condenser inlet temperature, the evaporator and condenser mass flow and the control signal of an external simulated controller.

The output of the condenser and the evaporator is calculated based on characteristic curves which are usually supplied by manufacturer of the heat pump. The curves show the condenser output and the electric power as a function of the evaporator inlet temperature and the condenser outlet temperature. These values are used to calculate coefficients of fitted biquadratic polynomials. The calculation of these coefficients has to be carried out separately. To increase the power of the heat pump by keeping the coefficient of performance constant, the condenser and the compressor power can be linearly scaled with a constant factor.

5.3.1.4 RPCMP model

The radiant panel is of a sheet and tube design. The cross section is show in the Figure 5.3. The thermal network with one PCM layer is shown in Figure 5.4. R_b and R_i is the combined convective and radiant heat transfer to room air T_a. T_i and T_p is the surface temperatures of insulation and PCM layer respectively. R_{ins} is the thermal resistance of insulating layer and R_{pcmp} is the thermal resistance of the PCM layer including the adhesive resistance and R_{pcm} is the thermal resistance of PCM layer. Calculation of R_p and of PCM layer properties will be described in the following sections. T_{pm} is the mean plate temperature and T_{pcm} is the mean PCM layer temperature. The terms U_b and U_f in Figure 5.3 represents the heat transfer through the panel front, back and edges, where the back heat loss coefficient is essentially the heat loss through insulation and front loss is the heat transfer through the PCM layer. The edge loss is ignored in this study. The total heat transfer U_l is the sum of U_b and U_f.

Main modeling assumptions:

- The metal contact temperature is assumed to be uniform;

- Thermal mass of the metal and insulating material is not considered;

- Edge losses are neglected;

- The headers provide uniform flow to tubes;

- Heat flow is one dimensional;

- Temperature gradients around tubes can be neglected;

- The temperature gradients in the flow and between the tubes can be treated independently;
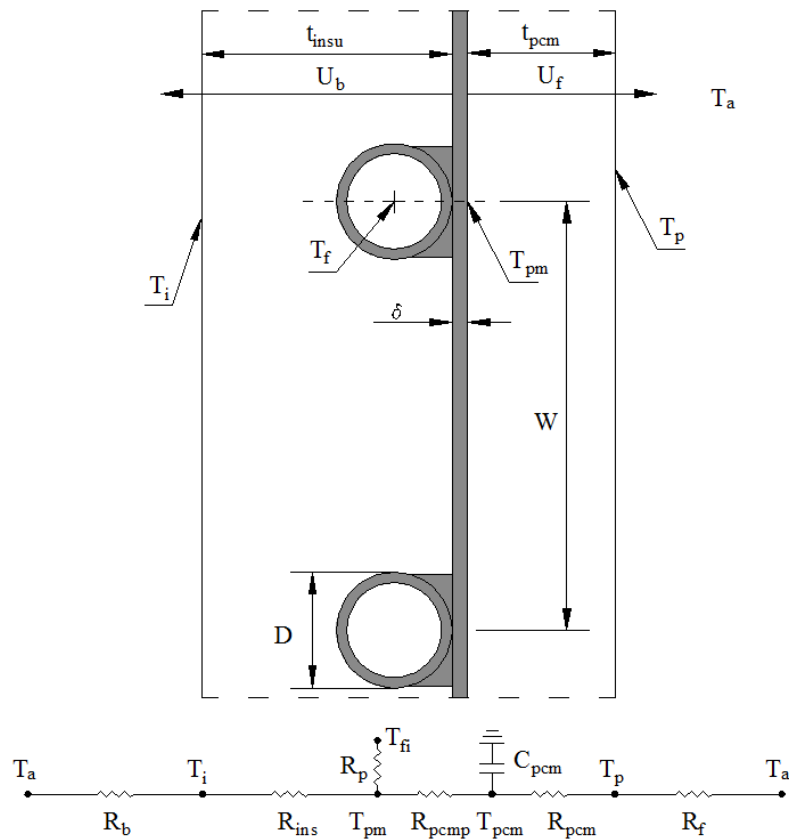
Figure 5.4: Simplified cross section scheme and thermal network of the wall RPCMP model. Radiant heat transfer to the room surfaces and radiant heat transfer to the wall surface from the back-side are not shown.

The sheet-tube configuration is visible in Figure 5.4. The distance between the tube centerlines is W, the tube exterior diameter is D, the thickness of the sheet is δ, the thickness of the insulation is t_{insu} and the thickness of PCM layer is t_{pcm}. T_b is the local base temperature. The solution to this problem can be treated as a classical fin problem (Duffie and Beckman, 2006).

The energy balance yields:

$$-U_L \Delta x (T - T_a) + \left(-\frac{k\delta dT}{dx}\right)\big|_x - \left(-\frac{k\delta dT}{dx}\right)\big|_{x+\Delta x} = 0 \qquad 5.6$$

where dx is elemental region of width, k is the conductivity of the metal plate. This energy balance is solved for the two regions of radiant panel. q_1 is the region that corresponds to the root section and q_2 is the one that corresponds to the fin section:

$$q_1 = (W - D)[-U_L(T_b - T_a)]\frac{\tanh m(W - D)/2}{m(W - D)/2} \qquad 5.7$$

where

$$m = \sqrt{U_L/k\delta} \qquad 5.8$$

And

$$q_2 = -U_L D(T_b - T_a) \qquad 5.9$$

The total heat transfer from the panel is written as:

$$q_u = q_1 + q_2 = ((W - D)F + D)[-U_L(T_b - T_a)] \qquad 5.10$$

Where

$$F = \frac{\tanh[m(W - D)/2]}{m(W - D)/2} \qquad 5.11$$

By considering the water side resistance, contact and conduction resistance of bond between the tube and the sheet, the heat transfer from water to radiant panel is expressed as follows:

$$q_u = WF'\left[-U_L(T_f - T_a)\right] \tag{5.12}$$

where the collector efficiency factor F' is expressed as follows. In the following equation the bond conductance C_b, pipe interior diameter D_i and the heat transfer coefficient between the fluid and the wall h_{fi} is introduced.

$$F' = \frac{1/U_l}{W\left[\dfrac{1}{U_L[D + (W - D)F]} + \dfrac{1}{C_b} + \dfrac{1}{\pi D_i h_{fi}}\right]} \tag{5.13}$$

The heat transfer inside the pipe h_{fi} for turbulent flow is expressed using Gnielinski correlation (Bergman et al., 2011) for Nusselt number:

$$h_{fi} = \frac{Nu\,k}{D_i} \tag{5.14}$$

$$Nu_D = \frac{(f/8)(Re_D - 1000)Pr}{1 + 12.7(f/8)^{1/2}(Pr^{2/3} - 1)} \tag{5.15}$$

where Re is Reynolds number, Pr is the Prandlt number and f is the friction factor, that can be obtained from the following equation:

$$f = (0.79\log(Re) - 1.64)^{-2} \tag{5.16}$$

For laminar flow, the Nusselt number is Nu=4.364.

The bond conductance is very important, since it can result in a significant loss of the panel efficiency. The bond conductance should be greater than 30 W/m °C for appropriate performance of the sheet and tube construction (Duffie and Beckman, 2006).

The average temperature of the panel can be obtained by performing integration along the water flow direction of one panel. The energy balance is as follows:

$$\left(\frac{\dot{m}}{n}\right)C_p T_f|_y + \left(\frac{\dot{m}}{n}\right)C_p T_f|_{y+\Delta y} + \Delta y q'_u = 0 \tag{5.17}$$

where $\dot{m}$ is the total mass flow rate of the panel, n is the number of parallel tubes, y and $\varDelta y$ are length and element region of length of the pipe. Substituting L for y, dividing through by $\varDelta y$, finding the limit as $\varDelta y$ approaches zero and substituting q_u with the previously mentioned expression, we obtain the expression of the fluid outlet temperature T_{fo} to fluid inlet temperature T_{fi}:

$$T_{fo} = T_a + \exp(\frac{-U_L A_c F'}{\dot{m} C_p})(T_{fi} - T_a)$$ 5.18

A quantity relating the actual sensible heat of a panel to the sensible heat if the whole panel surface were at the fluid inlet temperature is called panel heat removal factor F_R and is calculated as follows:

$$F_R = \frac{\dot{m} C_p (T_{fo} - T_{fi})}{A_p U_L (T_a - T_{fi})}$$ 5.19

Then the overall heating or cooling capacity of the panel can be calculated either applying the concept of the heat recovery factor or using the panel mean temperature:

$$Q_u = -A_c F_R U_L (T_{fi} - T_a)$$ 5.20

$$Q_u = A_c U_L (T_a - T_{pm)}$$ 5.21

Based on the previous equations, the mean plate temperature T_{pm} can be calculated as follows:

$$T_{pm} = T_{fi} + \frac{Q_u / A_c}{F_R U_L}(1 - F_R)$$ 5.22

5.3.1.5 The PCM layer model

The PCM model is based on measurements by V. Dermardiros (2015) in the same team as the present authors. The specific heat of the PCM panels is expressed using a continuous curve based on a skewed normal distribution, which offers a simplified method to input characterization data and improves simulation time of the PCM material.

$$C_p(T) = \Delta h \frac{1}{\sqrt{2\pi}} \exp\left(\frac{-(T-T_c)^2}{2\omega^2}\right)\left[1 + erf\left(\frac{skew(T-T_c)}{\sqrt{2}\omega}\right)\right] + C_{p,average} \qquad \text{5.23}$$

where Δh is the enthalpy of fusion, T_c is the approximate temperature of peak phase change, w is the temperature range of change, *skew* is the skewness factor and $C_{p,average}$ is the average specific heat of PCM in the sensible range. The 5 determined parameters needed for the proposed method of PCM modeling are given in Table 5.3.

Table 5.3: Specific heat equation input values V. Dermardiros (2015).

Parameters	Melting	Freezing
Δh, kJ-kg^{-1}	13 100	12 600
T_c, °C	23.6	20.8
ω, °C	4.5	4.7
Skew	-10	-4
$C_{p,average}$, kJ-kg^{-1}	3500	3500

The conductivity of the PCM material is expressed as follows:

$$k(T) = k_{solid} + \frac{k_{solid} - k_{liquid}}{2}[1 - erf(slope(T - T_k))] \qquad \text{5.24}$$

where k_{solid} is the conductivity of the solid phase, k_{liquid} is the conductivity of the liquid phase, *slope* is the slope of the transition between phases and T_k is the approximate temperature of peak change.

5.3.2 Numerical results

5.3.2.1 Spandrel BIPV/T output

The BIPV/T air collector energy is described by varying air collection mass flow rates at different irradiation and wind speed levels, since these are the most significant environmental factors affecting the output of the solar air collectors, see Figures 5.5-5.7. Thermal heat and temperature

difference between the ambient air and collector output are shown in Figure 5.5 for different solar radiation levels. At mass flow rates below 0,1 kg/s a temperature rise from 10 – 25°C can be achieved. For mass flow rates above 0,4 kg/s the air temperature difference from 1 - 7°C is still possible. Obviously the thermal output changes with different collector designs. For example, a collector with enhanced heat removal from the absorber plate introducing multiple air intakes into the channel, can increase the efficiency of this collector by more than 5% (Bigaila et al., 2015).

Wind speed has a significant effect on the temperature difference for mass flow rates below 0,15 kg/s, but when the mass flow rate increases, the temperature difference is not affected significantly by exterior wind speed as seen from Figure 5.6. In fact higher wind speeds result in better cooling of the PV panel, which in certain cases can increase the combined output of a hybrid collector.

As shown in Figure 5.7, mass flow rates above 0.6 - 0.7 kg/s start to show a decreasing net power output from spandrel integrated BIPV/T air collector system. This implies, that mass flow rates above 0,7 kg/s are considered outside of the normal operating air collector range and should be not considered, when selecting an appropriate spandrel integrated application.

For fresh air-preheating, this system is considered as a feasible solution for cold climate office buildings. For a south facing office perimeter zone in Saskatoon, Canada, this air collector can be used for fresh air supply, night cooling, in an economizer mode and for space heating. A combined 59% reduction in overall heating load and 36% in cooling load is possible, with electric power generation of 92.65 kWh/m² a (Bigaila and Athienitis, 2016).

For heat pump application a careful selection of a heat pump is important. The market available small scale air source heat pumps that operate at smaller source side air flow rates are either domestic exhaust air-to-water or small scale air-to-water heat pumps, as observed by the authors of this paper. The exhaust air-to-water heat pumps are operated so that the source side air mass flow rates could be adjusted to building ventilation needs, which is from 30 to 70 l/s or 0,04 – 0,08 kg/s

of air at 25°C. However, this results in smaller heating output of the heat pump of approximately 1,5 kW with COPs from 3,34 to 5,43, due to higher source side temperature Gustafsson et al. (2014). A small scale air-to-water heat pump source side mass flow rates are in the range of 0,1 – 0,6 kg/s operating at ambient conditions with COPs from 1,5 – 4,5 and nominal heating capacity of 2,92 kW (Touchie and Pressnail, 2014). The following type was chosen due to the fact that it is operated at ambient conditions with higher outputs and higher mass flow rates on the source side, that fall within the BIPV/T operating range.
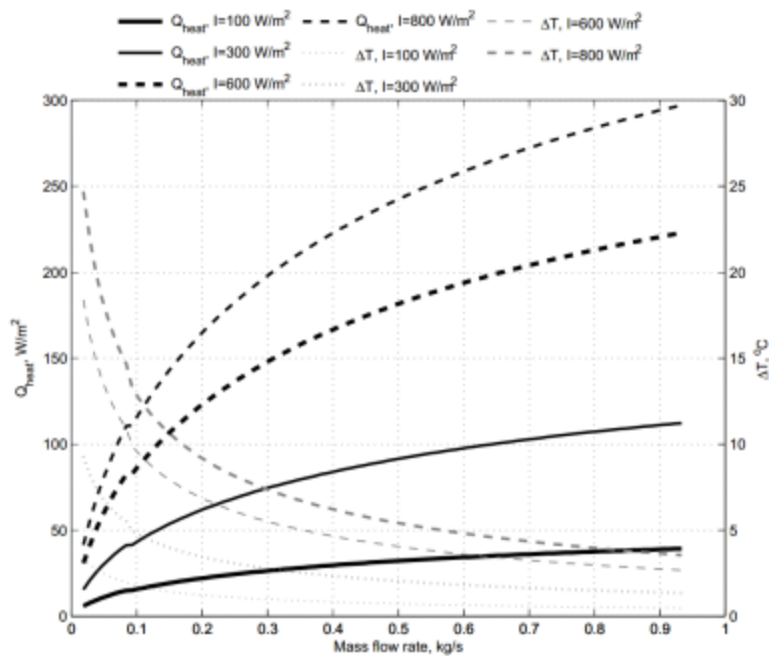
Figure. 5.5: Area weighted thermal output and temperature rise as a function of mass flow rate and irradiation for the described spandrel integrated BIPV/T air collector.
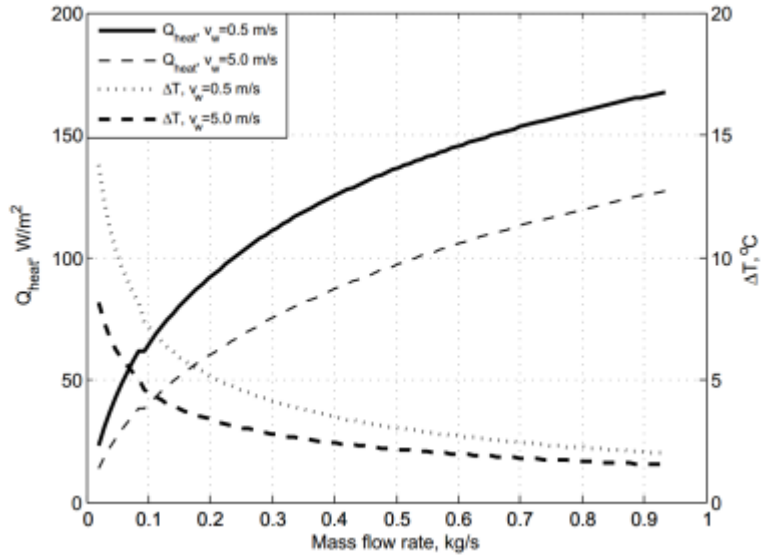
Figure. 5.6: Area weighted thermal output and temperature rise as a function of exterior wind speed at 450 W/m² for the described spandrel integrated BIPV/T air collector.
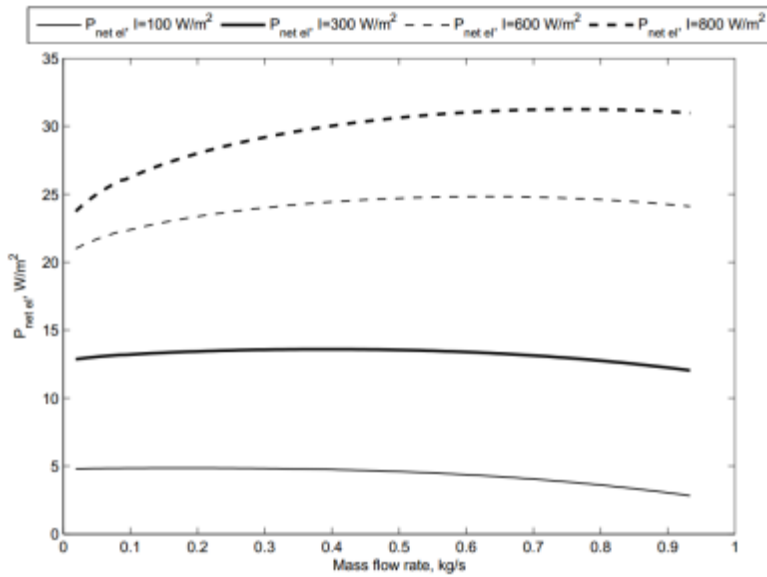
Figure 5.7: Net electric power of the BIPV/T (generation by the PV cells subtracted by the fan electricity consumption) as a function of mass flow rate.

167

5.3.2.2   RPCMP performance

A parametric analysis of the proposed design RPCMP is performed. Since the radiant panel is a multifunctional device, both supplying sensible heating/cooling to the space and acting as a short term storage device, optimization of the supply temperature for heating/cooling application and heat storage for later use must be performed. To increase the heat storage capacity panel PCM layer thickness must be evaluated taking into consideration the diminishing radiant panel heating capacity with thicker front PCM layer. To keep the radiant heat delivery to the room at adequate levels supply water temperature can be increased. However, this can lead to operating the PCM panel outside of the phase change range, which can result in reduced thermal capacitance for the short term storage applications. Radiant panel area in that case is an important design parameter. Another option is to find PCM panels that have optimal phase change temperature, however PCM panel product range is not flexible enough for this case.

Panel performance in heating mode

The wall panel heating capacity is shown in Figure 5.8. The heating capacity depends from supply water temperature and mass flow rate. The results in Figure 5.8 are given at 0.03 kg/s water supply mass flow rate. The insulation thickness is 0.1 m rigid PU insulation with 0.025 W/m K conductivity and PCM thickness of 0.1 m. The heating capacity for the wall panel at 30°C supply water temperature is 50 W/m^2 if the room temperature is 20°C and 200 W/m^2 at 58°C supply water temperature. The room air temperature affects the heat flux by 10 W/m^2 per °C for wall panels.
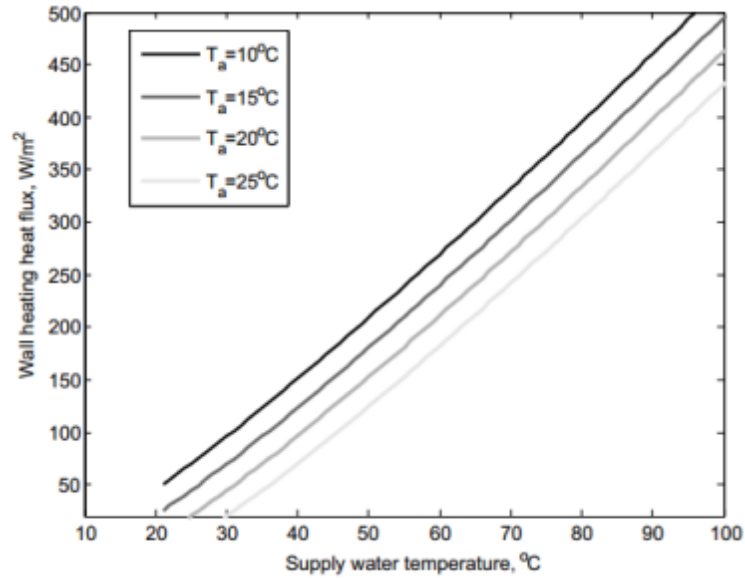
Figure 5.8: Wall panel heating flux vs. panel surface temperature for different constant room air temperatures.

RPCMP sensitivity analysis of steady state performance

The PCM layer thickness influence on heating output is shown in Figure 5.9, where the room air and surface temperatures were kept at 20°C, supply water temperature was from 21 to 100°C, PCM thickness was varied from 0 to 0.1 m and the supply water mass flow rate was 0.03 kg/s. As can be seen, the increasing thickness at the same supply water temperature decreases the heating output of the RPCMP. For example for 40°C supply water temperature the heat output of a wall panel without PCM layer on the front side would be 120 W/m² and with 0.1 m thickness PCM layer the heat output would be 29 W/m².
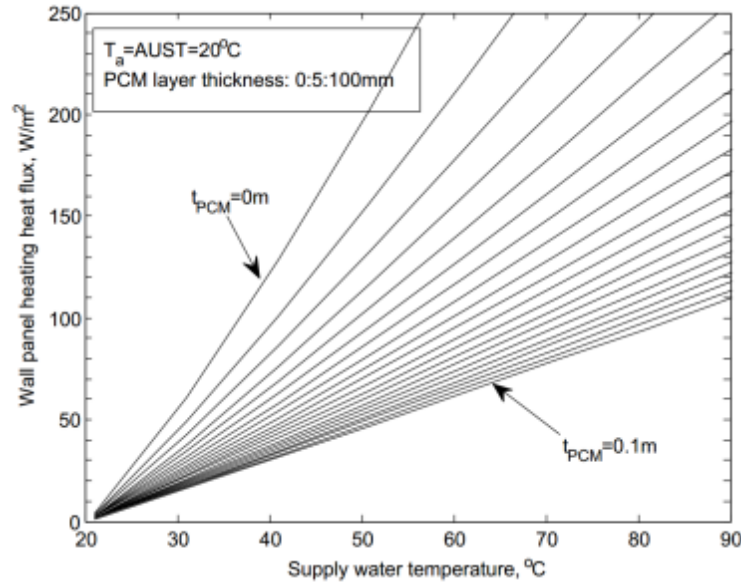
Figure 5.9: Wall RPCMP heat flux with different PCM layer thickness vs. supply water temperatures.

Top side thermal resistance effect on the panel heat output

Figure 5.10 presents the RPCMP heat output dependence on top side insulation parameters. The insulation thickness was varied from 5 mm to 125 mm which results in RSI values from 0.1 to 2.5. The water supply temperature was 25°C, T_{room} and all surfaces at 20°C and supply water mass flow rate was 0.03 kg/s. The temperature of the PCM layer at this condition is at the phase change range. The simulations were performed for wall panels. The general tendency is that the largest effect on the heat flux from the insulation is when the insulation is from 0.1 to 0.5 RSI as seen in Figure 5.10. After RSI 0.5 the effect is negligible. Thus, the optimal back-side insulation design thickness is approximately 2.5 cm for a rigid PU panel with conductivity of 0.025 W/m-K, which results in 0.5 RSI. In the Figure Q_u is the overall heat flux from panel to air and the Q_{back} and Q_{front} is the heat flux through insulation and PCM layer respectively. The higher flux through front is a result of lower convective heat transfer coefficient in the natural convection mode. This heat is stored in PCM layer and later passively released.

170
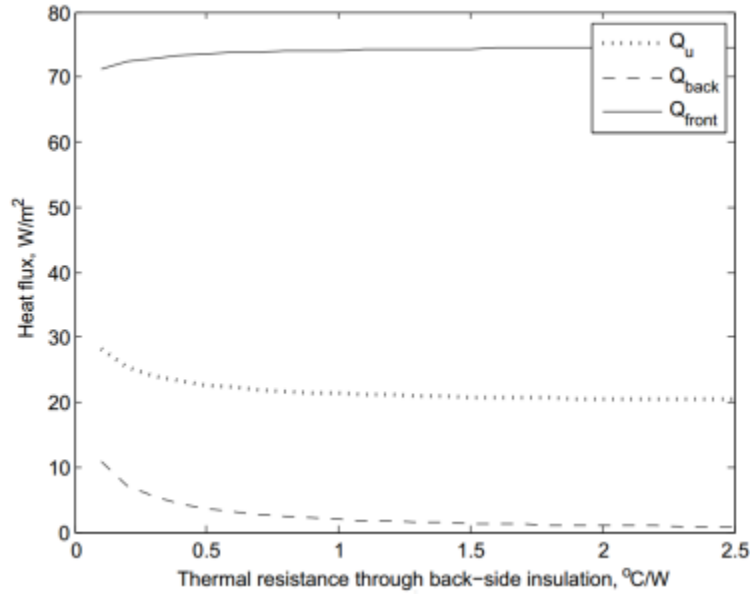
Figure 5.10: Wall radiant panel heat flux Q_u (from plate to front and back surfaces) and heat flux through front and back (from plate to front and back surfaces) vs. thermal resistance through back-side insulation.

The impact of PCM layer thickness on RPCMP storage capacity

The RPCMP thermal storage capacity effectiveness is estimated using the dynamic model. The study is aimed at finding the effect of the PCM panel thickness on the storage capacity while actively charging the panel with 30°C supply water temperature and applying constant 50 W/m² heat flux to the air node. Four thicknesses of PCM panel were investigated: the base case 5mm, 10mm, 15mm and 20mm. The phase change region for charging the PCM panels is from 20 to 24°C. The effective storage capacity is estimated applying the mentioned heating load of 50 W/m² for the charge period. The results are shown in Figure 5.11 and Table 5.4.

171
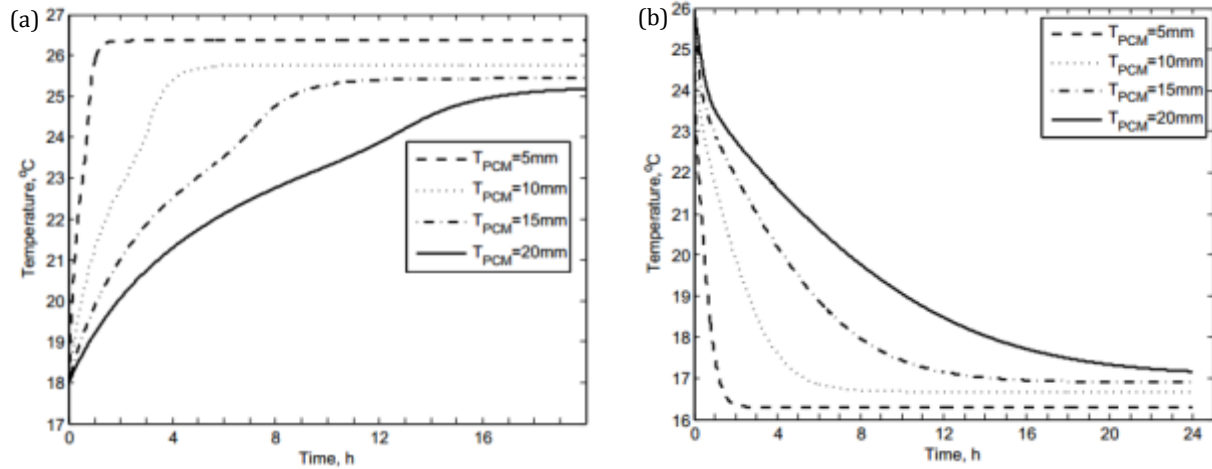
Figure 5.11: Charge (a) and discharge (b) PCM temperature profiles with different PCM layer thickness.

Table 5.4: Storage capacity of RPCMPs.

Thickness of PCM layer, mm	Charging time, h	Storage capacity, Wh/m²
5	0.6	29
10	2.5	123
15	5.7	287
20	10.5	524

5.3.3 Façade application study

5.3.3.1 Temperature profiles for design days

The operation concept of the whole system is shown in Figure 5.12 for a 4 consecutive design days during a heating season. The south facing perimeter zone has a 48% window-to-wall ratio, 25 m² floor area with a single duct variable air volume (VAV) system. The profiles are demonstrated for an optimized façade design in a retrofit case by Bigaila et al. (2016). The selected heat pump is a 3 kW air-to-water HP by Veissman (Gustafsson et al., 2014) connected to a 6 m² RPCMP with 10 cm thick PCM layer. The HP is assumed to be operated using a basic proportional-integral controller.

The temperature profiles of room air (T_{room}), RPCMP PCM surface facing the room ($T_{PCM,surf}$), panel water supply ($T_{w,supply}$), outdoor air supply ($T_{supply.OA}$), BIPV/T outlet air ($T_{out.BIPV/T}$) and heat pump condenser heat input ($Q_{out.hp}$) profile are shown. In this case the selected 3 kW heat pump is charging the PCM panel for 3-4 hours. The heat pump is turned-off when there is no heating demand. As seen from the simulations, during afternoon, the temperature of the room is varying within the heating and cooling setpoints. Later in the day, the temperature starts to drop and the passively and actively collected heat is released back into the room and no auxiliary heat is needed for all 4 design days.

If compared to a conventional VAV system, the total electricity consumption during the design days was nearly 8% lower, which is in fact the additional electricity consumption of the heat pump, plus additional electricity generation with the spandrel integrated BIPV/T collector. If the decentralized fresh air supply would be implemented, the electricity consumption difference would be much higher, since the fan electricity consumption for air distribution from central system would be eliminated. The supply air heating coil energy consumption reduction was 5%. The difference could be larger, because during the first hours of the simulation the air temperature is below the setpoint and auxiliary heat plus heat pump are activated.
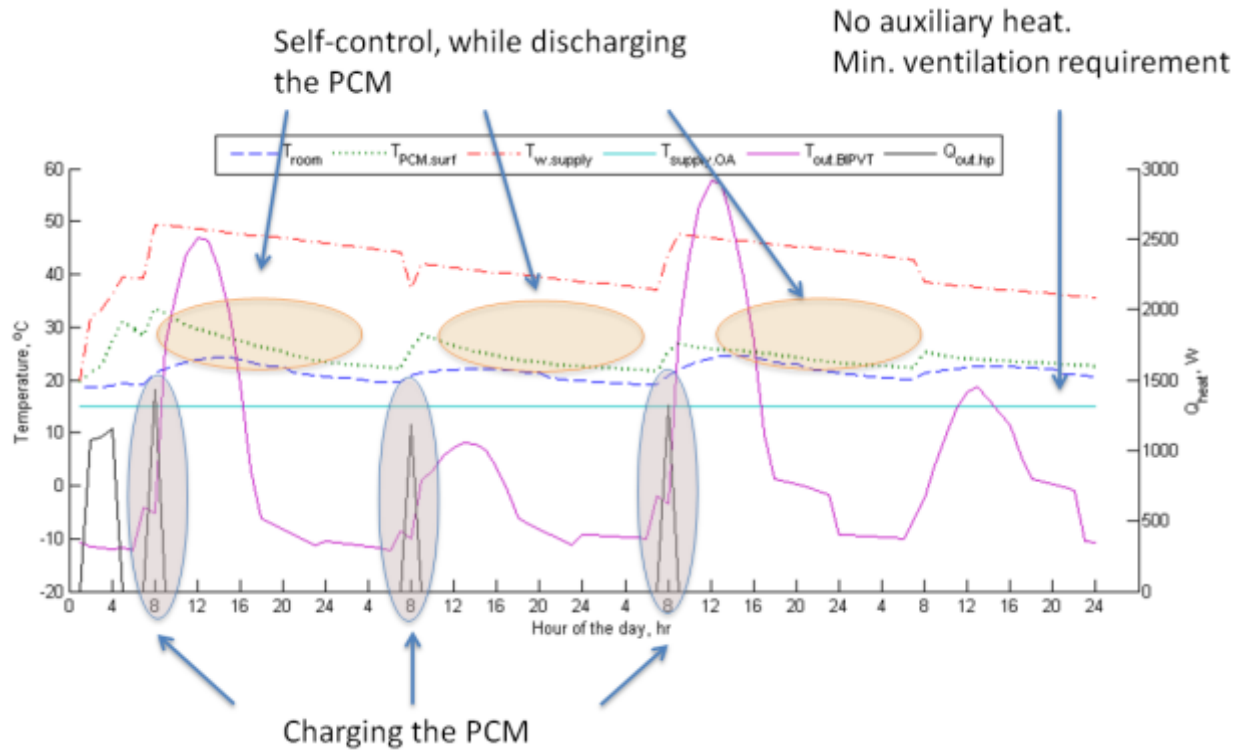
Figure 5.12: Decentralized system performance for south facing office building perimeter zone.

5.3.3.2 Heating season energy performance evaluation in a retrofit case

Simulations of several retrofit scenarios were performed and are shown in Table 5.5. For reference, the base case and an optimal façade retrofit design based on the solar façade retrofit methodology presented by Bigaila et al. (2016) is shown alongside two cases with decentralized façade integrated BIPV/T assisted systems. Case 2 is a replacement of an all-air heating system with the presented concept. Case 3 is an option to recover the rest of the potential solar heat from BIPV/T air collector, upgrade it with a heat pump and store it using sensible heat storage, like water tanks. In this case there would be a potential to further increase the electric power production of the BIPV, have a higher seasonal COP of the heat pump and recover more available heat with the air collector and use it in building zones, that require space heating, when necessary. The potential is high, since as shown in Figure 5.12, the heat pump is charging the RPCMP latent storage only for a few hours in the morning, when the heating demand is high and during the rest of the day, the heat pump is not

operated and the BIPV cells are not cooled. The simulations show that for a climate like Saskatoon, Canada, a 71% solar fraction can be achieved for case 3. For case 4, there is a significant increase in electricity production, due to reduced BIPV cell temperature and increased seasonal COP of the heat pump. The solar fraction in this case would be 90%. The stored sensible heat is not considered for the south perimeter heating, which means, that if it would be used in the south perimeter zone a positive energy balance potentially could be reached.

Table 5.5: Heating season (January-April) performance for Saskatoon climate.

	$Q_{heat}+Q_{vent,}$ kWh	$Q_{fans,pumps,}$ kWh	$P_{appliances,lighting,}$ kWh	$P_{BIPV,}$ kWh	$P_{HP,}$ kWh	$Q_{HP,}$ kWh	P_{BIPV}/P_{tot}	COP_{HP}
Before retrofit	1170,5	193,1	739,1	N/A	N/A	N/A	N/A	N/A
Case 1 - Facade retrofit based on [18]	1068,9	121,3	739,1	N/A	N/A	N/A	N/A	N/A
Case 2 - decentralized BIPV/T-HP-PCM on South	789,8	165,2	739,1	1003,2	514,7	1369,2	0,71	2,66
Case 3 - decentralized BIPV/T-HP-PCM with hydronic heat storage	789,8	181,7	739,1	2578,2	1930,0	6639,2	0,90	3,44

5.3.3.3   *Potential for building Net Zero Energy balance*

A Net Zero energy balance is possible, using the decentralized systems with local power production using BIPV, reducing the energy demand for space conditioning and other electrical loads and introducing low temperature heating sources with integrated thermal storage in them. The electric energy balance for Cases 3 and 4 is shown in Figure 5.13 for Saskatoon climate from January to April. The cooling season is not considered in this study, where a potential to go to Net Positive balance is possible, due to higher solar radiation levels and reduced cooling demand through appropriate passive design (Bigaila et al., 2016).
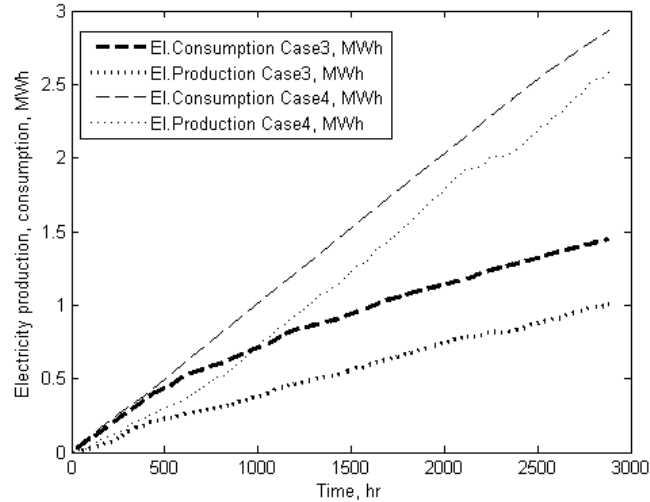
Figure 5.13. Cumulative electrical energy balance for retrofit cases 2 and 3.

5.4   **Conclusions**

A decentralized façade-integrated solar system is described and modeled in this paper. The system consists of a spandrel integrated air-based building-integrated photovoltaic/thermal collector (BIPV/T), a small scale air-to-water heat pump and a radiant panel with phase change material (RPCMP) for heating of south and west facing perimeter zones in a cold climate. The system is designed for retrofit applications, since some light and medium commercial buildings can benefit from relatively simple additional thermal mass application during the façade retrofit, which can be actively charged using façade integrated solar system with a heat pump.

Replacement of existing façade with the proposed decentralized system would help to perform both envelope and HVAC upgrades at the same time, which would result in time and cost reduction during the construction. If a complete façade replacement is not feasible, the system components can still be installed, however the benefits of prefabricated construction are not achieved.

Obviously, in order to perform a retrofit with prefabricated systems high precision measurement, design and manufacturing is crucial. Feasibility also depends on the distances between the panel

176

manufacturer and the construction site. Add to that, the site constraints can limit the access to the building façade as well.

Further work includes system operation optimization to shift the morning peak demand to off-peak hours. Effect of the heat pump and RPCMP sizing on combined energy performance and comfort parameters must be evaluated. An important aspect is the decentralized ventilation design options, since they can increase the operational energy savings significantly, due to reduced air distribution losses when compared to central systems.

The simulation results of the south facing perimeter office with decentralized solar assisted system shows promising results from operational energy point of view. With the developed numerical model the concept is compared to an all-air system for several consecutive design days. Electric power demand reduction of 14,5% for these design days can be achieved, if the façade integrated photovoltaic system would be supplying power to the perimeter zone for heating and plug load applications. A reduction in heating coil heating power demand of 11.3% is achieved for the mentioned design days if compared to all-air system.

6 Conclusions

Key results and conclusions of the thesis relating to are summarized by the following below:

- A BIPV/T prototype for spandrel applications integrated in a prefabricated façade element was designed and constructed utilizing the multiple inlet concept for the air intake. The developed prototype demonstrated 5% higher thermal efficiency and 0,5% higher electrical efficiency as compared to a BIPV/T system installed on Concordia University JMSB building. A standard performance characterization method was suggested for open loop BIPV/T air collectors utilizing a 5-plot system for comparison of different BIPV/T designs. This characterization method can be utilized at the preliminary HVAC and envelope integrated design stage;

- A multiple inlet BIPV/T numerical model was developed for façade-integrated system application studies including the multiple inlet effect – flow network and Nusselt number correlations were suggested for framed panels;

- The BIPV/T numerical model was improved with a solar transmission patch, to address one of the BIPV architectural integration requirements, the module texture and color effect on energy output. A library is created, where various innovative coatings, colors and pattern effects on the spectral light transmittance are reported. This information can be used for EPoG design or performance simulations;

- The numerical model was used to perform a parametric study of several BIPV/T design parameters to identify future development opportunities;

- A design methodology of BIPV and BIPV/T air collectors was introduced;

- A case study building in Saskatoon was modeled and a solar façade retrofit study was performed. A retrofit methodology was presented to estimate the most promising cases when a solar façade design in a retrofit project is considered. Spandrel-integrated BIPV and

BIPV/T, STPV glazing, shading devices with BIPV and second skin façade with BIPV was considered. The study was conducted for several Canadian climatic regions and general recommendations of the most feasible cases were presented. It was observed, that with current energy prices, EPoG costs, existing grid metering, self-consumption or feed-in-tariff programs the EPoG applications have a very high potential in retrofit projects, sometimes more feasible than conventional façade upgrades for the several Canadian climatic regions studied;

- A decentralized solar-assisted façade integrated system for retrofits was developed and modeled. The numerical model was included in a toolbox for solar system studies and a retrofit project case was investigated. The developed model was used to demonstrate, that on an annual basis, the decentralized system has a potential to substantially increase the building energy efficiency and close to net-zero perimeter zone performance is possible. The developed model can be used for system optimization and control studies.

6.1   Contributions

The contributions are summarized as follows:

- A design methodology for building integrated photovoltaics suitable for retrofits was developed (including BIPV/T and STPV design options);

- A numerical model for air-based framed BIPV/T solar collector with multiple inlets for spandrel façade retrofits was developed. Nusselt number correlations for this type of collector were identified. A library for BIPV glass optical parameters is created;

- A standard characterization method was developed for open-loop BIPV/T solar air collectors based on a proposed 5-plot system;

- A facade retrofit methodology for solar façade is developed and applied to a case study;

- A model of a BIPV/T assisted heat pump system and a radiant panel with a short term phase change thermal storage with PCM (RPCMP) was developed and extensively studied for potential retrofit systems.

- A decentralized façade system assisted by air-based BIPV/T solar collector was modeled with Matlab and implemented in Simulink-based toolbox *CARNOT (2017)* for future design and operation studies.

Journal publications:

Bigaila E. and Athienitis A.K., A study of a BIPV/T collector prototype for building façade applications, Energy Procedia, Volume 78, November 2015, pp. 1931-1936, https://doi.org/10.1016/j.egypro.2015.11.374.

Bigaila E. and Athienitis A.K., A study of solar façade potential in a cold climate office building retrofit, Applied Energy, article submitted to Special Issue, Aug. 2018.

Bigaila E. and Athienitis A.K., Modeling and simulation of a photovoltaic/thermal air collector assisting a façade integrated small scale heat pump with radiant PCM panel, Energy and Buildings, Volume 149, 2017, pp.298-309, https://doi.org/10.1016/j.enbuild.2017.05.045.

6.2 **Outlook and future research needs**

The potential for future research and development in this field is high and several main areas for future development are as follows:

- Better and more robust integrated tools are needed to design and optimize advanced solar facades in all design phases of new or old buildings;

- The development of tools that create BIM (building information model) based objects for BIPV, EPoG or BIPV/T products and can be used in building design stages for

implementation of these extremely competitive construction materials, particularly in early design stages. A dynamic link to energy simulation tools is necessary;

- A systematic approach to characterize the BIPV/T products is needed for the building designers to be able to include the air based BIPV/T collectors into their energy system (HVAC) designs. For this, a standard performance characterization for air-based BIPV/T or PV/T is required with available product databases;

- HVAC products for façade integration need to be developed. The design goals can be defined by theoretical studies setting the required performance maps for heat-pumps or radiant panel with PCM storage;

- Active modular thermal and electrical storage technologies and control strategies are crucial in not only providing the optimal comfort and performance of the solar-assisted systems, but also in reducing the PV and HVAC plant sizes and reaching net-zero energy building targets after retrofit;

- Development of an international BIPV standard that is addressing the multifunctionality of the active photovoltaic glass. A standard, that bridges both the structural and electrical performance requirements of the BIPV or EPoG for building industry and clearly separates the BIPV panels from the standard panel certification procedures, but does not eliminate the standard applications.

References

ASHRAE. (1997). ASHRAE Fundamentals. Handbook. Chapter 28: Nonresidential cooling and heating load calculations.

ASHRAE. (2001). ASHRAE Standard 55. Climate, comfort and natural ventilation: a new adaptive comfort standard.

ASHRAE. (2007). ANSI/ASHRAE Standard 62.1-2007. Ventilation for acceptable indoor air quality.

Athienitis, A., Bambara J., O'Neil, B., Faille, J. (2010). A prototype Photovoltaic/Thermal system integrated with transpired collector. Sol. Energy (85); p. 139-153.

Athienitis, A. K., Bambara, J., O'Neill, B., Faille, J. (2011). A prototype photovoltaic/thermal system integrated with transpired collector, Solar Energy 85 139-153, http://doi:10.1016/j.solener.2010.10.008.

Arkar, C., Medved, S. (2015). Optimization of latent heat storage in solar air heating system with vacuum tube air solar collector, Solar Energy 111 10-20, http://dx.doi.org/10.1016/j.solener.2014.10.013.

Backman, C., German, A., Daikin, B., Springer, D. (2016). Air-to-Water Heat Pump With Radiant Delivery in Low Load Homes, available at: http://apps1.eere.energy.gov/buildings/publications/pdfs/building_america/airtowater_heat_pumps.pdf, last accessed on April 8.

Baldini, L., Kim, M. K., & Leibundgut, H. (2014). Decentralized cooling and dehumidification with a 3 stage LowEx heat exchanger for free reheating. Energy and Buildings, 76, 270-277. doi:http://dx.doi.org/10.1016/j.enbuild.2014.02.021

Bambara, J., Athienitis, A. K., & O'Neill, B. (2011). Design and Performance of a Photovoltaic/Thermal System Integrated with Transpired Collector. ASHRAE Transactions, 117.

Bazilian, M., Groenhout, N., Prasad, D. (2001). Simplified numerical modelling and simulation of photovoltaic heat recovery system. Munich, Germany: 17th European photovoltaic solar energy conference, p 2387-2390.

Bazilian, M. D., & Prasad, D. (2002). Modelling of a photovoltaic heat recovery system and its role in a design decision support tool for building professionals. Renewable Energy, 27(1), 57-68. doi:http://dx.doi.org/10.1016/S0960-1481(01)00165-3

BC Hydro. (2018 a). BC Hydro business customers electricity rates, https://app.bchydro.com/accounts-billing/rates-energy-use/electricity-rates/business-rates.html#mgs (cited 02/07/2018).

BC Hydro. (2018 b). BC Hydro self-generation policy, https://www.bchydro.com/work-with-us/selling-clean-energy/net-metering/how_to_apply.html (cited 02/07/2018).

Bergmann, I., & Weiss, W. (2002). Fassadenintegration von thermischen Sonnenkollektoren ohne Hinterluftung: AEE Intec.

Bergman, T. L., Lavine, A. S., Incopera, F. P., Dewitt, D. P. (2011). Fundamentals of Heat and Mass Transfer, Seventh Edition, John Wiley & Sons, Inc., Hoboken, New Jersey, USA.

Berkley Windows and Daylighting Laboratory, 2018, https://windows.lbl.gov/software/window (sited 07/07/2017).

Bigaila, E., Rounis, E., Luk, P., & Athienitis, A. K. (2015). A study of a BIPV/T Collector prototype for Building Facade Applications. Paper presented at the IBPC 2015, Turin.

Bigaila, E., Hachem, C., El-Sayed, M., & Athienitis, A. (2016). Solar energy potential for commercial building facade retrofit. Paper presented at the eSim 2016, Hamilton, Canada.

Bigaila, E., Athienitis, A. K. (2016) Numerical study of spandrel integrated air-based BIPV/T system for façade retrofit projects in cold climates, in: 11th Advanced Building Skins Conference, Bern, Switzerland.

Bigaila, E., Athienitis, A. K. (2017). Modeling and simulation of a photovoltaic/thermal air collector assisting a façade integrated small scale heat pump with radiant PCM panel, Energy and Building 149, 298-309, http://dx.doi.org/10.1016/j.enbuild.2017.05.045.

Bine.info. (2009). Decentralised ventilation and climate control of office buildings.

Robinson, D., Campbell, N., Gaiser, W., Kabel, K., Le-Mouel, A., Morel, N., Stone, A. (2007). SUNtool – A new modelling paradigm for simulating and optimising urban sustainability, Solar Energy 81(9) 1196-1211, doi:http://dx.doi.org/10.1016/j.solener.2007.06.002.

Bobinson, D., Haldi, F., Kampf, J., Leroux, P. (2009). CITYSIM: Comprehensive micro-simulation of resource flows for sustainable urban planning, Paper presented at the Eleventh International IBPSA Conference, Glasgow, Scotland.

BOMA, (2015). Best, Module Definitions and Performance Benchmarks. Boma Best Application Guide.

Brinkworth, B. J. (2000). Estimation of FLow and Heat Transfer for the Design of PV Cooling Ducts. Solar Energy, 69, 413-420.

Buresch, M. (1983). Photovoltaic energy systems - design and installation. New York: McGraw-Hill.

Canadian Solar. (2015). Modules. Canadiansolar.com. Retrieved from http://www.canadiansolar.com/fileadmin/user_upload/downloads/datasheets/Datasheet_MaxPower_CS6X-P_en.pdf

Candanedo, J., Pogharian, S., Athienitis, A., Fry, A. (2007). Design and simulation of a net zero energy healthy home in Montreal. 2nd Canadian Solar Buildings Conference 1; p. 1-8.

Candanedo, J., & Athienitis, A. (2008). Simulation of the Performance of a BIPV/T system Coupled to a Heat Pump in a Residential Heating Application. Paper presented at the 9th International IEA Heat Pump Conference, Zurich.

Candanedo, L., Athienitis, A., Candanedo, J., & O'Brien, W., Yu Xiang. (2010). SIMPLIFIED MODEL FOR OPEN-LOOP AIR-BASED BIPV/T SYSTEMS. Paper presented at the sbrn. http://sbrn.solarbuildings.ca/c/sbn/file_db/Pres_Pdf/A-Simplified-Model-for-Open-Loop-Air-Based-BIPV-T-Systems.pdf

Candanedo, L. (2010). Modelling and Evaluation of the Performance of Building-Integrated Open Loop Air-based Photovoltaic/Thermal Systems. (PhD), Concordia University, Montreal, Canada.

Candanedo, J. (2011). A Study of Predictive Control Strategies for Optimally Designed Solar Homes. (PhD), Concordia University, Montreal. Retrieved from http://spectrum.library.concordia.ca/7704/

Cappel, C., Streicher, W., Lichtblau, F., & Maurer, C. (2014). Barriers to the Market Penetration of Façade-integrated Solar Thermal Systems. Energy Procedia, 48, 1336-1344. doi:http://dx.doi.org/10.1016/j.egypro.2014.02.151

Carnot, (2017). https://it.mathworks.com/matlabcentral/fileexchange/68890-carnot-toolbox

CEN-EN. (2001). European Committee for Standartization. Thermal solar systems and components – Solar Collectors – Part 2: Test methods. EN 12975-2. European Committee for Standardization.

CEN/TC 288. (2006). Standard prEN 15377-3:2006: Heating systems in buildings - Design of embedded water based surface heating and cooling systems - Part 3: Optimizing for use of renewable energy sources.

City of Saskatoon . (2018). City of Saskatoon Customer-Based Generation Programs, Feed-in-tariffs for in site solar electricity generation and electrical rates for commercial customers https://www.saskatoon.ca/services-residents/power-water/saskatoon-light-power/customer-based-generation-programs (cited 11/06/18).

Charron, R. (2004). One-and two-dimensional modeling of ventilated facades with integrated photovoltaic. (Masters thesis), Concordia University.

Charron, R. (2006). One-and two-dimensional modelling of ventilated facades with integrated photovoltaic panles. Sol Energy Engineering, ASME 128, p. 160-167.

Chen, Y., Athienitis, A., Berneche, B., Poissant, Y. (2007). Design and simulation of a building integrated photovoltaic thermal system and thermal storage for a solar home. Calgary, Canada: 2nd Canadian Solar Buildings Conference.

Chen, Y. (2009). Modeling and design of a solar house with focus on a ventilated concrete slab coupled with a building-integrated photovoltaic/thermal system. (M A Sc), Dept. of Building, Civil and Environmental Engineering, Concordia University. Retrieved from http://0-proquest.umi.com.mercury.concordia.ca/pqdweb?did=2073607551&sid=1&Fmt=2&clientId=10306&RQT=309&VName=PQD

Chen, Y. (2013). Methodology for Design and Operation of Active Building-Integrated Thermal Energy Storage Systems, PhD thesis, Concordia University, Montreal, Canada.

Christensen, C., Anderson, R., Horowitz, S., Courtney, A., Spencer, J. (2006). BEopt Software for building energy optimization: features and capabilities, U.S. Department of Energy, National Renewable Energy Laboratory, (NREL/TP-550-39929).

Clarke, J. A. (2012). Energy simulation in Building design: Taylor & Francis.

Compagno, A. (2002). Intelligent glass facades: material, practice, design. Basel: Birkhauser.

Cordeau, S., & Barrington, S. (2011). Performance of unglazed solar ventilation air pre-heaters for broiler barns. Solar Energy, 85(7), 1418-1429. doi:http://dx.doi.org/10.1016/j.solener.2011.03.026

Delisle, V., & Kummert, M. (2012). Experimental Study to Characterize the Performance of Combined Photovoltaic/Thermal Air Collectors. Journal of Solar Energy Engineering, 134(3), 031010-031010. doi:10.1115/1.4006576

Dermardiros, V. (2015). Modelling and Experimental Evaluation of an Active Thermal Energy Storage System with Phase-Change Materials for Model-Based Control, Master thesis, Concordia University, Montreal, Quebec, Canada.

Dermentzis, G., Ochs, F., Siegele, D., & Feist, W. (2014). A Facade Integrated Micro-Heat Pump - Energy Performance Simulations. Paper presented at the BauSIM 2014, Aachen.

Dittus, F., Boelter, L. (1930). Heat transfer in automobile radiators of tubular type. University of California Publications 2; p. 433-461.

DOE. (2005). Buildings Energy Databook: DOE.

DOE. (2012). EIA Commercial Buildings Energy Consumption Survey: CBECS.

Duffie, J. A., & Beckman, W. A. (2006). Solar Engineering of Thermal Processes. New Jersy: John Wiley & Sons.

Dymond, C., & Kutscher, C. (1996). Development of a flow distribution and design model for transpired solar collectors. Solar Energy, 60(5).

DuPont Energain. (2016). Available at: http://www.siginsulation.co.uk/Literature/dupont_energain_ prod%20info.pdf, last accessed July 10, 2016.

Ebbert, T. (2010). Refurbishment strategies for the technical improvement of office facades. (PhD), Technical University of Delft, Bochum.

ECBCS, I. (2009). IEA ECBCS Annex 44 Integrating Environmentally Responsive Elements in Buildings. Expert Guide - Part 2 Responsive Building Elements: IEA.

Eckstein, J. H. (1990). Detailed Modeling of Photovoltaic Components, M.S. Thesis, University of Wisconsin, Madison.

Esclapés, J., Ferreiro, I., Piera, J., Teller, J. (2014). A method to evaluate the adaptability of photovoltaic energy on urban façades, Solar Energy 105 414-427, doi:http://dx.doi.org/10.1016/j.solener.2014.03.012.

Egolf, P., Noume, A., Vuarnoz, D., & Gottschalk, G. (2014). Breathing building: A decentralized facade-integrated solar air-conditioning system (Vol. 381, pp. 381). Indistria & Formazione - International special issue 2014-2015.

Eicker, U. (2003). Solar technologies for buildings. New York: Wiley.

Eicker, U., Demir, E., Gurlich, D. (2015). Strategies for cost efficient refurbishment and solar energy integration in European Case Study buildings, Energy and Buildings 102 (2015) 237-249, http://dx.doi.org/10.1016/j.enbuild.2015.05.032.

Eisenhower, B., O'Neill, Z., Narayanan, S., Fonoberov, V. A., Mezić, I. (2012). A methodology for meta-model based optimization in building energy models, Energy and Buildings 47 292-301. doi:http://dx.doi.org/10.1016/j.enbuild.2011.12.001.

EN 12975-1. (2011). pr EN 12975-1:2011 „Thermal solar systems and components. Solar collectors. General requiremnts.".

Energir. (2018). Energir business customers natural gas rates. https://www.energir.com/en/business/price/pricing/ (cited 02/07/2018).

EUROSTAT. (2012). Final Energy Consumption by Sector, http://epp.eurostat.ec. europa.eu/tgm/refreshTableAction.do?tab=table&plugin=1&pcode=tsdpc320&language=e n (cited 11/06/2017).

Evola, G., Margani, G. (2016). Renovation of apartment blocks with BIPV: Energy and economic evaluation in temperature climate, Energy and Buildings 130 794-810, http://dx.doi.org/10.1016/j.enbuild.2016.08.085.

EN ISO. (2014). EN ISO 9806:2013 „Solar energy - Solar thermal collectors -Test methods".

Fallahi, A. (2009). Thermal Performance of Double-Skin Facade with Thermal Mass. (PhD), Concordia University, Montreal.

Feist, W. (1993). Building thermal simulation – a critical review of different modeling approaches, C.F. Muller, Karlsruhe, Germany, (In German).

Fleck, B., Meier, R., & Matovic, M. (2002). A field study of the wind effects on the performance of an unglazed transpired solar collector. Solar Energy, 73(3).

Fraunhofer ISE. (2012). EU-project „Cost-Effective". Resource- and Cost-effective integration of renewables in existing high-rise buildings. Germany: Fraunhofer ISE.

Frontini, F., Bonomo„ P, Hecker, R. (2016). Photovoltaic glass in building skin. A tool for customized BIPV in a BIM-based process.

Fortis BC. (2018). Fortis BC business customers natural gas rates. https://www.fortisbc.com/NaturalGas/Business/Rates/Mainland/Pages/LMRate3.aspx (cited 02/07/2018).

Fuentes, M. (2007). Integration of PV into the built environment. Brita in PuBs - Bringing retrofit innovation to application in public buildings, EU 6th framework program Eco-building. London, UK.

Gap Solutions. (2014). Solutions GAP Air. Technical manual.

Gap Solutions GmbH. (2014). GAP:air mit meltem luftungsgegerat mit warmeruck-gewinnung. Leonding.

German Solar Energy Society. (2010). Planning and installing solar Thermal Systems London: James & James.

Gluck, B. (1982). Strahlungsheizung - Theorie und Praxis. Karlsruhe: Verlag C. F.

Gnanam, B. (2013). Smart Energy Suburbs: Retrofitting Suburban Communities. Paper presented at the Quest 2013: Integrated Energy Solutions for Everyday Community. Conference and Tradeshow Markham, Ontario.

Gruner, M. (2012). The Potential of Facade-Integrated Ventilation Systems in Nordic Climate. Advanced decentralized ventilation systems as sustainable alternative to conventional systems. (Masters), NTNU.

Gugliermetti, F., Bisegna, F. (2006). Daylighting with external shading devices: design and simulation algorithms, Building and Environment 41(2) 136-149, doi:http://dx.doi.org/10.1016/j.buildenv.2004.12.011.

Guiavarch, A., Peuportier, B. (2006). Photovoltaic collectors efficiency according to their integration in buildings, Solar Energy 80 65-77, http://doi:10.1016/j.solener.2005.07.004.

Gunnewiek, L., Hollands, K., & Brundrett, E. (2002). Effect of wind on flow distribution in unglazed transpired-plate collectors. Solar Energy, 72(4).

Guo, J.; Lin, S.; Bilbao, J.I.; White, S.D.; Sproul, A.B., (2017). A review of photovoltaic thermal (PV/T) heat utilisation with low temperature desiccant cooling and dehumidification, Renewable and Sustainable Energy Reviews, vol. 67, pp. 1 - 14, http://dx.doi.org/10.1016/j.rser.2016.08.056

Gustafsson, M., Dermentzis, G., Myhren, J. A., Bales, C., Ochs, F., Holmberg, S., Feist, W. (2014). Energy performance comparison of three innovative HVAC systems for renovation through dynamic simulation, Energy and Buildings 82 512-519, http://doi:10.1016/j.enbuild.2014.07.059

Gustafsson, M., Dermentzis, G., Myhren, J., Bales, C., Ochs, F., Holmber, S., & Feist, W. (2015). Energy performance comparison of three innovative HVAC systems for renovation through dynamic simulation.

Gutermann, A. (2002). Mehrfamilien-Passivhaus mit solarem Luftsystem. Winterthur, Switzerland.

Hafner, B., Plettner, J., Wemhoner, C., & Wenzel, T. (1999). Conventional and Renewable energy systems optimization toolbox. Solar-Institut Juelich.

Haller, M., Winteler, C., Bertram, E., Bunea, M., Lerch, W., & Ochs, F. (2014). Solar and heat pump systems - summary of simulation results of the IEA SHC Task 44/HPP ANNEX 38. Paper presented at the 11th IEA Heat pump conference, Montreal.

Halverson, M., Rosenberg, M., Wang, W., Zhang, J., Mendon, V., Athalye, R. (2014). ANSI/ASHRAE/IES Standard 90.1-2013 Preliminary Determination: Quantitative Analysis, U.S. Department of Energy under Contract DE-AC05-76RL01830.

Hastings, S. R. (1999). Solar Air Systems: Built Examples. New York: James & James.

Hauser, G., & Heibel, B. (1998). Performance of curtain walls for pre-heating air. Paper presented at the SITHOK-3 International Congress, Maribor, Slovenia.

Heikkinen, P., Kaufmann, H., Winter, S., Larsen, K. E. (2016). TES EnergyFacade – prefabricated timber based building system for improving the energy efficiency of the building envelope. TES Manual, http://tesenergyfacade.com/ downloads/TES Manual-ebook FINAL.pdf, last accessed April 21.

Hegazy, A. A. (2000). Comparative study of the performances of four photovoltaic/thermal solar air collectors. Energy Conversion & Management, 41, 861-881.

Henning, H.-M. (2007). Solar-Assisted Air-Conditioning in Buildings: Springer Vienna Architecture.

Henning, H. M., Doll, J. (2012). Solar systems for heating and cooling of buildings, Energy Procedia 30 633 - 653.

Heo, Y., Choudhary, R., Augenbroe, G. A. (2012). Calibration of building energy models for retrofit analysis under uncertainty, Energy and Buildings 47 550-560, doi:http://dx.doi.org/10.1016/j.enbuild.2011.12.029.

Hydro Quebec. (2018 a). Hydro Quebec business customer electricity rates, 2018, http://www.hydroquebec.com/business/customer-space/rates/rate-g-general-rate-small-power.html (cited 02/07/2018).

Hydro Quebec. (2018 b). Hydro Quebec self-generation policy, http://www.hydroquebec.com/self-generation/faq.html (cited 02/07/2018).

Hovels, J. (2007). The Open Modular Facade Concept. Delft: Delft University of Technology.

Hug, R. (2010). Sun, Light and Heat: Light Control and Optimizing Energy in Offices and Other Buildings.

IEA. (2013). International Energy Agency (IEA). Transition to sustainable buildings. Paris, France: OECD/IEA;.

IEA. (2014). IEA SCH Task 47: Solar Renovation of Non-Residential Buildings.

IEA. (2015). International Agency Solar Heating and Cooling Programme Task 43. URL. http://task43.iea-shc.org/.

IEA ECBCS. (2011). IEA ECBCS Annex 50: Prefabricated Systems for Low Energy Renovation of Residential Buildings. Switzerland.

IEC. (2005). International Electrotechnical Commission. Crystalline silicon terrestrial photovoltaic (PV) modules – Design qualification and type approval. IEC 61215:2005.

IEC. (2006). IEC 61215/IEC 61646 ''Crystaline cilicium terrestrial photovoltaic (PV) Modules - Design qualification and type approval".

IEC. (2016). International Electrotechnical Commission. Concentrator photovoltaic (CPV) modules and assemblies – Design qualification and type approval. IEC 62108. International Electrotechnical Commission.

ISO. (2006 a). ISO 14064-1:2006 Greenhouse gases – Part 1: Specification with guidance at the organization level for qualification and reporting of greenhouse gas emissions and removals. URL https://www.iso.org/standard/38381.html.

ISO. (2006 b). ISO 14040:2006 Environmental management – Life ctycle assessment – Principles and framework. URL https://www.iso.org/standard/37456.html

Infield, D., Mei, L., & Eicker, U. (2004). Thermal performance estimation for ventilated PV facades. Solar Energy, 76(1–3), 93-98. doi:http://dx.doi.org/10.1016/j.solener.2003.08.010

Izquierdo, M., de Augustin-Camacho, P. (2015). Solar heating by radiant floor: Experimental results and emission reduction obtained with a micro photovoltaic–heat pump system, Applied Energy 147 297-307, http://dx.doi.org/10.1016/j.apenergy.2015.03.007.

IRENA. (2012). Solar Photovoltaics. Renewable Energy Technologies: Cost Analysis Series. Retrieved from

ISSOL. (2018). URL http://www.issol.eu/.

Ito, S., Miura, N., & Wang, K. (1999). PERFORMANCE OF A HEAT PUMP USING DIRECT EXPANSION SOLAR COLLECTORS1. Solar Energy, 65(3), 189-196. doi:http://dx.doi.org/10.1016/S0038-092X(98)00124-8

Kim, J.-H., & Kim, J.-T. (2012). A Simulation Study of Air-Type Building-Integrated Photovoltaic-Thermal System. Energy Procedia, 30, 1016-1024. doi:http://dx.doi.org/10.1016/j.egypro.2012.11.114

Kim, M. K., & Baldini, L. (2016). Energy analysis of a decentralized ventilation system compared with centralized ventilation systems in European climates: Based on review of analyses. Energy and Buildings, 111, 424-433. doi:http://dx.doi.org/10.1016/j.enbuild.2015.11.044

Kim, M. K., Leibundgut, H., & Choi, J.-H. (2014). Energy and exergy analyses of advanced decentralized ventilation system compared with centralized cooling and air ventilation systems in the hot and humid climate. Energy and Buildings, 79, 212-222. doi:http://dx.doi.org/10.1016/j.enbuild.2014.05.009

King, P. (2016). Procurement and design for existing buildings, http://www.bath.ac.uk/cwct/cladding_org/fdp/paper10.pdf, last accessed June 21.

Kirimtat, A., Koyunbaba, B. K., Chatzikonstantinou, I., Sariyildiz, S. (2016). Review of simulation modeling for shading devices in buildings, Renewable and Sustainable Energy Reviews 53 23-49, doi:http://dx.doi.org/10.1016/j.rser.2015.08.020.

Klein, S., & Nellis, G. (2012). Thermodynamics. New York: Cambridge University Press.

Klein, S. A., Beckmn, W. A., Mitchell, J. W., & Duffie, J. A. (2012). Trnsys 17. Volume 4 Mathematical Reference of standard components. Madison, U.S.A.: Solar Energy Laboratory, University of Wisconsin-Madison.

Knaack, U., Klein, K., & Auer, T. (2007). Facades - principles of construction. Basel.

Komp, R. (1982). Practical photovoltaics - electricity from solar cells. Michigan: aatec pubications

Koschenz, M. (2000). Thermpaktive Bauteilsysteme TABS. EMPA.

Koschenz, M., & Lehmann, B. (2004). Development of a thermally activated ceiling panel with PCM for application in lightweight and retrofitted buildings. Energy and Buildings, 36(6), 567-578. doi:http://dx.doi.org/10.1016/j.enbuild.2004.01.029

Kramer, K. (2011). Interaction of Regulation and Innovation: Solar Air Heating Collectors.

Kramer, K. (2013). IEA-SHC Task 43: Solar rating and certification procedures: IEA-SHC.

Kutscher, C. (1994). Heat exchange effectiveness and pressure drop for air flow through perforated plates with and without crosswind. Journal of Heat Transfer (94) p 391-399.

Lai, C. M., Hokoi, S. (2015). Solar façades: A review, Building and Environment 91 152-165, doi:http://dx.doi.org/10.1016/j.buildenv.2015.01.007.

Lechner, N. (2014). Heating, Cooling, Lighting. Sustainable methods for architects. New Jersey, The USA, Wiley.

Lee, S. H., Hong, T., Piette, M. A., Taylor-Lange, S. C. (2015). Energy retrofit analysis toolkits for commercial buildings: A review. Energy 89 1087-1100, doi:http://dx.doi.org/10.1016/j.energy.2015.06.112.

Mattei, M., Notton, G., Cristofari, C., Muselli, M., Poggi, P. (2006). Calculation of the polycrystalline PV module temperature using a simple method of energy balance, Renewable Energy 31(4) 553-567, doi:http://dx.doi.org/10.1016/j.renene.2005.03.010.

Mahler, B., & Himmler, R. (2008). Results of the evaluation study DeAL: Decentralized facade integrated ventilation systems. Paper presented at the 8th International Conference for Enhanced Building Operations, Berlin.

Manz, H., Egolf, P. W., Suter, P., & Goetzberger, A. (1997). TIM–PCM external wall system for solar space heating and daylighting. Solar Energy, 61(6), 369-379. doi:http://dx.doi.org/10.1016/S0038-092X(97)00086-8

Martinez, A., Patterson, M., Carlson, A., Noble, D. (2000). Fundamentals in Façade Retrofit Practice. Procedia Engineering 118, 934-941, doi:http://dx.doi.org/10.1016/j.proeng.2015.08.534.

Martinez, A. (2014). A. Carlson, State of the Art Methodology to Assess Energy Facade Retrofits. Paper presented at the ARCC/EAAE 2014: Beyond Architecture: New Intersections & Connections.

Márquez-García, A., Varo-Martínez, M., López-Luque, R. (2013). Toolbox engineering software for the analysis of sunlight on buildings, International Journal of Low-Carbon Technologies, doi:10.1093/ijlct/ctt062.

Maurer, C., Cappel, C., & Kuhn, T. E. (2015). Methodology and First Results of an R&D Road Map for Façade-integrated Solar Thermal Systems. Energy Procedia, 70, 704-708. doi:http://dx.doi.org/10.1016/j.egypro.2015.02.179

Maurer, C., Kuhn, T. E. (2012). Variable g value of transparent façade collectors, Energy and Buildings 51 177-184, doi:http://dx.doi.org/10.1016/j.enbuild.2012.05.011.

MEEFS. (2013). Multifunctional Energy Efficient Facade System for Building Retrofitting across Europe.

Mei, L., Infield, D., Eicker, U., Loveday, D., & Fux, V. (2006). Cooling potential of ventilated PV façade and solar air heaters combined with a desiccant cooling machine. Renewable Energy, 31(8), 1265-1278. doi:http://dx.doi.org/10.1016/j.renene.2005.06.013

Metais, B., Eckert, E. R. G.,.Trans. ASME J. Heat Transfer, 86 (1964), p. 295

Moaveni, S., Tebbe, P., Schwartzkopf, L., Gehrke, J., & Simones, M. (2011). The magnitude of the thermal energy stored in a building wall adjacent to an unglazed transpired solar collector. Paper presented at the ASME.

Noguchi, M., Athienitis, A., Delisle, V., Ayoub, J., Berneche, B. (2008). Net zero energy homes of the future: A case study of the EcoTerraTM House in Canada. Glasgow, Scotland: Renewable Energy Congress.

NRCan. (2004). Heating and cooling with a heat pump. Gatineau: Energy Publications, Office of Energy Efficiency, Natural Resources Canada.

NRCan-OEE. (2013a). Energy Efficiency Trends in Canada, 1990 to 2010. Retrieved from Ottawa, Ontario:

NRCan-OEE. (2013b). Survey of Commercial and Institutional Energy Use - Buildings 2009 (Detailed Statistical Report March 2013). Retrieved from Natural Resources Canada, Ottawa:

NRTEE. (2009). Geared for Change: Energy Efficiency in Canada's Commercial Building Sector. Ottawa.

Ochs, F. (2014). iNSPiRe Newsletter.

Ooshaksaraei, P., Sopian, K., Zulkifli, R., & Zaidi, S. (2013). Characterization of air-based photovoltaic thermal panels with bifacial solar cells. International Journal of Photoenergy, 2013.

Paiho, S., Seppa, I. P., Jimenez, C. (2015). An energetic analysis of a multifunctional façade system for energy efficient retrofitting of residential buildings in cold climates of Finland and Russia, Sustainable Cities and Society 15 75-85, http://dx.doi.org/10.1016/j.scs.2014.12.005.

Pasqualini, P., & Pressnail, K. (2002). The DBZ and Wall Surface Temperatures: canadianarchitect.com.

PAS. (2011). PAS 2050:2011 Specification for the assessment of the life cycle greenhouse gas emissions of goods and services. URL https://shop.bsigroup.com/forms/PASs/PAS-2050/.

Peng, J., Lu, L., Yang, H., & Han, J. (2013). Investigation on the annual thermal performance of a photovoltaic wall mounted on a multi-layer facade. Applied Energy, 646-656.

Pfeifer, J. B. B. (1984). Germany Patent No.: DPMA.

Quesada, G., Rousse, D., Dutil, Y., Badache, M., Hallé, S. (2012). A comprehensive review of solar facades. Opaque solar facades. Renewable and Sustainable Energy Reviews 16(5) 2820-2832. doi:http://dx.doi.org/10.1016/j.rser.2012.01.078

Redweik, P., Catita, C., Brito, M. (2013). Solar energy potential on roofs and facades in an urban landscape, Solar Energy 97 332-341, doi:http://dx.doi.org/10.1016/j.solener.2013.08.036.

Richman, R., & Pressnail, K. (2010 a). The solar dynamic buffer zone (SDBZ) curtain wall: Theory and simulation.

Richman, R., & Pressnail, K. D. (2010 b). Quantifying and predicting performance of the solar dynamic buffer zone (SDBZ) curtain wall through experimentation and numerical modeling. Energy and Buildings, 42(4), 522-533. doi:http://dx.doi.org/10.1016/j.enbuild.2009.10.021

Roth, K., Dieckmann, J., Brodrick, J. (2009). Heat Pumps for Cold Climates, ASHRAE Journal (February).

Rounis, E. D. (2015). Multiple-inlet Building Integrated Photovoltaics: Modeling and Design Including Wind Effects. (MASc), Concordia University.

Rounis, E. D., Bigaila, E., Luk, P., Athienitis, A., & Stathopoulos, T. (2015). Multiple-inlet BIPV/T modeling: wind effects and fan induced suction. Paper presented at the IBPC 2015, Turin.

Rysanek, A. M., Choudhary, R. (2013). Optimum building energy retrofits under technical and economic uncertainty, Energy and Buildings 57 324-337, doi:http://dx.doi.org/10.1016/j.enbuild.2012.10.027.

Ruschenburg, J., Baisch, K., Courtot, F., Oltersdorf, T., & Herkel, S. (2011). Experimental and Simulation Results on a Solar-Assisted Heat Pump Prototype for Decentral Applications. Paper presented at the 10th IEA Heat Pump Conference, Tokyo.

Saelens, D. (2002). Energy performance assessment of a single storey multiple-skin facades. (PhD), Catholic University of Leuven, Leuven.

Saranti, A., Tsoutsos, T., Mandalaki, M. (2015). Sustainable Energy Planning. Design Shading Devices with Integrated Photovoltaic Systems for Residential Housing Units, Procedia Engineering 123 479-487, doi:http://dx.doi.org/10.1016/j.proeng.2015.10.099.

Sarralde, J. J., Quinn, D. J., Wiesmann, D., Steemers, K. (2015). Solar energy and urban morphology: Scenarios for increasing the renewable energy potential of neighbourhoods in London, Renewable Energy 73 10-17, doi:http://dx.doi.org/10.1016/j.renene.2014.06.028.

Silva, P. C. P., Almeida, M., Braganca, L., Masquita, V. (2013). Development of prefabricated retrofit module towards nearly zero energy buildings, Energy and Buildings 56 115-125, http://dx.doi.org/ 10.1016/j.enbuild.2012.09.034.

Sharples, S., Charlesworth, P. (1998) Full-scale measurements of wind-induced convective heat transfer from a roof-mounted flat plate solar collector. Solar Energy (62); p. 69-77.

Smart-Flex. (2017) Cordis Project – Smart-flex: Demonstration at industrial scale of the FLeXible manufacturing of SMART multifunctional photovoltaic building elements. URL;. fhttp://www.smartflex-solarfacades.eu/project/

The German Energy Society. (2008). Planning & Installing Photovoltaic Systems: A Guide for installers, architects and engineers. London: Sterling VA.

Thornton, J. W., Bradley, D. E., McDowell, T. P., Blair, N. J., Duffy, M. J. (2012). Electrical Library mathematical Reference, TESSLibs17. Component Libraries for the TRNSYS Simulation Environment. Solar Energy Laboratory, University of Wisconsin – Madison.

Tonui, J. K., & Tripangnostopoulos, Y. (2007). Air-cooled PV/T solar collectors with low cost performance improvements. Solar Energy, 81, 498-511.

Torío, H., Angelotti, A., & Schmidt, D. (2009). Exergy analysis of renewable energy-based climatisation systems for buildings: A critical view. Energy and Buildings, 41(3), 248-271. doi:http://dx.doi.org/10.1016/j.enbuild.2008.10.006

Transsolar GmbH. (2012). Multizone building modeling with Type56 and TRNBuild: Integrated model for Thermo-Active Building Elements.

Tregenza, P. (1987). Subdivision of the sky hemisphere for luminance measurements, Lighting Research and Technology 19 13-14.

Touchie, M. F., Pressnail, K. D. (2014)) Evaluating a proposed retrofit measure for a multi-unit residential building which uses an air-source heat pump operating in an enclosed balcony space, Energy and Buildings 85 107-114, http://dx.doi.org/10.1016/j.enbuild.2014.08.048.

Tzempelikos, A., Athienitis, A. K. (2007). The impact of shading design and control on building cooling and lighting demand, Solar Energy 81(3) 369-382, doi:http://dx.doi.org/10.1016/j.solener.2006.06.015.

Ubertini, S., & Desideri, U. (2003). Design of a solar collector for year-round climatization. Renewable Energy, 28(4), 623-645. doi:http://dx.doi.org/10.1016/S0960-1481(02)00071-X

U.S. DOE (2017). Energy Plus. http://apps1.eere.energy.gov/buildings/energyplus/: U.S. Department of Energy & NREL.

van Dijk, H., Spiekman, M., de Wilde, P. (2005). A monthly method for calculating energy performance in the context of European building regulations. Paper presented at the Ninth International IBPSA Conference, International Building Performance Simulation Association, Montreal, Canada.

van Moeseke, G., Bruyère, I., De Herde, A. (2007). Impact of control rules on the efficiency of shading devices and free cooling for office buildings, Building and Environment 42(2) 784-793, doi:http://dx.doi.org/10.1016/j.buildenv.2005.09.015.

Vats, K., & Tiwari, G. (2012). Performance evaluation of a building integrated semitransparent photovoltaic thermal system for roof and façade. Energy and Buildings, Volume 45, Pages 211-218.

Vats, K., Tomar, V., & Tiwari, G. N. (2012). Effect of packing factor on the performance of a building integrated semitransparent photovoltaic thermal (BISPVT) system with air duct. Energy and Buildings, 53, 159-165. doi:http://dx.doi.org/10.1016/j.enbuild.2012.07.004

Voss, K., (2000). Solar energy in building renovation - results and experience of international demonstration buildings, Energy and Buildings 32, 291-302.

Waide, P., & Amann, J. (2007). Energy efficiency in the North American existing building stock: International Energy Agency.

Welz, C., Maurer, C., Lauro, P., Stryi-Hipp, G., Hermann, M. (2013). Mass flow, pressure drop, and leakage dependent modeling and characterization of solar air collectors. Freiburg, Germany: International Conference on Solar Heating and Cooling for Buildings and Industry.

Welz, C., Maurer, C., Di Lauro, P., Stryi-Hipp, G., & Hermann, M. (2014). Mass Flow, Pressure Drop, and Leakage Dependent Modeling and Characterization of Solar Air Collectors. Energy Procedia, 48, 250-263. doi:http://dx.doi.org/10.1016/j.egypro.2014.02.030

Yang, T., Athienitis, A. (2014). A study of design options for a building integrated photovoltaic/thermal (BIPV/T) system wih glazed air collector and multiple inlets. Sol. Energy;. http://dx.doi.org/10.1016/j.solener.2014.01.049

Yang, T. (2015). A Numerical and Experimental Investigation of Enhanced Open-Loop Air-Based Building-integrated Photovoltaic/Thermal (BIPV/T) Systems. Retrieved from Montreal:

Zeimes, M. (1979). Heizanlage mit luft/wasser-waermepumpe fuer raumheizung und/oder brauchwasserbereitung, mit einem luftkkollektor zur umwandlung der sonnenenergie in waerme: Google Patents.

Zhang, X., Shen, J., Lu, Y., He, W., Xu, P., Zhao, X., Dong, X. (2015). Active Solar Thermal Facades (ASTFs): From concept, application to research questions. Renewable and Sustainable Energy Reviews 50 32-63, doi:http://dx.doi.org/10.1016/j.rser.2015.04.108.

Zondag, H. A. (2008). Flat-plate PV-Thermal collectors and systems: A review. Renewable & Sustainable Energy Reviews, 891-959.

Appendix A - Solar façade PV inputs

Table A.1: Overhang and shutter parameters.

BIPV overhang model	South	East	West
Length of the wall, m	42.70	47.20	47.20
Installed peak power, kWp	4.47	4.95	4.95
Annual electricity production, MWha	6.52	5.14	5.04
BIPV shutter			
Panel area, m2	1.92	1.92	1.92
Wall area with PV, m2	62.90	51.80	51.80
Installed peak power, kWp	10.32	8.50	8.50
Annual electricity production, MWha	9.61	6.06	6.08

Table A.2: Spandrel-integrated BIPV parameters.

	South	East	West	South	East	West
WWR	0.8	0.8	0.8	0.4	0.4	0.4
Wall area, m2	25.16	19.6	19.6	75.48	62.2	62.2
Installed peak power, kWp	4.49	3.49	3.49	13.46	11.09	11.09
Annual electricity production, MWha	5.59	3.66	3.74	16.8	11.5	11.7

Table A.3: Second skin with BIPV parameters.

Second skin model (Orientation)	South				
Packing Factor	0.1	0.2	0.4	0.6	0.8
Wall area, m2	125.8				
Installed peak power, kWp	2.24	4.48	8.96	13.44	17.92
Annual electricity production, MWha	3.17	5.03	10.06	19.01	25.35
Second skin model (Orientation)	**East**				
Packing Factor	0.1	0.2	0.4	0.6	0.8
Wall area, m2	103.6				
Installed peak power, kWp	1.84	3.69	7.38	11.07	14.76
Annual electricity production, MWha	2.03	3.58	7.16	12.12	16.26
Second skin model (Orientation)	**West**				
Packing Factor	0.1	0.2	0.4	0.6	0.8
Wall area, m2	103.6				
Installed peak power, kWp	1.84	3.69	7.38	11.07	14.76
Annual electricity production, MWha	2.06	3.66	7.32	12.38	16.51

Table A.4: STPV parameters.

Second skin model (Orientation)	South								
Packing factor	0.17			0.39			0.52		
WWR	0.8	0.4	0.3	0.8	0.4	0.3	0.8	0.4	0.3
Window area, m2	100.64	50.32	37.74	100.64	50.32	37.74	100.64	50.32	37.74
Installed peak power, kWp	3.05	1.52	1.14	6.99	3.49	2.62	9.32	4.66	3.49
Annual electricity production, MWha	3.99	2.29	1.77	8.74	4.38	3.58	10.24	5.12	4.38
Second skin model (Orientation)	**East**								
Packing factor	0.17			0.39			0.52		
WWR	0.8	0.4	0.3	0.8	0.4	0.3	0.8	0.4	0.3
Window area, m2	84	41.4	31.1	84	41.4	31.1	84	41.4	31.1
Installed peak power, kWp	2.54	1.25	0.94	5.83	2.88	2.16	7.78	3.83	2.88
Annual electricity production, MWha	2.68	1.42	1.08	5.99	2.96	2.33	7.42	3.68	2.96
Second skin model (Orientation)	**West**								
Packing factor	0.17			0.39			0.52		
WWR	0.8	0.4	0.3	0.8	0.4	0.3	0.8	0.4	0.3
Window area, m2	84	41.4	31.1	84	41.4	31.1	84	41.4	31.1
Installed peak power, kWp	2.54	1.25	0.94	5.83	2.88	2.16	7.78	3.83	2.88
Annual electricity production, MWha	2.73	1.44	1.09	3.05	3.02	2.37	7.60	3.76	3.02

Appendix B - Energy saving analysis results

Table B.1: Overhang and shutter effect on perimeter zone performance.

Name	Energy savings for perimeter zones (min-max), %	Name	Energy savings for perimeter zones (min-max) for cases with EPoG, %
Ins(S),W(S),WWR(S)+O(S)	-1.48 – 2.87	*Ins(S),W(S),WWR(S)+EPoG-O(S)*	0.51 – 4.86
Ins(EW),W(EW),WWR(EW)+O(E)	-1.18 – 10.58	*Ins(EW),W(EW),WWR(EW)+ EPoG -O(E)*	0.39 – 12.15
Ins(EW),W(EW),WWR(EW)+O(W)	-0.31 – 10.93	*Ins(EW),W(EW),WWR(EW)+ EPoG -O(W)*	1.22 – 12.47
Ins(S),W(S,EW),WWR(S,EW)+O(S,E,W)	-0.74 – 12.66	*Ins(S),W(S,EW),WWR(S,EW)+ EPoG -O(S,E,W)*	4.35 – 17.75
Ins(S),W(S),WWR(S)+Sh(S)	-3.09 – 2.40	*Ins(S),W(S),WWR(S)+ EPoG -Sh(S)*	-0.16 – 5.33
Ins(EW),W(EW),WWR(EW)+Sh(E)	-1.17 – 10.69	*Ins(EW),W(EW),WWR(EW)+ EPoG -Sh(E)*	0.67 – 12.53
Ins(EW),W(EW),WWR(EW)+Sh(W)	-0.70 – 10.91	*Ins(EW),W(EW),WWR(EW)+ EPoG -Sh(W)*	1.15 – 12.76
		Ins(S),W(S,EW),WWR(S,EW)+ EPoG -Sh(S,E,W)	3.01 – 18.93

Table B.2: Spandrel integrated BIPV parameters.

Group nr.	Name	Energy savings for perimeter zone façade retrofit (min-max), %	*Energy savigns for façade retrofit with addition of South, East, West spandrel-integrated EPoG (min-max), %*	*Energy savigns for façade retrofit with addition of South spandrel-integrated EPoG (min-max), %*
1	*Ins(S,EW,N)*	0-2	4-8	2-6
2	*Ins(S,EW,N),Inf(1.2)*	24-31	27-33	24-30
3	*Ins(S,EW,N),Inf(1.2),W(S)*	26-39	29-42	26-39
4	*Ins(S,EW,N),Inf(1.2),W(EW)*	29-37	32-39	29-37
5	*Ins(S,EW,N),Inf(1.2),W(N)*	25-32	27-34	25-31
6	*Ins(S,EW,N),Inf(1.2),W(W1,EW,N)*	31-40	34-43	32-40
7	*Ins(0.588),Inf(1.2),W(S,EW,N),WWR(EW(0.4))*	31-38	40-47	33-40
8	*Ins(0.588),Inf(1.2),W(S,EW,N),WWR(S(0.4),EW(0.4))*	32-37	46-51	39-44
9	*Ins(0.183),Inf(1.2),W(S,EW,N),WWR(EW(0.4))*	35-42	44-51	37-44
10	*Ins(0.183),Inf(1.2),W(S,EW,N),WWR(S(0.4),EW(0.4))*	37-42	50-56	43-49
11	*Ins(0.109),Inf(1.2),W(S,EW,N),WWR(EW(0.4))*	36-43	45-52	38-45
12	*Ins(0.109),Inf(1.2),W(S,EW,N),WWR(S(0.4),EW(0.4))*	38-43	51-57	44-50
13	*Ins(0.077),Inf(1.2),W(S,EW,N),WWR(EW(0.4))*	36-43	45-52	38-45
14	*Ins(0.077),Inf(1.2),W(S,EW,N),WWR(S(0.4),EW(0.4))*	38-43	52-57	44-50
15	*Ins(S,EW,N),Inf(0.6)*	53-59	53-58	51-56
16	*Ins(0.588),Inf(0.6),W(S,EW,N),WWR(EW(0.4))*	60-66	67-73	60-66
17	*Ins(0.588),Inf(0.6),W(S,EW,N),WWR(S(0.4),EW(0.4))*	62-66	74-79	67-71
18	*Ins(0.183),Inf(0.6),W(S,EW,N),WWR(EW(0.4))*	64-70	71-77	64-70
19	*Ins(0.183),Inf(0.6),W(S,EW,N),WWR(S(0.4),EW(0.4))*	66-71	78-83	71-76
20	*Ins(0.109),Inf(0.6),W(S,EW,N),WWR(EW(0.4))*	65-70	71-77	64-70
21	*Ins(0.109),Inf(0.6),W(S,EW,N),WWR(S(0.4),EW(0.4))*	67-71	79-83	72-76
22	*Ins(0.077),Inf(0.6),W(S,EW,N),WWR(EW(0.4))*	65-71	71-78	64-70
23	*Ins(0.077),Inf(0.6),W(S,EW,N),WWR(S(0.4),EW(0.4))*	68-72	79-84	72-77

Table B.3: Energy savings in a façade retrofit with a second skin and BIPV glazing.

Name	Energy savings for perimeter zones (min-max), %	Name	Energy savings for perimeter zones (min-max) for cases with EPoG glazing, %
Second skin south façade addition	2	*Second skin south façade addition with EPoG (PF1)*	3
		Second skin south façade addition with EPoG (PF2)	4
		Second skin south façade addition with EPoG (PF3)	5
		Second skin south façade addition with EPoG (PF4)	8
		Second skin south façade addition with EPoG (PF5)	10
Second skin East and West facades addition	4	*Second skin East and West facades addition with EPoG (PF1)*	6
		Second skin East and West facades addition with EPoG (PF2)	7
		Second skin East and West facades addition with EPoG (PF3)	8
		Second skin East and West facades addition with EPoG (PF4)	10
		Second skin East and West facades addition with EPoG (PF5)	11
Second skin North facade addition	1		

Table B.4: Retrofit with STPV Windows energy savings.

Name	Energy savings for perimeter zones (min-max), %
W(S,EW),WWR(S,EW)+STPV_PF1(S,EW)	1.7-11.3
W(S,EW),WWR(S,EW)+STPV_PF2(S,EW)	1.9-11.9
W(S,EW),WWR(S,EW)+STPV_PF3(S,EW)	2.3-12.7

Appendix C - Cost analysis results
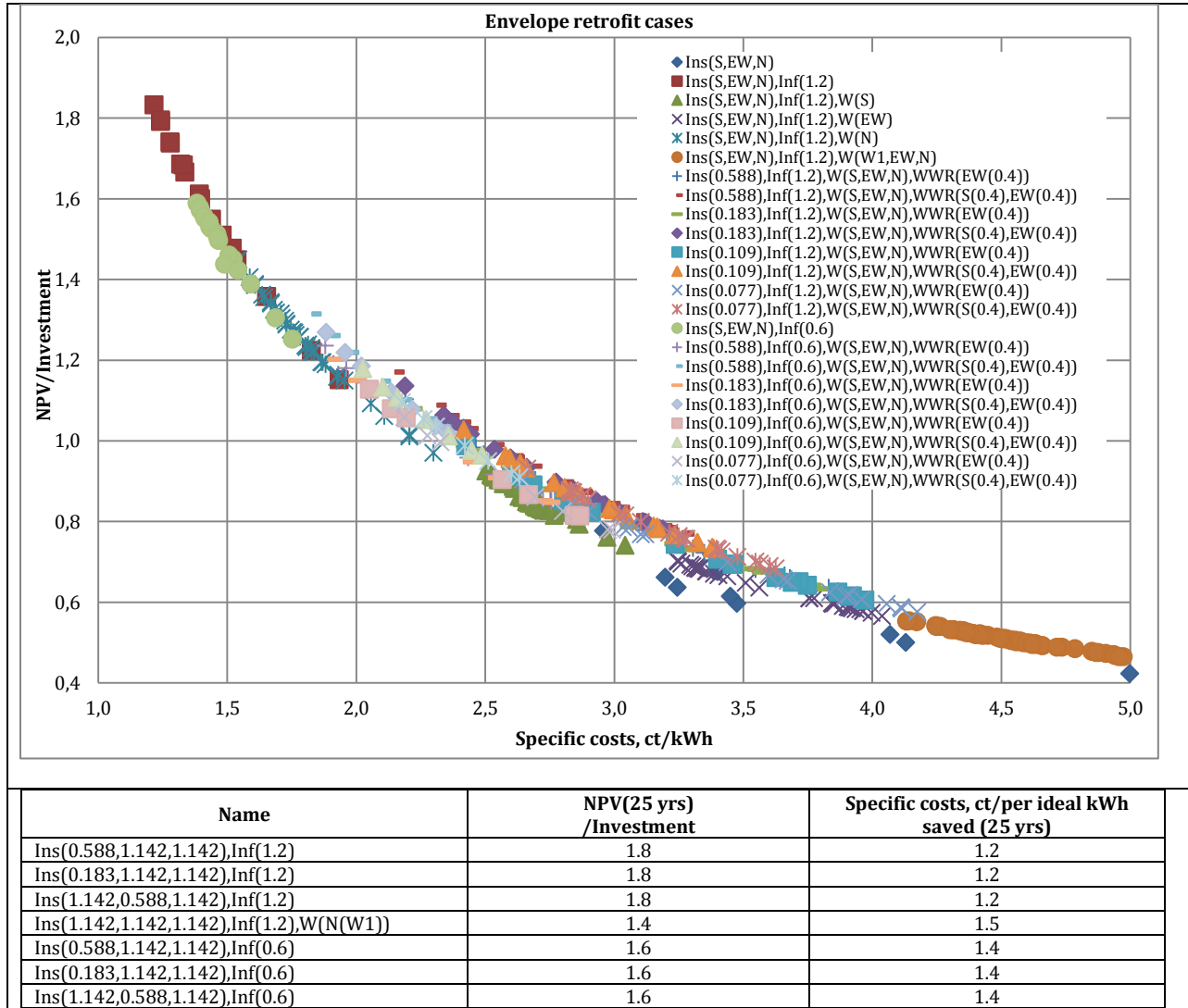
Figure C.1: Facade retrofit cases.

Name	NPV(25 yrs) /Investment	Specific costs, ct/per ideal kWh saved (25 yrs)
Ins(0.588,1.142,1.142),Inf(1.2)	1.8	1.2
Ins(0.183,1.142,1.142),Inf(1.2)	1.8	1.2
Ins(1.142,0.588,1.142),Inf(1.2)	1.8	1.2
Ins(1.142,1.142,1.142),Inf(1.2),W(N(W1))	1.4	1.5
Ins(0.588,1.142,1.142),Inf(0.6)	1.6	1.4
Ins(0.183,1.142,1.142),Inf(0.6)	1.6	1.4
Ins(1.142,0.588,1.142),Inf(0.6)	1.6	1.4

Envelope retrofit cases

Legend:
- Ins(S,EW,N)
- Ins(S,EW,N),Inf(1.2)
- Ins(S,EW,N),Inf(1.2),W(S)
- Ins(S,EW,N),Inf(1.2),W(EW)
- Ins(S,EW,N),Inf(1.2),W(N)
- Ins(S,EW,N),Inf(1.2),W(W1,EW,N)
- Ins(0.588),Inf(1.2),W(S,EW,N),WWR(EW(0.4))
- Ins(0.588),Inf(1.2),W(S,EW,N),WWR(S(0.4),EW(0.4))
- Ins(0.183),Inf(1.2),W(S,EW,N),WWR(EW(0.4))
- Ins(0.183),Inf(1.2),W(S,EW,N),WWR(S(0.4),EW(0.4))
- Ins(0.109),Inf(1.2),W(S,EW,N),WWR(EW(0.4))
- Ins(0.109),Inf(1.2),W(S,EW,N),WWR(S(0.4),EW(0.4))
- Ins(0.077),Inf(1.2),W(S,EW,N),WWR(EW(0.4))
- Ins(0.077),Inf(1.2),W(S,EW,N),WWR(S(0.4),EW(0.4))
- Ins(S,EW,N),Inf(0.6)
- Ins(0.588),Inf(0.6),W(S,EW,N),WWR(EW(0.4))
- Ins(0.588),Inf(0.6),W(S,EW,N),WWR(S(0.4),EW(0.4))
- Ins(0.183),Inf(0.6),W(S,EW,N),WWR(EW(0.4))
- Ins(0.183),Inf(0.6),W(S,EW,N),WWR(S(0.4),EW(0.4))
- Ins(0.109),Inf(0.6),W(S,EW,N),WWR(EW(0.4))
- Ins(0.109),Inf(0.6),W(S,EW,N),WWR(S(0.4),EW(0.4))
- Ins(0.077),Inf(0.6),W(S,EW,N),WWR(EW(0.4))
- Ins(0.077),Inf(0.6),W(S,EW,N),WWR(S(0.4),EW(0.4))

Name	NPV(25 yrs) /Investment	Specific costs, ct/per ideal kWh saved (25 yrs)
EPoG(S,E,W)	1.79	9.02
Ins(1.142,1.142,0.183)+EPoG(S,E,W)	1.55	5.61
Ins(0.588,1.142,1.142),Inf(1.2)+EPoG(S,E,W)	1.82	2.19
Ins(1.142,0.588,1.142),Inf(1.2)+EPoG(S,E,W)	1.81	2.20
Ins(1.142,0.183,1.142),Inf(1.2)+EPoG(S,E,W)	1.79	2.14
Ins(1.142,1.142,1.142),Inf(1.2),W(N(W1))+EPoG(S,E,W)	1.60	2.48
Ins(0.588,1.142,1.142),Inf(1.2),W(N(W1))+EPoG(S,E,W)	1.63	2.43
Ins(0.588,1.142,1.142),Inf(0.6)+EPoG(S,E,W)	1.66	1.86
Ins(1.142,0.588,1.142),Inf(0.6)+EPoG(S,E,W)	1.65	1.86
EPoG(S)	1.97	8.02
Ins(0.588,1.142,1.142),Inf(1.2)+EPoG(S)	1.89	1.61
Ins(1.142,0.588,1.142),Inf(1.2)+EPoG(S)	1.88	1.62
Ins(0.588,1.142,1.142),Inf(1.2),W(N(W1))+EPoG(S)	1.61	1.88
Ins(0.588,1.142,1.142),Inf(0.6)+EPoG(S)	1.65	1.57
Ins(1.142,0.588,1.142),Inf(0.6)+EPoG(S)	1.65	1.57

Figure C.2: Facade retrofit with BIPV cases.

Figure C.3: Facade retrofit with solar shading and BIPV as solar shading cases.

Name	NPV(25 yrs) /Investment	Specific costs, ct/per ideal kWh saved (25 yrs)
Ins(1.142,0.588,1.142),W(EW(W1)),WWR(EW(0.4))+EPoG-O(East)	1.4	3.6
Ins(1.142,0.183,1.142),W(EW(W1)),WWR(EW(0.4))+EPoG-O(East)	1.4	3.2
Ins(1.142,0.588,1.142)+EPoG-O(W)	3.2	1.5
Ins(1.142,0.183,1.142)+EPoG-O(W)	1.9	6.1
Ins(1.142,0.588,1.142)+W(EW(W1)+WWR(EW(0.4)+EPoG-O(W)	1.4	3.5
Ins(0.588,1.142,1.142)+EPoG-O(S,E,W)	2.3	5.9

Envelope retrofit cases

Legend:
- Ins(S,EW,N)
- Ins(S,EW,N),Inf(1.2)
- Ins(S,EW,N),Inf(1.2),W(S)
- Ins(S,EW,N),Inf(1.2),W(EW)
- Ins(S,EW,N),Inf(1.2),W(N)
- Ins(S,EW,N),Inf(1.2),W(W1,EW,N)
- Ins(0.588),Inf(1.2),W(S,EW,N),WWR(EW(0.4))
- Ins(0.588),Inf(1.2),W(S,EW,N),WWR(S(0.4),EW(0.4))
- Ins(0.183),Inf(1.2),W(S,EW,N),WWR(EW(0.4))
- Ins(0.183),Inf(1.2),W(S,EW,N),WWR(S(0.4),EW(0.4))
- Ins(0.109),Inf(1.2),W(S,EW,N),WWR(EW(0.4))
- Ins(0.109),Inf(1.2),W(S,EW,N),WWR(S(0.4),EW(0.4))
- Ins(0.077),Inf(1.2),W(S,EW,N),WWR(EW(0.4))
- Ins(0.077),Inf(1.2),W(S,EW,N),WWR(S(0.4),EW(0.4))
- Ins(S,EW,N),Inf(0.6)
- Ins(0.588),Inf(0.6),W(S,EW,N),WWR(EW(0.4))
- Ins(0.588),Inf(0.6),W(S,EW,N),WWR(S(0.4),EW(0.4))
- Ins(0.183),Inf(0.6),W(S,EW,N),WWR(EW(0.4))
- Ins(0.183),Inf(0.6),W(S,EW,N),WWR(S(0.4),EW(0.4))
- Ins(0.109),Inf(0.6),W(S,EW,N),WWR(EW(0.4))
- Ins(0.109),Inf(0.6),W(S,EW,N),WWR(S(0.4),EW(0.4))
- Ins(0.077),Inf(0.6),W(S,EW,N),WWR(EW(0.4))
- Ins(0.077),Inf(0.6),W(S,EW,N),WWR(S(0.4),EW(0.4))

Name	NPV(25 yrs)/Investment	Specific costs, ct/per ideal kWh saved (25 yrs)
2nd Skin South with EPoG (PF4)	0.51	21
2nd Skin South with EPoG (PF5)	0.67	18
2nd Skin East, West with EPoG (PF5)	0.54	29

Figure C.4: Facade retrofit by adding a second skin with BIPV.

Window replacement with STPV

Legend:
- W(S,EW),WWR(S,EW)+STPV_PF1(S,EW)
- W(S,EW),WWR(S,EW)+STPV_PF2(S,EW)
- W(S,EW),WWR(S,EW)+STPV_PF3(S,EW)
- W(S(W2),EW(W2))
- W(S(W2),EW(W2)),WWR(S(0.3),EW(0.3))
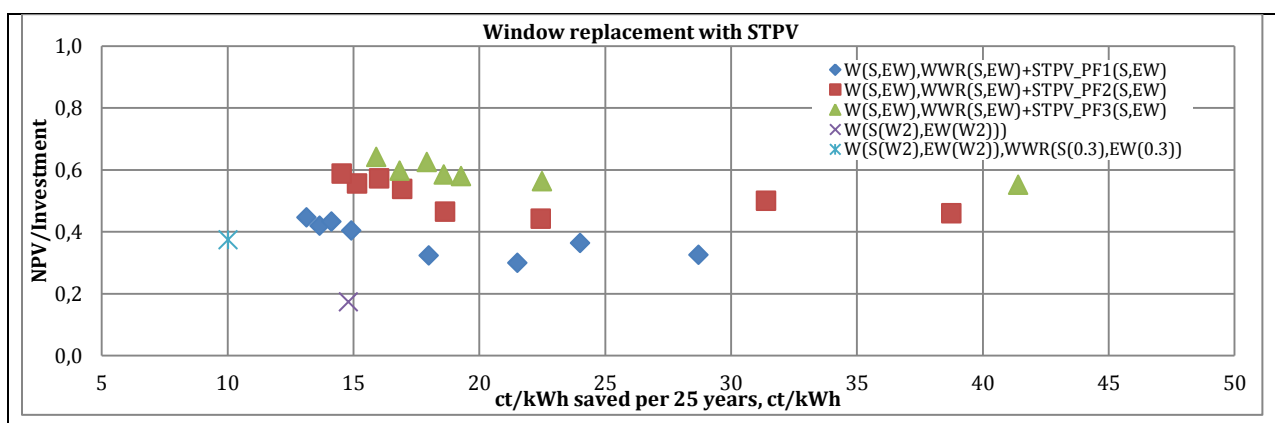
Name	NPV(25 yrs)/Investment	Specific costs, ct/per ideal kWh saved (25 yrs)
W(S(W2),EW(W2)),WWR(S(0.3),EW(0.3))+STPV_PF1(S,EW)	0.45	13
W(S(W2),EW(W2)),WWR(S(0.3),EW(0.3))+STPV_PF2(S,EW)	0.59	15
W(S(W1),EW(W1)),WWR(S(0.3),EW(0.3))+STPV_PF3(S,EW)	0.63	18
W(S(W2),EW(W2)),WWR(S(0.3),EW(0.3))+STPV_PF3(S,EW)	0.64	16

Figure C.5: Façade retrofit by replacing windows with STPV.

199

Name	NPV(25 yrs) /Investment	Specific costs, ct/per ideal kWh saved (25 yrs)
Ins(0.588,1.142,1.142),Inf(1.2)	1.8	1.2
Ins(0.183,1.142,1.142),Inf(1.2)	1.8	1.2
Ins(1.142,0.588,1.142),Inf(1.2)	1.8	1.2
Ins(1.142,1.142,1.142),Inf(1.2),W(N(W1))	1.4	1.5
Ins(0.588,1.142,1.142),Inf(0.6)	1.6	1.4
Ins(0.183,1.142,1.142),Inf(0.6)	1.6	1.4
Ins(1.142,0.588,1.142),Inf(0.6)	1.6	1.4
EPoG(S,E,W)	1.8	9.0
Ins(1.142,1.142,0.183)+EPoG(S,E,W)	1.5	5.6
Ins(0.588,1.142,1.142),Inf(1.2)+EPoG(S,E,W)	1.8	2.1
Ins(1.142,0.588,1.142),Inf(1.2)+EPoG(S,E,W)	1.8	2.1
Ins(1.142,0.183,1.142),Inf(1.2)+EPoG(S,E,W)	1.8	2.1
Ins(1.142,1.142,1.142),Inf(1.2),W(N(W1))+EPoG(S,E,W)	1.6	2.4
Ins(0.588,1.142,1.142),Inf(1.2),W(N(W1))+EPoG(S,E,W)	1.6	2.4
Ins(0.588,1.142,1.142),Inf(0.6)+EPoG(S,E,W)	1.7	1.8
Ins(1.142,0.588,1.142),Inf(0.6)+EPoG(S,E,W)	1.7	1.8
EPoG(S)	2.0	8.0
Ins(0.588,1.142,1.142),Inf(1.2)+EPoG(S)	1.9	1.6
Ins(1.142,0.588,1.142),Inf(1.2)+EPoG(S)	1.9	1.6
Ins(0.588,1.142,1.142),Inf(1.2),W(N(W1))+EPoG(S)	1.6	1.8
Ins(0.588,1.142,1.142),Inf(0.6)+EPoG(S)	1.7	1.5
Ins(1.142,0.588,1.142),Inf(0.6)+EPoG(S)	1.6	1.5
Ins(1.142,0.588,1.142),W(EW(W1)),WWR(EW(0.4))+EPoG-O(East)	1.4	3.6
Ins(1.142,0.183,1.142),W(EW(W1)),WWR(EW(0.4))+EPoG-O(East)	1.4	3.2
Ins(1.142,0.588,1.142)+EPoG-O(W)	3.2	1.5
Ins(1.142,0.183,1.142)+EPoG-O(W)	1.9	6.1
Ins(1.142,0.588,1.142)+W(EW(W1)+WWR(EW(0.4)+EPoG-O(W)	1.4	3.5
Ins(0.588,1.142,1.142)+EPoG-O(S,E,W)	2.3	5.9
2nd Skin South with EPoG (PF4)	0.5	21.5
2nd Skin South with EPoG (PF5)	0.7	18.1
2nd Skin East, West with EPoG (PF5)	0.5	29.3
W(S(W2),EW(W2)),WWR(S(0.3),EW(0.3))+STPV_PF1(S,EW)	0.4	13.1
W(S(W2),EW(W2)),WWR(S(0.3),EW(0.3))+STPV_PF2(S,EW)	0.6	14.5
W(S(W1),EW(W1)),WWR(S(0.3),EW(0.3))+STPV_PF3(S,EW)	0.6	17.9
W(S(W2),EW(W2)),WWR(S(0.3),EW(0.3))+STPV_PF3(S,EW)	0.6	15.9

Figure C.6: Facade retrofit with BIPV best cases per each approach summary.